Longitudinal handling characteristics of a tailless gull-wing aircraft

Daniël Sarel Agenbag

July 28, 2008

UNIVERSITEIT VAN PRETORIA
UNIVERSITY OF PRETORIA
YUNIBESITHI YA PRETORIA

Longitudinal handling characteristics of a tailless gull-wing aircraft

by

Daniël Sarel Agenbag

A dissertation submitted in partial fulfilment
of the requirements for the degree

Master of Engineering

(Mechanical Engineering)

in the

Faculty of Engineering, Built Environment and Information Technology

University of Pretoria

July 2008

Synopsis

Longitudinal handling characteristics of a tailless gull-wing aircraft

Author	:	Daniël Sarel Agenbag
Student number	:	9701128-3
Study leader	:	Prof. N.J. Theron
Co-leader	:	Mr. R.J. Huyssen
Degree	:	Master of Engineering (Mechanical)
Department	:	Department of Mechanical and Aeronautical Engineering

A handling quality investigation was performed on the swept gull-wing configuration. The swept gull-wing configuration is tailless and has a wing with a transition in the sweep and dihedral angle. An example of this type of aircraft is the Exulans. This aircraft is currently under development at the University of Pretoria. The handling quality study was focussed on pitch axis dynamics. The Exulans is a research testbed that will be used to investigate the swept gull-wing configuration and its special controls by means of full-scale flight testing. Variable wing sweep, twisting elevons and winglets will be investigated as means of control. These control devices are configured in such a way as to have minimum impact on the performance of the aircraft. The handling qualities of the swept gull-wing configuration have to be acceptable while using these different control strategies.

The study was launched to investigate whether a gull-wing configuration aircraft will have satisfactory handling qualities at CG positions associated with the most favourable aerodynamic performance. There is an aerodynamic performance gain in designing an aircraft so that the CG falls on the so-called 'E-point'. The E-point is the centre of pressure for an elliptical circulation distribution. An ellip-

tical circulation distribution is associated with the highest Oswald efficiency for an aircraft.

Time domain simulation techniques and frequency domain analysis techniques were used to analyse the handling qualities of the gull-wing configuration. The C-star criterion was used to analyse handling qualities with time domain simulation data as input. Comparative time domain simulations were performed between the Exulans and other aircraft to compare handling qualities. Eigenvalue analysis was used together with the thumbprint criterion to investigate inherent gull-wing airframe dynamics. The Shomber-Gertsen and Military Specification 8785 criteria were also used for the same purpose. The Neal-Smith method was used to investigate the effect of control authority on handling qualities and the effect of a pilot. The Mönnich and Dalldorff criterion was used to evaluate gust handling qualities. An analysis chart by Fremaux and Vairo was used to evaluate the tumbling susceptibility of the gull-wing configuration.

The pitch handling quality investigation shows sufficient promise that the swept gull-wing configuration will have acceptable handling qualities with the CG placed at positions associated with optimised aerodynamic performance. Analysis showed that the swept gull-wing configuration is potentially prone to tumbling. With low static margins, the configuration should exhibit improved handling qualities in gusty conditions when compared to existing tailless aircraft.

It is recommended that a lateral handling quality study be performed before full scale flight testing commences on the Exulans. In addition, the possibility of wingtip stall must be investigated for the case of the swept gull-wing configuration.

KEYWORDS: Tailless aircraft; Handling qualities; Gust handling qualities; E-point; O-point; Flight simulation; Swept gull-wing configuration; Mönnich and Dalldorff criterion; C-star criterion; Thumbprint criterion; Shomber-Gertsen analysis; Neal-Smith analysis; Pilot induced oscillation; Pecking; Tumbling; Exulans; Variable static margin; Variable sweep wing; Pilot mathematical model; Oswald efficiency.

Opsomming

Longitudinale hanteringseienskappe van 'n stertlose meeuvlerkvliegtuig

Skrywer	:	Daniël Sarel Agenbag
Studentenommer	:	9701128-3
Studieleier	:	Prof. N.J. Theron
Mede-studieleier	:	Mnr. R.J. Huyssen
Graadbenaming	:	Magister in Ingenieurswese (Meganies)
Departement	:	Departement Meganiese en Lugvaartkundige Ingenieurswese

'n Ondersoek is geloods aangaande die vlughanteringseienskappe van die meeuvlerkuitleg. Hierdie uitleg is 'n stertlose ontwerp waarvan die vlerk 'n oorgang in veeg en diëderhoek het. Die Exulans sweeftuig, tans onder ontwikkeling by die Universiteit van Pretoria, is 'n voorbeeld van hierdie uitleg. Die studie het gefokus op heivlak dinamika. Die Exulans is 'n navorsingsplatform wat gebruik sal word om die spesiale vlugbeheerstelsel van die meeuvlerkuitleg te ondersoek deur volskaalse vlugtoetse. Veranderbare vlerkveeg, asook wringbare hoogterolroere en rigtingroere op entvlerke word gebruik om die Exulans te stuur. Die beheeroppervlaktes is ontwerp om die impak op die werksverrigting van die vliegtuig te minimeer. Die hanteringseienskappe van die meeuvlerkuitleg moet aanvaarbaar wees met die gebruik van hierdie stuurmeganismes.

Die ondersoek moes bepaal of die meeuvlerkuitleg gunstige hanteringseienskappe sal vertoon terwyl die vliegtuig se swaartepunt geplaas is op 'n posisie wat assosieer word met die mees gunstige aerodinamiese werksverrigting. Daar is 'n voordeel met betrekking tot aerodinamiese werksverrigting wanneer 'n vliegtuig ontwerp word sodat die swaartepunt ooreenstem met die sogenaamde 'E-punt'.

Die E-punt is die sentroïede van die drukverdeling van 'n elliptiese sirkulasieverspreiding. 'n Elliptiese sirkulasieverspreiding word assosieer met die mees gunstige Oswald rendement van 'n vliegtuig.

Tyddomein simulasietegnieke en frekwensiedomein analises is gebruik om die hanteringseienskappe van die meeuvlerkuitleg te ondersoek. Die C-ster kriterium is gebruik om hanteringseienskappe te ondersoek met behulp van tyddomein simulasie resultate. Tyddomein simulasies was gebruik om die Exulans en ander vliegtuie te vergelyk met betrekking tot hanteringseienskappe. Eiewaarde analise is gebruik tesame met die 'vingerafdruk' kriterium om die inherente lugraamhanteringseienskappe van die meeuvlerk te ondersoek. Die Shomber-Gertsen en Militêre Standaard 8785 kriteria is ook vir dieselfde doel gebruik. Die Neal-Smith metode is gebruik om die effek van beheeroutoriteit op hanteringseienskappe en die invloed van 'n vlieënier te ondersoek. Die Mönnich-Dalldorff kriterium is gebruik om die effek van rukwindtoestande op hanteringseienskappe te ondersoek. 'n Analisekaart deur Fremaux en Vairo is gebruik om die vatbaarheid van die meeuvlerkuitleg vir tuimeling te ondersoek.

Die heivlak hanteringseienskapstudie het getoon dat die meeuvlerkuitleg genoegsame belofte van gunstige hanteringseienskappe toon wanneer die swaartepunt geplaas word op posisies wat assosieer word met hoë aerodinamiese werksverrigting. Analise het ook onthul dat die meevlerkuitleg vatbaar is vir tuimeling. Die studie het verder ook aangetoon dat die uitleg meer gunstige hanteringseienskappe het as bestaande stertlose ontwerpe tydens turbulente omstandighede, mits dit met 'n lae stabiliteitsgrens ontwerp word.

Dit word aanbeveel dat 'n laterale hanteringseienskapstudie van stapel gestuur word voor enige volskaalse vlugtoetse met die Exulans onderneem word. Die moontlikheid van staking by die vlerkpunte moet ook ondersoek word vir die meeuvlerkuitleg.

SLEUTELWOORDE: Stertlose vliegtuig; Hanteringseienskappe; E-punt; O-punt; Vlugsimulasie; Teruggeveegde meeuvlerkkonfigurasie; Mönnich en Dalldorff kriterium; C-ster kriterium; Vingerafdruk kriterium; Shomber-Gertsen analise; Neal-Smith analise; Vlieënierinsetossilasies; Knikossilasies; Tuimelvlug; Exulans; Veranderbare stabiliteitsgrens; Veranderbare vlerkveeghoek; Oswald rendement.

Credits

The author of this document would like to thank the following persons who have played a part in the successful completion of this study:

- S. Ackerman
- M. Agenbag
- Mev. Annamarie Bezuidenhout
- A.V. Bergh
- C.P. Crosby
- E. Güther
- M. Heyns
- R.J. Huyssen
- W.E. Misselhorn
- C. Sandrock
- R. Sogno
- J. Sutherland
- N.J. Theron
- C.G. van Deventer

Artificial flight may be defined as that form of aviation in which a man flies at will **in any direction**, by means of an apparatus attached to his body, the use of which requires **dexterity** of the user.

Otto Lilienthal, 1895

Kunstflug bedeutet willkürliches Fliegen eines Menschen mittels eines an seinem Körper befestigten Flugapparates, dessen Gebrauch persönliche geschicklichkeit voraussetzt.

Typeset using LaTeX 2_ε

Contents

List of Figures

List of Tables

Nomenclature

Mathematical Symbols

A	Linearised state space matrix (see Equation B.6)
A	Wing area (Only Figure E.1) [m^2]
a_0	Section lift curve slope for a section normal to the quarter-chord line when placed in the direction of the free stream [/rad]
b	Wing span of aircraft [m]
$\overline{c}$	Mean aerodynamic chord [m]
c	Damping term matrix of a multi-degree-of-freedom system
C^*	C-star response []
C_D	Aircraft drag coefficient
C_L	Aircraft lift coefficient
C_M	Aircraft moment coefficient
C_{D_0}	Parasitic drag coefficient
C_{D_α}	Drag coefficient derivative w.r.t. angle of attack
C_{D_e}	Equilibrium drag coefficient
C_{D_i}	Coefficient of induced drag
C_{D_V}	Drag coefficient derivative w.r.t. true airspeed

$C_{D_{\delta_e}}$ Drag coefficient derivative w.r.t. angle of elevator (or elevon) deflection

C_{L_0} y-intercept of lift coefficient curve

C_{L_q} Lift coefficient due to the pitch rate of the aircraft

C_{L_V} Lift coefficient derivative w.r.t. true airspeed

C_{L_α} Lift coefficient curve slope [/rad]

$C_{L_{\delta_e}}$ Lift coefficient due to the elevator (or elevon) deflection

$C_{L_{\dot{\alpha}}}$ Lift coefficient derivative w.r.t. the rate of change of angle of attack

C_{M_0} y-intercept of moment curve

C_{M_q} Pitch moment coefficient of aircraft due to pitch rate, or pitch damping [/rad]

C_{M_V} Moment coefficient derivative w.r.t. true airspeed

C_{M_α} Moment coefficient curve slope of the aircraft [/rad]

$C_{M_{\dot{\alpha}}}$ Pitch moment coefficient of aircraft due to rate of change of angle of attack. This coefficient relates to aerodynamic damping due to the interaction between the forward lifting surface and aft lifting surface (the horizontal stabiliser for most aircraft). [/rad]

$C_{M_{\delta_e}}$ Change of moment coefficient w.r.t. elevon deflection angle [/rad]

d Time delay

e Oswald's span efficiency factor

$\overline{F}$ Excitation force vector of a multi-degree-of-freedom system

F_s Elevator (or elevon) stick force, positive for pull [N]

g Gravitational acceleration [m/s^2]

I	Identity matrix
i	The complex part of a complex number
I_{xx}	X-X moment of inertia (aircraft body axis system) [kg·m^2]
I_{yy}	Y-Y moment of inertia (aircraft body axis system) [kg·m^2]
I_{zz}	Z-Z moment of inertia (aircraft body axis system) [kg·m^2]
k	Stiffness matrix of a multi-degree-of-freedom system
K_1	Normal acceleration scaling constant of the C* analysis [].
K_2	Pitch rate scaling constant of the C* analysis [seconds].
K_3	Pitch acceleration scaling constant of the C* analysis [seconds^2].
K_θ	The 'airframe only' gain
K_p	Steady state pilot gain
K_q	Steady state gain, elevator to pitch rate transfer function
l	Distance from aircraft centre of gravity to the head of the pilot. [m]
L_α	$\frac{\rho V_T^2 S C_{L_\alpha}}{2mV_T}$, the dimensional derivative of the aerodynamic lift in the wind axis system w.r.t. angle of attack. In the case of an aircraft with negligible control surface lift this parameter is an approximation of the inverse of τ_{θ_2}. [1/second]
L_{δ_e}	$\frac{\rho V_T^2 S C_{L_{\delta_e}}}{2mV_T}$, the dimensional derivative of the aerodynamic lift in the wind axis system w.r.t. elevon deflection [1/second]
m	Aircraft mass [kg]
m	Mass (inertia) matrix of a multi-degree-of-freedom system
M_α	Dimensional derivative of the aerodynamic pitch moment in the wind axis system w.r.t. angle of attack

M_q Dimensional derivative of the aerodynamic pitch moment in the wind axis system w.r.t. pitch rate of the aircraft

M_V Dimensional derivative of the aerodynamic pitch moment in the wind axis system w.r.t. true airspeed

M_{δ_e} Dimensional derivative of the aerodynamic pitch moment in the wind axis system w.r.t. elevator (or elevon) deflection

$M_{\dot{\alpha}}$ Dimensional derivative of the aerodynamic pitch moment in the wind axis system w.r.t. the rate of change of the angle of attack

M_{F_s} $M_{\delta_e}\left(\frac{\delta_e}{F_s}\right)_{SS}$, the derivative of aerodynamic moment around the pitch axis with respect to elevator (or elevon) stick force at steady state conditions.

n Aircraft load factor $\frac{L}{mg}$, or the normal acceleration of aircraft [g's]

n_α Load factor gradient [g/rad]

$\overline{q}$ Dynamic pressure or $\frac{1}{2}\rho V_T^2$ [N/m^2]

q Pitch rate of aircraft [rad/s]

q_g Pitch rate due to gust velocity [rad/s]

q_{rel} Pitch rate of aircraft relative to surrounding air [rad/s]

S Wing area [m^2]

s Laplace operator [1/rad]

s Quarter chord sweep angle [°]

s_r Eigenvalue with index r, of a generic multi degree of freedom system

s_r^* The complex conjugate of s_r

T_{2_p} Time to double, the time for the dynamic mode to double in amplitude [seconds]

V_e True airspeed at trim condition [m/s] or [km/h]

V_T True airspeed [m/s]

$\dot{w}_g$ Partial derivative of vertical component of gust velocity with respect to time [m/s^2]

W_g Maximum value of the vertical gust [m/s]

w_g Vertical component of gust velocity as function of time [m/s]

$\ddot{\overline{x}}$ Acceleration vector of a multi-degree-of-freedom system

$\dot{\overline{x}}$ Velocity vector of a multi-degree-of-freedom system

$\dot{\mathbf{x}}$ State vector in state space representation

$\overline{X}$ Longitudinal distance rearward from the aircraft CG to the wing aerodynamic centre

$\overline{x}$ Displacement vector of a multi-degree-of-freedom system

X_α Dimensional derivative of the aerodynamic force in the X-direction of the wind axis system w.r.t. angle of attack

X_V Dimensional derivative of the aerodynamic force in the X-direction of the wind axis system w.r.t. true airspeed

X_{δ_e} Dimensional derivative of the aerodynamic force in the X-direction of the wind axis system w.r.t. elevator (or elevon) deflection

x_{cg} Distance between the leading edge of the wing on the symmetry axis of the aircraft and the CG [m]

$\dot{\overline{y}}$ Acceleration vector of a multi-degree-of-freedom system (State space substitution)

$\overline{y}$ Velocity vector of a multi-degree-of-freedom system (State space substitution)

$\dot{z}$ State space substitution variable

z Derivative of state space substitution variable

Z_α Dimensional derivative of the aerodynamic force in the Z-direction of the wind axis system w.r.t. angle of attack

Z_q Dimensional derivative of the aerodynamic force in the Z-direction of the wind axis system w.r.t. pitch rate of the aircraft

Z_V Dimensional derivative of the aerodynamic force in the Z-direction of the wind axis system w.r.t. true airspeed

Z_{δ_e} Dimensional derivative of the aerodynamic force in the Z-direction of the wind axis system w.r.t. elevator (or elevon) deflection

$Z_{\dot{\alpha}}$ Dimensional derivative of the aerodynamic force in the Z-direction of the wind axis system w.r.t. the rate of change of the angle of attack

α Angle of attack [rad or degrees]

$\dot{\alpha}$ Rate of change of angle of attack [rad/s]

γ Outboard wing sweep angle (See Figure 4.2). [rad or degrees]

δ_e Elevator (or elevon) deflection angle [rad]

ζ Damping ratio []

ζ_p Phugoid mode damping ratio []

ζ_r The damping ratio of the r^{th} mode of a generic multi degree of freedom system []

ζ_{sp} Short period mode damping ratio []

$\ddot{\theta}$ Pitch acceleration of the aircraft. [rad/s^2]

$\dot{\theta}$ Pitch rate [rad/s]

θ Pitch angle [rad or degrees]

θ_e Error between the commanded pitch attitude and the aircraft pitch attitude [rad]

Λ Angle of sweep of wing quarter-chord line [degrees]

λ Wavelength of the vertical gust disturbance [m]

ρ Density of air [kg/m^3]

τ_{θ_2} Numerator time constant (airframe lead time constant) of pitch rate to elevator deflection transfer function [seconds]

τ_{p_1} Time constant of control system lead element [seconds]

τ_{p_2} Time constant of control system lag element [seconds]

χ Aspect ratio, $\frac{b^2}{S}$ []

ω Circular frequency [rad/s]

ω_d Damped natural frequency [rad/s]

ω_r The natural frequency of the r^{th} mode of a generic multi degree of freedom system [rad/s]

ω_{n_p} Phugoid mode natural frequency [rad/s]

$\omega_{n_{sp}}$ Short period mode natural frequency [rad/s]

$\angle$ Signifies Bode phase angle of a transfer function

$\left(\frac{\theta}{\theta_e}\right)^*$ $\frac{\theta}{\theta_e}$ transfer function with uncompensated pilot. This transfer function is considered as uncompensated when only a gain was used to achieve the Neal-Smith performance standards.

$\left(\frac{\delta_e}{F_s}\right)_{SS}$ Steady state gearing between elevator (or elevon) deflection and elevator stick force [rad/N]

$\frac{\theta}{\theta_c}$ The closed-loop transfer function of the aircraft plus control system plus pilot

$\frac{\theta}{\theta_e}$ The open-loop transfer function of the aircraft plus control system plus pilot

$\frac{\theta}{F_s}$ The open-loop transfer function of the aircraft plus control system

Abbreviations

AR Aspect ratio of wing

BW Bandwidth [rad/s]

BW_{MIN} Minimum bandwidth frequency

BWB Blended Wing Body

CAP Control anticipation parameter

CFD Computational Fluid Dynamics

CG Centre of Gravity

dB Decibel units for Bode amplitude, where amplitude in $dB = 20 \log_{10}$ [amplitude]

GPS Global Positioning System

IP Initial point (for a bombing run)

$J-UCAS$ Joint Unmanned Combat Air System

PIO Pilot induced oscillation

PR Pilot rating (of aircraft handling qualities)

UAV Unmanned Air Vehicle

VLM Vortex Lattice Method

Subscripts

e Elevon, as used in δ_e

e Equivalent, as used with V_e

g	Gust
r	Index number, typically of an eigenvalue, circular natural frequency or damping ratio
rel	Relative
SS	Steady state

Chapter 1

Introduction

The tailless swept gull-wing configuration is based on the wing shapes that exist in nature. The inboard and outboard wing sections of the gull-wing configuration have a transition in the sweep and dihedral angles.

The handling qualities of a new example of the gull-wing configuration were investigated. This gull-wing aircraft is called the Exulans. The Exulans is a research testbed that will be used to investigate the performance advantages of tailless flight by means of full-scale flight testing. Variable wing sweep, twisting elevons and all-flying winglets will be used to control the Exulans. These control devices are configured to have the minimum impact on the performance of the aircraft. The handling qualities of the swept gull-wing configuration have to be acceptable while using these different control strategies.

A performance gain can be achieved if the gull-wing configuration aircraft is designed with the CG on the so-called E-point. The Exulans is required to have inherently acceptable handling qualities with its CG positioned on this point, since no form of artificial stability augmentation will be used in its design.

The handling quality investigation was performed with analysis techniques obtained from literature. Time domain simulation techniques and frequency domain techniques were used to analyse handling qualities of the configuration. The geometry and parameters of the Exulans aircraft were

used as inputs to the analyses.

1.1 The Swept Gull-Wing Configuration

The swept gull-wing configuration is defined here as a tailless configuration having a wing with a transition in the sweep and dihedral angles.

A number of design examples exist with a gull-wing configuration. The Minimoa (see Figure 1.1) is an example of a 'tailed gull-wing configuration'. The Wenk Weltensegler (see Figure 2.1) and the Nietoperz (see Figure 2.7) are examples of swept gull-wing configurations. The swept gull-wing configuration should not be confused with the plain or unswept gull-wing configuration. The plain gull-wing configuration has a wing with dihedral crank, but no significant spanwise sweep changes. Examples of this configuration are the DFS Habicht and the DFS Reiher aircraft.

The Exulans (see Section 1.2) is modern example of a tailless swept gull-wing configuration. This particular example of the configuration has forward sweep on the inboard wing, with the outboard wing section swept backwards. The inboard wing section has dihedral, while the outboard wing section has anhedral. The inboard wing section stretches from the wing root to the semi-span of the aircraft. The swept gull-wing configuration in itself is not novel, but this combination of dihedral, sweep and planform as applied to the Exulans design is unique. The handling qualities of this example of the swept gull-wing configuration will be investigated.

Figure 1.1: The Göppingen Gö 3 or 'Minimoa' (Anonymous, 2006).

1.2 The Exulans Project

The Exulans II aircraft is shown in Figure 1.2. A noteworthy feature of the Exulans is the variable sweep outboard wing (see Figure 1.3) that is used for longitudinal trim control. The pilot can control the sweep angle by means of the flight controls. The range of sweep is 20° to 36°. Variable sweep trim control has the advantage (amongst several other) that the useful range of the elevons is not reduced by trimming.

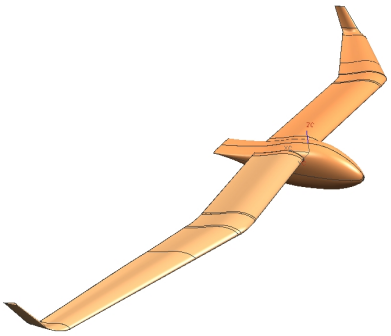

Figure 1.2: A computer generated image of the Exulans II.

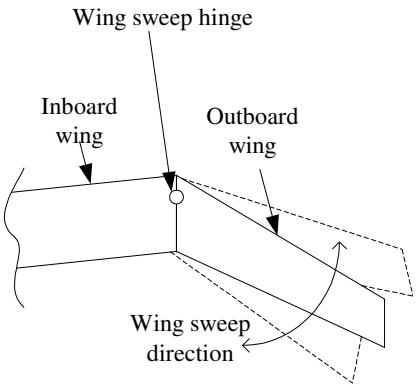

Figure 1.3: The variable outboard wing sweep as implemented on the Exulans.

The Exulans project started in 1989 as a final year project when a scale flying model was designed and built. The model was used to investigate the possible stability and control issues of the swept gull-wing configuration.

The full scale Exulans I was built following the scale prototype. The aircraft was subjected to ground tow tests and limited flight testing (see Figure 1.4). The Exulans I was designed to be a foot-launchable glider and did not have winglets. The Exulans II is designed as an ultra-light glider. It will employ all-flying winglets for directional control and yaw damping. The Exulans IIM is a possible future development that will be a motorglider.

Figure 1.4: Exulans I hanging from balloon prior to launch

The Exulans has been the research topic of a number of academic projects. The feasibility of the gull-wing configuration was investigated in the work of Huyssen (1994). Extensive research was also done on performance aspects of the Exulans glider by Crosby (1997). The architecture of a design flight simulator for the Exulans was investigated by Cronje (1999). This research was followed by another project (Agenbag, 2000) in which the flight model characterisation for the Exulans was done and applied to the simulator architecture.

1.3 The Goal

The goal of the study is the investigation of the handling qualities of a swept gull-wing configuration aircraft, specifically with the CG of the aircraft placed on or in close proximity of the E-point or the O-point. There is an aerodynamic performance gain associated with having the gull-wing configuration CG coincident with these positions.

The E-point is the centre of pressure for an elliptical circulation distribution. The O-point is similar to the E-point, but is the centre of pressure for an aircraft with winglets. Placing the CG of the aircraft on these points eliminates the need for additional trimming moments, thereby resulting in an undisturbed elliptical circulation distribution that is associated with a high Oswald efficiency.

The study was used to analyse pitch handling qualities of the Exulans at different static margins in advance of full scale flight testing. The results were used to investigate whether or not a region of static margin exists that is associated with both good handling qualities as well as high Oswald efficiency.

1.4 Methodology and Limitations

The pitch handling qualities of the tailless swept gull-wing configuration were analysed by means of the following methods and criteria:

- The C-star flying qualities criterion.

- Comparison of the gull-wing configuration pitch dynamics with other aircraft. Time domain simulations are used to make the comparison.
- Thumbprint criterion.
- Military flying qualities specifications.
- Shomber-Gertsen criterion.
- The Neal-Smith criterion.
- The Mönnich & Dalldorff criterion.
- Tumbling analysis.

The following assumptions were made in performing the handling qualities investigation:

- The investigation was restricted to the pitch handling qualities of the swept gull-wing configuration. The study of lateral handling qualities (eg. roll and yaw) is suggested as a subject for future research. This was done since many handling quality issues surrounding tailless aircraft are related to the pitch handling qualities. Pitch handling qualities are often studied in isolation because the aircraft longitudinal equations of motion can be decoupled from the lateral equations of motion. The equations can be decoupled when it is assumed that the roll rate, yaw rate and sideslip angle are zero. This approach allows the scientific study of pitch handling qualities by elimination of other variables.
- It is assumed that the aircraft has inherently favourable tip stall characteristics. Tip stall is a non-linear phenomenon that falls outside the scope of this study. Tip stall can be the cause of undesirable handling qualities, but an aircraft without tip stall problems can still exhibit poor handling qualities. As such, it needs to be studied in isolation.
- The flight simulations used as part of the analyses presented here, model only linear aerodynamics, except for non-linear drag modelling.

In the case of the gull-wing configuration only gliding flight was considered.

- All handling quality analyses presented here assume that the aircraft structure is completely rigid. The structural dynamics of the aircraft can have a large influence on the overall aircraft dynamics. This study will focus on investigating overall gull-wing configuration handling qualities, thus eliminating the variable of aeroelasticity. The structure of each aircraft is different in size and concept and therefore a separate study is required for each example of the gull-wing configuration in order to show that the aeroelastic modes of the structure do not influence handling qualities negatively. The effects of aeroelasticity on handling qualities therefore falls outside the scope of this study.

Chapter 2

A History of Tailless Aircraft

A large variety of tailless aircraft have been built in the past. The low aerodynamic pitch damping and pitch inertia give tailless aircraft unique handling qualities. This chapter is intended to provide some background on tailless aircraft designs and their handling characteristics.

A 'tailless' aircraft has no horizontal stabiliser, but can have vertical stabilisers (sometimes called 'fins', e.g. the SB-13 Arcus). An aircraft is a 'flying wing' (e.g. the Horten II) when it has no horizontal or vertical stabilisers (Nickel & Wohlfahrt, 1994:4).

One of the earliest tailless designs is the 'Weltensegler', a design by Fritz Wenk, dating back to 1921. This Weltensegler is shown in Figure 2.1. This aircraft is an early example of the swept gull-wing configuration (Huyssen, 1994).

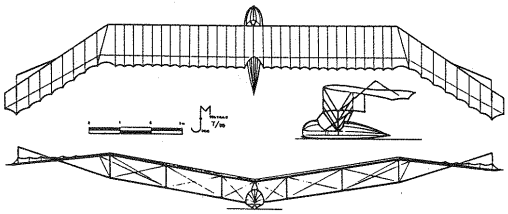

Figure 2.1: The tailless sailplane 'Weltensegler' (Nickel & Wohlfahrt, 1994:12).

Tailless aircraft aircraft technology developed rapidly during the 1930's with the designs of the Horten brothers from Germany. The two brothers

produced several aircraft until the end of the Second World War. Dr. Reimar Horten continued to design and build tailless aircraft in Argentina after the War. The Horten aircraft designs have a wide variety of planform shapes. A few of the Horten aircraft are shown in Figure 2.2.

Figure 2.2: Photo of the sailplanes Horten H II, H III, H IV. (Nickel & Wohlfahrt, 1994)

Each Horten aircraft had unique flying qualities. The first Horten aircraft (H I) shown in Figure 2.3 had a triangular (strongly tapered) planform. The elevators and ailerons were not combined into an elevon in this design. The elevators were inboard, with the ailerons outboard. The H I had undesirable handling qualities. This can be attributed to the aircraft's high taper ratio, the sweepback angle of the wing and the centered elevators (Nickel & Wohlfahrt, 1994:460). The elevators in the centre of the wing caused it to have negative wash-out when deflected upwards. This can lead to wing tip stall. Alexander Lippisch, a contemporary of the Horten brothers, designed an aircraft with a very similar planform to the Horten I, the Delta I. This aircraft had the same poor handling qualities as the Horten I.

Later Horten aircraft designs improved on the flying qualities of the Horten I. These designs had larger span and aspect ratio. These aircraft combined the functions of the elevator and ailerons and the control surfaces were placed outboard spanwise. The Horten aircraft had high taper ratios. Today the high taper ratio is viewed as an undesirable design characteristic, since this can lead to tip stalling and reduced performance.

The Horten brothers experimented with various CG positions on the Hor-

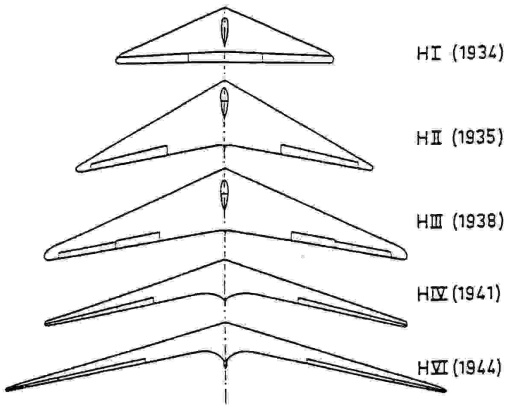

Figure 2.3: Different Horten wing planforms (Nickel & Wohlfahrt, 1994).

ten III aircraft (ibid.: 198). They found that rearward *CG* positions were associated with poor handling qualities.

The Horten IV aircraft had desirable handling qualities (ibid.: 465). The second version of this aircraft was constructed with a rearward centre of gravity and the laminar wing profile of the Mustang fighter aircraft. The design changes on the second version were made to improve performance, but instead it caused the aircraft to have unfavourable spin characteristics. These characteristics caused a flutter problem.

The Horten IX design was used as the basis of the design of the Gotha Go-229 (Horten IX) aircraft, which was designed to operate at a speed of 1000 km/h with a range of 1000 km.

The Me-163 Komet (Figure 2.4) designed by Alexander Lippisch was also a tailless design. This aircraft had acceptable handling qualities. The design had low aspect ratio and high sweepback. This gave the configuration high values of aerodynamic damping. The Me-163 flew at much higher speeds than the Horten sailplanes. This made the aerodynamic damping force of the aircraft higher.

Jack Northrop developed tailless aircraft before and after World War 2. The XB-35 and the YB-49 (Figure 2.5) bombers are examples.

Northrop engineers found through extensive testing experience that tailless designs had advantages. They have high lift and low drag characteristics,

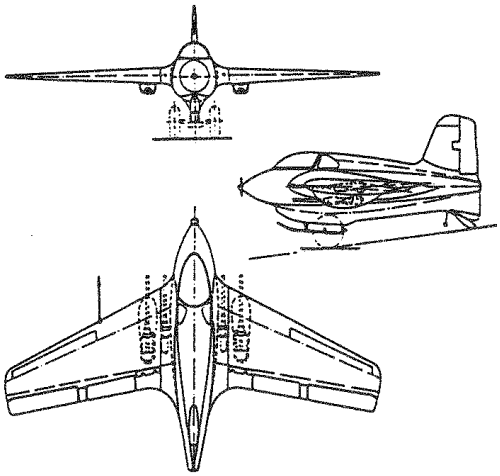

Figure 2.4: The Messerschmitt Me-163 Komet (Nickel & Wohlfahrt, 1994).

meaning that they can transport more cargo faster and farther than conventional aircraft. Structurally, the tailless aircraft is simpler to manufacture. For military usage, the smaller cross-section of the design also presented a smaller target for anti-aircraft fire. Years later the significance of smaller cross-sections became even greater as this meant smaller radar signature. This is an important part of design for stealth. The Northrop YB-49 flight test programme showed that the aircraft was not a stable enough weapons platform due to its inherent dynamics. The Northrop YB-49 displayed pitch and yaw problems that made it very slow in settling to the initial point (IP) for a bombing run. (Anonymous, n.d. a). Plans were made to fit it with an autopilot with which some of the problems could be fixed. Funding for the project was stopped before this could be done. Many factors prevented the Northrop designs from being mass produced, but these designs provided the basis for a later bomber design, namely the B-2 Spirit Stealth Bomber.

Since the designs of the Horten brothers and the Northrop company, the tailless aircraft concept has been championed by many private aircraft builders. A concise review of these designs will now be made.

Hang gliders are tailless aircraft and have been developed since the 1950's. They are not prone to the fast α oscillation known as 'pecking'. Pecking is a

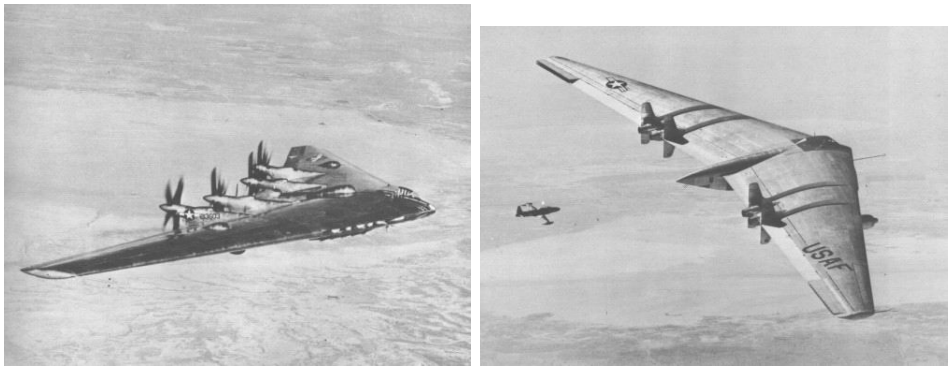

(a) XB-35 (b) YB-49

Figure 2.5: Two Northrop tailless aircraft designs. (Anonymous, n.d. g)

rapid oscillatory motion around the pitch axis of the aircraft. Hang gliders are sometimes susceptible to tumbling. (Nickel & Wohlfahrt, 1994:388) Tumbling is an autorotative pitching motion primarily about an axis parallel to a vehicle's lateral axis, plus translation in a vertical plane along an inclined flight path. (Fremaux & Vairo, 1995)

The Frenchman Charles Fauvel designed and developed a range of tailless aircraft during the 50's and 60's of the twentieth century. The AV-36 is shown in Figure 2.6. This type of tailless aircraft is known as a 'flying plank'. A flying plank is a tailless aircraft with very little or no wing sweep. When such an aircraft has a rudder, it has a small lever arm between the rudder and the aircraft centre of gravity. This type of plane has been known to display α oscillations in gusty weather conditions. The frequency of the oscillations is around 0.5 Hz. Many examples of the aircraft have been built and in general it displays acceptable handling characteristics, except during take-off and landings. During landing, the aircraft's susceptibility to 'pancaking' is especially visible. Pancaking is a flight characteristic of an aircraft that occurs when the elevator is deflected upwards, resulting in a loss of lift and altitude. This is especially visible during landing in ground effect. Tailless aircraft are more susceptible to this phenomenon than aircraft with horizontal

stabilisers. This is because the elevators (elevons) of tailless aircraft are on the main lifting surface and therefore the amount of lift lost due to control deflections is significant. The phenomenon appears to have the effect of an elevator reversal and is therefore sometimes incorrectly called 'control inversion'.

Figure 2.6: The Fauvel AV-36. (Anonymous, n.d. b)

A Polish design, the SZD-6x Nietoperz of the 1950's showed a forward-backward wing sweep design. The Nietoperz is a swept gull-wing configuration aircraft. Another design of the period is the SZD-20x Wampir. These designs are shown in Figure 2.7. The SZD-6x Nietoperz had poor handling qualities in gusty conditions. It displayed unpleasant pitching while flying in the turbulent wake during aerotowing operations. (Zientek, 1992) The SZD-20x Wampir also had poor gust handling qualities (worse than that of the Nietoperz). The Wampir eventually broke up in mid-air during flight testing due to aeroelastic problems.[1]

[1]The pilot survived the crash with only minor injuries since he was able to use his parachute (Zientek, 1992).

(a) Nietoperz (Anonymous, n.d. f)

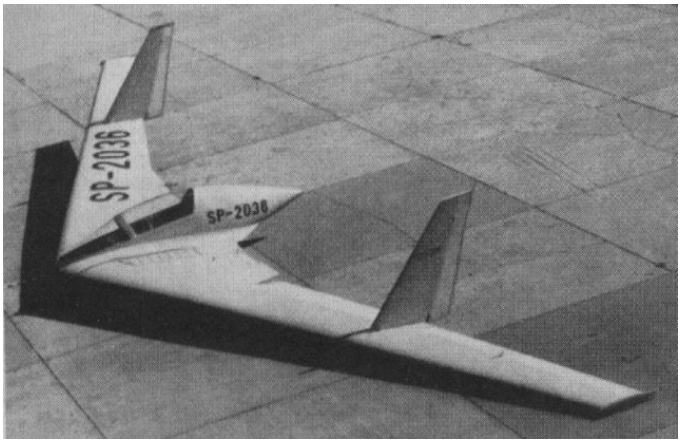

(b) Wampir (Anonymous, n.d. e)

Figure 2.7: Polish tailless aircraft designs of the 50's.

The G.A.L./56 (see Figure 2.8) is a post-war tailless aircraft. It exhibited poor handling characteristics. Problems were experienced on this aircraft due to landing gear geometry and an aft centre of gravity. It had a tail heavy pitching moment near ground due to an increase in lift as a result of ground effect (Nickel & Wohlfahrt, 1994:225).

Figure 2.8: The G.A.L./56 tailless aircraft. (Nickel & Wohlfahrt, 1994:217-222)

The American Jim Marske is a leading designer of tailless aircraft in the United States. One of his designs is shown in Figure 2.9

Figure 2.9: A Jim Marske design. (Anonymous, n.d. d)

The 1980's produced the more modern low taper ratio tailless sailplanes. A number of examples of this type of aircraft exist. Most notable of these designs are the Akaflieg Braunschweig SB-13 and the Flair 30 of Günther

Rochelt. These aircraft offer improved efficiency and better handling characteristics than earlier designs. The SWIFT (Kroo et al., 1991) from the University of Stanford and the Pyxis glider (Anonymous, n.d. h) also fall in this class of tailless aircraft, see Figure 2.10.

The SB-13 had poor gust handling qualities. It is prone to 'pecking'. (Nickel & Wohlfahrt, 1994:104) The aircraft also displayed a coupling of the angle of attack oscillations with the wing bending mode. These oscillations are difficult to control since they have frequencies larger than 1 Hz, which is out of the controllable range of a human pilot.

Many modern glider designs originate from universities. The SWIFT (Figure 2.11) began as the theme of a course in aircraft design at Stanford University. This aircraft is foot-launched and combines the versatility of hang gliders with the performance of sailplanes. BrightStar gliders of California (USA) have produced a commercial version of the SWIFT aircraft called the Millennium. It folds more compactly and costs less to produce. (Kroo, 2000)

(a) Akaflieg Braunschweig's SB-13 (Nickel & Wohlfahrt, 1994)

(b) A model of the Flair 30. (Anonymous, n.d. i)

(c) The Pyxis. (Anonymous, n.d. h)

Figure 2.10: Modern low taper ratio sailplanes.

Figure 2.11: The SWIFT foot launched glider. (Kroo et al., 1991)

Tailless aircraft have seen a resurgence in the last two decades. This type of design offers many advantages such as stealth, performance improvements and structural efficiency. The advent of unmanned air vehicles (UAV's), improved control systems and the importance of stealth has again made the concept popular with designers. Aircraft such as the X-36 are a testimony to this. The X-36 has a set of redundant control effectors for increased survivability. The aircraft is made controllable by digital control systems. These control system rely heavily on an extensive aerodynamic database and modern control theory. (Calise et al., 2000)

The B-2 bomber is another example of a modern tailless aircraft. The inherent dynamics of the aircraft is masked by using digital control systems. This solves the inherent problems experienced by the earlier YB-49 design.

New passenger aircraft tailless concepts are currently being investigated with the Blended Wing Body (BWB) concept. These airliners will be more efficient[2] in carrying passengers and offer engine noise reduction advantages (Anonymous, 2005) due to the position of the propulsion system. (Figure 2.12)

[2]The reduction of drag due to the absence of an empennage structure will lead to fuel savings. Mass is saved by integrating the passenger cabin with the wing.

Figure 2.12: The Blended Wing Body Concept from Cambridge University (Anonymous, 2005:12).

The X-43 (see Figure 2.13) is an example of a hypersonic tailless aircraft. This aircraft is to use scramjet technology in order to travel at speeds in excess of Mach 10. (Wilson, 2003)

The X-45 (see Figure 2.13) is an example of a tailless aircraft that will be used in a Joint Unmanned Combat Air System ($J-UCAS$). (Wilson, 2003) It is a UAV that is able to perform combat missions in unison with other similar UAV's. These UAV's are autonomous to a large degree.

The Boeing ScanEagle (see Figure 2.14)is an example of a tactical UAV used for reconnaissance. The current model of this aircraft has a wing span of 3 metres (10 feet). It is land or shipped launched with a pneumatic wedge catapult launcher and is recovered with a 'Skyhook' system. This system is used to land the aircraft by catching a rope hanging from a pole. (Holly, 2005) This aircraft is used to fly pre-programmed or operator initiated missions by using GPS and its onboard flight control system. This UAV was developed to be a low cost, long endurance autonomous air vehicle. As a tailless aircraft, the aircraft offers the inherent increase in aerodynamic efficiency due to reduced drag, making it suitable for long endurance missions.

(a) X-43

(b) X-45

Figure 2.13: Tailless experimental aircraft. (Wilson, 2003:23-24)

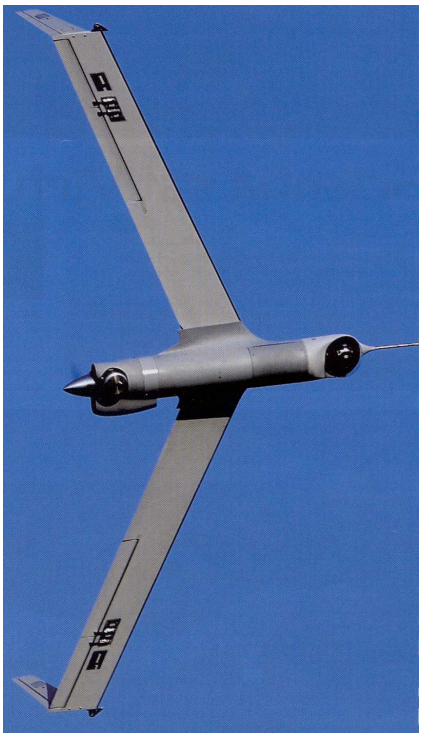

Figure 2.14: The Boeing ScanEagle *UAV* (Holly, 2005:37).

Chapter 3

Handling Quality Criteria

In order to evaluate aircraft handling qualities, it is necessary to define what constitutes good handling qualities. This chapter will present various handling quality analysis methods.

3.1 Cooper Harper Flying Qualities Rating Scale

The Cooper Harper evaluation criterion (Cooper & Harper, 1969) is a subjective method of evaluating aircraft handling qualities. This is different from all the other evaluation methods presented in this study, since the other methods are mathematical/empirical in nature. This method gives the pilot a way of having an influence on the design of the aircraft. This is important since the pilot is the end user of the aircraft.

With this method, the pilot rates the aircraft controllability on a scale from 1 to 10, with 1 being the most favourable rating. The Cooper Harper evaluation criterion is presented in Table A.1.

The Cooper Harper scale can only be used if an aircraft is available for flight testing or if an accurate flight simulator of the aircraft exists. The flight simulator should be able to simulate pitching motion as well as normal (up and down) acceleration. In addition to the hardware a group of pilots is also required in order to be able to conduct a handling qualities study.

The pilot opinion of the aircraft is then obtained by letting the various pilots either test fly the aircraft or letting the pilots interact with the the simulator. A questionnaire is then used to determine the Cooper Harper rating of the aircraft.

The Cooper Harper criterion will not be used in the gull-wing handling qualities study since neither a pitch flight simulator nor an aircraft were available for testing at the time of completion of this study.

3.2 The Zacher Protocol

The Zacher Flight Test Protocol (Thomas, 1993) was developed by Hans Zacher specifically for sailplanes and uses flight tests and a questionnaire to evaluate the flying qualities of an aircraft. This protocol was not applied to the gull-wing configuration since a prototype was not available for flight testing.

3.3 Thumbprint Criterion Analysis

The handling quality criterion presented here is based on the research presented in O'Hara (1967). An application of the thumbprint criterion can be found in Chun & Chang (2001:17). The method is based on the natural frequency and damping ratio of the aircraft dynamic modes.

The criterion is summarised in the graph presented in Figure 3.1. This graph is also known as the 'thumbprint'. An aircraft has satisfactory handling qualities when its short period damping ratio and natural frequency can be plotted in the centre of the contours of the 'thumbprint' graph.

The pilot opinion contours shown in the 'thumbprint' (Figure 3.1) were constructed from flight tests. Pilots were used to evaluate the handling qualities of so-called 'variable stability' aircraft such as the USAF/CAL T-33 aircraft. The damping ratio and natural frequencies of a variable stability aircraft can be varied by adjusting the CG of the aircraft. Pilot opinions of several CG configurations were compiled in the form of Figure 3.1. The pilot

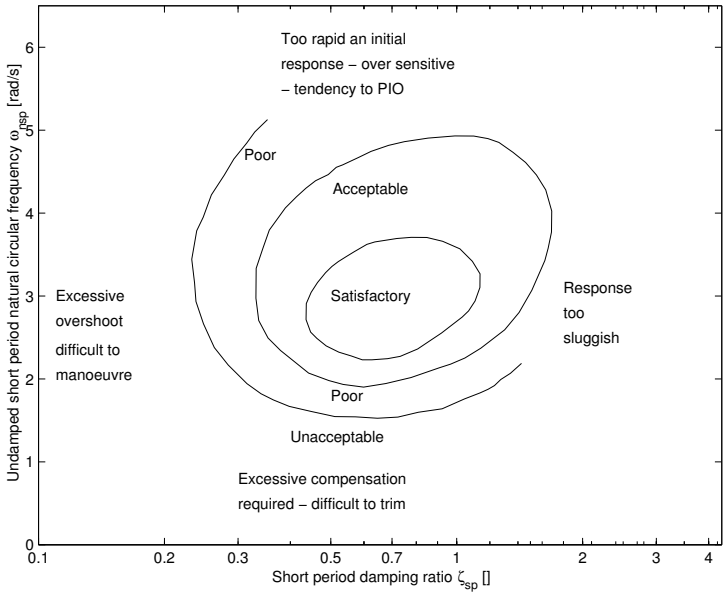

Figure 3.1: Typical pilot opinion contours for the short period mode (O'Hara, 1967).

opinions of the different configurations were expressed in pilot ratings (PR). The pilot ratings correspond to the Cooper-Harper scale. The thumbprint criterion requires two assumptions:

- The predominant variable sensed by the pilot is normal acceleration, as opposed to pitching acceleration.
- The short period response may be represented by that of a linear second order system.

The thumbprint criterion is important for aircraft that do not have stability augmentation systems. A linear second order system might not be able to approximate the dynamics of an aircraft that is stability augmented.

In order to use the thumbprint criterion, it is necessary to know the natural frequency and the damping ratio of the short period mode of an aircraft. These values may be determined by means of the following methods:

- Flight testing can be used to excite the short period aircraft mode independently of the phugoid mode. The damping ratio and natural

frequency can then be established by means of curve fitting techniques from flight test data.

- A mathematical model can be created that describes the dynamics of the aircraft. This is done using equations of motion and the aerodynamic coefficients of the aircraft. These equations are usually a non-linear set of differential equations. The equations have to be linearised at a certain trim point in order to perform an eigenvalue analysis. An eigenvalue analysis is then performed on the linearised equations of the aircraft model. The eigenvalue analysis yields the short period damping ratio and natural frequency.

The thumbprint criterion analysis of the gull-wing configuration was performed by means of numerical eigenvalue analysis. The method of eigenvalue analysis as applied to the gull-wing configuration is described in Appendix B. This method was chosen as an aircraft was not available for flight testing at the time of analysis. A mathematical model of the gull-wing configuration was created (see Section 4.7). The equations of the model were linearised for a range of outboard wing sweep angles and CG positions of the gull-wing configuration. Eigenvalue analysis was performed on the linearised equations. The results of the eigenvalue analysis were plotted on thumbprint graphs like the one presented in Figure 3.1.

The thumbprint criterion is important since it is useful in determining whether an aircraft will be prone to 'pecking'. Pecking occurs during gusty conditions or α disturbances in the case of flying wing aircraft. High and low frequency occurrences of pecking have been found (Nickel & Wohlfahrt, 1994). The SB-13 Arcus experienced pecking problems. At high static margins the aircraft displayed α oscillations of 1 to 2 Hz which pilots found difficult or impossible to control. The pecking problem improved with lower static margins because the frequency of the oscillations dropped to 0.5 to 1 Hz. The pilots of the SB-13 found it difficult to control the α oscillations because it had the same frequency as that of the human reaction (1 to 3 Hz). If the natural frequency of the α oscillations (i.e. the short period mode) were to be in the range of 0.398 to 0.637 Hz (2.5 to 4 rad/s, that falls outside

the human response frequency), the pecking problem of the aircraft should be theoretically solved.

3.4 Military Flying Qualities Specifications

The military handling quality criteria are presented in MIL-F-8785C (1980). Short period mode requirements as well as phugoid mode requirements are presented in this specification.

The natural frequencies and damping ratios of the aircraft dynamic modes are used as input to this method. The values of these parameters are calculated by numerical eigenvalue analysis. The Control Anticipation Parameter or CAP is then calculated with the short period natural frequency. The value of the CAP is then plotted against short period damping ratio on the military flying qualities specifications graph. The military flying qualities specifications are graphically represented in Figure 3.2. An aircraft has the most favourable handling qualities when the aircraft's dynamic mode properties can be placed in the centre of the 'Level 1' bounding box of this figure. The phugoid damping ratio of the aircraft is compared to the requirement presented in Table 3.1.

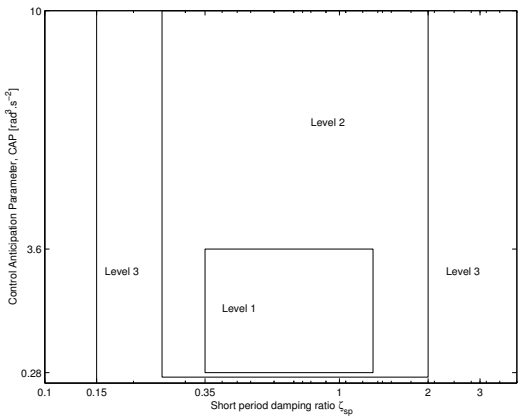

Figure 3.2: Category A control anticipation parameter and ζ_{sp} requirements (Chun & Chang, 2001).

The control anticipation parameter used in Figure 3.2 is defined in Equa-

tion 3.2. It is a function of short period natural frequency and aircraft load factor gradient (n_α). This parameter is related to the time constant of the aircraft pitch response. It is a measure of how predictable an aircraft's handling characteristics are to a human pilot. The optimum value of the CAP lies in the centre of the 'Level 1' block in Figure 3.2.

$$n_\alpha = \frac{\frac{1}{2}\rho V_T^2 S \frac{\partial C_L}{\partial \alpha}}{mg} \tag{3.1}$$

$$CAP = \frac{\omega_{n_{sp}}^2}{n_\alpha} \tag{3.2}$$

The boundaries for a Level 1 aircraft[1] and a Level 2 aircraft[2] are shown in Figure 3.2. The boxes drawn in the graphs are for the Category A flight phases[3]. The Category C flight phases[4] have the same short period damping ratio limits according to Table IV of MIL-F-8785C (1980:13), but different CAP requirements away from the optimum damping ratio/CAP point. The lower limit on the Level 1 and 2 boxes for the CAP are 0.16 and 0.096 rad^3·s^{-2} respectively for Category C[5] flight envelopes. Simply put, if an aircraft's dynamics are such that a plot of its CAP versus its short period damping ratio is a point in the centre of the 'Level 1' box of the Category A criterion, then it has optimal handling characteristics regarding Category A *as well as* Category C manoeuvres. The classifications regarding 'Level' and 'Category' are according to MIL-F-8785C (1980).

The Level 1 requirements for longitudinal manoeuvring characteristics according to MIL-F-8785C (1980:13-14) are summarised in Table 3.1. These requirements are reflected in Figure 3.2. Table 3.1 also lists a specification for the phugoid mode of the aircraft.

[1]Flying qualities adequate for the mission flight phase.

[2]Flying qualities adequate for the mission flight phase, but some increase in pilot workload or degradation in mission effectiveness exists.

[3]Nonterminal flight phases generally requiring rapid manoeuvring e.g. air-to-air combat or aerobatic flying

[4]Terminal flight phases normally accomplished using gradual manoeuvres and usually requiring accurate flight-path control e.g. take-off and landing

[5]These values are 0.28 and 0.16 rad^3·s^{-2} for the Level 1 and 2 boxes respectively for Category A as shown in Figure 3.2.

Table 3.1: Level 1 requirements for MIL-F-8785C

Phugoid damping requirements	$\zeta_p \geq 0.04$
Short period damping ratio limits	$0.35 \leq \zeta_{sp} \leq 1.30$
Short period undamped natural frequency	$0.28 \leq \frac{\omega_{nsp}^2}{n_\alpha} \leq 3.6$ rad^3·s^{-2}

3.5 The C-star Flying Qualities Criterion

The C-star criterion (Tobie et al., 1966) is a time-history envelope criterion. The criterion was developed by using flight test data. This criterion uses pitch rate, pitch acceleration and normal acceleration response to define desirable aircraft handling characteristics. These three responses are combined into one response by an equation. The resulting combined response is divided by the pilot stick response and then normalised by the steady state value of the response. The normalised response is then plotted on the C-star time history envelope (Figure 3.3). If the combined response falls inside the envelope, handling qualities are acceptable.

There are two C-star time history envelopes that are shown in Figure 3.3. The solid lines of the envelope represents the 'up and away' or normal manoeuvring flight envelope of favourable handling. This envelope was determined from flight tests with the F-94 variable stability aircraft. The thick dashed line represents the boundaries of favourable handling for a powered landing approach as established with flight tests from a Boeing 367-80 aircraft. If a response falls within these lines, the aircraft has a pilot opinion rating of 3.5 on the Cooper Harper scale, whether it be in the 'up and away' or the landing scenario.

The C-star criterion uses a time history envelope to evaluate handling characteristics. Aircraft step responses are used as input to the method. The C-star criterion is not 'necessary and sufficient' to evaluate handling characteristics. It is necessary to judge the aircraft response within the acceptable envelope by merit. As an example of this, the response of an aircraft may

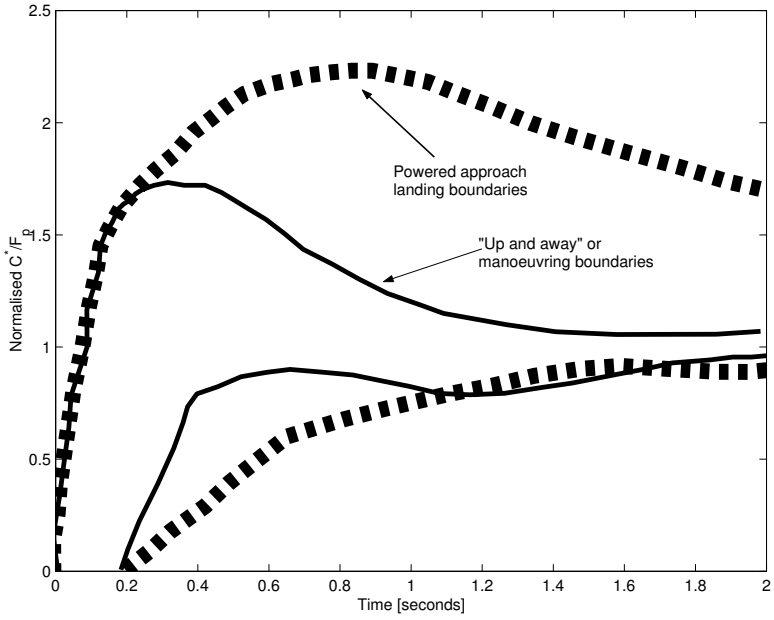

Figure 3.3: The C-star time history envelopes from Tobie et al. (1966).

fall in the acceptable boundaries of the C-star criterion, while still having a non-desirable lightly damped high frequency mode superimposed on the dominant response.

The step elevator input response required for the C-star analysis may be determined in the following two ways:

- Flight testing can be used to measure the step response of an aircraft.
- Flight simulation may be used to obtain the step response. This approach was used to analyse the gull-wing configuration aircraft.

The C-star method is useful when evaluating a stability augmented aircraft because the lumped dynamics of the airframe and the control system are evaluated. The C-star criterion is a time domain method. It shows the influence of numerator dynamics (zeros dynamics) and non-linear effects on handling qualities. Tobie et al. (1966:95) states that aircraft pitch motion cues are very important with respect to handling qualities. The 'thumbprint' criterion does not take into account these motion cues.

The C-star response is calculated by combining the normal acceleration with the pitch acceleration that is sensed by the pilot. The pilot's position is not at the centre of gravity of the aircraft (for the majority of designs) and therefore he or she will experience increased acceleration levels compared to those of the centre of gravity. The additional acceleration due to pitching has to be calculated at the position of the pilot's head, since this is where the sensory organs are located. The following formula is used to combine normal acceleration and pitch acceleration and pitch rate:

$$C^* = K_1 n + K_2 \dot{\theta} + K_3 \ddot{\theta} \tag{3.3}$$

where the value of K_1 is 1 (dimensionless) and K_2 equals 12.4 (units of [seconds]) as derived in Tobie et al. (1966:96). The 'n' parameter is the normal acceleration of the aircraft in g's. $\dot{\theta}$ and $\ddot{\theta}$ are the pitch rate (in rad/s) and pitch acceleration (rad/s^2) respectively of the aircraft. l is positive when the pilot is situated in front of the CG and negative when the pilot is situated behind the CG. The K_3 constant is calculated with the following equation:

$$K_3 = \frac{l}{g} \tag{3.4}$$

The l parameter is the distance from the pilot's station to the centre of gravity of the aircraft and g is gravitational acceleration. K_3 has the units of [seconds^2]. The pilot of the Exulans does not sit upright as with most aircraft, but lies in the prone position as with a hang glider. The Exulans is used here as an example of a gull-wing configuration , but this does not imply that all gull-wing configurations will have the pilot in the prone position. For the Exulans, l is calculated as the sum of the distance from the aircraft centre of gravity to the hips of the pilot and the distance from the hips to the eyes. The last mentioned distance (884 mm) was obtained from Anonymous (1997) for a 97'th percentile UK aircrew male.

The C-star response calculated with Equation 3.3 is divided by the pilot stick input force or F_s. This is done in order to plot the response on Figure 3.3. Neal & Smith (1970) presents a pilot handling qualities study where the C-star method is also illustrated. The examples from this reference calculate

stick force with a linear stick force gradient. Neal & Smith (1970:18) indicates that favourable handling qualities correspond to a stick force gradient of 20 to 31 N/g. A value of 25.5 N/g was chosen for use in the gull-wing configuration C-star analysis. The arbitrary value was used since the actual gearing of the aircraft was not known at the completion of this study.

The step responses presented in Section I.1 were used in the evaluation of the Exulans.

3.6 The Shomber-Gertsen criterion

This evaluation criterion was proposed in Shomber & Gertsen (1967). This article presents pilot opinion contours that are based on the zeros of the elevator input to pitch response transfer function. The work of Shomber & Gertsen (1967) is also closely related to the fixed base simulator study performed by Chalk (1963).

The transfer function of Equation 3.5 is the basis of the zeros criterion of Shomber & Gertsen (1967). The zero of this transfer function is influential in the handling qualities of the aircraft because it influences the phase and magnitude of the aircraft pitch response. The zeros of the elevator input to pitch response transfer function varies with airspeed. As a result, the method is useful in determining how handling qualities vary at different airspeeds. The relationship of pilot opinion to different flight conditions was set up using flight test data and fixed base simulator studies.

$$\frac{q(s)}{\delta_e(s)} = \frac{K_q(1+\tau_{\theta_2}s)}{\frac{s^2}{\omega_{n_{sp}}^2} + \frac{2\zeta_{sp}}{\omega_{n_{sp}}}s + 1} \tag{3.5}$$

The Shomber-Gertsen handling qualities analysis entails the calculation of the values of the following parameters for an aircraft at a given operating condition (trim speed): n_α, $\omega_{n_{sp}}$, ζ_{sp} and $1/(\tau_{\theta_2}\omega_{n_{sp}})$. These parameter values are then plotted on Figures 3.4 or 3.5. If $n_\alpha \leq 15$ g/rad, the values are plotted on Figure 3.4, otherwise the values are plotted on Figure 3.5. The closer the plotted point is to the 'Satisfactory' region, the better the handling qualities. The zeros rating method is related to the Cooper Harper rating

scale. Figures 3.4 and 3.5 have iso pilot rating contours that are related to the Cooper-Harper scale.

The natural frequencies and damping ratios of the aircraft modes required for this method are calculated by means of numerical eigenvalue analysis.

The $1/\tau_{\theta_2}$ parameter can be approximated by L_α. This is true when the longitudinal control surface located aft of the centre of gravity exhibits negligible control surface lift (Shomber & Gertsen, 1967):

$$\frac{1}{\tau_{\theta_2}} = \frac{L_\alpha - M_\alpha(L_{\delta_e}/M_\delta)}{1 - M_{\dot{\alpha}}(L_{\delta_e}/M_\delta)} \approx L_\alpha \tag{3.6}$$

For a tailless aircraft, control surface lift is not negligible because the elevon is on the main wing of the aircraft. The elevon is also close to the centre of gravity of the aircraft. The full expression must therefore be used to calculate $1/(\tau_{\theta_2}\omega_{n_{sp}})$ when evaluating the handling characteristics of a tailless aircraft such as the gull-wing configuration. Even though Figure 3.4 shows L_α/ω_{n_sp} appearing on the y-axis, the value of $1/(\tau_{\theta_2}\omega_{n_{sp}})$ will be used to plot the y-coordinate of the values on this graph, since the gull-wing configuration is tailless.

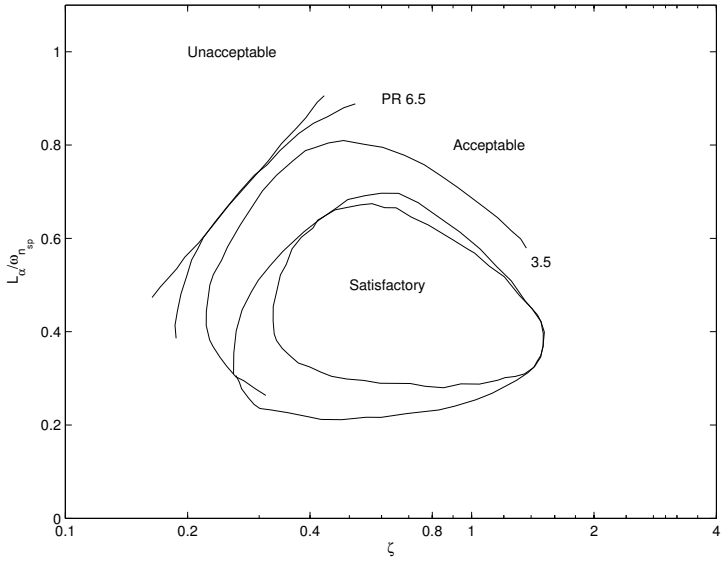

Figure 3.4: The longitudinal short-period criterion of Shomber & Gertsen (1967) for $n_\alpha \leq 15$ g/rad.

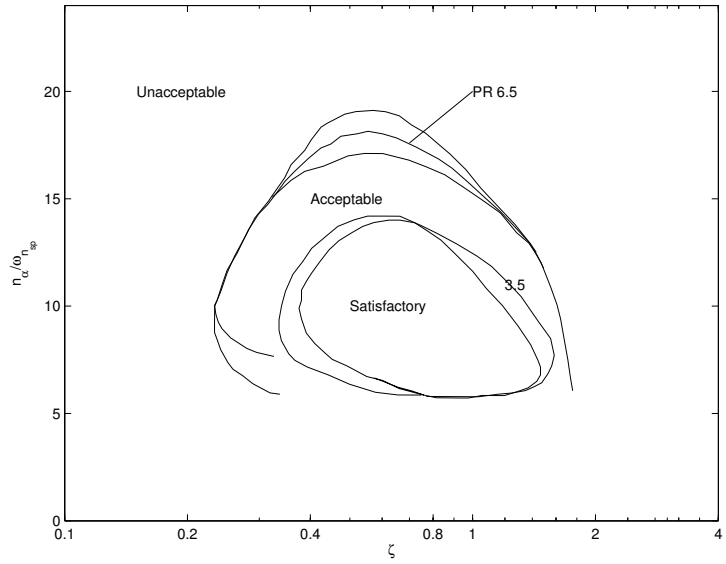

Figure 3.5: The longitudinal short-period criterion of Shomber & Gertsen (1967) for $n_\alpha \geq 15$ g/rad.

n_α (Equation 3.7) is the incremental load factor per unit angle of attack. This parameter is varied by changing the trim airspeed of the aircraft, since the other variables of this parameter (e.g. mass, wing area, lift curve slope) are constants.

$$n_\alpha = \frac{\frac{1}{2}\rho V^2 S C_{L_\alpha}}{mg} \tag{3.7}$$

3.7 The Neal-Smith Criterion

The Neal-Smith aircraft handling quality evaluation method was originally developed in order to assess the handling qualities of fighter aircraft equipped with flight control systems (Neal & Smith, 1970). The method requires a pilot transfer function model and an aircraft pitch attitude to stick force transfer function. This is used to quantitatively evaluate the amount of compensation that a pilot needs to make in order to control the aircraft. The result of the evaluation is then plotted on an opinion chart that was created using flight test data and pilot opinion. This chart is presented in Figure 3.6.

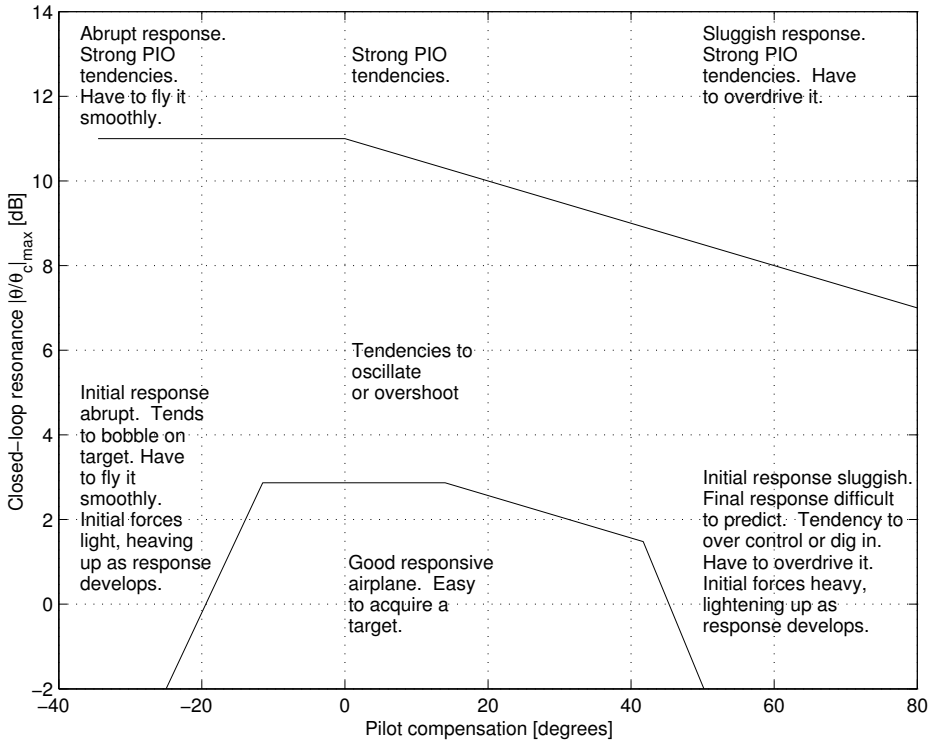

Figure 3.6: The Neal-Smith criterion for fighter manoeuvring dynamics.

The Neal-Smith evaluation criterion can also be applied to an aircraft without a flight control system. This was the case with the gull-wing configuration, since the inherent controllability (without a control system) of the aircraft was investigated. The control system dynamics were simply omitted in the aircraft transfer function in order to accommodate this type of aircraft.

The transfer function model of the pilot and the aircraft was obtained from Neal & Smith (1970:38). The pilot model ($\frac{F_s}{\theta_e}$) is presented in the following equation:

$$\frac{F_s}{\theta_e} = K_p e^{-0.3s} \frac{\tau_{p_1} s + 1}{\tau_{p_2} s + 1} \tag{3.8}$$

This type of model is known as a compensatory tracking model. It includes a time delay as well as lead and lag compensation and a gain. The time delay models the neuromuscular lag of a human pilot. Neal & Smith (1970)

indicates that the time delay may vary between 0.2 and 0.4 seconds. The value of 0.3 seconds was used in the analysis of the gull-wing configuration.

The unaugmented aircraft model (derivation is shown in Appendix L) that was used to model the pitch dynamics of the gull-wing configuration is presented in the following equation:

$$\frac{\theta}{F_s} = \frac{K_\theta(\tau_{\theta_2}s + 1)}{s(\frac{s^2}{\omega_{n_{sp}}^2} + \frac{2\zeta_{sp}}{\omega_{n_{sp}}}s + 1)} \tag{3.9}$$

where the airframe gain K_θ is:

$$K_\theta = \frac{g}{V_T(F_s/n)_{SS}} \tag{3.10}$$

$\frac{F_s}{n}_{SS}$ will eventually be determined by means of flight test when the Exulans is built and flown. A $\frac{F_s}{n}_{SS}$ value of 25.5 N/g was used in the analysis presented here. This value was chosen because flight test pilots of the Neal-Smith evaluation programme found the most favourite gradients to lie between 20 and 31 N/g. (Neal & Smith, 1970:18)

The following transfer function and 'open loop' and 'closed-loop' definitions are important to understand the Neal-Smith method. These definitions are taken from Neal & Smith (1970:39).

$\frac{\theta}{F_s}$ is the *open-loop* transfer function of the aircraft plus control system. In the case of the gull-wing configuration this would refer to the aircraft transfer function alone because the aircraft is analysed without a flight control system.

$\frac{\theta}{\theta_e}$ is the *open-loop* transfer function of the aircraft, control system and pilot.

$\frac{\theta}{\theta_c}$ is the *closed-loop* transfer function of the aircraft, control system and pilot.

The terms 'open-loop' and 'closed-loop' are meant to apply to the block diagram shown in Figure 3.7.

The following definitions are also important:

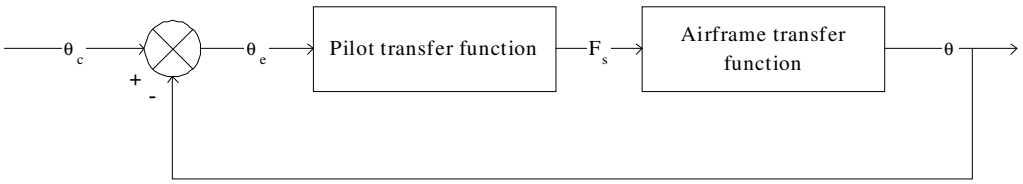

Figure 3.7: Mathematical model of pitch attitude tracking.

Bandwidth (BW): Bandwidth is defined as the frequency for which the closed-loop Bode phase, $\angle(\frac{\theta}{\theta_c})$, is equal to -90 degrees. In the context of fighter design, it is a measure of how quickly the pilot can move the aircraft's nose toward the target.

Droop Droop is defined as the maximum excursion of the closed-loop Bode amplitude, $|\frac{\theta}{\theta_c}|$, below the 0 dB line for frequencies less than BW (see Figure 3.8). Once again, in the context of fighter design and in the absence of large oscillations, droop is a measure of how slowly the nose settles down on a target.

Standard of Performance A minimum bandwidth, $(\text{BW})_{min}$, of 3.5 rad/s, and a maximum droop of 3 dB: For frequencies of ω less than 3.5, $\angle(\frac{\theta}{\theta_c})$ must be greater than -90 degrees and the $|\frac{\theta}{\theta_c}|$ must be greater than -3 dB.

PIO Tendency The tendency to oscillate or *PIO* is defined in terms of the Bode magnitude of any closed-loop resonant peak, $|\frac{\theta}{\theta_c}|_{max}$, that results from the pilot's efforts to achieve the performance standards. This standard of performance was developed using the flight test data and pilot opinion of the fixed base instrument flight rules (IFR) simulator tests that are documented in the work of Neal & Smith (1970).

Pilot Compensation The pilot's physical and mental workload required to achieve the standard of performance is defined in terms of the phase

of his compensation at ω =$(\mathrm{BW})_{min}$:

$$\angle_{pc} = \angle\left(\frac{i\omega\tau_{p_1}+1}{i\omega\tau_{p_2}+1}\right) \tag{3.11}$$

Maximum closed loop resonance This resonant peak ($|\frac{\theta}{\theta_c}|_{max}$) is shown and graphically defined in Figure 3.8.

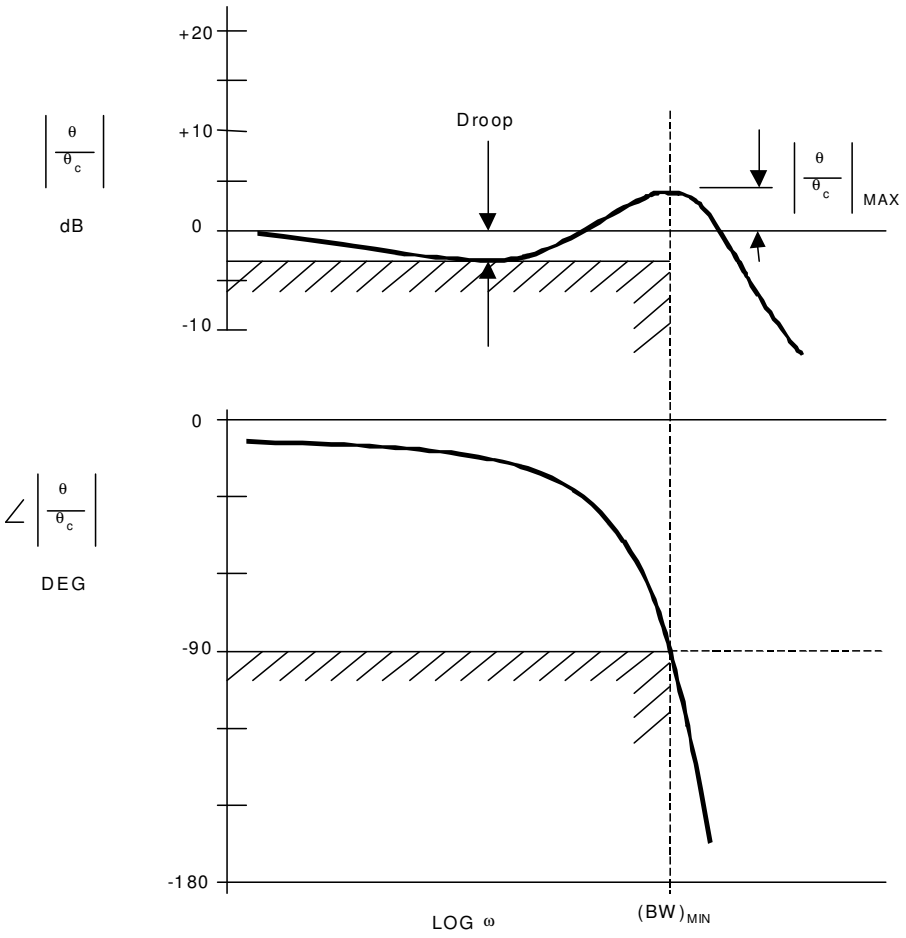

Figure 3.8: Tracking performance standards used in the Neal-Smith analysis(Neal & Smith, 1970:44).

The way the Neal-Smith method was applied in this work is summarized as follows:

1. The Bode amplitude and phase characteristics of the aircraft's pitch attitude response to stick-force inputs ($|\frac{\theta(i\omega)}{F_s(i\omega)}|$ and $\angle\frac{\theta(i\omega)}{F_s(i\omega)}$) have to be obtained. The amplitude and phase characteristics for the gull-wing configuration were obtained using the $\frac{\theta}{F_s}$ transfer function together with the aerodynamic coefficients presented in Chapter 4, but the characteristics may also be measured during flight testing. The frequency range of interest according to the Neal-Smith report is from 0.5 rad/s to at least 10 rad/s.

2. The open-loop Bode amplitude and phase characteristics for the aircraft and the pilot delay is then calculated at some nominal value of K_p (e.g. 1.0). The superscript asterisk signifies that the uncompensated pilot, i.e. only the pilot gain and time delay is modelled in the transfer function.
$$\left(\frac{\theta}{\theta_e}\right)^* = 1.0 \times e^{-0.3s}\left[\frac{\theta}{F_s}\right] \tag{3.12}$$

3. $|\frac{\theta}{\theta_e}|^*$ is then plotted versus $\angle\frac{\theta}{\theta_e}^*$ and overlaid on a Nichols chart. The resulting curve is then translated until the performance standards of Figure 3.8 are just met.

4. If $|\frac{\theta}{\theta_c}|_{max}$ is greater than 0 dB, then pilot compensation is required. The compensation can be determined by adding the amplitude and phase of Figure 3.10 to the uncompensated amplitude-phase curve, for several trial values of τ_{p_1} or $\frac{\tau_{p2}}{\tau_{p_1}}$. The value of τ_{p_1} or $\frac{\tau_{p2}}{\tau_{p_1}}$ that results in the smallest value of $|\frac{\theta}{\theta_c}|_{max}$ will be that which causes the bandwidth to exactly equal 3.5 rad/s and the maximum droop to exactly equal 3 dB.

5. $|\frac{\theta}{\theta_c}|_{max}$ is then obtained from Figure 3.9 and $\angle_{pc}$ is read directly from Figure 3.10 (for $\omega = 3.5$ and the particular value of τ_{p_1} or $\frac{\tau_{p2}}{\tau_{p_1}}$ used.)

6. The values of pilot compensation ($\angle_{pc}$) and closed loop resonance ($|\frac{\theta}{\theta_c}|_{max}$) are then plotted on the opinion chart of Figure 3.6. The handling qualities of the aircraft are then determined from the opinion chart. The lower line on this figure represents a Pilot Rating (PR) of 3.5, while the

top line represents a Pilot Rating of 6.5. The term Pilot Rating refers to the evaluation rating of the Cooper-Harper scale (see Section 3.1.)

The performance standards of the Neal-Smith method (Figure 3.8) are represented on a Nichols chart in Figure 51 of Neal & Smith (1970). This Nichols chart is presented in Figure 3.9.

The amplitude-phase curves for 'optimum' pilot compensation is presented in Figure 52 of Neal & Smith (1970). This graph is presented in Figure 3.10.

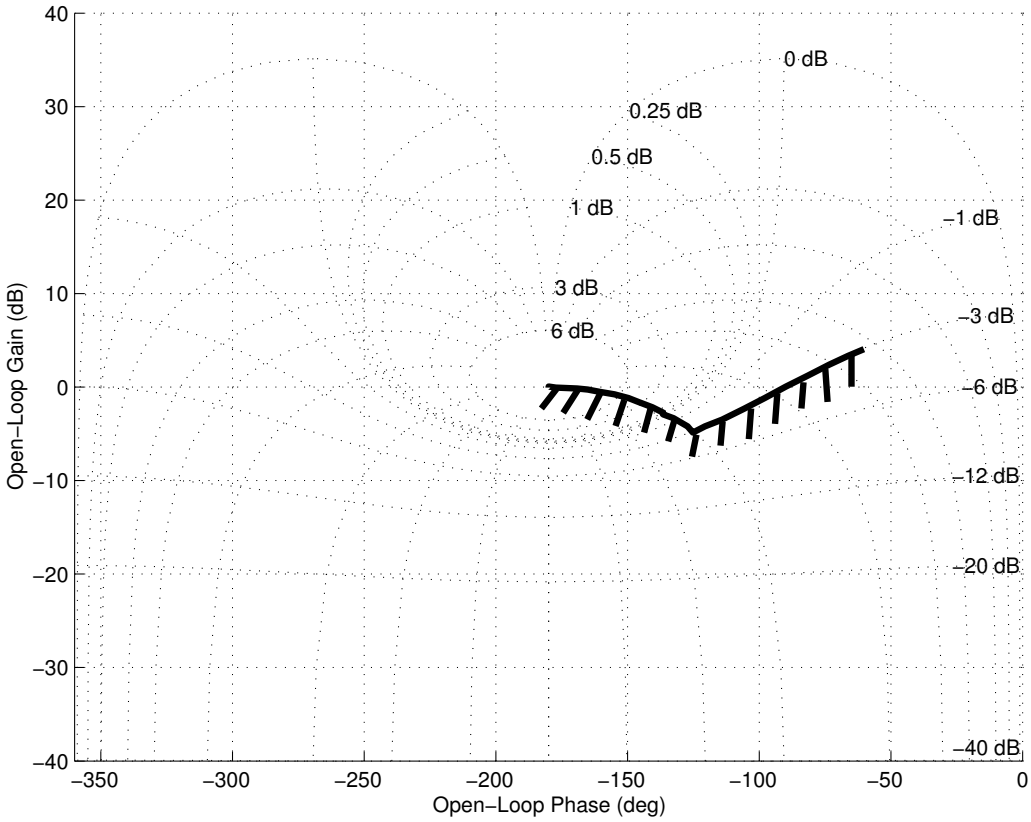

Figure 3.9: Nichols chart with performance standards.

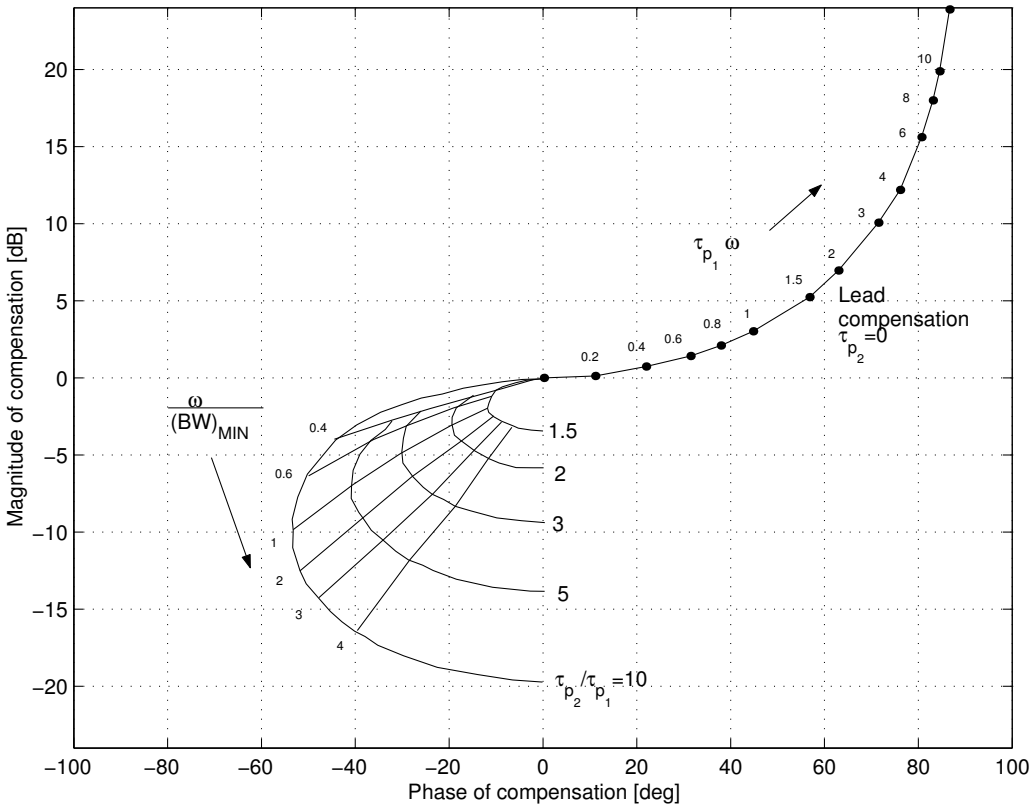

Figure 3.10: Amplitude-phase curves for 'Optimum' pilot compensation. (Neal & Smith, 1970:54)

3.8 A Turbulence Handling Criterion

The previous paragraphs covered handling quality investigation methods that may be applied to any type of aircraft. Tailless aircraft have unique handling quality issues in turbulent atmospheric conditions as a result of their low damping and low pitch inertia.

The inequality shown in Equation 3.13 (Mönnich & Dalldorff, 1993) has been presented as a handling quality criterion for tailless aircraft in turbulent conditions. If the inequality is true, good flying qualities can be expected of an aircraft in turbulent conditions. For most tailed aircraft this inequality would be true. Tailless aircraft usually have low aerodynamic pitch damping when compared to tailed aircraft. This means that the value of C_{M_q} is usually sufficiently low for tailless aircraft that the inequality of Equation 3.13 becomes false.

$$\frac{C_{M_\alpha}}{C_{M_q}} < (C_{L_\alpha} + C_{D_e})\frac{\rho S\overline{c}}{2m} \tag{3.13}$$

The only requirement for applying this criterion is that the aerodynamic coefficients, the mass (m), wing area (S) and mean aerodynamic chord ($\overline{c}$) of the aircraft be known. It is also required to know the density altitude (ρ) at which the aircraft will operate. The aerodynamic parameters include the pitch damping coefficient (C_{M_q}), the moment curve slope (C_{M_α}), the lift curve slope (C_{L_α}) and the equilibrium drag coefficient (C_{D_e}). The values for these parameters are then simply substituted into Equation 3.13 to evaluate the inequality relationship of the criterion.

Chapter 4

Mathematical Model

A mathematical model of aircraft dynamics is required to study handling qualities. The mathematical models described in this chapter will be used to perform the following two functions:

- The calculation of the short period and phugoid mode properties of an aircraft, eg. the natural frequency and the damping ratio.
- The execution of flight simulations with which time domain responses for an aircraft are calculated.

The Exulans, Piper Cherokee, ASW-19 and the SB-13 mathematical models are presented in this chapter. The gust disturbance model used in time domain simulations is also presented.

4.1 Definition of Aircraft Axis System

A frame of reference is required for calculating the magnitudes of aircraft aerodynamic coefficients, aircraft positions and rotations. Axis systems that are frequently used in flight mechanics (Stevens & Lewis, 1992:62) were chosen for this purpose.

The axis systems that are used throughout this document are shown in Figure 4.1. This figure contains a gull-wing aircraft and the wind and body axis systems. Both are right handed axis systems. All rotations about an

axis are taken positive when they satisfy the right hand rule for rotations. The pitch rotations and attitude angles that are simulation outputs follow this convention.

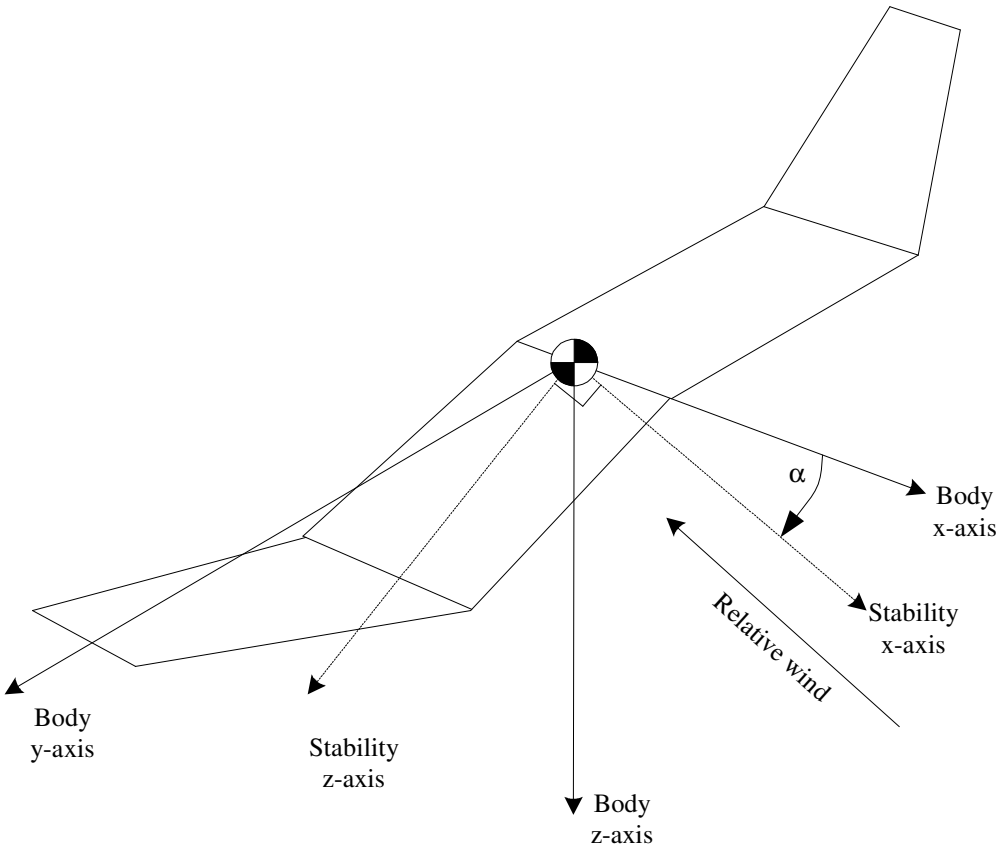

Figure 4.1: Aircraft axes system used in this document.

All aerodynamic coefficients used in this study are calculated in the wind axis system (stability axis system) with the CG as reference point. The body axis system is used internally by the simulation code used in this study.

4.2 Aircraft Model Characterisation

A simulation model requires aerodynamic coefficients and aircraft mass distribution data as input. The literature used to calculate these characteristics

for a typical aircraft is described here. This study contains model descriptions of four aircraft namely the Piper Cherokee, the ASW-19, the SB-13 and the Exulans.

Aerodynamic parameters such as the lift and moment curve slopes were obtained from vortex lattice methods.

Aerodynamic characteristics of the Exulans aircraft were also obtained from Crosby (2000). Mass distribution data of the Exulans aircraft was obtained from Huyssen (2000). The aircraft inertia was calculated using the mass distribution data.

The methods presented in Abbot & von Doenhoff (1959) were used in some cases to provide estimates for overall lift of linearly tapered wings. This reference provides aerodynamic data for a wide variety of wing sections. It also provides checks for the effect of control surface deflections on overall lift and moment coefficients that are calculated by means of vortex lattice methods.

Aerodynamic data on the Piper Cherokee was obtained from McCormick (1995).

The wind tunnel data presented in Althaus & Wortmann (1981) was used to obtain the aerodynamic characteristics of the wing profiles of the ASW-19 aircraft.

Aerodynamic data on the airfoil sections of the SB-13 was obtained from Horstmann & Shürmeyer (1985).

Where no wind tunnel airfoil data was available, the XFOIL panel method was used to calculate the characteristics. (Drela & Youngren, 2000)

Stability derivatives, such as C_{Mq} are very important with respect to the modelling of tailless aircraft. According to the literature, four types of techniques are mostly used for estimating stability derivatives:

- wind tunnel results (Fremaux & Vairo, 1995)
- System identification using flight test results like the studies performed by Moes & Iliff (2002) and Browne (2003)
- Numerical methods such as Computational Fluid Dynamics or CFD

(Park, 2000) and Vortex Lattice methods or VLMs (Kuethe & Chow, 1998)).

- Manual calculation techniques based on empirical data (Roskam, 1971).

Experimental (wind tunnel) methods were not used to measure aerodynamic characteristics of the gull-wing configuration. This was avoided because the handling qualities of a general configuration was investigated in this study, as opposed to that of a final design. The different aerodynamic parameters influencing handling qualities have to be varied for such an investigation. The added value of accurately measured properties diminishes when a range of values are to be investigated. An additional consideration was that it is difficult to achieve acceptable dynamic similarity between small and full-scale models for the specific case of the Exulans. This is due to the geometry of the aircraft and the low true airspeed (maximum true airspeed is less than 110 km/h) for which it is designed.

System identification was not employed because a representative gull-wing aircraft was not available for flight testing at the time of completion of this study.

It was decided not to use CFD as part of this study since specialised expertise is necessary in creating models to perform analysis with sufficient accuracy.

Two Vortex Lattice Methods were used to calculate the stability derivatives of the aircraft that were modeled in this study. The two VLM implementations are Tornado (Melin, 2001) and JKVLM (Kay et al., 1996). Vortex Lattice Methods can accommodate complex aircraft geometry and require little computational effort. It has been shown (Kay et al., 1996) that methods such as JKVLM have produced results that give good correlation with wind tunnel data and DATCOM results. Toll & Queijo (1948) gives approximate relations for the stability derivatives for wings of different taper and sweepback. The calculations based on this source were used to check the Vortex Lattice Method results.

The methods of Roskam (1971) are based on empirical data and manual calculation techniques and were also used for estimating the magnitudes of

stability derivatives.

An example of how model characterisation is done for a tailless aircraft is presented in Ashkenas & Klyde (1989). The techniques presented in this reference was used in this study.

Nickel & Wohlfahrt (1994:468) provided some information on the performance of the SB-13, such as the optimum glide ratio.

Drag polar information as well as mass information of the ASW-19 was found on the internet (Anonymous, n.d. c).

4.3 Stability Derivatives

The stability derivatives will be used to create the aircraft mathematical model. These parameters are defined using the axis system defined in Section 4.1.

Many aerodynamic coefficients are approximately constant or vary in an approximately linear way over a range of angles of attack. This is advantageous since this fact can be used to simplify the aircraft mathematical model. The stability derivatives are simply the gradients of aerodynamic coefficients with respect to an angle (e.g. angle of attack, α).

The stability derivatives have their origins from the linear small perturbation equations (Bryan, 1911).

The stability derivatives for motion in the pitch plane are shown in Table 4.1.

Table 4.1: Longitudinal dimensional and dimensionless derivatives (Stevens & Lewis, 1992:105).

$X_V = -\frac{\bar{q}S}{mV_T}(2C_D + C_{D_V})$	$C_{D_V} \equiv V_T \frac{\partial C_D}{\partial V_T}$
$X_\alpha = \frac{\bar{q}S}{m}(C_L - C_{D_\alpha})$	$C_{D_\alpha} \equiv \frac{\partial C_D}{\partial \alpha}$
$X_{\delta_e} = -\frac{\bar{q}S}{m} C_{D_{\delta_e}}$	$C_{D_{\delta_e}} \equiv \frac{\partial C_D}{\partial \delta_e}$
$Z_V = -\frac{\bar{q}S}{mV_T}(C_D + C_{L_V})$	$C_{L_V} \equiv V_T \frac{\partial C_L}{\partial V_T}$
$Z_\alpha = -\frac{\bar{q}S}{m}(C_D + C_{L_\alpha})$	$C_{L_\alpha} \equiv \frac{\partial C_L}{\partial \alpha}$
$Z_{\dot{\alpha}} = -\frac{\bar{q}S\bar{c}}{2mV_T} C_{L_{\dot{\alpha}}}$	$C_{L_{\dot{\alpha}}} \equiv \frac{2V_T}{\bar{c}} \frac{\partial C_L}{\partial \dot{\alpha}}$
$Z_q = -\frac{\bar{q}S\bar{c}}{2mV_T} C_{L_q}$	$C_{L_q} \equiv \frac{2V_T}{\bar{c}} \frac{\partial C_L}{\partial q}$
$Z_{\delta e} = -\frac{\bar{q}S}{m} C_{L_{\delta e}}$	$C_{L_{\delta e}} \equiv \frac{\partial C_L}{\partial \delta_e}$
$M_v = \frac{\bar{q}S\bar{c}}{I_{yy}V_T}(2C_M + C_{M_V})$	$C_{M_V} \equiv V_T \frac{\partial C_M}{\partial V_T}$
$M_\alpha = \frac{\bar{q}S\bar{c}}{I_{yy}} C_{M_\alpha}$	$C_{M_\alpha} \equiv \frac{\partial C_M}{\partial \alpha}$
$M_{\dot{\alpha}} = \frac{\bar{q}S\bar{c}}{I_{yy}} \frac{\bar{c}}{2V_T} C_{M_{\dot{\alpha}}}$	$C_{M_{\dot{\alpha}}} \equiv \frac{2V_T}{\bar{c}} \frac{\partial C_M}{\partial \dot{\alpha}}$
$M_q = \frac{\bar{q}S\bar{c}}{I_{yy}} \frac{\bar{c}}{2V_T} C_{M_q}$	$C_{M_q} \equiv \frac{2V_T}{\bar{c}} \frac{\partial C_M}{\partial q}$
$M_{\delta_e} = \frac{\bar{q}S\bar{c}}{I_{yy}} C_{M_{\delta_e}}$	$C_{M_{\delta_e}} \equiv \frac{\partial C_M}{\partial \delta_e}$

4.4 Equations of Motion

The equations of motion of the mathematical model are shown in Equation 4.1. The equations are presented in a state space format. These equations are a set of differential equations that may be solved with a suitable numerical integration method in order to calculate time domain responses.

The state space representation of the equations of motion presented here (Equation 4.1) is based on Equations 2.4-23 to 2.4-26 (Stevens & Lewis, 1992:88-89). Similar equations of motion are presented in the work of Etkin (1972).

$$\dot{\mathbf{x}} = \begin{bmatrix} \dot{V}_T \\ \dot{\alpha} \\ \dot{\theta} \\ \dot{q} \end{bmatrix} = \begin{bmatrix} \frac{-\frac{1}{2}\rho V_T^2 S C_D}{m} - g\sin(\theta-\alpha) \\ \frac{-\frac{1}{2}\rho V_T^2 S C_L + m(V_T q + g\cos(\theta-\alpha))}{mV_T} \\ q \\ \frac{\frac{1}{2}\rho V_T^2 S\bar{c}(C_M + \frac{\frac{1}{2}\bar{c}\cdot C_{Mq} q}{V_T})}{I_{yy}} \end{bmatrix} + \begin{bmatrix} \frac{-\frac{1}{2}\rho V_T^2 S C_{D_{\delta_e}} \cdot \delta_e}{m} \\ \frac{-\frac{1}{2}\rho V_T^2 S C_{L_{\delta_e}} \cdot \delta_e}{mV_T} + q_g \\ 0 \\ \frac{\frac{1}{2}\rho V_T^2 S\bar{c}(C_{M_{\delta_e}} \cdot \delta_e + \frac{\frac{1}{2}\bar{c}\cdot C_{Mq} q_g}{V_T})}{I_{yy}} \end{bmatrix} \tag{4.1}$$

4.5 Analytical Approximations for Short Period and Phugoid Modes

The damping ratios and natural frequencies of the short period and phugoid longitudinal modes were used to evaluate the flying qualities of three different aircraft. The aircraft models were required to have a sufficient level of model accuracy in order to calculate the natural frequencies and damping ratios.

Analytical approximations for both the short period and phugoid modes were used to identify the parameters that have the largest effect on the accuracy of the natural frequency and damping ratio calculation. From the approximations it was possible to determine which parameters have the most significant influence of the natural frequencies and damping ratios. The analytical approximation equations were obtained from Stevens & Lewis (1992:206-210).

4.5.1 The Short Period Approximation

An expression for the natural frequency of the short period mode is presented in Equation 4.2 and an expression for the damping ratio is presented in Equation 4.3.

C_D is a parameter of $\omega_{n_{sp}}$ (see Equation 4.2). The equilibrium drag coefficient is normally much smaller than the lift curve slope and therefore its influence on the frequency is less significant than the other parameters.

It is clear from the $\omega_{n_{sp}}$ equation that C_{M_q} and C_{M_α} are important parameters with respect to natural frequency.

In the case of a light weight aircraft, the contribution of pitch stiffness (C_{M_α}) to $\omega_{n_{sp}}$ becomes less significant than that of (C_{M_q}).

The mass moment of inertia around the Y-Y axis of the aircraft is a very important parameter in the natural frequency and the damping ratio. When the inertia is large, $\omega_{n_{sp}}$ becomes smaller.

$$\omega_{n_{sp}} = \frac{1}{2}\rho V_T S\bar{c}\left[\frac{-C_{M_q}(C_D + C_{L_\alpha}) - (4m/\rho S\bar{c}C_{M_\alpha})}{2mI_{yy}}\right]^{\frac{1}{2}} \tag{4.2}$$

Pitch damping (C_{M_q}) and the damping effect of the empennage ($C_{M_{\dot{\alpha}}}$) are important parameters of the short period damping ratio. The damping ratio increases in magnitude as C_{M_q} and $C_{M_{\dot{\alpha}}}$ increases. The short period damping ratio decreases as inertia increases.

$$\zeta_{sp} = \frac{-\bar{c}}{4}\left[\frac{m}{I_{yy}}\right]^{\frac{1}{2}} \frac{C_{M_q} + C_{M_{\dot{\alpha}}} - 2I_{yy}(C_D + C_{L_{\dot{\alpha}}})/(\bar{c}^2 m)}{[-\frac{1}{2}C_{M_q}(C_D + C_{L_{\dot{\alpha}}}) - 2mC_{M_\alpha}/(\rho S\bar{c})]^{1/2}} \tag{4.3}$$

4.5.2 The Phugoid Approximation

The analytical approximation for the phugoid mode natural frequency is shown in the following equation:

$$\frac{\omega_{n_p}^2}{g} = \frac{(C_D + C_{L_\alpha})(2C_M + C_{M_V}) - C_{M_\alpha}(2C_L + C_{L_V})}{-\frac{1}{2}\bar{c}C_{M_q}(C_D + C_{L_\alpha}) - C_{M_\alpha}[mV_T^2/(\bar{q}S) - \frac{1}{2}\bar{c}C_{L_q}]} \tag{4.4}$$

The above equation can be simplified with some assumptions. This simplification is described in Stevens & Lewis (1992:209) and shortly summarised in the following paragraphs, as it is important to understand the relative importance of the different parameters of the equation.

The derivation of Equation 4.4 assumes that the engine (if the aircraft has one) thrust vector passes through the centre of gravity, in order that the equilibrium aerodynamic pitching moment is zero.

The natural frequency is a function of a number of parameters, one of which is the drag coefficient. Under most circumstances C_D is small in comparison with C_{L_α}. Let us assume (for the sake of simplification) that $C_D \ll C_{L_\alpha}$. Also take into account that $C_M \approx 0$ at a trim flight condition. When the C_{M_V}, C_{L_V} and C_{L_q} coefficients are neglected (the magnitude of these coefficients are small close to a trim condition and small relative to other contributions), Equation 4.4 can be simplified as follows:

$$\frac{\omega_{n_p}^2}{g} = \frac{2C_{m_\alpha}C_L}{\frac{1}{2}\bar{c}C_{m_q}C_{L_\alpha} + 2mC_{m_\alpha}/(\rho S)} \tag{4.5}$$

This equation shows that the phugoid natural frequency is proportional to the square root of the lift coefficient when the other derivatives in the

equation are constant. Inspection of Equation 4.5 also shows that the phugoid mode natural frequency decreases as damping (C_{M_q}) increases.

The analytical approximation for the phugoid damping ratio is presented in Equation 4.6. This expression is not very accurate Stevens & Lewis (1992:210), but is shown as a matter of completeness.

$$2\zeta_p\omega_{n_p} = -(X_V + X_{T_V}cos\alpha_e + \frac{X_\alpha[M_q(Z_V - X_{T_V}sin\alpha_e) - (V_T + Z_q)(M_V + M_{T_V})]}{M_qZ_\alpha - M_\alpha(V_T + Z_q)} \quad (4.6)$$

4.5.3 Tailed aircraft Sensitivity Analysis

A sensitivity analysis was used to explore the effects of aircraft parameters on natural frequency and damping ratio. The analytical approximations of natural frequency and damping ratio were used for the sensitivity study.

The properties of the aircraft modes of a Piper Cherokee aircraft were calculated in the sensitivity study. It was assumed that the aircraft is travelling at a fixed height and speed.

The damping ratio and natural frequency of the short period is calculated for the baseline configuration of the aircraft. The different parameters of the equations of these properties are then varied by 5% above and below the baseline. The effect of these changes on natural frequency and damping ratio are then calculated. Equations 4.2 and 4.3 were used to calculate short period natural frequency and damping ratio. The results of the study are presented in Table 4.2. The same analysis was performed on the phugoid natural frequency (using Equation 4.4) and the results are presented in Table 4.3.

This analysis was used as a precursor to the one presented in Chapter 5 and was used to select the parameters for the sensitivity study.

The analysis was performed for a density altitude of 1524m (5000ft) and a speed of 161km/h (100mph). The analysis was done for power-off gliding flight at a static margin of 23.75% and a 2.2° angle of attack.

The following conclusions were drawn:

- Air density (ρ), true airspeed (V_T), pitch moment of inertia (I_{yy}) and

the pitch stiffness (C_{M_α}) (and hence the static margin) have a large effect on short period natural frequency.

- The aerodynamic damping coefficient (C_{M_q}) has a large influence on the aircraft short period damping ratio. The damping effect due to the interaction between the main lifting surface and the horizontal tail ($C_{M_{\dot{\alpha}}}$) has an effect on the aircraft short period damping ratio, but its effect is smaller than that of the aerodynamic damping coefficient. Air density (ρ), the pitch moment of inertia (I_{yy}) and the pitch stiffness (C_{M_α}) also have a large influence on the damping ratio of the short period mode.

- The phugoid natural frequency is influenced by air density (ρ), the lift curve slope (C_{L_α}), aircraft mass (m) and pitch stiffness (C_{M_α}). These parameters influence the phugoid natural frequency because this mode involves an exchange in potential energy with kinetic energy.

It is important to note that C_{M_0}, C_{L_0} and $C_{M_{\delta_e}}$ are not very important parameters in the natural frequencies or the damping ratios of either of the aircraft dynamic modes. These quantities are more important with respect to the trim attitude. The $C_{M_{\delta_e}}$ variable also determines and the control gain of the aircraft in the pitch plane.

Table 4.2: Results of the sensitivity analysis of the short period mode. (The absolute values of the changes in magnitude of the properties are shown)

Parameter	% change	$\lvert\%\Delta\omega_{n_{sp}}\rvert$	$\lvert\%\Delta\zeta_{sp}\rvert$
ρ	+5%	2.48%	2.45%
ρ	-5%	2.55%	2.52%
V_T	+5%	5.00%	0.00%
V_T	-5%	5.00%	0.00%
C_{M_q}	+5%	0.015%	3.622%
C_{M_q}	-5%	0.015%	3.623%
C_D	+5%	0.000%	0.001%
C_D	-5%	0.000%	0.001%
C_{L_α}	+5%	0.015%	0.015%
C_{L_α}	-5%	0.015%	0.015%
m	+5%	0.014%	0.062%
m	-5%	0.014%	0.069%
I_{yy}	+5%	2.41%	2.41%
I_{yy}	-5%	2.60%	2.60%
C_{M_α}	+5%	2.45%	2.40%
C_{M_α}	-5%	2.52%	2.58%
$C_{M_{\dot{\alpha}}}$	+5%	0.00%	1.28%
$C_{M_{\dot{\alpha}}}$	-5%	0.00%	1.28%

Table 4.3: Results of the sensitivity analysis of the phugoid mode. (The absolute values of the changes in magnitude of the properties are shown)

Parameter	% change	$\lvert\%\Delta\omega_{n_p}\rvert$
ρ	+5%	2.45%
ρ	-5%	2.52%
C_{M_q}	+5%	0.015%
C_{M_q}	-5%	0.015%
C_D	+5%	0.015%
C_D	-5%	0.015%
C_{L_α}	+5%	1.810%
C_{L_α}	-5%	1.844%
m	+5%	2.396%
m	-5%	2.582%
I_{yy}	+5%	0.00%
I_{yy}	-5%	0.00%
C_{M_α}	+5%	1.78%
C_{M_α}	-5%	1.93%
$C_{M_{\dot{\alpha}}}$	+5%	0.00%
$C_{M_{\dot{\alpha}}}$	-5%	0.00%

4.6 Aircraft Mathematical Models

The mathematical model parameter values for the aircraft used in this study are listed in Table 4.4.

The following four aircraft types are used for a comparative handling characteristics analysis (see Section 6.2) with the gull-wing configuration:

- Piper Cherokee PA-28-180 - This aircraft is used because all the parameter values could be obtained from published data (McCormick, 1995). This model was also used for benchmarking of the simulation code. The aircraft is representative of a conventional powered aircraft.
- The ASW-19 standard glider - This aircraft is representative of a standard glider known to have very good handling qualities.
- The Akaflieg SB-13 Arcus sailplane - This aircraft is representative of a tailless glider, that has good flying qualities, except in turbulent conditions.
- The Exulans gull-wing configuration - The subject of the handling quality evaluation. Table 4.4 shows the mathematical model parameter values for an aircraft with the outboard wing sections swept back at 30°.[1] The sweep case presented in the table has a 10.7% static margin at the 30° sweep angle.

The planforms of these aircraft are shown in Appendix C.

All the coefficients relating to aircraft moments in Table 4.4 use the aircraft centre of gravity as the reference point. This convention will be followed throughout this document.

The gull-wing aircraft (Exulans) has low damping and pitch inertia when compared to aircraft with horizontal stabilisers. The values are low when compared to another tailless aircraft such as the SB-13. The difference between the SB-13 and gull-wing configuration is that the SB-13 does not have

[1] The design wing sweep angle for cruising flight.

Table 4.4: The aircraft mathematical model parameters used in this study.

Parameter	Unit	Cherokee	ASW-19	SB-13	Gull-Wing
S	m^2	14.86	11.79	11.79	12.00
$\overline{c}$	m	1.6	0.822	0.797	1.02
m	kg	1089	408	435	160
I_{yy}	kg·m^2	1694	548	149.5	28.2
C_{L_α}	/rad	4.50	5.92	5.51	5.15
$C_{L_{\delta_e}}$	/rad	0.343	0.220	0.469	0.638
C_{M_α}	/rad	-1.069	-0.633	-0.5896	-0.55
C_{M_q}	/rad	-7.83	-17.68	-5.37	-2.55
$C_{M_{\dot{\alpha}}}$	/rad	-2.76	-3.05	0.00	0.00
$C_{M_{\delta_e}}$	/rad	-0.63	-1.033	-0.59	-0.533
C_{D_0}		0.03125	0.0100	0.00977	0.014
C_{D_i}		0.09291	0.0196	0.01543	0.0285

the forward backward swept cranked wing like the gull wing, but only backwards sweep.

The $C_{M_{\delta_e}}$ parameter was calculated for the gull-wing aircraft and SB-13 using a vortex lattice method.

4.7 Gull-Wing Configuration Model

The geometry of the Exulans was used to create a mathematical model. The Exulans data that were presented in Table 4.4 represents one wing sweep case. The mathematical model for the full range of wing sweep angles is presented in this section.

The variable wing sweep configuration (and therefore variable static margin) of the Exulans necessitates that static margin has to be specified at a certain sweep angle. In this document the static margin layouts are specified at 30° outboard wing sweep. 30° wing sweep was arbitrarily chosen since this is the cruise flight setting. Static margin varies with wing sweep angle for two reasons: A change in wing sweep has a significant effect on the aircraft CG and on the position of the neutral point of the aircraft.

Four different static margin layouts were investigated in this study. The four different layouts were chosen so that a large range of static margins could be evaluated with respect to handling qualities. The four layouts were 2%, 5%, 10.7% and 15% static margin at 30° wing sweep. It is important not to confuse the static margin change due to wing sweep with the different static margin layouts that are investigated.

The following observations were made with regards to the Exulans:

- The longitudinal CG of the aircraft varies with outboard wing sweep angle, since the masses of the outboard wing sections are a meaningful percentage of the all-up mass.
- The magnitude of aerodynamic damping changes significantly with a change in CG.
- Control authority is a function of longitudinal CG (and static margin) because of the short moment arm between the elevons and the CG.
- The pilot mass is a significant fraction of total aircraft mass.

The Exulans has a wing area of 12m^2 and a mean aerodynamic chord of 1.08m.

The methods used to calculate the parameter values used in the mathematical model set-up are explained in the following subsections. The parameter values (e.g. control authority, damping and pitch inertia) presented in this section will be referred to as 'baseline' values in subsequent sections.

4.7.1 Inertial Parameters

The inertial parameters relevant to the modelling of the Exulans glider are its mass, moment of inertia about the Y-Y axis and its CG.

Mass

The all-up mass of the Exulans glider comprises of the mass of the pilot, the mass of the wings and the mass of the fuselage. The pilot mass was assumed

to be 90 kg. According to Huyssen (2000) the mass of the inboard and outboard part of one wing of the Exulans glider are 13 and 9 kg respectively. The mass of each winglet on the outboard wing is 2 kg. The mass of each of the hinges of the variable sweep wings is 1 kg. The mass of the fuselage is 20 kg. The total aircraft mass (including pilot) is 160 kg.

Centre of gravity and static margin

The centre of gravity of the Exulans was calculated for different wing sweep angles. The CG's of different components are shown in Figure 4.2. Sample mass and balance data for the Exulans layout is presented in Table 4.5.

The distance x_{cg} is measured from the leading edge of the wing on the centerline of the aircraft to the CG position. x_{cg} is positive for a CG behind the leading edge. The change in x_{cg} will be approximated as linear for the wing sweep range under investigation.

Static margin was calculated using the position of the neutral point and CG of the aircraft. The neutral point of the Exulans was calculated using a vortex lattice method. The calculation method is described in Appendix G.2.

The neutral point was calculated for different cases of wing sweep. The CG of the four static margin layouts were chosen so that the following four layouts resulted: 2%, 5%, 10.7% and 15% static margin at 30° wing sweep. The CG's between the four layouts were altered by changing the CG's of the fuselage and the pilot in the mass and balance calculation of the aircraft. The CG graphs for the four layouts are presented in Figure 4.3 as a function of wing sweep. The neutral point is also shown on this graph as a function of sweep. The magnitude of the static margin for a given CG layout can be visualised as the vertical distance on the graph between the neutral point line and the line of a specific CG layout. The four CG layouts of the study are referred to by their respective static margins at 30° sweep. The static margin at this sweep angle can also be visualised by means of Figure 4.3, where a bold dashed line is drawn as a measure of static margin. The line shows static margin as a percentage of mean aerodynamic chord. The graph presented in Figure 4.3 was used to calculate static margin as a function of

Table 4.5: Longitudinal mass and balance data of the Exulans (30° sweep, 10.7% @ 30° static margin layout).

Component	Mass [kg]	x_{cg} [m]	Pitch inertia around aircraft CG [kg·m^2]
Pilot	90	0.167	1.05
Fuselage	20	-0.300	6.62
Inboard wing sections	26	0.393	0.36
Wing sweep hinges	2	-0.315	0.70
Outboard wing sections	18	1.001	9.48
Winglets	4	1.855	9.98

wing sweep for the four CG layouts and the result of this is presented in Figure 4.4.

Figure 4.4 shows that the gull-wing configuration is not statically stable across the wing sweep range for two of the four different static margin layouts. These two configurations become statically unstable at the low wing sweep angles corresponding to negative static margin. In practice this means that these configurations will have a diverging nose pitch attitude if the pilot does not constantly provide correcting control inputs.

Y-Y moment of inertia

The swept gull-wing configuration has low pitch inertia when compared to other aircraft and even when compared to other tailless aircraft. Pitch inertia varies with wing sweep.

A simple approach was followed to estimate I_{yy} as a function of sweep. The aircraft was divided into different sections (Figure 4.2), as with the x_{cg} calculation, each having their own centre of gravity.

The different aircraft sections were approximated as point masses at their geometrical centroids.

The pilot was approximated as a rigid body and a point mass. This was done to simplify the inertia model. In reality, the pilot is not a rigid body or a point mass and, in the case of the Exulans, he/she is not rigidly connected

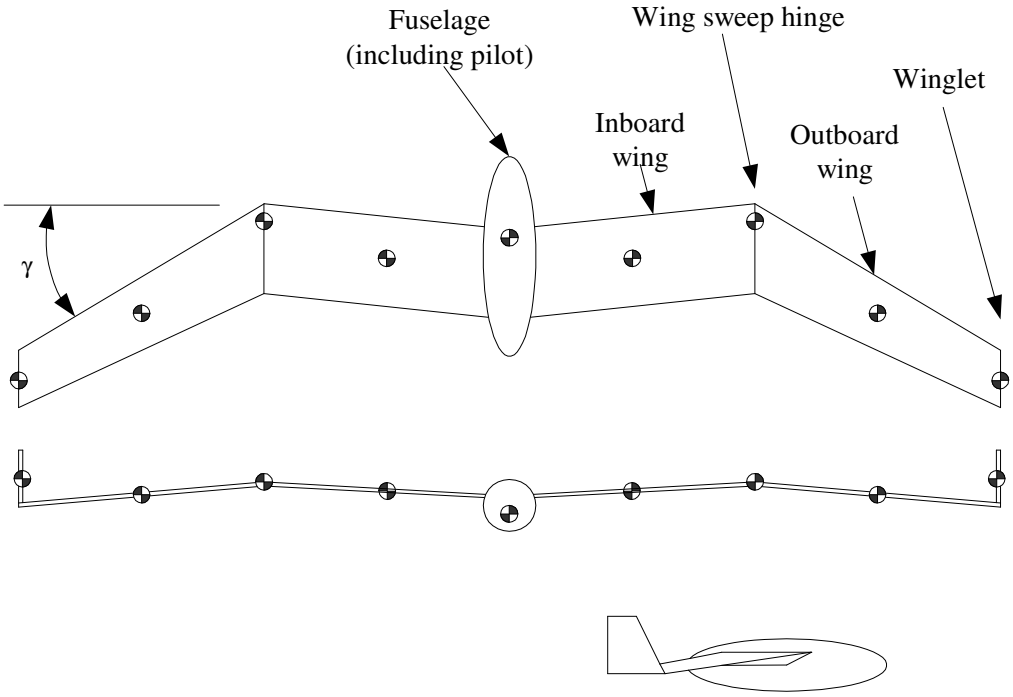

Figure 4.2: Three views of the Exulans glider showing assumed *CG* locations of different aircraft components. (Outboard wing sweep angle (γ) at 31°).

to the aircraft. This is because the pilot lies in the prone position in a harness mounted to the fuselage. Since the pilot is not rigidly connected to the airframe, he/she contributes less to the aircraft pitch inertia. The inertia calculation simplification can be tolerated since it is shown later (Section 5.2) that the effect on handling qualities is small if the estimation error of inertia is within 10%.

Equation 4.7 was used to evaluate I_{yy} for different wing sweep angles. The variable i in this equation represents the number of an aircraft section. The pitch inertia graphs for the four different static margin layouts are presented in Figure 4.5. An example of the pitch inertias for the different aircraft sections is presented in Table 4.5.

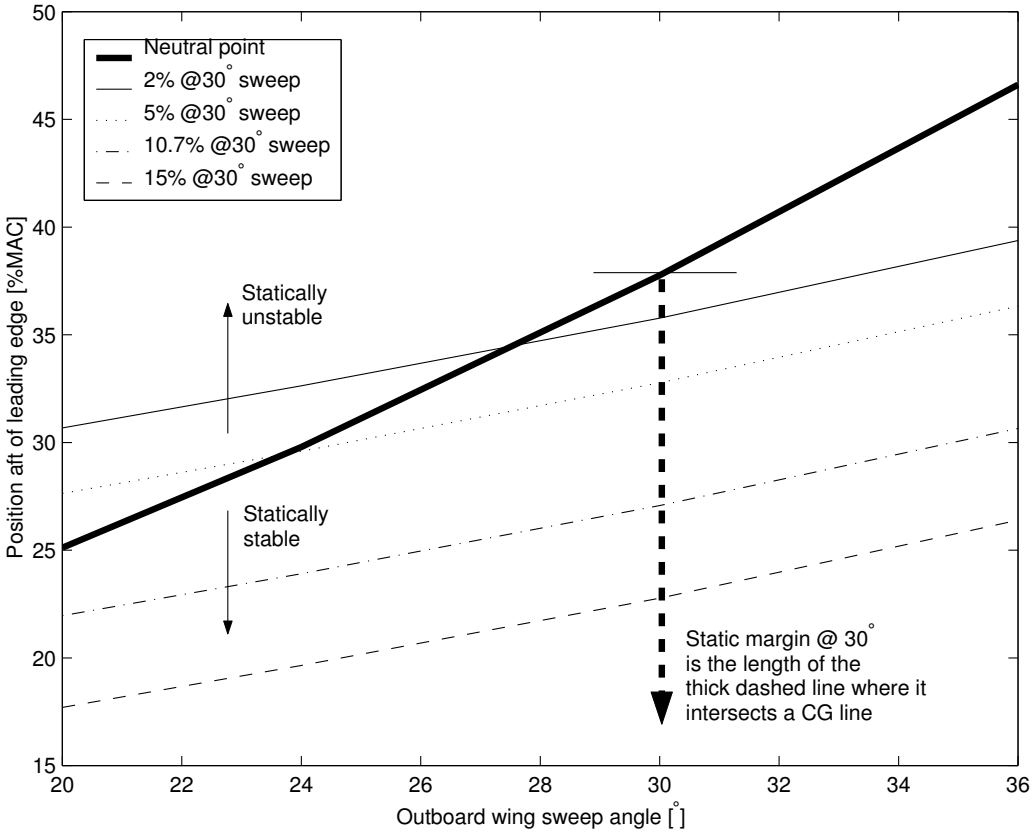

Figure 4.3: Four different *CG* locations and the neutral point as a function of sweep.

$$I_{yy} = \sum_{i=1}^{n} (x_{CG_{aircraft}} - x_{CG_i})^2 m_i \tag{4.7}$$

4.7.2 Aerodynamic Parameters

The calculation methods and results for the aerodynamic parameters are presented in this section.

Lift and pitch moment model

The lift parameters of the aircraft were obtained by consulting an aerodynamicist (Crosby, 2000) and by using a vortex lattice computer algorithm.

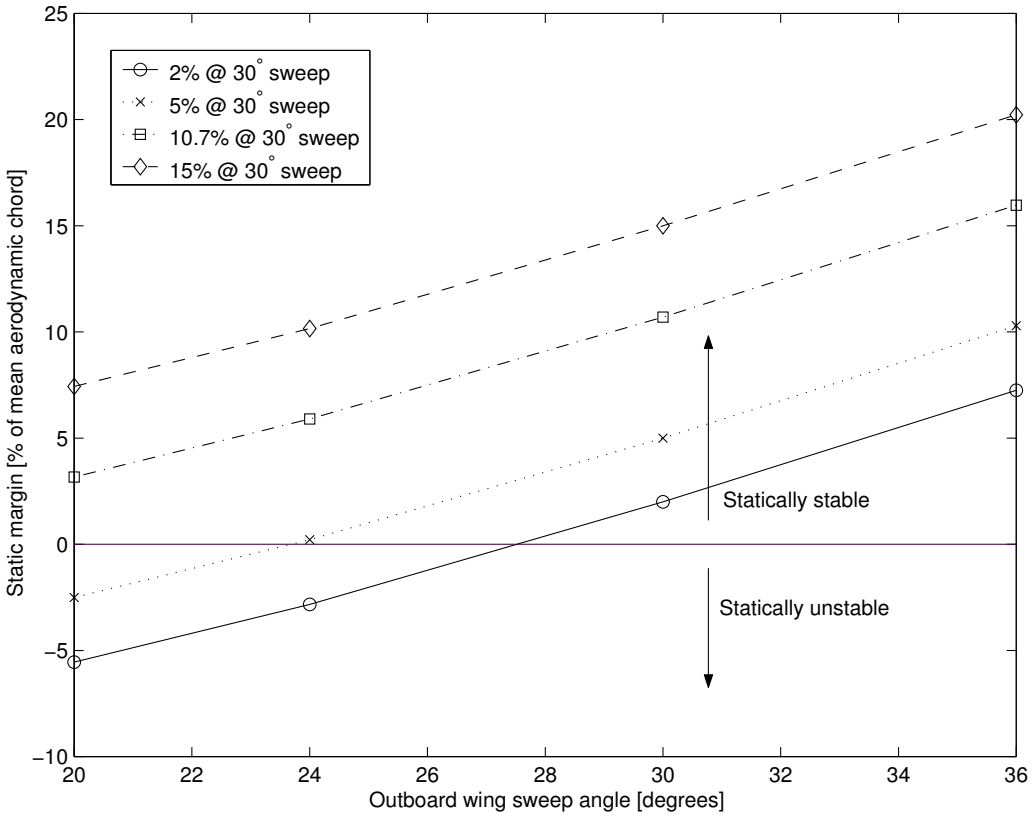

Figure 4.4: Aircraft static margin as a function of sweep angle for four different CG locations.

The total aircraft lift coefficient and the pitch moment coefficient are calculated by means of Equations 4.8 and 4.9.

$$C_L = C_{L_0} + C_{L_\alpha}\alpha + C_{L_{\delta_e}}\delta_e \tag{4.8}$$

$$C_M = C_{M_0} + C_{M_\alpha}\alpha + C_{M_{\delta_e}}\delta_e + \frac{\overline{c}}{2V_T}(C_{Mq}\dot{\theta}) \tag{4.9}$$

The aerodynamic coefficients of the Exulans were calculated for the linear aerodynamic region. The JKVLM vortex lattice method (Kay et al., 1996), was used to calculate the values of these parameters. The JKVLM code was used since it has a fast execution time and because it has a relatively simple input and output interface. JKVLM was subjected to a benchmarking

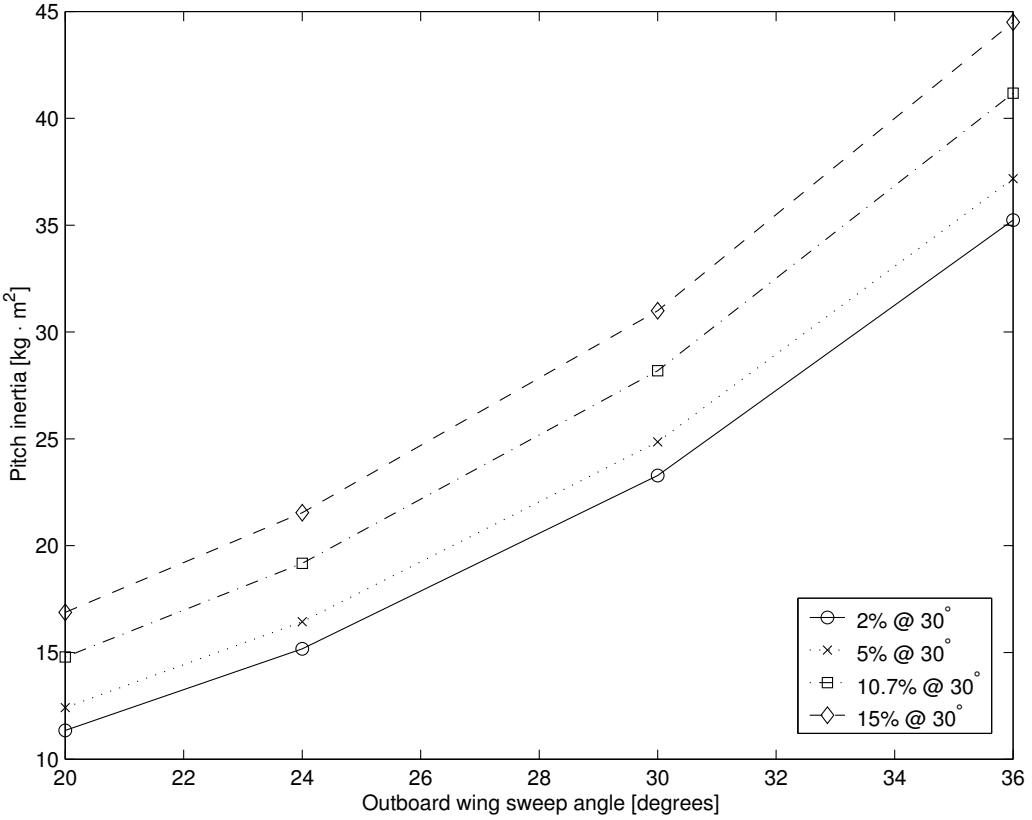

Figure 4.5: Pitch inertia (I_{yy}) as function of sweep angle for four different static margin configurations.

procedure (see Appendix G).

The following assumptions and simplifications were made in constructing the vortex lattice model of Exulans:

- The aircraft was modeled by a wing surface only. The aerodynamic effects of the fuselage were not taken into account.
- The wing was modeled as an infinitely thin plate. The effect of camber was not modeled as flat plates were used to model the wing surface. The dihedral angle of the inboard wing section and the anhedral angle of the outboard wing section were modeled.
- The outer wings were modeled as having 4 degrees of positive wing

twist (leading edge downwards). The forward sections of the flat plates are warped downwards to model wing twist.

- The effects of boundary layer flow and cross flow are not modeled with a VLM.
- The neutral point was calculated for an angle of attack of zero degrees.
- The outboard wing span (the lateral distance between the wing sweep hinge and the wing tip) of the Exulans VLM model was kept constant at 3 metres for all sweep angles that were analysed. This was done to simplify the geometry of the model. The wing chord values at the wing sweep hinge (1.1 m) and at the wing tip (0.7 m) were also kept the same for all sweep angles.

The results of the lift curve slope calculations performed with the vortex lattice method are shown in Figure 4.6.

The zero lift angle of attack was calculated incorrectly because the wing of the Exulans was modeled as an infinitely thin plate. Symmetrical sections such as the infinitely thin flat plate have a zero lift angle of attack of 0°. In reality the Exulans has a very thick wing section. This meant moment coefficients were also calculated incorrectly.

Even though the zero lift angle of attack was calculated incorrectly by JKVLM, the other stability derivative values calculated by the programme are sufficiently accurate. This was shown with the JKVLM benchmark study presented in Appendix E.

The lift curve information in Table 4.6 was obtained from Crosby (2000). This data was used to estimate the zero lift angle of attack and C_{L_0}. The information from Crosby (2000) is compared with the JKVLM values in Table 4.7.

Appendix E showed that the JKVLM C_{L_α} calculation is more accurate than that of C_{M_α}. The moment curve slope was therefore calculated by means of the relationship in Equation 4.10 using the static margin (which is specified) and the JKVLM C_{L_α} value.

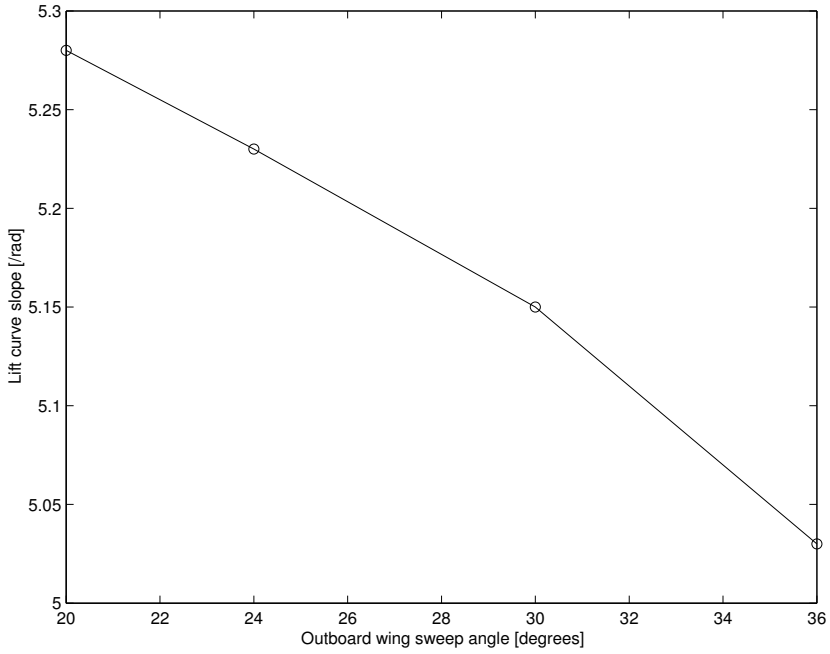

(a) Lift curve slope for different outboard wing sweep angles.

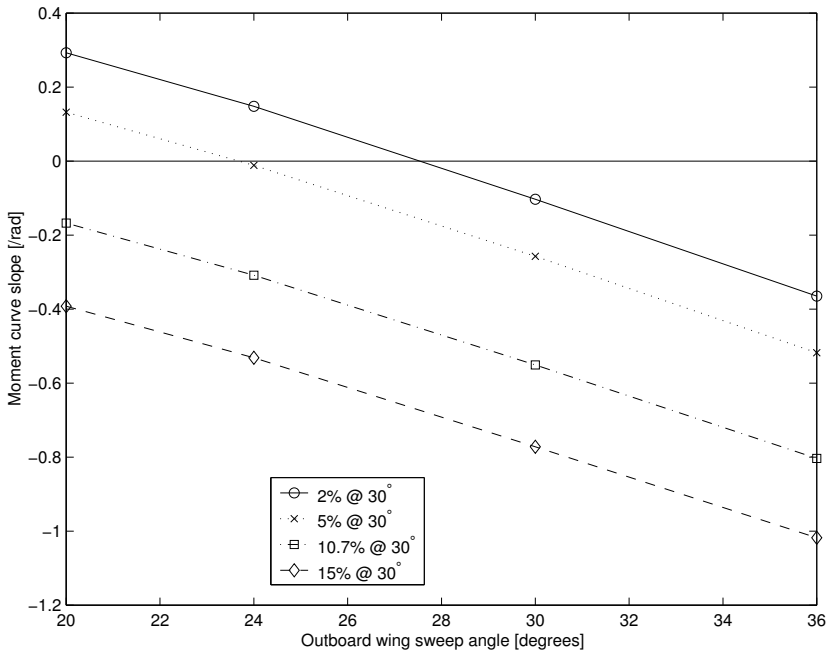

(b) Moment curve slope for different outboard wing sweep angles.

Figure 4.6: C_{L_α} and C_{M_α} for different outboard wing sweep angles.

Table 4.6: Lift curve information from Crosby (2000)

Outboard wing sweep [degrees]	α [degrees]	C_L
24	0	0.06908
	17.8	1.7
26	6	0.625
	8	0.818
29.5	0	0.06
	2	0.244

Table 4.7: Comparison of aerodynamic data from Crosby (2000) to JKVLM results

Outboard wing sweep [degrees]	C_{L_α}	C_{L_0}	C_{L_α} JKVLM
24	5.250	0.069	5.242
26	5.529	0.046	5.215
29.5	5.271	0.060	5.159

$$\begin{aligned} SM &= -\frac{\partial C_M}{\partial C_L} \\ \therefore \frac{\partial C_M}{\partial \alpha} &= -\frac{\partial C_L}{\partial \alpha} \times SM \end{aligned} \tag{4.10}$$

Table 4.7 shows that a reasonable comparison exists between JKVLM results and that of Crosby (2000). C_{L_0} varies with respect to wing sweep. The C_{L_0} value was taken as a constant value of 0.06 in order to simplify the mathematical model.

The JKVLM results for the lift curve slope (Figure 4.6) and the C_{L_0} value were used to create the lift curve for different angles of wing sweep. The JKVLM results for C_{L_α} are used instead of the aerodynamicist's information (Crosby, 2000), because it is available for a larger range of sweep angles.

In order to estimate C_{M_0}, the following procedure is followed: The physical properties of the Exulans (wing area, mass) and the estimated trim speed for a range of sweep angles are substituted into Equation 4.11. The relevant trim speeds were obtained from Crosby (2000). The air density was assumed to be 1.16 kg·m^{-3}. A corresponding range of corresponding lift coefficients can be calculated with this information.

$$\frac{1}{2}\rho V_T^2 S C_L = mg \tag{4.11}$$

The lift coefficients can be used together with the lift equation to estimate the effective trim angle of attack. The trim angle of attack and C_{M_α} are then used to calculate a range of values for C_{M_0}. This is done by means of a moment balance around the CG of the aircraft and by noting that the moment balance equals zero for trimmed flight (see Equation 4.12).

$$\begin{aligned} C_{M_0} + C_{M_\alpha} \cdot \alpha + C_{M_{\delta_e}} \delta_e &= 0 \\ C_{M_0} &= -C_{M_\alpha} \cdot \alpha - C_{M_{\delta_e}} \delta_e \end{aligned} \tag{4.12}$$

The values for $C_{M_{\delta_e}}$, $C_{L_{\delta_e}}$ and C_{Mq} were calculated using JKVLM. The elevon control surfaces on the VLM model had a chordwise dimension of 25% of the mean aerodynamic chord. The extent of the elevons were taken to be 67.5% of the semi-span to the wingtip. The results are presented Figures 4.7 and 4.8. Benchmarking of the vortex lattice method was performed for the C_{Mq} and $C_{M_{\delta_e}}$ parameters (see Appendix E and F) using wind tunnel data.

$C_{L_{\delta_e}}$ was not used in the tailed sensitivity analysis since the lift of an elevator of a tailed aircraft is small compared to the contribution of the main lifting surface. The lift produced by the elevon deflection on a tailless aircraft is significant and therefore $C_{L_{\delta_e}}$ is included in the mathematical model.

Drag Polar

The drag polar is based on the following specifications (Crosby, 2000) and the formula for a drag polar, Equation 4.13:

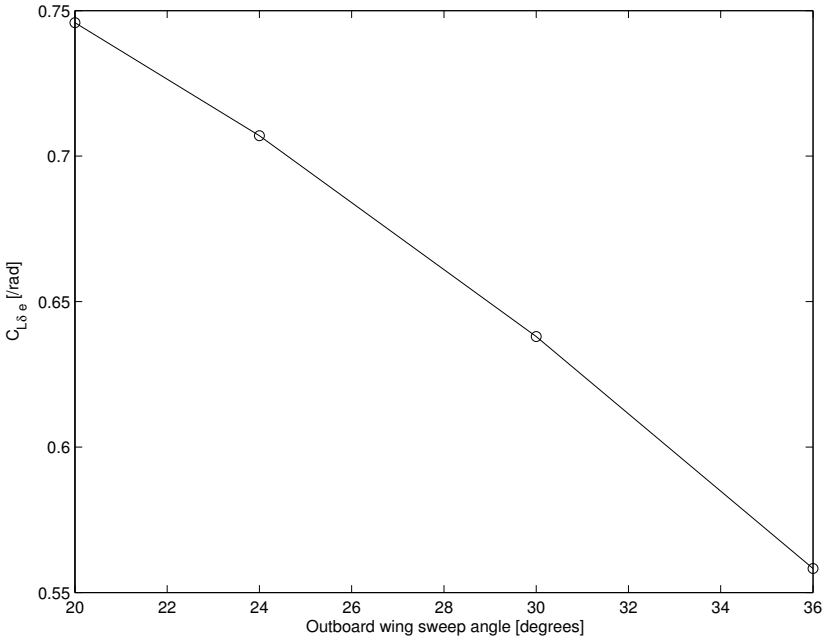

(a) $C_{L_{\delta_e}}$ for different outboard sweep angles.

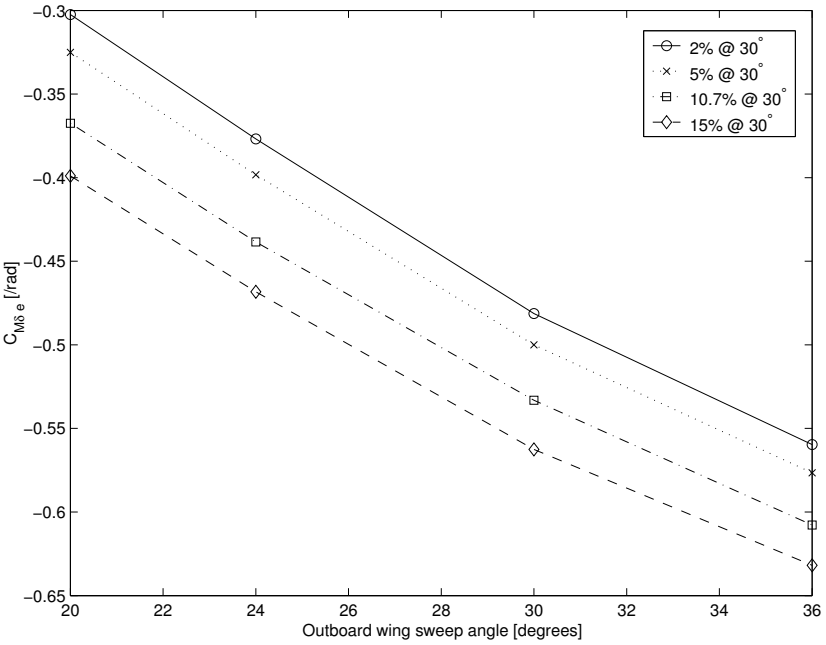

(b) $C_{M_{\delta_e}}$ for different outboard wing sweep angles.

Figure 4.7: $C_{L_{\delta_e}}$ and $C_{M_{\delta_e}}$ for different outboard wing sweep angles.

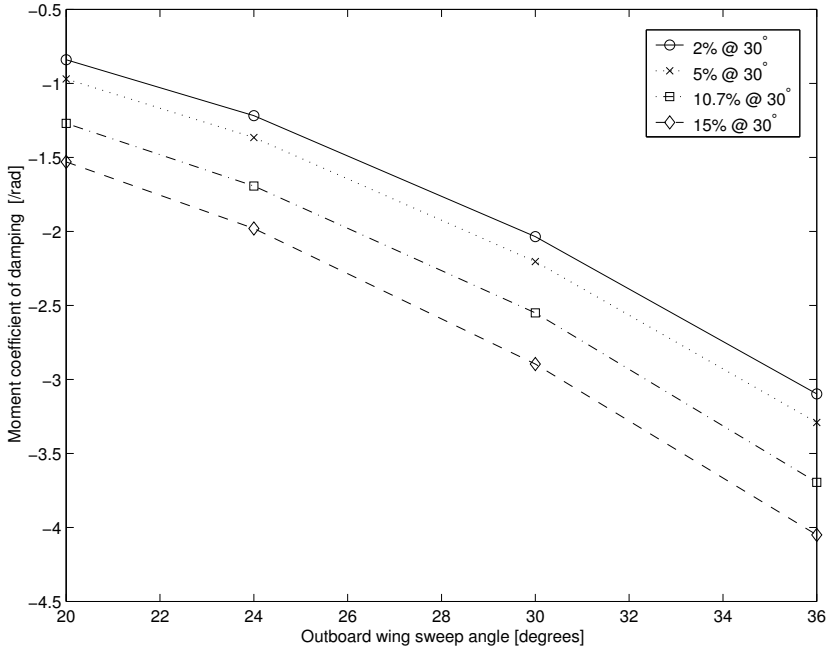

Figure 4.8: Pitch damping coefficient (C_{Mq}) for different outboard sweep angles.

- Best $\frac{L}{D}$ ratio $= 25$ at $C_L = 0.7$
- At the best $\frac{L}{D}$, $C_{D_0} = C_{D_i}$

$$C_D = C_{D_0} + \frac{C_L^2}{\pi AR\text{e}} \tag{4.13}$$

The values of C_{D_0} and the ARe product (clean aircraft and no flap or elevon deflection) were calculated as 0.014 and 11.1408 respectively.

4.7.3 E-point, O-Point and C-point of the Gull-Wing Configuration

Tailless aircraft offer potential advantages in terms of low drag. An elliptical lift distribution is optimal with respect to induced drag. For a tailless aircraft (without any other pitching moments acting) the maximum Oswald efficiency factor can only be achieved if the centre of gravity of the aircraft lies on the centre of pressure for an elliptical lift distribution. This point is called the 'E-point' according to Nickel & Wohlfahrt (1994:74).

The shape of the optimum circulation distribution for a tailless aircraft with winglets approximates the shape of a half-ellipse on the semi-span basic wing (see Figure 4.9). The centre of gravity position that coincides with the centre of lift for this lift distribution is named the O-point (ibid.: 74). The O-point is aft of the E-point in the case of a rearward swept wing, because the lift distribution corresponding with the O-point has a higher local magnitude at the wing tip than in the case of the E-point.

In addition to the E-point and the O-point, the C-Point is also defined (ibid.: 74). This is a position on the longitudinal axis that is the centre of pressure for a constant local lift coefficient along the span of the wing. This lift distribution corresponds to the maximum lift that the particular wing could possibly generate. The C-point does not correspond to an optimum lift to drag ratio. The lowest possible stall speed could be achieved if the CG was located in the C-point. This arrangement would be desirable for takeoff and landing, provided the handling qualities are acceptable.

In order to investigate the handling qualities of the gull-wing configuration at its optimum design point, it is required to determine whether this aircraft type has desirable handling qualities with the CG at the E-point (for an aircraft with a plain wing) and with the CG at the O-point (for an aircraft with winglets).

In the case of the Exulans, the winglets are of the all-flying type. This means that the angle of the winglets relative to the free stream may be altered by the rigging of the control run. As such the winglets can be used to produce varying magnitudes of lift. This means that the winglets can also

produce zero lift when the winglet is at the zero lift angle of attack. As a result, the aircraft could potentially be operated at either the E-point or the O-point. It is therefore required to investigate the handling qualities of the aircraft with the *CG* placed at the E-point and the O-point and the locations in between.

The O-point of the Exulans was calculated at various wing sweep angles. A graphical method (Figure 4.9) was used for the calculation along with the following assumptions:

- The optimum lift distribution can be approximated by the part of a half-ellipse on the basic wing planform without the winglet. This assumption is taken from Horstmann (1988).
- The wing sections of the aircraft have zero pitching moment.
- The balance of pitching moments is produced without flaps by a (hypothetical) wing torsion or wing wash-out.

The O-point calculation of the gull-wing configuration in Figure 4.9 was performed by projecting the centroid of the assumed elliptical lift distribution along the quarter chord line of the wing planform. The intersecting points of the first two sections were joined by a line. The centroid of the semi-span part of the ellipse (Section 1 + 2) was projected onto this line and projected onto the wing line of symmetry. In summary, the (ellipse) weighted average of the quarter chord line of the wing is calculated to yield the O-point. The E-point and C-point was calculated in a similar way.

The C-Point and the O-Point are close to each other in the case of the gull-wing configuration. The O-Point is behind the C-point. This is a potential handling quality problem when the flight test data of the SB-13 is taken into account. Nickel & Wohlfahrt (1994) states that the centre of gravity should be a suitable distance (at least 5% of mean aerodynamic chord) in front of the C-point in the case of a tailless aircraft in order for the aircraft to be stable. This indicates that the O-point might be inaccessible as a possible position for the centre of gravity for the gull-wing configuration. The C-point and

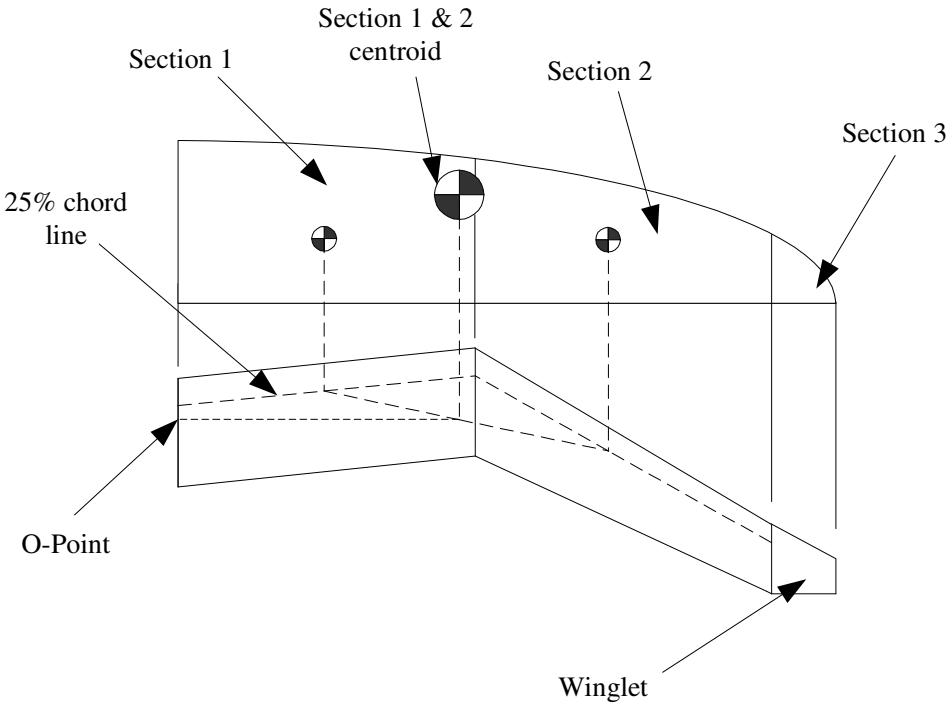

Figure 4.9: Calculation of O-Point by means of graphical method for a wing with an outboard sweep angle of 30°.

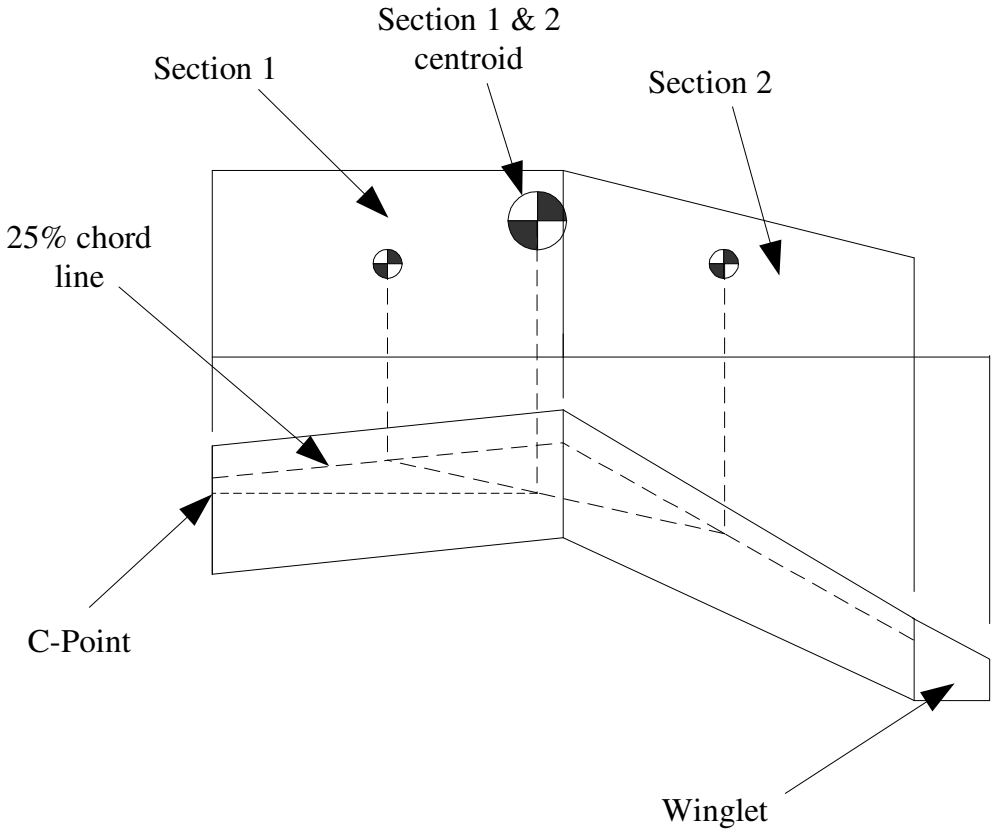

Figure 4.10: Calculation of C-Point by means of graphical method for a wing with an outboard sweep angle of 30°.

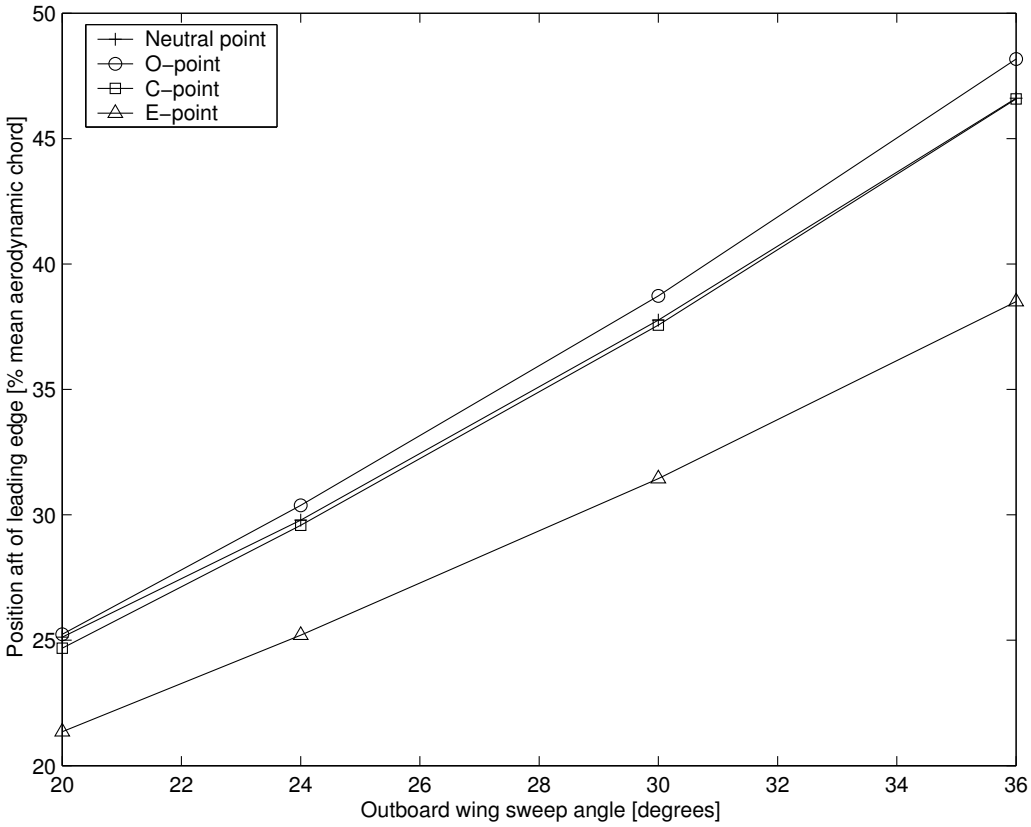

Figure 4.11: The O-point, C-point, E-point and the neutral point of the gull-wing configuration for a range of outboard wing sweep angles.

the neutral point are almost identical for the gull-wing configuration. The E-point is in front of the C-point, but it is still situated at a low static margin. It is important to verify whether good handling qualities can be expected at the CG positions close to the E-point and the O-point. It is also necessary to determine whether the maneuverability point[2] lies forward or aft of the O-point. If it is forward of the O-point, a pilot would not be able to control the aircraft without the assistance of stability augmentation.

The rest of the study is devoted to the investigation of whether or not the Exulans aircraft, as an example of a gull-wing configuration, has satisfactory handling characteristics with its CG positioned at various magnitudes of static margin. Special consideration will be given to static margins that have CG positions that are coincident with either the E-point or the O-point.

4.8 Disturbance models

The disturbance models used for simulation of wind gusts and elevon inputs are described here. These disturbance models were used for the gull-wing configuration sensitivity study chapter and simulation results presented in subsequent chapters.

4.8.1 Gust Disturbance

A vertical wind gust is modeled by using the equations of the angle of attack and the pitch rate. The disturbance is introduced as described in Equation 4.1. This gust model is presented by Etkin (1972) and simulation results using this gust model are presented by Mönnich & Dalldorff (1993). The gust model uses the assumption that the effect of a vertical gust on an aircraft flying through the gust is equivalent to a pitch rate disturbance. A graphical representation of the pitch rate disturbance is presented in Figure 4.12.

The implementation of the gust disturbance is presented in Equation 4.14.

[2]The maneuverability point is a CG position where the aircraft has low or negative static margin, but where the pilot is still able to fly the aircraft without excessive pilot workload.

$$q_{rel} = q + q_g \tag{4.14}$$
$$= q + \dot{w}_g/V_e \tag{4.15}$$

The variations in trim airspeed are assumed to be small according to small disturbance theory and are therefore held constant. The vertical gust velocity (w_g) and its derivative with respect to time are presented in Equation 4.16

$$\begin{aligned} w_g &= W_g\left(\frac{1}{2}\right)(1-\cos(\omega t)) \\ w_g &= W_g\left(\frac{1}{2}\right)\left(1-\cos\left(2\pi\left(\frac{V_e}{\lambda}\right)t\right)\right) \\ \dot{w}_g &= \left(\frac{W_g \pi V_e}{\lambda}\right)\sin\left(2\pi\left(\frac{V_e}{\lambda}\right)t\right) \end{aligned} \tag{4.16}$$

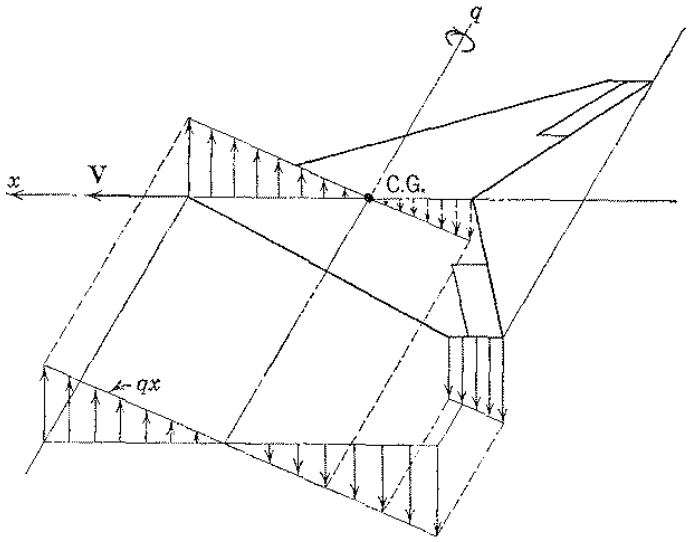

Figure 4.12: Wing velocity distribution due to pitching. (Etkin, 1972:270)

Equation 4.14 is valid for long wavelengths only. The wavelength of the vertical gust inputs for all the simulations was taken as 50m and $W_g = 2$ m/s.

The vertical gust was introduced after 1 second of simulation time for all the simulations that were performed on the different aircraft models.

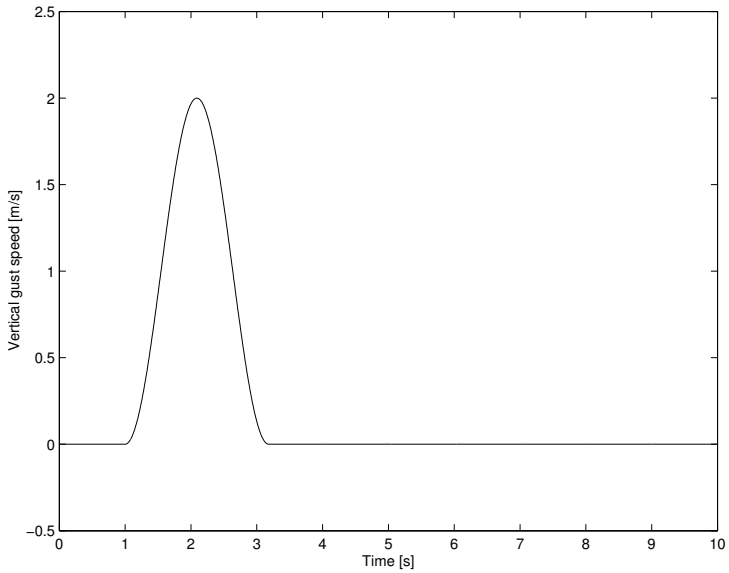

Figure 4.13: The $1 - \cos$ vertical gust disturbance. (Mönnich & Dalldorff, 1993)

4.8.2 Elevon Step Input

A step input was used for the pitch control response simulations that were performed in this study. The input was introduced after 1 second for all simulations. The step input that was used had a magnitude of negative 1 degree elevon deflection (δ_e). The sign convention followed throughout the study means that the negative elevon deflection (elevon up) causes an aircraft nose up rotation.

The boundary layer around the elevon is not modeled in the simulation and as a result no control stick dead band is simulated. The simulation results show that the aircraft responds immediately to the control input because of this. This was done to investigate the effect of control input in isolation with regards to the effects of other dynamics.

Chapter 5

Gull-Wing Sensitivity Analysis

The results and conclusions of the gull-wing configuration handling quality study are dependent on the values of the input parameters of the aircraft model. The exact magnitudes of these parameters have not been measured, but were estimated by calculation. In order to have sufficient confidence in the conclusions of this study, it was required to gauge the effect of estimation errors on the predicted pitch response (and hence, handling qualities) of the aircraft. The sensitivity study was used to assess the confidence level of the predicted aircraft pitch responses and as a result, the conclusions presented in this study.

The static margin, damping coefficient, pitch inertia and control authority were identified in Section 4.5.3 as the most influential variables with respect to pitch dynamics. The CG can be varied (within practical limits) on an actual aircraft to achieve a certain static margin. The static margin can then be verified by measurements, but the remaining variables cannot be altered as easily. The accuracy with which these parameter values are predicted is therefore important. As a result, the sensitivity study was focussed on the parameters other than static margin.

5.1 Baseline and method

The Exulans mathematical model was used for the analysis. The sensitivity study was performed on an Exulans with 30° outboard wing sweep angle and a static margin of 10.7% at 30° wing sweep. This applies to all simulation results presented in this chapter. The study comprises of time domain simulations with a gust disturbance after 1 second. The gust disturbance is as documented in Section 4.8. The parameter values of the Exulans mathematical model were varied over the following ranges for the purpose of the sensitivity study:

- The pitch inertia was varied from -10% to +10% with respect to the baseline. This narrow range was chosen for pitch inertia since it can be determined within reasonable accuracy prior to the construction of an aircraft. It can also be fine tuned (within practical limits) once an aircraft is built.

- The pitch damping coefficient was varied from -50% to +50% with respect to the baseline. This range was chosen with the guidance of the C_{M_q} benchmark study (Appendix E). The benchmark work indicated that pitch damping estimated with a VLM differs by as much as 50% from the actual value.

- The elevon control authority was varied from -20% to +20% with respect to the baseline. This range was chosen with the guidance of the $C_{M_{\delta_e}}$ benchmark study (Appendix F). The benchmark work indicated that the pitch control authority estimated with a VLM differs by as much as 20% from the actual value.

The baseline parameter values of the sensitivity analysis are presented in Table 4.4 under the gull-wing column. The parameter values were varied individually during each simulation, while all the other parameters were kept at the baseline values. All time domain simulations were performed with a true airspeed speed of 82.4 km/h, which is the design trim speed at 30° outboard wing sweep according to Crosby (2000). The simulations of the

sensitivity study were performed with a time step of 0.01 seconds (i.e., samples at 100 Hz). The justification for this choice of time step size is presented in Appendix D.

The modal parameters (natural circular frequency and damping) were also calculated for the baseline model and the different models of the sensitivity study. The sensitivity with respect to a certain parameter was evaluated by visual inspection of the time domain simulation results and the change in the modal parameter values from the baseline. The baseline values for the sensitivity study and the modal parameters are presented in Table 5.1.

Table 5.1: Baseline parameter values used for the sensitivity study (30° sweep gull-wing configuration with a 10.7% static margin at 30° sweep).

Parameter	Unit	Baseline value
I_{yy}	kg·m^2	28.2
C_{M_q}	/rad	-2.55
$C_{M_{\delta_e}}$	/rad	-0.533
$\omega_{n_{sp}}$	rad/s	10.28
ζ_{sp}		0.592
ω_{n_p}	rad/s	0.49
ζ_p		0.075

The modal characteristics were estimated using numerical techniques (theory presented in Appendix B), as opposed to the analytical approximations of Section 4.5. The numerical techniques are more accurate since fewer assumptions are made in the estimation than in the case of the analytical answer. The numerical technique uses a linearised model associated with some trim condition to calculate the modal characteristics. A comparison between the two methods is presented in Table 5.2. The phugoid mode frequency approximation does not show good agreement with that of the numerical method. The phugoid damping approximation was not calculated because the approximation is known to be inaccurate. The short period mode approximation shows better correlation with the numerical method. These results are in agreement with the discussion on the accuracy of the approximations as presented in Stevens & Lewis (1992:210).

Table 5.2: Comparison of modal characteristics estimated by numerical methods and analytical approximations (30° sweep gull-wing configuration with a 10.7% static margin at 30° sweep).

Parameter	Unit	Numerical	Analytical
$\omega_{n_{sp}}$	rad/s	10.28	8.44
ζ_{sp}		0.59	0.44
ω_{n_p}	rad/s	0.49	0.10

5.2 Pitch Axis Inertia

The results of the pitch inertia sensitivity study simulations are presented in Figures 5.1 to 5.4.

The pitch inertia of the Exulans is low compared to its roll and yaw inertia. The pitch inertia was varied from 10% below to 10% above the baseline value of 28.2 kg·m^2 (the 30° sweep value at 10.7% static margin). The inertia changes had a small effect on pitch rate and attitude. The phugoid mode is almost unaffected by a change in inertia, but the short period mode is affected by the change. This can be seen from the change in the small 'hump' (left side of the graph in Figure 5.4) of the attitude response. The inertia changes had a noticeable effect on angle of attack dynamics.

The sensitivity of pitch inertia with respect to the natural frequency and damping ratios of the aircraft modes is shown in Tables 5.3 and 5.4. The 10% change in pitch inertia has no effect on phugoid natural frequency and a small effect on phugoid and short period damping ratio. It causes a 5% change in short period natural frequency. The effect of this on handling qualities can be assessed by using the thumbprint criterion (see Section 3.3). If one bears in mind that the lines on the thumbprint graph do not represent absolute borders, but rather smooth transitions, it can be argued that a 0.6 rad/s (or 5% from the baseline) change in short period natural frequency does not represent a drastic change in handling qualities. Such a difference would not have the effect of changing the pilot opinion rating from 'Satisfactory' to 'Poor'. The estimation error of inertia can be contained within 10% and therefore the baseline value of inertia can be used for all handling qualities

analyses in this study.

Table 5.3: Sensitivity of circular natural frequency with respect to pitch inertia.

Inertia [% change]	ω_{n_p}	[% change]	$\omega_{n_{sp}}$	[% change]
-10	0.493	No change	10.842	5.44
Baseline	0.493		10.283	
10	0.493	No change	9.808	-4.62
Average sensitivity [%/%]		None		-0.50

Table 5.4: Sensitivity of damping ratio with respect to pitch inertia.

Inertia [% change]	ζ_p	[% change]	ζ_{sp}	[% change]
-10	0.076	1.60	0.598	1.06
Baseline	0.075		0.592	
10	0.074	-1.47	0.587	-0.79
Average sensitivity [%/%]		-0.15		-0.09

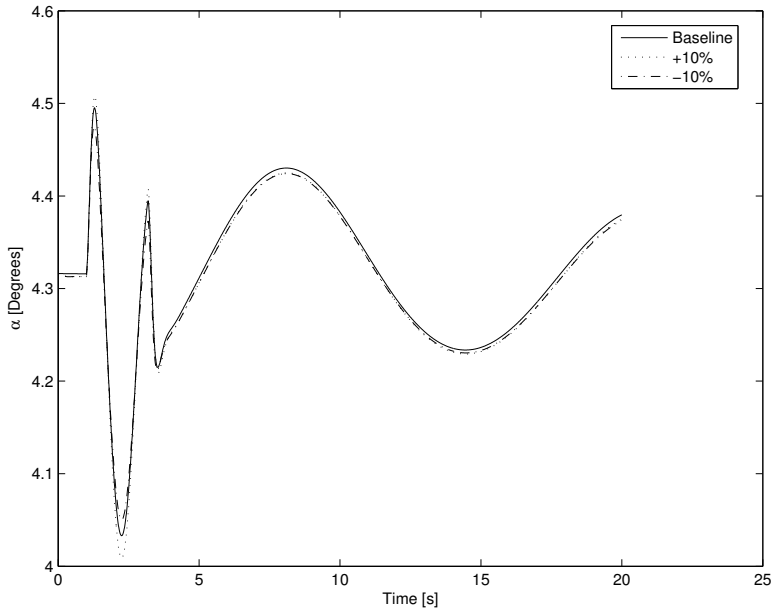

Figure 5.1: Gust response of aircraft angle of attack (α) at different pitch axis inertias.

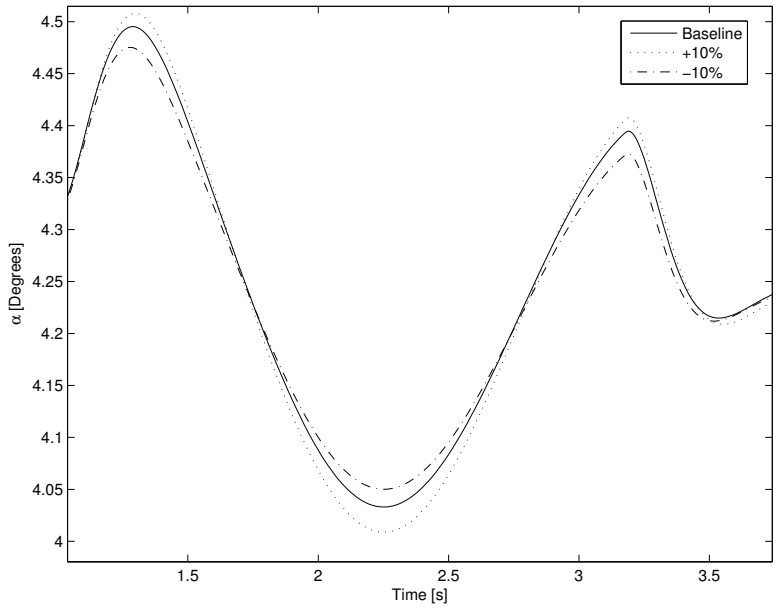

Figure 5.2: Magnified gust response of aircraft angle of attack (α) at different pitch axis inertias.

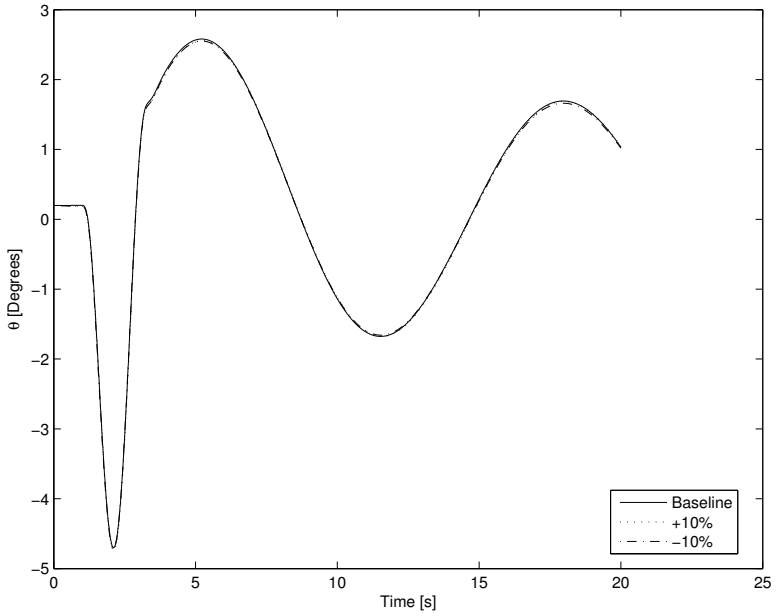

Figure 5.3: Gust response of aircraft attitude (θ) at different pitch axis inertias.

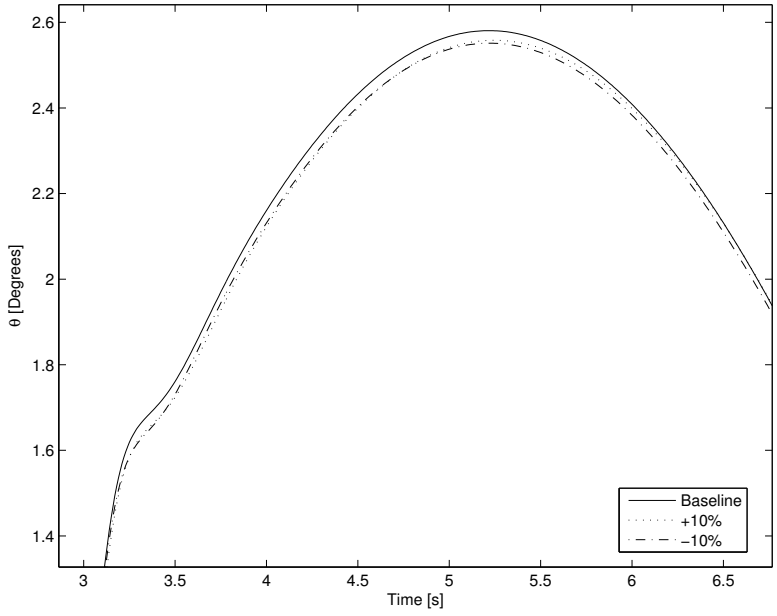

Figure 5.4: Short period gust response of aircraft attitude (θ) at different pitch axis inertias.

5.3 Pitch Damping Coefficient

The pitch damping coefficient changes significantly with respect to CG in the case of a tailless aircraft. In the case of a tailed aircraft the distance from the tail to the centre of gravity and the lift curve slope of the tailplane are the most important parameters in the calculation of the aerodynamic damping coefficient of the aircraft. Changes in centre of gravity are usually small as a percentage of the distance to the tail and hence the change in damping coefficient due to a centre of gravity change is also small. This is not the case for a tailless aircraft, since its damping ratio is a function of the planform of the main lifting surface. A change in the CG position therefore has a significant effect on the damping coefficient of a tailless aircraft.

Simulations with the gull-wing model were performed where the static margin was held constant at the baseline configuration of 10.7%. The pitch inertia was also held constant. The pitch damping coefficient was varied by 50% above and below the baseline. The results of these simulations are presented in Figures 5.5 and 5.6. The natural frequency and damping ratio of the aircraft modes were calculated for the different aerodynamic damping cases. These results are presented in Table 5.5 and 5.6.

The results of the sensitivity study show that a 50% change in the aerodynamic damping coefficient causes a larger than 7% change in phugoid and short period frequency. The change in damping has a significant effect on damping ratio for both the short period (larger than 19% change) and the phugoid (larger than 14% change) damping ratio. When the thumbprint graph (Figure 3.1) is examined, it can be seen that such a change in short period damping ratio can have a significant effect on pilot opinion. The inaccuracy in the calculation of the value of the damping ratio is not so severe that it will invalidate the conclusions produced by the handling quality study. A 50% change in damping ratio will not change the pilot opinion result to the extent that the analysis is invalid. Appendix E showed that a 50% inaccuracy is a worst case scenario for C_{M_q}. It is more likely for the case of the Exulans (with forward and backward wing sweep) that the inaccuracy will be 20%. It can therefore be concluded that the uncertainty in the aerodynamic

damping ratio is large enough for it to be a variable in the handling quality investigation, but that C_{M_q} should be varied by 20% above and below the baseline.

Table 5.5: Sensitivity of natural frequency with respect to pitch damping coefficient.

Damping [% change]	ω_{n_p}	[% change]	$\omega_{n_{sp}}$	[% change]
-50	0.540	9.68	9.375	-8.83
Baseline	0.493		10.283	
50	0.456	-7.55	11.121	8.16
Average sensitivity [%/%]		-0.17		0.17

Table 5.6: Sensitivity of damping ratio with respect to pitch damping coefficient.

Damping [% change]	ζ_p	[% change]	ζ_{sp}	[% change]
-50	0.064	-14.17	0.458	-22.72
Baseline	0.075		0.592	
50	0.086	14.30	0.709	19.76
Average sensitivity [%/%]		0.28		0.42

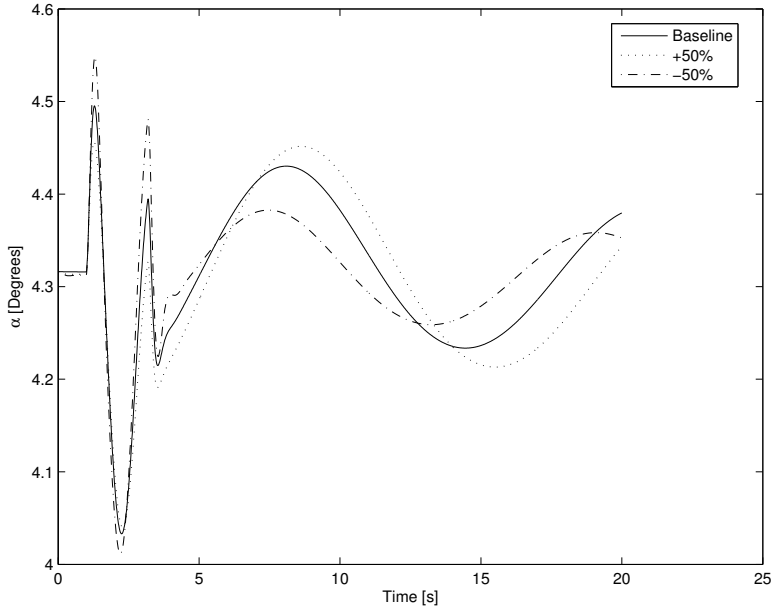

Figure 5.5: Gust response of aircraft angle of attack (α) at different damping coefficient values.

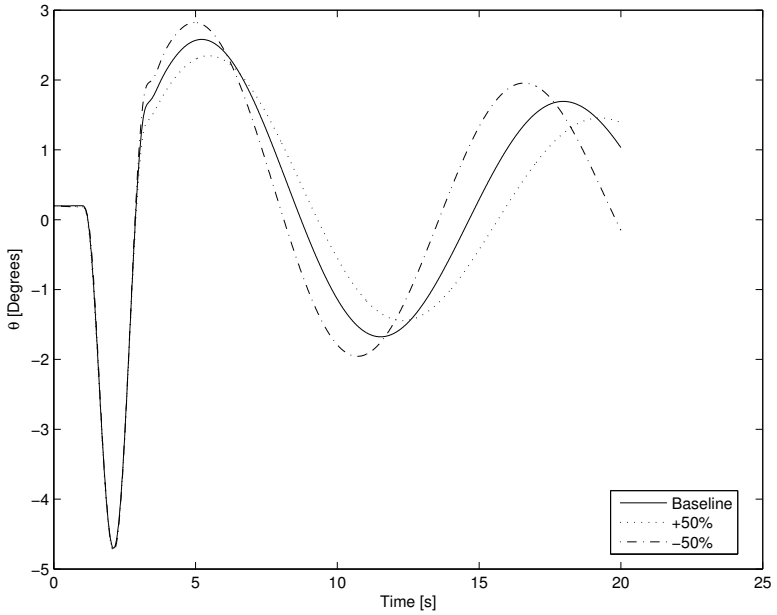

Figure 5.6: Gust response of aircraft attitude (θ) at different damping coefficient values.

5.4 Elevon Control Authority

The sensitivity of the aircraft pitch attitude response to varying degrees of control authority was investigated with time domain simulations. This was done to assess the impact of the estimation error of the $C_{M_{\delta_e}}$ parameter on handling qualities. $C_{L_{\delta_e}}$ is predicted with sufficient accuracy (see Appendix F) and therefore the sensitivity of the aircraft response with respect to this parameter was not investigated.

Control authority (the magnitude of $C_{M_{\delta_e}}$) of the elevons influences the magnitude of the response to an elevon control input. Control authority must not be confused with the gearing to the elevon, since it is a function of the control surface aerodynamics. The control authority can be modelled as a gain in the aircraft attitude control loop.

Three cases of control authority were investigated in the sensitivity analysis. The baseline control authority as presented in Table 4.4 for an aircraft with an outboard wing sweep of 30° was used in one simulation. Pitch inertia, static margin and aerodynamic damping were kept constant in simulations while control authority was varied. For one simulation the control authority was 20% higher than the baseline and for the other the control authority was 20% lower than the baseline. This variance in the control authority corresponds to the estimation error of the parameter (Appendix F). The lift due to elevon deflection or $C_{L_{\delta_e}}$ was kept at the baseline value for all simulations.

The simulations were performed with a -1° elevon step input at 1 second after the start of the simulation. The simulation results are presented in Figures 5.7 to 5.8.

The simulation results show that the natural frequencies and damping ratios of the aircraft's dynamic modes are unchanged by different control authorities. Control authority has a significant influence on the magnitude of the pitch attitude of the aircraft following a control input. The effect on the magnitude is shown in Table 5.7. These results show that the magnitude changes by 1% (on average) from the baseline for every 1% change in the control authority. This is a significant change and therefore the estimation

error for this parameter will have a definite effect on handling qualities. The $C_{M_{\delta_e}}$ parameter therefore has to be varied by 20% from the baseline for handling quality studies involving control authority.

Table 5.7: Sensitivity of pitch attitude (θ) amplitude with respect to $C_{M_{\delta_e}}$.

$C_{M_{\delta_e}}$ [% change]	Maximum θ amplitude [°]	[% change]
-20	4.910	-21.54
Baseline	6.258	
20	7.645	22.16
Average sensitivity [%/%]		1.09

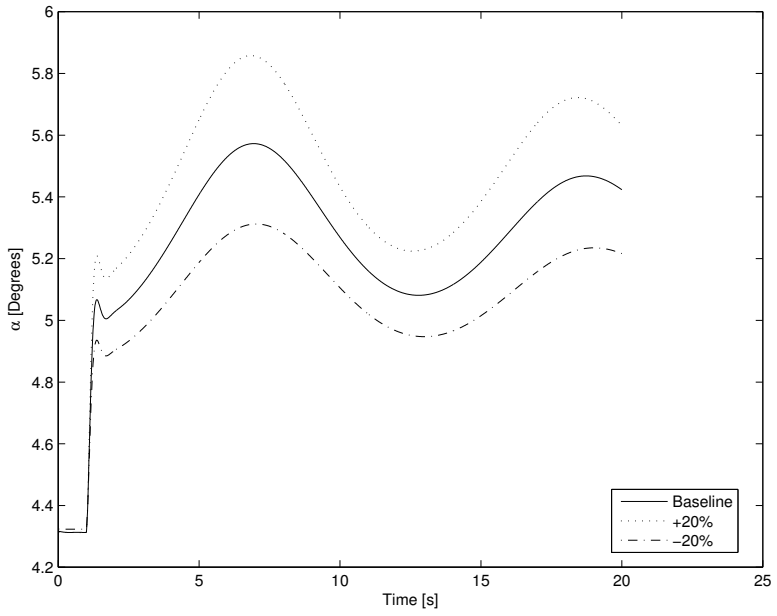

Figure 5.7: Control input step response of aircraft angle of attack (α) at different control authority aircraft configurations.

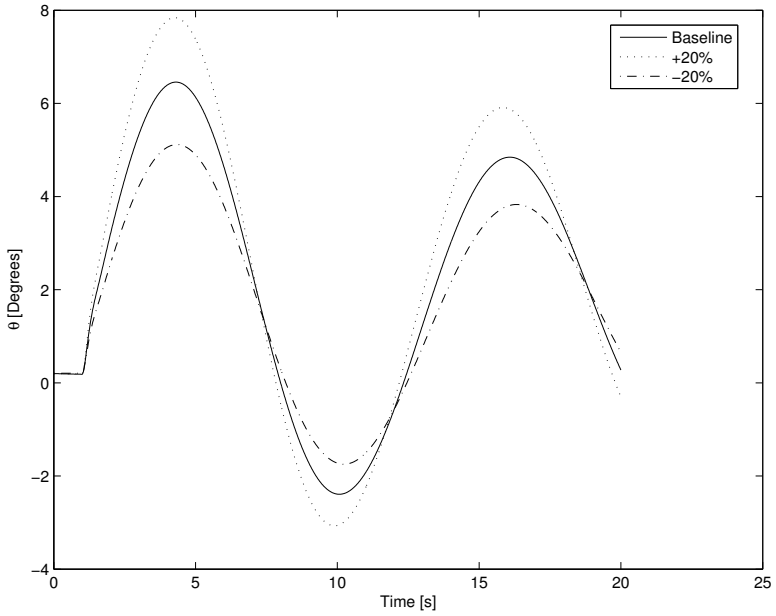

Figure 5.8: Control input step response of aircraft attitude (θ) at different control authority aircraft configurations.

5.5 Conclusion of Sensitivity Analysis

The estimation error of pitch inertia (for an aircraft the size of the Exulans) is not significant enough to have a noticeable effect on the outcome of a handling quality analysis of the gull-wing configuration. The inertia will therefore not be a variable in the handling quality analyses presented here.

Aerodynamic pitch damping has a significant influence on the aircraft attitude, natural frequency and damping ratio of the aircraft modes. The C_{M_q} parameter value will be varied by 20% in the handling quality study because this is the estimation error of this parameter. The effects of this error on handling qualities need to be assessed.

Elevon control authority has a significant influence on aircraft attitude following a control input. The estimation error of this parameter is 20% above and below the baseline value. The handling quality study will therefore include this variance to investigate the effects of this estimation error.

The effects of only static margin, aerodynamic pitch damping and elevon control authority were investigated in the handling quality analyses documented in subsequent chapters. The influence of pitch inertia is not investigated further. This is because it does not have a sufficiently significant effect on the dynamic modes and because it can be estimated with reasonable accuracy.

Chapter 6

Time Domain Analysis

Time domain handling quality analyses of the Exulans are presented in this chapter. The handling characteristics of the gull-wing configuration (using the Exulans as representative example) were investigated by means of step elevon control input simulations and gust response simulations. The C-star handling quality criterion was applied to the simulation results. The Exulans gust responses were also compared to those of an existing tailed glider (ASW-19), an existing tailless glider (SB-13 Arcus) and a powered aircraft (Piper Cherokee) in gliding (engine off) flight.

6.1 C-star Criterion Analysis

The C-star analysis method is explained in Section 3.5. This type of analysis was applied to different combinations of sweep and static margin of the Exulans. The different cases of the gull-wing configuration that were analysed are defined in Appendix I.1.

The results of one set of C-star analyses are presented here (Figure 6.1) and the rest are presented in Appendix I.5. Figure 6.1 is presented as an arbitrary sample of a C-star analysis result.

The following conclusions can be made from the C-star analysis:

A response is favourable with respect to the C-star criterion when it falls inside the C-star boundaries and when it does not exhibit a lightly

damped oscillation. The C-star response of most of Exulans cases that were investigated fall outside the favourable C-star boundaries. This is especially evident during the first 0.6 seconds of the normalised response. After the initial 0.6 seconds most of the responses fall within the C-star boundaries. Almost none of the cases exhibited a lightly damped oscillation, as the steady state C-star response converges quickly. It may therefore be concluded that the initial response of the Exulans to a step response is unfavourable. The handling qualities improve after the initial response according to this method.

Static margin and outboard wing sweep have the largest influence on handling qualities according to the C-star analysis. This is evident from Figures I.51 and I.52: The 24° sweep cases almost fall within the 'powered landing' (thick dashed line) C-star boundaries, while the 30° cases have a very high initial overshoot outside the C-star boundaries. The lower sweep cases seem to have more favourable handling qualities according to this observation.

The estimation error of control authority has a significant effect on C-star handling qualities at low sweep angles (24°). Higher moment control authority has the consequence of a large initial overshoot as can be seen in Figure 6.1. This figure shows that the low control authority case falls completely within the 'powered landing' boundaries, while the high and baseline cases have an initial overshoot. Figure I.54 shows that the effect of the estimation error is of lesser importance at 30° sweep since all the cases fall outside the acceptable boundaries. The general trend is that less moment control authority leads to a more favourable C-star handling quality evaluation.

Figure I.55 shows the effect on the estimation error of the aerodynamic damping coefficient on the handling qualities as predicted by the C-star method. This results indicate that damping does have an influence on handling qualities, but that it is not significant.

The C-star response has an important conclusion with regards to the CG position of the pilot relative to that of the aircraft CG. The third term of Equation 3.3 tends to translate the C-star response to the right. This means that pitch acceleration and the distance l have a significant effect on the handling qualities. l is the distance from the aircraft CG to the acceleration

sensory organ of the pilot (the ear). It is advisable for the aircraft designer to minimise this distance, because if the pilot is far from the CG he or she will experience unpleasant pitch accelerations, leading to poor handling qualities. In the case of the gull-wing configuration this is best achieved by placing the pilot on the aircraft CG if other design considerations permit this. The distance l is zero with an upright sitting pilot coincident with the aircraft CG. l is equal to the distance from the pilot hip to the head for a pilot in the prone position (with the hip coincident with the aircraft CG).

The C-star analysis method has some limitations, which have an influence on the value of the conclusions made from it:

- Statically unstable and marginally stable cases of sweep and static margin (eg. configurations 45 and 54) can not be evaluated using the C-star method. The reason for this is that stick fixed simulations results are used to calculate the C-star response. The stick fixed simulations are divergent for marginally stable and unstable cases and therefore the C-star criterion cannot be applied.

- The effect of a pilot can not be evaluated with the C-star method as in the case of the Neal-Smith method (see Section 7.4).

- The C-star criterion is more difficult to interpret than other handling qualities criteria. If a response falls outside the boundary, it does not give a good indication of how the response could be improved. This is one of the deficiencies of the method as described in Neal & Smith (1970).

These limitations make it necessary to evaluate the conclusions of the C-star method together with other handling quality analysis methods. This will be done in Section 7.5 where the C-star results will be compared with frequency domain analysis results. Without comparison to other methods, the general conclusion of the C-star method is that the Exulans will have marginally acceptable handling qualities during landing (associated with low sweep angles) and unacceptable handling qualities during rapid manoeuvring.

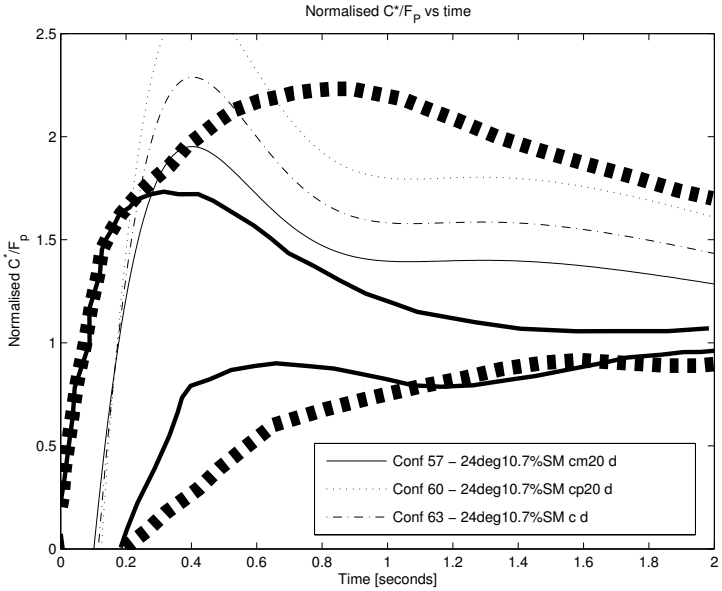

Figure 6.1: The C-star analysis for all control authority variations at 24° sweep with the baseline aerodynamic damping at a 10.7% (at 30°) static margin configuration. (Configurations 57, 60, 63)

6.2 Comparative Simulations

The gust response of the Exulans was compared with a similar class tailless aircraft and a similar class tailed aircraft. As a matter of interest, the Exulans response was also compared to the response of a powered aircraft in gliding flight. The Piper Cherokee was chosen as a representative powered aircraft.

The SB-13 was chosen as a representative tailless aircraft. This aircraft is a standard class glider and was developed in the 80's and 90's.

The ASW-19 was chosen as a representative conventional aircraft with which the Exulans can be compared. This aircraft is known to have very good handling characteristics as well as being a high performance glider.

'Stick-fixed' simulations were used to compare the different aircraft types. The time responses of the different aircraft were plotted on the same axes and evaluated.

A similar study has been performed which involved the SB-13 and the ASW-19 (Mönnich & Dalldorff, 1993). This study found that the gust

responses were important in determining the relative handling qualities of the two aircraft. A $1 - \cos$ gust disturbance was used in all simulations. The gust model is discussed in Section 4.8.1.

Three Exulans layouts were used as part of the comparative study. A low outboard wing sweep configuration (24°, static margin of 15% at 30°) and a high wing sweep configuration (36°, static margin of 5% at 30°) were used. A medium sweep (30°, static margin of 2% at 30°) case was also included in the analysis. The low and high sweep Exulans models have a static margin of 10% at the particular sweep angle. The SB-13 and the ASW-19 models used in the simulations also have static margins of 10%. The Exulans has lower trim design speeds than the other aircraft used in the comparative study. This makes a direct comparison between all the aircraft difficult and limits the analysis to a qualitative evaluation of the time responses. Both the ASW-19 and the SB-13 were trimmed at 120km/h for the simulations. The Exulans models were trimmed at 55.3, 82 and 109.4km/h for the 24°, 30° and 36° sweep cases respectively.

The results of the comparative study are presented in Figures 6.2 to 6.8. These figures show the attitude response to a $1 - \cos$ wind gust disturbance. The short period attitude reponses of Figure 6.3 were translated vertically (to change the reference attitude to zero degrees) and superimposed for comparison purposes. The result is presented in Figure 6.4. The same superposition and translation was done with the results of Figure 6.6 and the results are presented in Figure 6.7.

The following observations can be made from the results presented in this section:

- The SB-13 has a weakly damped short period oscillation. The short period oscillation is the 'bump' between 1.5 and 2 seconds after the start of the simulation. This may contribute to poor handling characteristics.
- The ASW-19 and Cherokee have strongly damped short period modes, to the point that it is not visible on the attitude response of the aircraft.
- The Exulans has a visible short period response (the 'bump') for the low (24°) and high (36°) sweep cases. Both these cases have a 10%

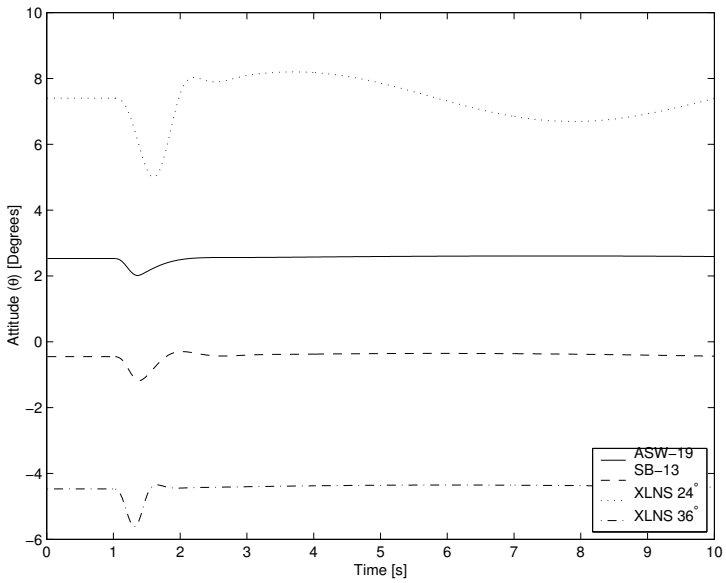

Figure 6.2: The response in aircraft attitude (θ) to a $1 - \cos$ gust, for the ASW-19, the SB-13, the 24° (15% static margin) and the 36° (5% static margin) sweep Exulans.

static margin at these sweep angles. The 30° sweep case has a 2% static margin. It has a strongly damped short period mode like the ASW-19 and the Cherokee. The 30° case has low static margin (2%) while the other cases have high static margin (10%). Since the low static margin case has a time response similar to those aircraft with favourable gust handling qualities, it is concluded that the Exulans has improved gust handling qualities at low static margins.

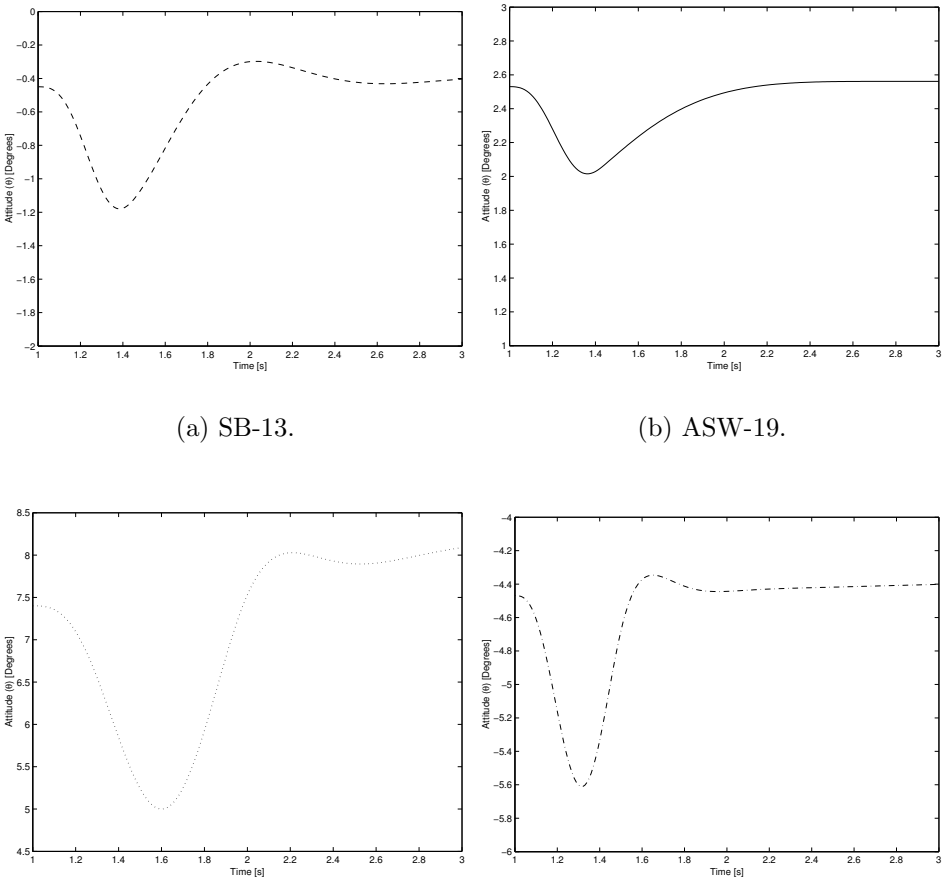

(a) SB-13.

(b) ASW-19.

(c) Exulans 24° sweep and 15% static margin.

(d) Exulans 36° sweep and 5% static margin.

Figure 6.3: Aircraft attitude (θ) to a $1 - \cos$ gust, during the period of the introduction of the gust, for the ASW-19, the SB-13 and Exulans.

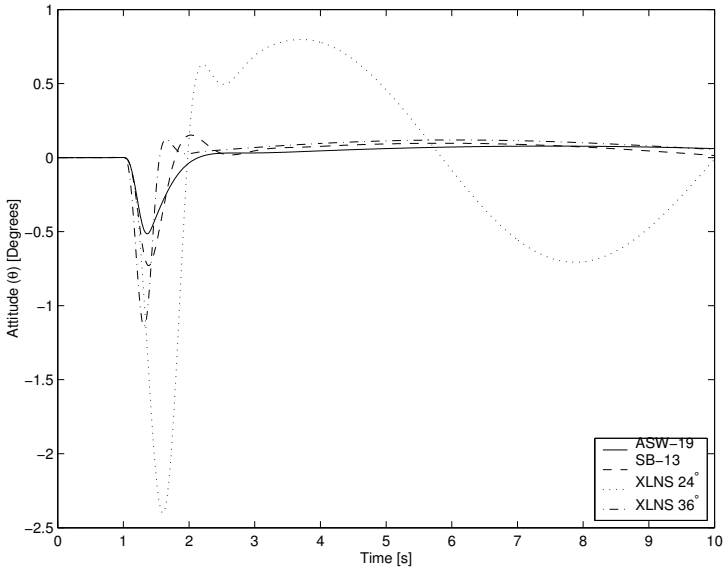

Figure 6.4: The superimposed response in aircraft attitude (θ) to a $1-\cos$ gust, for the ASW-19, the SB-13, the 24° (15% static margin) and the 36° (5% static margin) sweep Exulans.

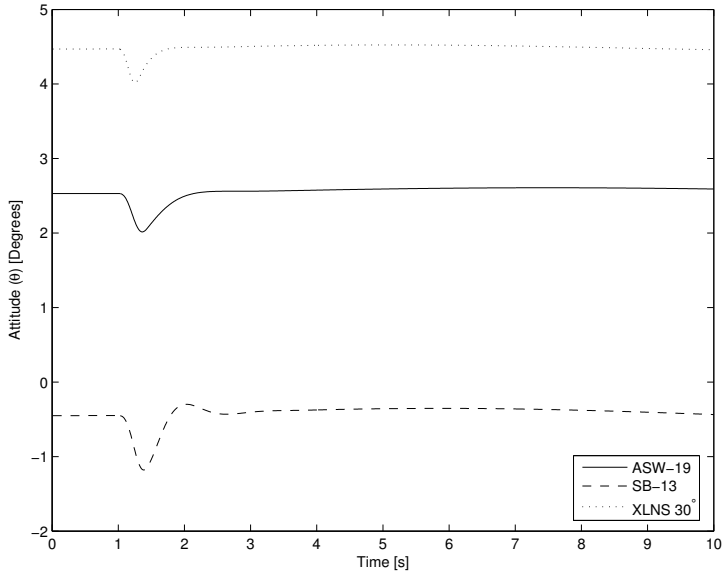

Figure 6.5: The response in aircraft attitude (θ) to a $1-\cos$ gust, for the ASW-19, the SB-13 and the 30° (2% static margin) sweep Exulans.

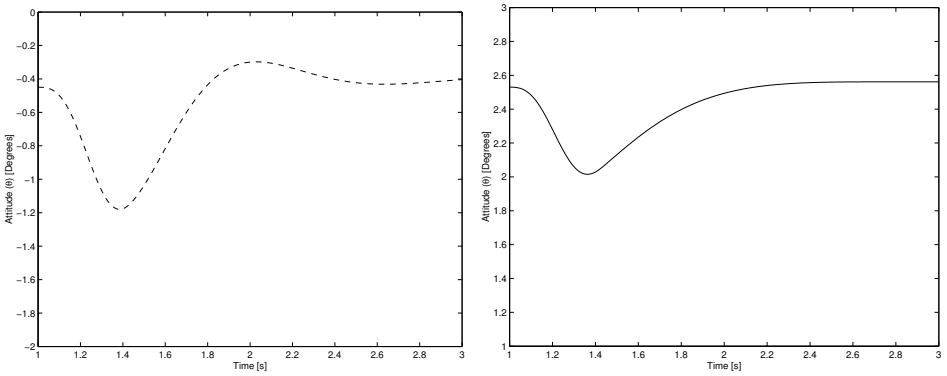

(a) SB-13.

(b) ASW-19.

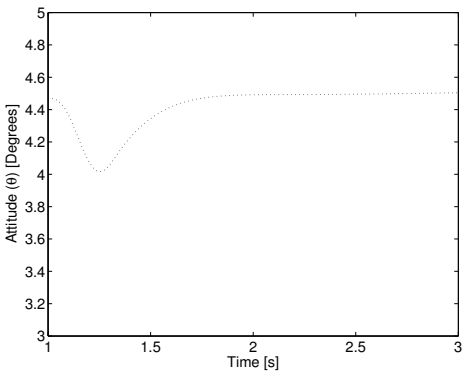

(c) Exulans 30° sweep and 2% static margin.

Figure 6.6: Zoomed aircraft attitude (θ) to a $1 - \cos$ gust, for the ASW-19, the SB-13 and Exulans.

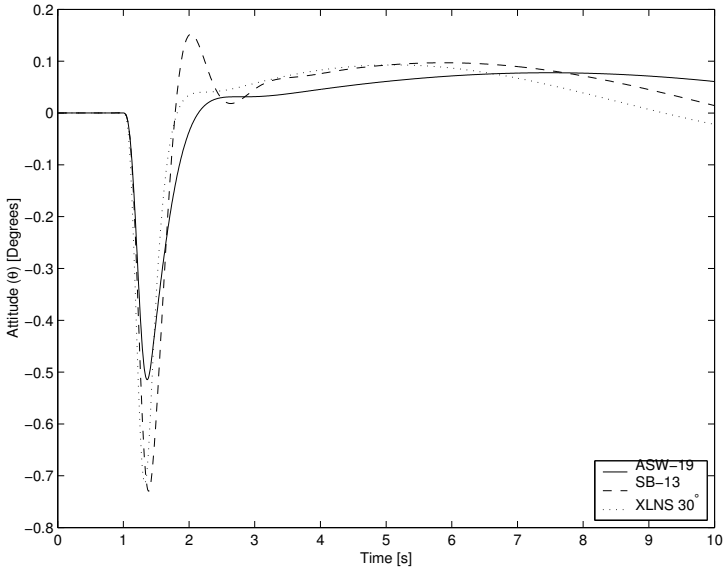

Figure 6.7: The superimposed response in aircraft attitude (θ) to a $1 - \cos$ gust, for the ASW-19, the SB-13 and the 30° (2% static margin) sweep Exulans.

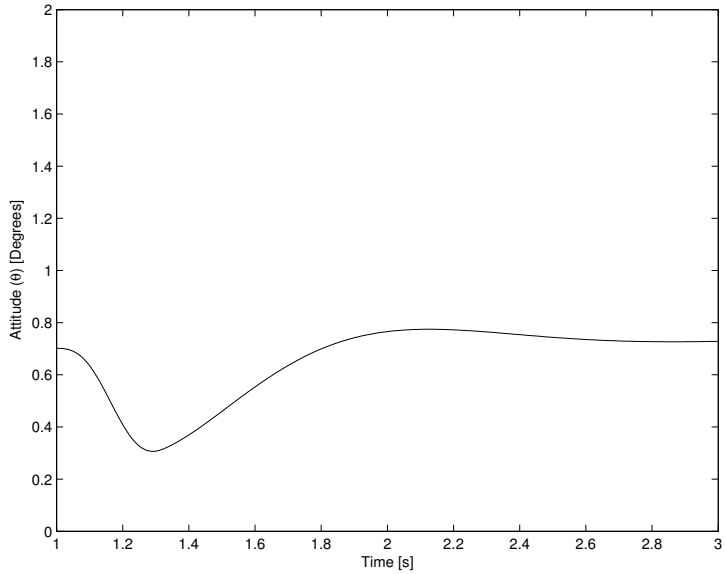

Figure 6.8: The response in aircraft attitude (θ) to a $1 - \cos$ gust, for the Piper Cherokee (gliding flight).

Chapter 7

Frequency Domain Analysis

Many of the analysis techniques listed in Chapter 3 are frequency domain techniques. The gull-wing configuration (with the Exulans as example) handling qualities were analysed by using these techniques. The results are presented here.

7.1 Thumbprint Criterion Analysis

The thumbprint criterion analysis methodology is presented in Section 3.3. This methodology was applied to the Exulans.

The handling qualities of different cases of sweep and static margin of the gull-wing configuration were investigated with the thumbprint analysis method. The cases were numbered for ease of reference. The numbering system is presented in Table H.2 of Appendix H. Different cases of sweep angle and static margin were investigated with the thumbprint criterion. The aerodynamic damping was kept at the baseline value for all cases. The 'baseline' values are defined as the parameter values presented in Section 4.7. The analysis was performed at four different values of static margin for the following cases:

- 20° outboard wing sweep (configurations 3, 6, 9, 12).
- 24° outboard wing sweep (configurations 15, 18, 21, 24).

- 30° outboard wing sweep (configurations 27, 30, 33, 36).
- 36° outboard wing sweep (configurations 39, 42, 45, 48).

The damping ratios and natural frequencies of the short period mode of the different cases were calculated by means of eigenvalue analysis (see Appendix B) and plotted on the short period opinion contours (the 'thumbprint' graph) of O'Hara (1967).

A typical result of the eigenvalue analysis is shown in Figure 7.1. The remainder of the results are included for reference purposes in Appendix J.1. The pilot opinions of different short period regions are shown as text labels. The short period natural frequencies and damping ratios of three configurations are plotted as circles. The number of each case or configuration (according to Table H.2) is shown as a text label next to the circle. The region of best handling qualities is indicated with a diamond shape on the plot. The damping ratio of the phugoid mode is also included on the plot, next to the aircraft configuration number.

Configurations 3, 6 and 15 are statically unstable. As a result of this, the thumbprint criterion cannot be applied to these cases. These configurations have to be analysed by means of another method such as the Neal-Smith method or a pilot in the loop simulation.

The thumbprint analysis results (Figure 7.1 and Figures J.1 to J.3) show that the Exulans will have the most favourable handling qualities at low static margins and at low sweep angles. From these results, it can be observed that configurations 9 and 18 are closest to the most favourable point on the thumbprint graph. These configurations have low static margin and wing sweep. Configurations 27 and 39 (see Figures J.2 and J.3) do not have good handling qualities according to the thumbprint criterion, but these cases have more favourable handling qualities than the other, higher static margin cases presented on the same graphs. The thumbprint analysis indicated that the high sweep and high static margin cases of the Exulans will be prone to pilot induced oscillation or PIO.

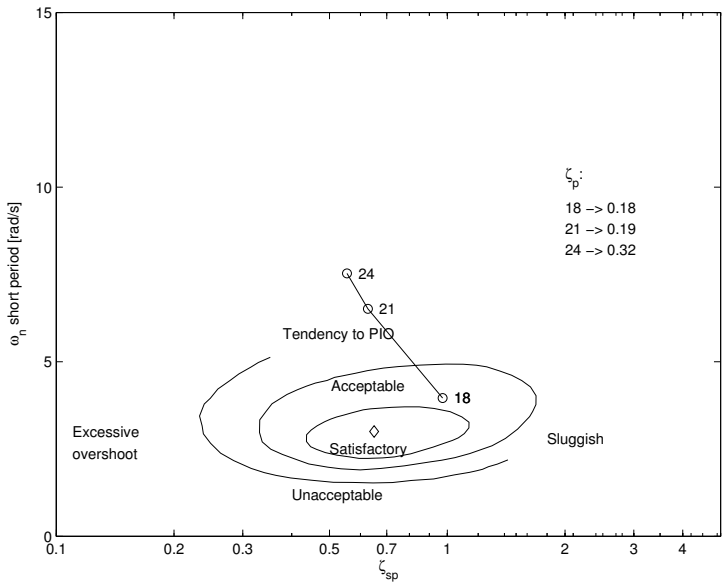

Figure 7.1: Thumbprint analysis for 24° outboard wing sweep, at various static margin cases, with the baseline aerodynamic damping. (Configuration nr. 18 is 24° 5% d, Configuration nr. 21 is 24° 10.7% d, Configuration nr. 24 is 24° 15% d, as per Table H.2)

7.2 Military Flying Qualities Specifications

Flying quality requirements are presented in MIL-F-8785C (1980). The methodology of the Military Flying Qualities analysis is presented in Section 3.4. The cases of the Exulans used for the thumbprint analysis were also analysed by means of the Military Flying Qualities analysis.

The results of the analysis are presented in Figure 7.2 and Figures J.4 to J.6.

The military flying qualities criteria require that the phugoid damping ratio $\zeta_p \geq 0.04$ for Level 1 flying qualities. This requirement was presented on the first line of Table 3.1. The phugoid damping ratio was presented as text on the graphs in Figure 7.1 and Figures J.1 to J.3. Configuration 18, for example has a phugoid damping ratio of 0.18 according to Figure 7.1. This is larger than the required minimum of 0.04. All the other Exulans cases that were investigated have phugoid damping ratios larger than 0.04 and therefore

satisfy Level 1 flying qualities with respect to this requirement.

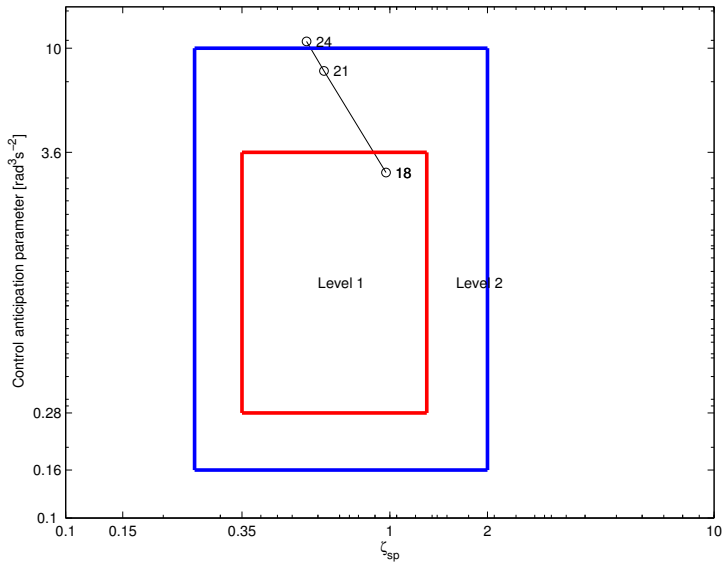

Figure 7.2: *CAP* for 24° outboard wing sweep, at various static margin cases, with the baseline aerodynamic damping. (Configuration nr. 18 is 24° 5% d, Configuration nr. 21 is 24° 10.7% d, Configuration nr. 24 is 24° 15% d, as per Table H.2)

Configuration 18 had Level 1 qualities with respect to the *CAP*. This configuration had 'acceptable' handling qualities according to the thumbprint criterion (see Figure 7.1). All other configurations had Level 2 flying qualities. This means that these configurations will have adequate flying qualities, with some increased pilot workload when compared to configuration 18.

When examining Figure 7.2 it can be observed that configuration 18 has better flying qualities than configuration 24, since the former is further away from the centre of the Level 1 bounding box. This indicates that lower static margins have more favourable handling qualities, since configuration 18 has a lower static margin than 21 or 24. The same trend can be observed with respect to wing sweep angle. The higher the wing sweep angle becomes, the poorer the handling qualities become. These results agree with the thumbprint analysis.

7.3 Shomber-Gertsen Analysis

This analysis method is presented in Section 3.6. The strength of the Shomber-Gertsen analysis method is that the handling qualities of an aircraft can be analysed at different airspeeds.

The different cases of Section I.1 of the pitch control input simulations were analysed using the Shomber-Gertsen method and the numbering system presented in Tables H.1 of Appendix H was used.

In order to vary the value of n_α, the above-mentioned cases were analysed with varying true airspeed (V) values. The speed was varied by 20% above and below the design trim speed.

Sample results from the analysis are presented in Figures 7.3 and 7.4. The remainder of the results are presented in Appendix J.3. The following observations (grouped per case set) can be made from the results of the analysis:

Group one (Static margin variations, 30° sweep, baseline aerodynamic damping, baseline control authority or Configurations 81, 90, 99, 108). The low speed case and the design speed had a $n_\alpha < 15$ g/rad and the high speed case had a $n_\alpha > 15$ g/rad. The cases with $n_\alpha < 15$ g/rad had acceptable to satisfactory handling characteristics. The cases with $n_\alpha > 15$ g/rad had unsatisfactory handling qualities. This indicates that speeds higher than the design speed will potentially have unsatisfactory handling qualities according to the Shomber-Gertsen method. This must be viewed as a serious flight limitation for the Exulans.

Group two (Static margin variations, 24° sweep, baseline aerodynamic damping, baseline control authority or Configurations 45, 54, 63, 72). No speed had a $n_\alpha > 15$ g/rad. Configurations 54, 63 and 72 has satisfactory to acceptable handling qualities. Configuration 45 (statically unstable case) could not be positioned on the contour map and therefore has unacceptable characteristics.

Group three (Static margin variations, 36° sweep, baseline aerodynamic damping, baseline control authority or Configurations 117, 126, 135,

144). All configurations and speeds that were investigated have unsatisfactory handling characteristics according the design speed and the high speed case. The 'lower than design speed' case has satisfactory handling qualities for all cases.

Group four (Control authority variations, 30° sweep, baseline aerodynamic damping, 10.7% static margin at 30° or Configurations 93, 96, 99). The low speed case and design speed case had values of $n_\alpha < 15$ g/rad and the high speed case had a $n_\alpha > 15$ g/rad. Design speeds and low speeds displayed acceptable handling characteristics. The high speed case had unacceptable handling qualities. The control authority variations had a small impact on handling characteristics. This means that a 20% accuracy on the prediction of the control authority is sufficient for this handling quality analysis, since the effect of prediction errors on the result is small.

Group five (Control authority variations, 24° sweep, baseline aerodynamic damping, 10.7% static margin at 30° or Configurations 57, 60, 63). The design speed and the low speed case had $n_\alpha < 15$ g/rad with satisfactory handling qualities. The high speed case had a $n_\alpha > 15$ g/rad with unacceptable handling qualities. Once again, the control authority variation had a small effect.

Group six (Damping variations, 30° sweep, 10.7% static margin at 30°, baseline control authority, or Configurations 97, 98, 99). The design speed, the low speed case and the high speed case for configurations 98 and 99 had $n_\alpha < 15$ g/rad. Configuration 97 had $n_\alpha < 15$ g/rad for the low speed case and the design speed case, while the high speed case had a $n_\alpha > 15$ g/rad. Design speeds cases and low speed cases all display acceptable handling qualities. Only the high speed case coupled with low damping displayed unacceptable handling qualities. The 20% variation in aerodynamic damping has an influence on the outcome of the handling quality study, but the effect is not so significant that it can change the pilot opinion. The airspeed is a much more significant

parameter with respect to handling qualities.

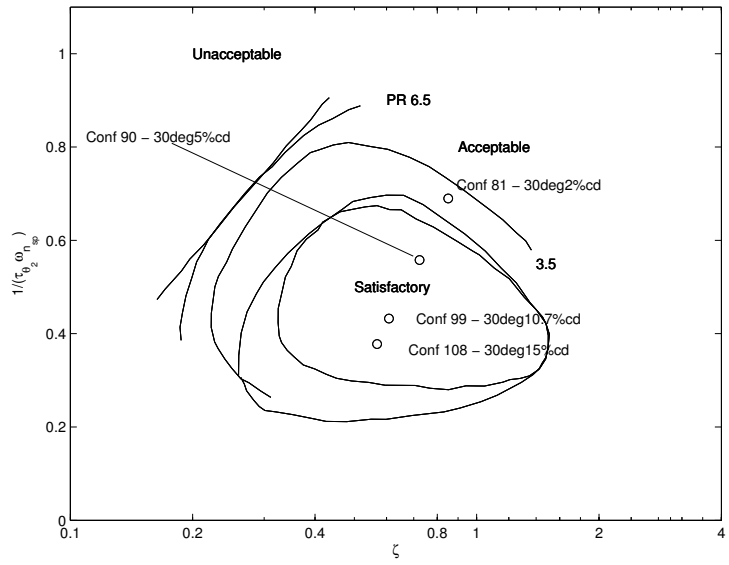

Figure 7.3: Group one analysis results for $n_\alpha < 15$ g/rad.

It may seem from the discussion in the previous paragraphs that there is a discontinuity between the results for $n_\alpha < 15$ and the results for $n_\alpha \geq 15$. It must however be remembered that handling qualities transition smoothly from acceptable to poor and that this discontinuity somewhat artificial because it is a result of how the handling quality criterion was defined in Shomber & Gertsen (1967).

The following conclusions can be drawn from the observations of the results:

- The estimation error of aerodynamic damping and control authority have an influence on handling quality predictions. A 20% variance in these parameter values will however not alter the conclusions of the handling quality study, since the effect is small enough.

- Speeds higher than the design trim speeds show a tendency to result in unacceptable handling qualities for the case of the Exulans. It follows as a recommendation that the Exulans should not be operated at speeds

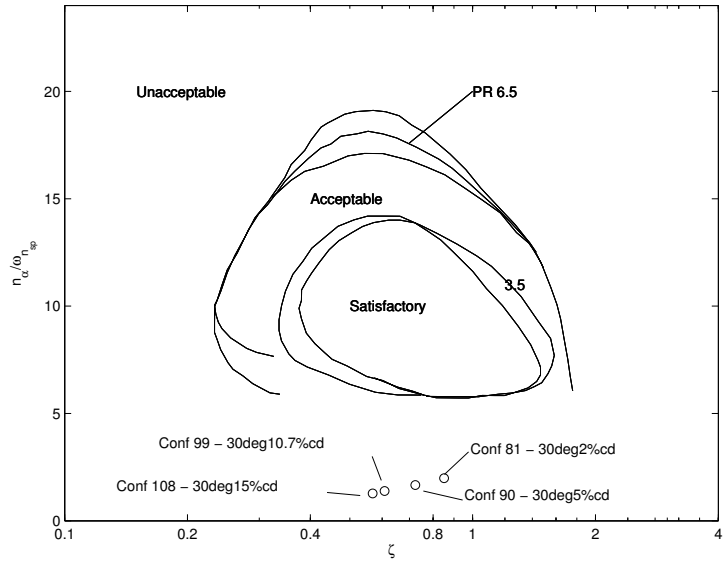

Figure 7.4: Group one analysis results for $n_\alpha \geq 15$ g/rad.

higher than the design speed (for a given sweep angle) as a risk reduction measure.

7.4 Neal-Smith Handling Qualities Analysis

The Neal-Smith analysis method is presented in Section 3.7. This method was applied to the Exulans. The Exulans configurations that were investigated in the pitch control step input analysis (see Section I.1) were also used as subjects for the Neal-Smith analysis. The Neal-Smith analysis was performed at the design airspeeds for each of the sweep cases that were analysed.

The results of the Neal-Smith analysis are presented in Figure 7.5.

The following conclusions can be drawn from the results:

- Most of the configurations that were investigated fall within the boundaries of favourable pilot opinion. The pilot rating for all these configurations are 3.5 or better. The exceptions are the statically unstable configurations (such as 24° sweep case with a 2% static margin at 30°). The Neal-Smith method indicated that the human pilot model with a 0.3s time delay could not compensate or control negative static margin cases. Since the statically unstable configurations did not achieve the minimum bandwidth criterion, it cannot be plotted on the Neal-Smith chart. This chart is only defined for configurations that achieve the compensation criterion.

- All the configurations that were investigated required lead compensation to achieve the bandwidth and droop criteria.

- The variation of $C_{M_{\delta_e}}$ of 20% with respect to the baseline had a very small impact on handling qualities. The estimation error of this parameter is therefore not a critical factor with respect to handling qualities. The methods used to estimate this parameter are therefore judged to be sufficiently accurate for the application.

- The analysis performed on configurations 97, 98 and 99 indicate that the 20% variation in damping due to estimation error has a small effect on the Neal-Smith opinion rating.

- The Neal-Smith analysis showed that the gull-wing configuration will

have good handling qualities for a wide range of sweep and static margin in calm conditions.

The Neal-Smith method is important because it provides a way to assess the effect of control authority and the pilot-in-the loop on handling qualities. The fact that a simulated pilot in the form of a transfer function model is used, is advantageous because it offers repeatability, where true pilot-in-the-loop analysis and simulation is never completely repeatable.

The pitch stick force gradient of the Exulans was taken as 25 N/g for the analyses performed. This value was obtained from Neal & Smith (1970). This stick force gradient was an initial assumption, since the aircraft was not constructed at the time of completion of this study. It must be investigated further and optimised for the case of the Exulans in a future study.

Bandwidth is a very important parameter with respect to pilot opinion in this method. When a pilot manoeuvres the aircraft very aggressively, more bandwidth is required compared to scenarios where more gradual manoeuvres are executed. The gull-wing configuration was evaluated with a bandwidth requirement of 3.5 rad/s. This was done because the Neal-Smith opinion chart was set up using this bandwidth requirement. The second reason for using 3.5 rad/s is because the gull wing planform aircraft might be used for aerobatic flying purposes, where higher bandwidth is required due to rapid flight manoeuvres. If the bandwidth criterion is relaxed, the configurations that showed unacceptable characteristics at high bandwidth, would show more acceptable handling characteristics.

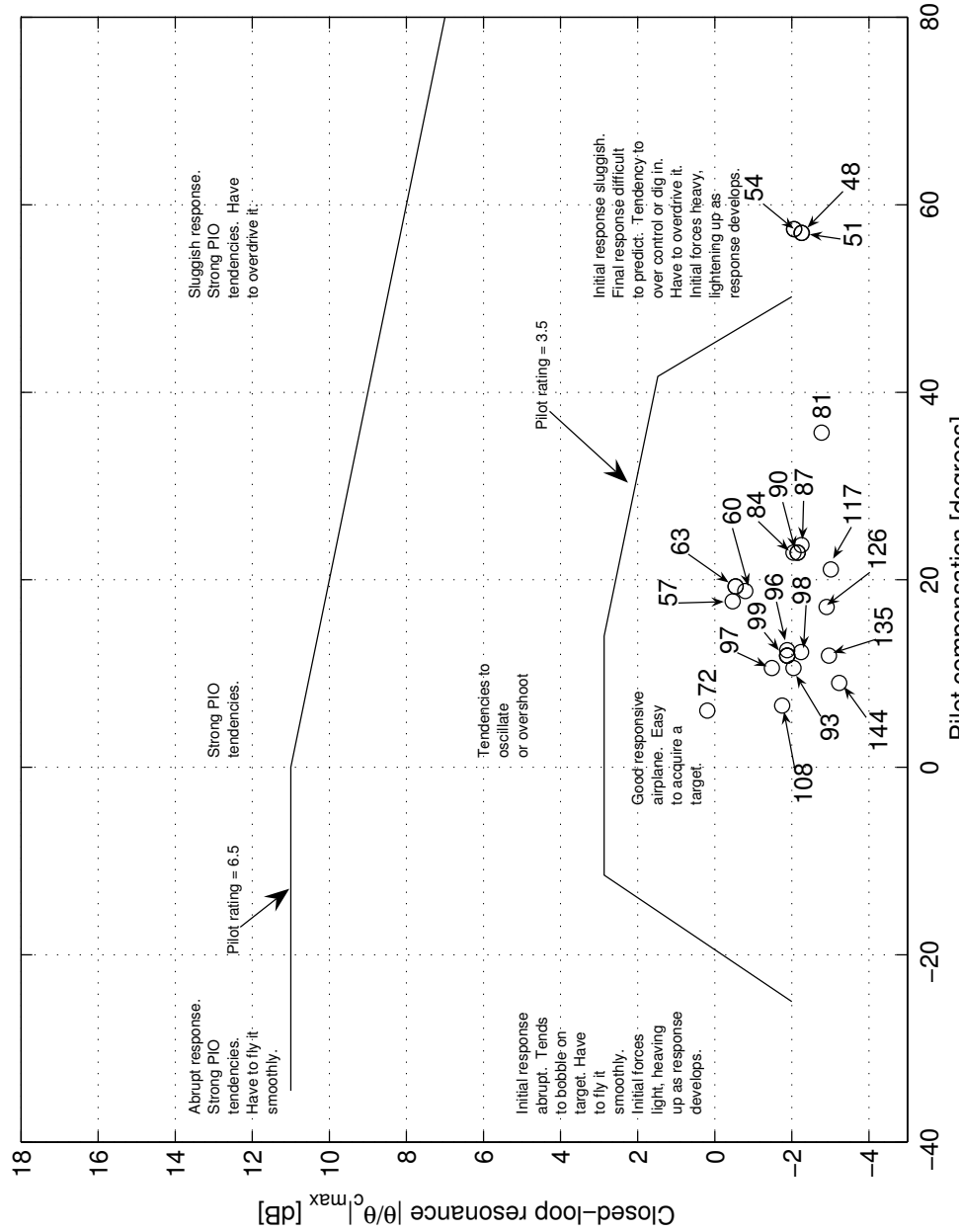

Figure 7.5: Results of the Neal-Smith study performed on various gull-wing configurations.

7.5 Frequency Domain Analysis Summary

Many important conclusions were drawn in this chapter regarding the handling qualities of the gull-wing configuration. Several analysis methods were used to predict handling qualities. The different methods are suitable for evaluating different aspects of handling qualities. Certain methods contradict each other and therefore an overview summary is required:

- The Military flying qualities criteria and the thumbprint analysis are useful for evaluating the inherent (raw) aircraft dynamics. These results indicated that the raw aircraft has some unpleasant characteristics, but that the handling qualities improve as static margin is decreased. These methods cannot evaluate marginally stable or unstable configurations.

- The Shomber Gertsen analysis is useful for evaluating handling qualities at different trim speeds. Airspeed is an important parameter in the zeros of the aircraft pitch transfer function. The zeros of the transfer function have an important influence on handling qualities. This method seems to indicate that the gull-wing handling qualities are generally acceptable, but not at speeds above the design trim speed.

- The Neal-Smith analysis is the most complete of all the methods used to evaluate the handling qualities. This method includes the stabilising effect of the pilot and is useful for the evaluation of marginally stable aircraft cases. It is also useful for preliminary pilot-in-the-loop studies and for evaluating the effect of varying control authority. The Neal-Smith results indicate that almost all the Exulans cases have good handling qualities, except for the marginally stable and unstable cases. This means that the CG region for acceptable handling qualities stops forward of the neutral point for the gull-wing configuration. The Neal-Smith method takes into account the stabilising effect of the pilot and as a result, its results should be used in preference to the less complete thumbprint and Military criteria.

- The C-star results of Chapter 6.1 predicts that the Exulans will have poor handling qualities for rapid manoeuvring and during landings. This contradicts the Neal-Smith results. When the two methods are compared it is evident that the stabilising effect of the pilot is not taken into account with the C-star method. Neal & Smith (1970) also states that the C-star method does not always correctly predict handling qualities. It is concluded that the Neal-Smith analysis results should rather be used since it is a more thorough method and because it has also been properly benchmarked (see Neal & Smith (1970)), whereas the C-star method is a mathematical method based on a summary of different studies (Tobie et al., 1966).

- The effects of control authority and damping variations on handling qualities were investigated. This investigation was required due to the presence of estimation errors in calculating these parameter values. The results indicated that these variations do not have a significant influence on handling qualities. It is concluded that the accuracy with which these parameters were estimated was sufficient.

In summary the Exulans should exhibit satisfactory handling qualities for a wide envelope of wing sweep and static margin, except at speeds higher than the design trim speed.

Chapter 8

Turbulence and Tumbling Criteria

Tailless aircraft have low pitch inertia and aerodynamic damping when compared to conventional aircraft. These characteristics cause tailless aircraft to have unique characteristics during gusty or turbulent conditions. Tailless aircraft are also more susceptible to tumbling than tailed aircraft for these reasons. Some special handling qualities criteria have been developed to analyse tailless aircraft with respect to gusty conditions and tumbling. These criteria were applied to the gull-wing configuration. The results are presented here.

8.1 Turbulence Handling Criterion

Some tailless aircraft have been known to display unfavourable handling characteristics in turbulent conditions. The unfavourable handling characteristics are associated with the pitching phenomenon of 'pecking'. Examples of aircraft that are prone to this condition are the SB-13 , the Horten H XV b and H XV m (Nickel & Wohlfahrt, 1994:104).

The work of Mönnich & Dalldorff (1993) investigated the handling qualities of flying wings in turbulent conditions. The SB-13 handling qualities were investigated and compared to a modern conventional sailplane, the ASW-19.

A tailless aircraft handling criterion (hereafter referred to as the Mönnich-Dalldorff criterion) for turbulent conditions was derived in the study. This was applied to the gull-wing configuration. The Mönnich-Dalldorff analysis was repeated in this study and the same results were achieved as documented in Mönnich & Dalldorff (1993).

The Mönnich-Dalldorff criterion states that a tailless aircraft (or any aircraft for that matter) shall have favourable handling qualities in turbulent conditions provided that the following inequality is satisfied for that particular aircraft:

$$\frac{C_{M_\alpha}}{C_{M_q}} < (C_{L_\alpha} + C_{D_e})\frac{\rho S\overline{c}}{2m} \tag{8.1}$$

The variables of the inequality are defined in the nomenclature list. If the inequality of Equation 8.1 is satisfied, the existence of a zero of the gust velocity to pitch attitude transfer function in the left half plane is guaranteed. The left half plane zero leads to favourable gust handling qualities. The inequality is true for almost all conventional aircraft, but this is not the case for all flying wing aircraft.

The Mönnich-Dalldorff criterion was applied to various static margin and sweep cases of the gull-wing configuration. The criterion was evaluated for air density values of 1.225 kg/m^3 and 0.855 kg/m^3. These density values correspond to sea level and an altitude of 12000 ft for the International Standard Atmosphere. The sea level altitude was chosen to represent the case of wake turbulence from an aerotow at sea level, while the upper altitude limit represents the maximum safe altitude without an oxygen supply on board. The aircraft parameters used in the evaluation were taken from Table 4.4. The trim lift C_L and equilibrium drag (C_{D_e}) were calculated using an angle of attack of 9.8° for 24° sweep, 4.1° for 30° sweep and 2.1° for 36° sweep for the gull wing planform aircraft. The parameter values mentioned were substituted into Equation 8.1 and the results are presented in Tables 8.2 to 8.5. The trim conditions used for the analysis are presented in Table 8.1. The result tables contain some of the parameters of the investigation as well as the numerical values of the left- and right hand side of the inequality of Equation 8.1. If

the right hand side value is larger in magnitude than the left hand side, the particular configuration will have satisfactory turbulent condition handling qualities. The analyses showed that the ratio of the moment curve slope and the aerodynamic damping coefficient had the most significant influence on the inequality of the Mönnich-Dalldorff criterion.

Table 8.1: Trim conditions used for the Mönnich-Dalldorff analysis of the gull-wing configuration.

Sweep (γ, °)	α, °	C_L	C_{L_α}	C_{D_e}
24	9.78	0.954	5.232	0.040
30	4.13	0.430	5.146	0.019
36	2.12	0.244	5.031	0.016

Table 8.2: The evaluation of the Mönnich-Dalldorff criterion for different outboard wing sweep angles of the gull-wing configuration aircraft for a 2% static margin at 30° sweep case.

Sweep (γ, °)	C_{M_α}	C_{M_q}	Left	Right Sea level	Right 12000 ft
24	0.148	-1.218	-0.121	0.247	0.172
30	-0.103	-2.035	0.051	0.242	0.169
36	-0.365	-3.097	0.118	0.236	0.165

The results (Tables 8.2 to 8.5) indicate that the turbulent handling qualities become less favourable with higher sweep angles. As the sweep angle increases, the left hand side of the inequality starts getting closer in magnitude to the right hand side. The results also show that turbulent handling qualities deteriorate with altitude. Table 8.4 indicates that the right hand side (12000 ft column) of the equation is less than the left hand side of the equation for all sweep angles of the 10.7% static margin (at 30° sweep) case. In contrast, the sea level column shows the right hand side to be larger for all sweep cases.

The inequality is favourable with respect to the Mönnich-Dalldorff criterion for most sweep angle and static margin configurations of the gull-wing

Table 8.3: The evaluation of the Mönnich-Dalldorff criterion for different outboard wing sweep angles of the gull-wing configuration aircraft for a 5% static margin at 30° sweep case.

Sweep (γ, °)	C_{M_α}	C_{M_q}	Left	Right	
				Sea level	12000 ft
24	-0.011	-1.365	0.008	0.247	0.172
30	-0.257	-2.204	0.117	0.242	0.169
36	-0.518	-3.291	0.157	0.236	0.165

Table 8.4: The evaluation of the Mönnich-Dalldorff criterion for different outboard wing sweep angles of the gull-wing configuration aircraft for a 10.7% static margin at 30° sweep case.

Sweep (γ, °)	C_{M_α}	C_{M_q}	Left	Right	
				Sea level	12000 ft
24	-0.309	-1.693	0.182	0.247	0.172
30	-0.551	-2.546	0.216	0.242	0.169
36	-0.804	-3.695	0.217	0.236	0.165

configuration aircraft. This indicates that the aircraft will have satisfactory gust handling characteristics over a large region of the operational envelope. The configuration with a 24° sweep and 2% static margin (at 30° sweep) is statically unstable. This implies that the inequality is true by default since the left hand side of the expression then becomes negative. All sea level cases except for the ones having a 15% static margin (at 30° sweep) have favourable handling qualities according to the criterion. The 12000 ft cases of all the 2% and 5% static margin cases have favourable handling qualities and the higher static margin cases all have unfavourable characteristics.

The low static margin cases are most favourable with respect to gust handling qualities according to the criterion. This compares well with the results from the thumbprint criterion analysis presented in Section 7.1. This is because a lower pitch moment stiffness (that goes along with lower static margin) causes the left hand side of the inequality to be smaller in magnitude. This causes the inequality of the criterion to be true. It may be

Table 8.5: The evaluation of the Mönnich-Dalldorff criterion for different outboard wing sweep angles of the gull-wing configuration aircraft for a 15% static margin at 30° sweep case.

Sweep (γ, °)	C_{M_α}	C_{M_q}	Left	Right	
				Sea level	12000 ft
24	-0.531	-1.980	0.268	0.247	0.172
30	-0.772	-2.895	0.267	0.242	0.169
36	-1.018	-4.051	0.251	0.236	0.165

concluded that the gull-wing configuration's ratio of pitching moment stiffness to aerodynamic damping is favourable with respect to gust handling qualities.

8.2 Tumbling

An aircraft can inadvertently enter an out-of-control tumbling motion under certain conditions. Tumbling can be defined as an autorotative pitching motion primarily about an axis parallel to a vehicle's lateral axis, plus translation in a vertical plane along an inclined flight path. This is a very serious condition that may lead to the loss of the aircraft. Tumbling may be caused by high pitch rates and conditions where an aircraft has entered a 'tail slide' (Fremaux & Vairo, 1995). A tail slide is entered when the air over the wing travels from the aft end of the aircraft to the front of the aircraft. A tail slide can therefore occur during stalls and violent spins.

The data of Fremaux & Vairo (1995) will be used to analyse the gull-wing configuration with respect to tumbling. The mentioned paper is the result of wind tunnel work that was used to identify the driving parameters of the tumbling phenomenon on tailless aircraft. The mechanisms of tumbling were also investigated in that study. No forward/backward swept (gull-wing configuration) models were tested in the study and hence the results from the evaluation should not be view as directly applicable to the gull-wing. The test models used are presented in Figure 8.1. In the absence of more appli-

cable wind tunnel data, this data may be relevant to provide a first order estimate assessment of tumbling behaviour. Fremaux & Vairo (1995) found that positive static stability does not necessarily preclude tumbling. Factors that influence tumbling are centre of gravity location, mass distribution and geometric aspect ratio. This study created a chart that indicates the combinations of static margin and aspect ratio that are likely to lead to tumbling tendencies with an aircraft.

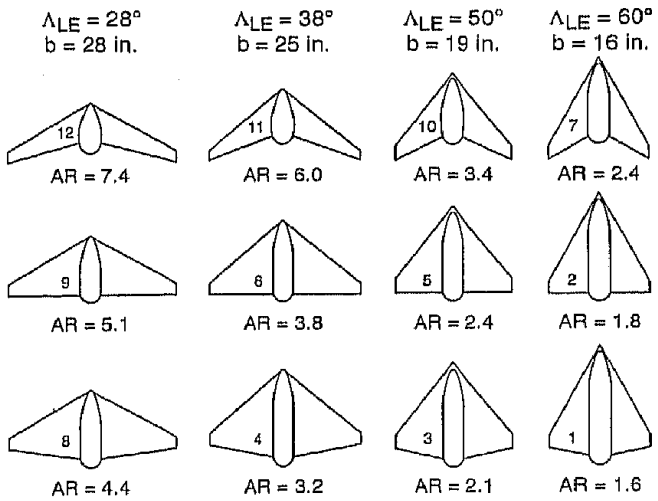

Figure 8.1: Generic flying wing models used for tumbling research. (Fremaux & Vairo, 1995)

Tumbling happens when $I_{xx} > I_{yy}$ ('wing-heavy' as Fremaux & Vairo (1995) refers to it) and when the aircraft static margin and aspect ratio falls within the boundaries as described in Figure 8.2.

Tailless aircraft are most likely to tumble while conventional configurations are the least likely to tumble. (Fremaux & Vairo, 1995) With this in mind, it is important to investigate whether the gull-wing configuration is also susceptible to this condition.

The gull-wing configuration under investigation has a high aspect ratio (12). It is expected that the aircraft will mostly be operated at low static margin (2 to 10%). The Exulans has an I_{xx} value of 585 kg·m^2. This means that the I_{xx} to I_{yy} ratio is at least larger than 13 (see Figure 4.5 for I_{yy} values

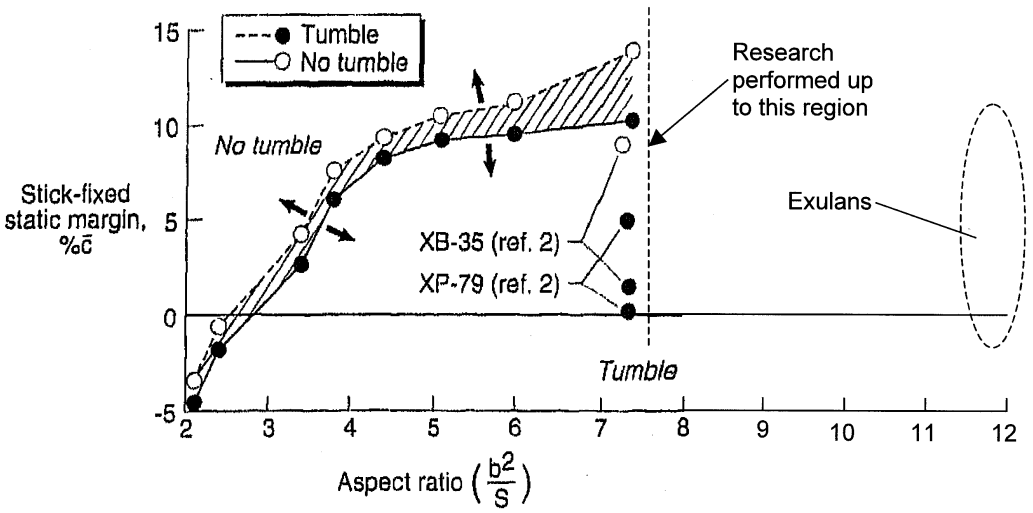

Figure 8.2: Static margin for tumbling as a function of aspect ratio for models with 'wing-heavy' (ie. $I_{xx} > I_{yy}$) loadings. (Fremaux & Vairo, 1995)

for the Exulans), depending on sweep angle. When these inertia ratios are compared to Figure 8.2 it can be concluded that the gull-wing configuration is likely to be susceptible to tumbling, assuming the trend can be extrapolated linearly to higher aspect ratios.

The tumbling research presented in Figure 8.2 was performed using thin flat plate wing models with a centre section to model the fuselage and acting as ballast. The research indicates that thick airfoil sections (Exulans has a thick airfoil section) have a tendency to be less susceptible to tumbling. Further research needs to be done on the gull-wing configuration's tumbling tendencies because engine nacelles, canopies, and any protrusion might have an effect on tumbling (Fremaux & Vairo, 1995). It is suggested that a detailed aerodynamic analysis be performed on the Exulans to determine whether its thick wing sections, winglets and fuselage could prevent tumbling behaviour.

As an initial estimate, there exists reasonable concern that the gull-wing configuration might be susceptible to tumbling. It may also be concluded that manoeuvres that may cause tumbling (high pitch rates, stalls and spins) should be avoided with the gull-wing configuration.

Chapter 9

Handling Qualities and Performance

Tailless flight should be able to offer attractive fundamental benefits to aviation. Practical implementation has revealed several shortcomings which render the benefits significantly compromised. At the core of the challenge lies the efficiency deterioration which results from the quality of the lift distribution over the main wing. The main wing of a tailless aircraft is responsible for the stability and control function (this is performed by the empennage on a tailed aircraft). It is therefore unavoidable to find variations of the lift distribution during flight. Flight efficiency demands that the lift distribution be of good quality to minimise the loss of energy in the wake of flight. This loss is manifested in vorticity in the wake resulting from gradients in the lift distribution. It is classified as induced drag in the drag brake-down.

In order to unlock the potential benefits of tailless flight it becomes necessary to achieve acceptable stability and control properties with a minimum penalty on the induced losses. Stability and control must be investigated together with performance issues to ensure that handling qualities are not optimised at the cost of performance.

When a tailless aircraft's CG is placed on the E-point (the O-point if the tailless aircraft has winglets) and the wing is designed to have an elliptical lift distribution, the aircraft will have the best Oswald efficiency. The region

between the E-point and the O-point is shown as hatched in Figure 9.1. This hatched region is associated with the best Oswald efficiency. In accordance with the argument of the first paragraph of this chapter, the tailless design would benefit if this region of best Oswald efficiency would somehow overlap with good handling qualities.

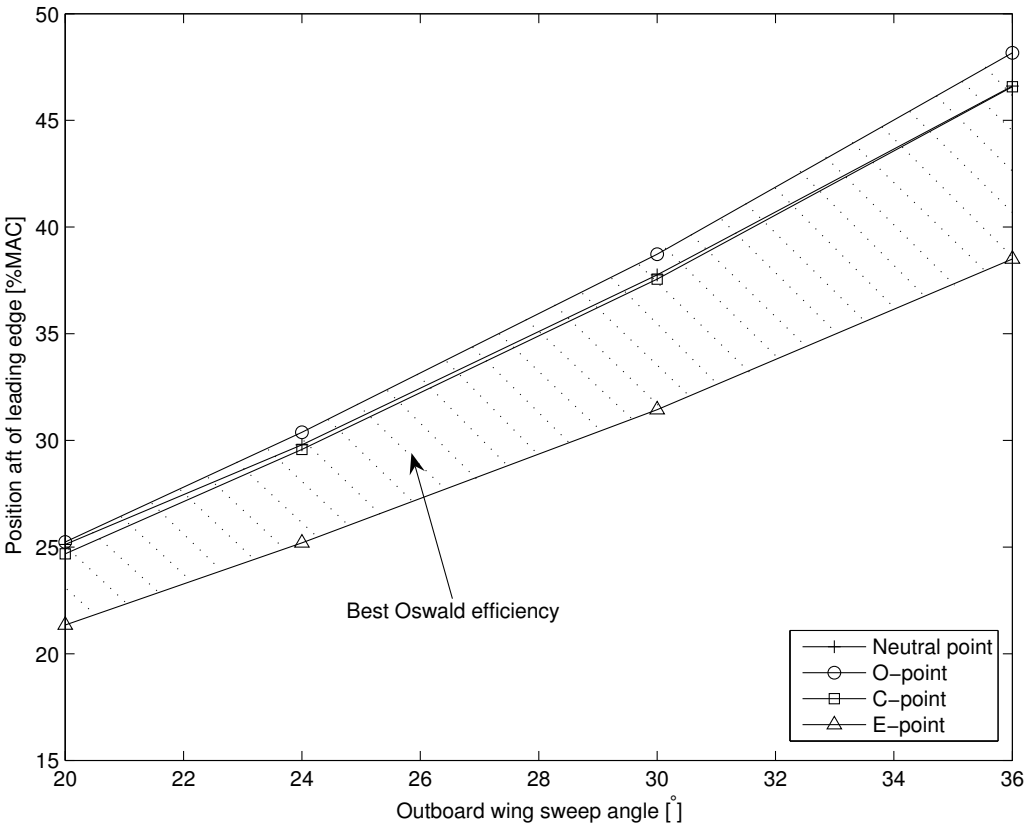

Figure 9.1: Region of best Oswald efficiency for the Exulans. The y-axis represents the distance behind the wing leading edge (at plane of symmetry).

A number of methods were used in Chapters 6 and 7 to evaluate the handling qualities. These methods were used to define a region of sweep and CG position with satisfactory (PR is 3.5 or better) handling qualities. Of these methods, the Neal-Smith method is the most complete method, since the dynamics of the pilot as a controller are not neglected. Compare

this to the thumbprint analysis that is more simplistic in nature. The pole analysis results ignore the contributions of the pilot and the zeros of the aircraft transfer function. The C* method takes into account the effects of the aircraft poles and zeros. The C* method is a time domain method and as such is also capable of handling a non-linear aircraft model. None of these methods investigate the effects of gusty conditions on handling qualities. The Mönnich-Dalldorff criterion was used to evaluate the gull-wing configuration with respect to turbulent conditions. Due to the strengths of the different analysis methods, a combination of all the analysis results was used to set up the boundaries of acceptable handling qualities in Figure 9.2.

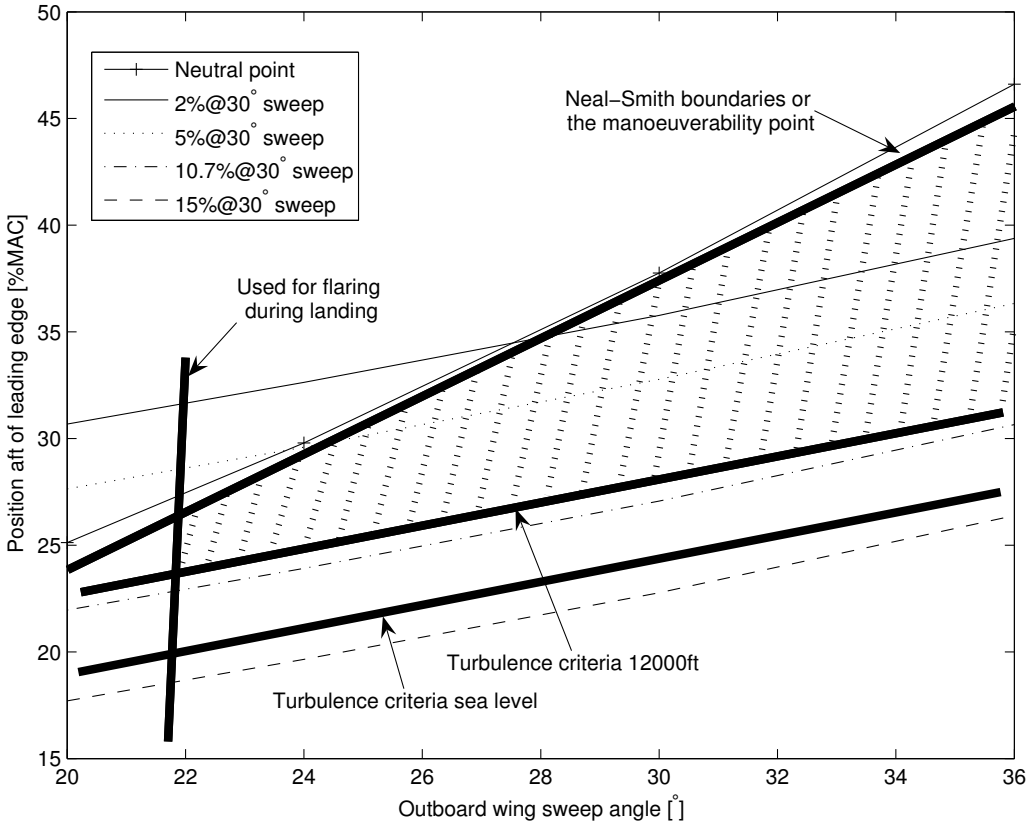

Figure 9.2: Region of acceptable handling qualities (PR is 3.5 or better) for the Exulans for different sweep angles and CG positions. The y-axis represents the distance behind the wing leading edge (at plane of symmetry).

Four lines in bold print are used to mark off the boundaries of acceptable handling characteristics in Figure 9.2. The line labelled 'Used for flaring' is used to mark off the low sweep angles. The handling qualities in this region were not investigated because these sweep angles are only used during the flare manoeuvre of landing and not during normal flight. The line used to mark off 'Turbulence criteria' was constructed by drawing a line parallel and just above the line of the 15%@30° sweep CG location function. This line represents the results of Section 8.1 where all CG locations indicated good gust handling qualities, except for the 15%@30° sweep CG location function. A similar line is used to indicate the region of good handling qualities at altitude. This is because gust rejection characteristics deteriorate with altitude. The fourth bold line on the graph represents the Neal-Smith results of Section 7.4. These results indicated that marginally stable and unstable configurations cannot be compensated by the average human pilot. The region of satisfactory handling qualities is hatched for purposes of clarity.

The four CG configurations investigated in this study are a function of outboard wing sweep and are specified as a percentage of mean aerodynamic chord at 30° wing sweep. The centre of gravity configurations are specified with respect to the static margin at 30° outboard wing sweep. 30° was chosen as a reference because the trim speed at this sweep angle is the cruise design speed. As an example, a legend caption in Figure 9.2 of '2%@30°' indicates a CG configuration that has a static margin of 2% at 30° outboard wing sweep. At wing sweep angles lower than 30°, this configuration will have a static margin lower than 2% and at wing sweep angles higher than 30°, it will have a static margin higher than 2%. The four CG configurations cover a wide range of static margins and were chosen so that the minimum static margin that is represented is not less than -5.5%. All the quantities are plotted as distances referenced to the mean aerodynamic chord of the aircraft, measured from the leading edge of the wing of the aircraft on the plane of symmetry[1] of the wing. Since all the quantities are plotted on a scale referenced to the mean aerodynamic chord, the static margin for any configuration and sweep angle may be read off as the distance between

[1]This is the position of y=0 on the body axis system described in Figure 4.1.

the *CG* for a particular configuration (at a particular sweep angle) and the neutral point at that sweep angle.

The regions for acceptable handling qualities and best Oswald efficiency have now been defined and in Figure 9.3 these two regions are superimposed. This figure shows that there is a significant overlap between the region of good performance and acceptable handling (the cross-hatched region).

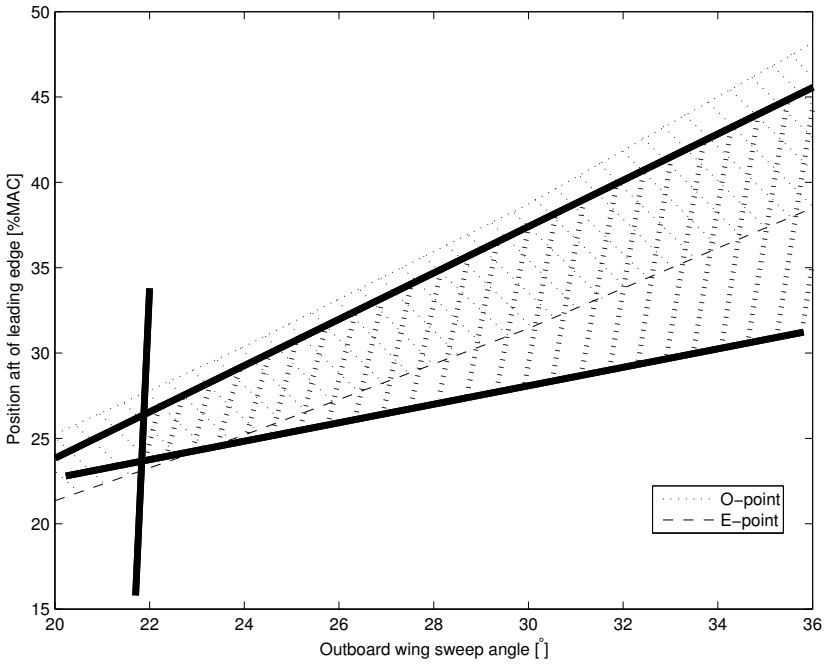

Figure 9.3: Superposition of regions of acceptable handling qualities and best Oswald efficiency for the Exulans. The y-axis represents the distance behind the wing leading edge (at plane of symmetry).

In Figure 9.4 the region of good handling and performance is presented together with the *CG* cases that were studied. Two of the configurations (2% at 30° and 5% at 30°) show a partial overlap with the favourable region. This represents the fundamental conclusion of this study:

A region of CG position and wing sweep exists for the gull-wing configuration that, given certain maximum speed constraints, the aircraft has satisfactory handling qualities in addition to the best Oswald efficiency.

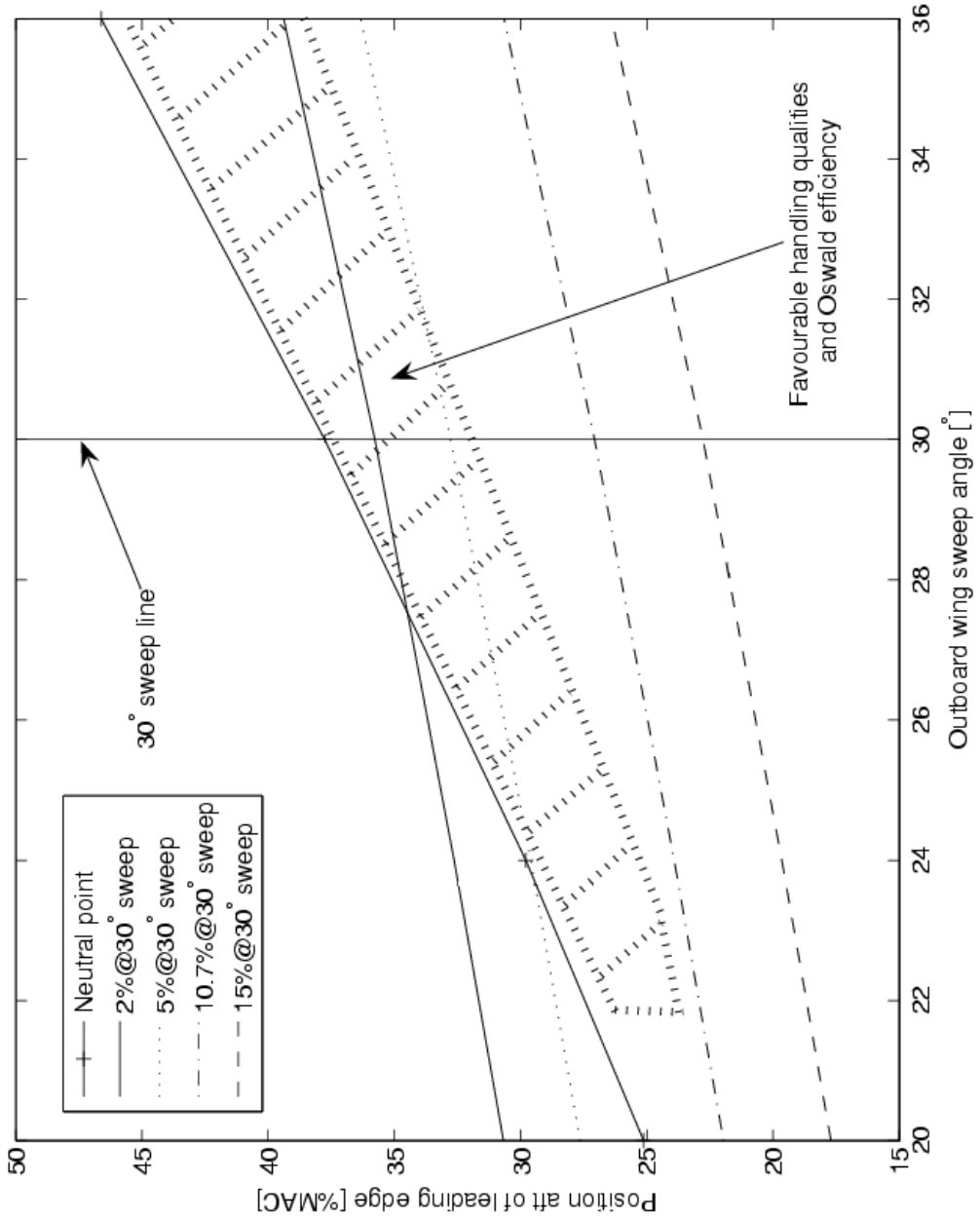

Figure 9.4: Region with both acceptable handling qualities and best Oswald efficiency for the Exulans. The y-axis represents the distance behind the wing leading edge (at plane of symmetry).

Chapter 10

Conclusion

A longitudinal handling quality investigation was performed on a tailless swept gull-wing configuration. An example of this type of aircraft is the Exulans that is under development at the University of Pretoria. The study assumed that lateral handling quality issues, such as tip stall and related spinning, will be handled in a separate study.

A mathematical model of the Exulans was created in order to investigate its pitch handling qualities. The handling qualities of the aircraft were evaluated using the mathematical model and methods obtained from literature.

In summary, the most important parameters that influence the handling qualities of the swept gull-wing configuration aircraft are static margin and the $\frac{C_{M_\alpha}}{C_{M_q}}$ ratio.

The following conclusions were drawn from the handling quality investigation:

- A region of CG position and wing sweep exists for the gull-wing configuration that, given certain maximum speed constraints, the aircraft has satisfactory handling qualities in addition to the best Oswald efficiency.

- The handling qualities of the Exulans in gusty conditions should be acceptable if the aircraft has a favourable $\frac{C_{M_\alpha}}{C_{M_q}}$ ratio. This ratio is acceptable with a static margin of below 5% (at 30°) together with an

aerodynamic damping coefficient of less than 3.2/rad (absolute value). Handling qualities in gusty conditions deteriorate with altitude, but is still acceptable at 12000 ft at low static margins. At low static margins, the short period mode of the aircraft is such that it has good disturbance rejection properties. This is a potential improvement on existing tailless designs that have exhibited poor disturbance rejection qualities.

- It is advisable to place the CG of the pilot as close as possible to the CG of the aircraft. A sitting pilot position with the ears of the pilot on the longitudinal aircraft CG position is optimal with respect to handling qualities. This type of pilot position has the effect of minimizing the magnitude of the pitch accelerations to which the pilot is subjected, which leads to improved handling qualities.

- The study indicated that the gull-wing configuration could be susceptible to tumbling. A gull-wing aircraft has a high aspect ratio and an unfavourable inertia ratio with respect to tumbling due to its geometry and mass distribution. Manoeuvres that may cause tumbling (high pitch rates, stalls and spins) should be avoided where possible with the gull-wing configuration.

- The Shomber-Gertsen handling qualities analysis showed that the Exulans will potentially have degraded handling qualities at true airspeeds above the design airspeeds. The Exulans is predicted to have satisfying handling qualities below and at the design speeds.

- The handling characteristics of the Exulans are insensitive to changes in pitch inertia that are within 10% from the baseline. This means that the handling qualities will not be sensitive to the placement of relatively large point masses such as batteries, as long as the CG of the aircraft is correctly placed.

- The variation of the $C_{M_{\delta_e}}$ and C_{M_q} parameters of 20% with respect to the baseline had a very small impact on handling qualities. The estimation errors of these parameters are therefore not a critical factor with respect to handling qualities. The methods used to estimate

these parameters are therefore judged to be sufficiently accurate for the application.

The pitch handling quality investigation shows that the swept gull-wing configuration and the Exulans has enough promise to warrant further investigation into its handling qualities. The recommendations for further investigation are outlined in the next section.

Chapter 11

Recommendations

The conclusions from the previous sections pointed out that the Exulans (as an example of a swept gull-wing configuration) should have acceptable longitudinal handling qualities. This section will list topics that were identified during the course of this study that will also have an influence on handling qualities in general.

The following topics for future work were identified:

- The lateral handling characteristics of the gull-wing configuration have to be evaluated. Required roll and yaw rate criteria need to be defined for the Exulans. Control surface sizes must then be evaluated to prove that these criteria can be met. Time domain simulation techniques can be used to evaluate whether roll and yaw rate criteria are satisfied.

- The gull-wing configuration must be analysed with respect to wingtip stall. The tip stall is manifested as a pronounced pitching and rolling instability. The tip stall also usually occurs in the region of the elevons, rendering flight controls ineffective. Tailless aircraft have been known to exhibit tip stall behaviour at low static margins. A detailed CFD and wind tunnel study must be performed at different pitch rates to investigate whether this occurs with the gull-wing configuration. The models that are used for the investigation must have low static margin configurations. Flight testing done previously with the SB-13 has shown tip stall problems to develop at low static margin. Fences or

other techniques must then be identified to solve this problem, should it occur.

- Detailed aerodynamic analysis and testing needs to be done to determine whether the shape of the fuselage could be used to prevent tumbling. Past research indicates that thick airfoil sections have a tendency to be less susceptible to tumbling. Engine nacelles, canopies and any protrusions from the aircraft could also have an effect on tumbling. A detailed aerodynamic analysis can possibly yield aerodynamic solutions to prevent the onset of tumbling.

- The pitch stick force gradient of the Exulans was used as 25 N/g for the analyses performed. This stick force gradient was an initial assumption, since the aircraft was not constructed at the time of completion of this study. This gradient must be optimised for the case of the Exulans. The optimised value should then be used as a design input to the gearing of the flight controls of the Exulans.

- A pilot in the loop simulator study should be performed. The work presented in this document eliminated the human pilot as a variable, although a mathematical pilot model was used for one analysis. The effect of the human pilot should now be studied on a pitch flight simulator. This must be done to quantify the effect of the variance of pilot skill on the Exulans handling qualities. The pitch stick force gradient mentioned in the previous point should be used as an input to the simulator study.

- A modal analysis should be performed on the structure of the Exulans. The structure should not have any resonant frequencies that are of same magnitude as that of the human pilot pitch stick input (2-3Hz). The structural resonant frequencies should also be higher than the frequencies of typical gust disturbances. Such a modal analysis can be performed with either a structural 'bonk' test or by means of finite element analysis.

- It is anticipated that the Exulans will have degraded handling qualities at speeds above the design airspeed. It is consequently a recommendation that the aircraft should be operated at speeds less than the design airspeed.

The following recommendations can be made with regards the safe expansion of the flight envelope during flight testing of the full-scale Exulans prototype. These recommendations are made based upon the results of the handling quality study:

- Flight testing should commence in calm conditions and at sea level, since gust rejection handling qualities are more favourable for these conditions.
- The static margin for the initial testing phase should be kept between 5% to 7%. The reason for this value is that tip stall is not expected at these values of static margin and handling qualities are expected to be acceptable.
- The landing manoeuvre should preferably be executed by means of a flaring manoeuvre that is achieved with forward wing sweep, as opposed to using elevons to pitch up the nose. This is because excessive use of the elevons increase the risk of the pancaking phenomenon.

Bibliography

Abbot, I. and von Doenhoff, A. (1959) *Theory of Wing Sections*, Dover Publications, Second edition.

Agenbag, D. (2000) "Development of a design real time pitch flight simulator for the Exulans glider", Final year thesis, Department of Mechanical and Aeronautical Engineering, University of Pretoria, RSA.

Althaus, D. and Wortmann, F. (1981) *Stuttgarter Profilkatalog I*, Vieweg, Braunschweig/Wiesbaden.

Anonymous (1997) "Human factors for designers of equipment. part 2: Body size.", Defence Standard DEF STAN 00-25 (Part 2)/Issue 2, British Ministry of Defence, UK.

Anonymous (2005) "Echoing to the sound of silence", *Aerospace Testing International, September issue*.

Anonymous (2006) "Göppingen Gö 3", Website, `http://en.wikipedia.org`, Accessed 19 December 2006.

Anonymous (n.d. a) "Flying wing history", Website, `www.yourzagi.com`, Accessed 19 May 2004.

Anonymous (n.d. b) "The flying wings of Charles Fauvel", Website, `http://www.nurflugel.com/Nurflugel/Fauvel/e_biograph.htm`, Accessed 4 May 2001.

Anonymous (n.d. c) "Goldfields gliding club homepage", Website, `www.ggc.co.za`, Accessed 27 October 2004.

Anonymous (n.d. d) "Jim Markse flying wings pioneer photo gallery", Website, `http://www.continuo.com/marske/pioneer/photogal.htm`, Accessed 4 May 2001.

Anonymous (n.d. e) "SZD 20 Wampir 2", Website, `http://www.vintagesailplanes.de/SZD_20.htm`, Accessed 19 May 2004.

Anonymous (n.d. f) "Nietoperz", Website, `http://www.vintagesailplanes.de/nietoper.htm`, Accessed 19 May 2004.

Anonymous (n.d. g) "Northrop flying wing", Website, `http://www.pilotfriend.com/century-of-flight/Aviation`, Accessed 19 May 2004.

Anonymous (n.d. h) "Pyxis", Website, `http://users.skynet.be/nestofdragons/pyxis.htm`, Accessed 18 June 2004.

Anonymous (n.d. i) "Rigid-wing models - The Flair 30", Website, `http://midtoad.homelinux.org/midwinter.ca/RigidWings/flair30.htm`, Accessed 25 May 2004.

Anonymous (n.d. j) "Schleicher ASW-19", Website, `http://www.gliding-in-melbourne.org/asw19.htm`, Accessed 19 January 2005.

Ashkenas, I. and Klyde, D. March (1989) "Tailless aircraft performance improvements with relaxed static stability", Contractor Report CR-181806, NASA, USA.

Browne, K. (2003) "The instrumentation and initial analysis of the short-term control and stability derivatives of an ASK-13 glider.", Master's thesis, Department of Electronic Engineering, University of Stellenbosch, Stellenbosch, RSA.

Bryan, G. (1911) *Stability in Aviation*, Macmillan, London.

Calise, A.; Lee, S. and Sharma, M. (2000) "Development of a reconfigurable flight control law for the X-36 tailless fighter aircraft", Conference paper, AIAA Guidance, Navigation, and Control Conference, 14-17 August, 2000/Denver, CO.

Chalk, C. (1963) "Fixed-base simulator investigation of the effects of L_α and true speed on pilot opinion of longitudinal flying qualities", Technical Documentary Report ASD-TDR-63-399, Flight Dynamics Laboratory Research and Technology Division Air Force Systems Command, Wright-Patterson Air Force Base, Ohio.

Chun, H. H. and Chang, C. H. (2001) "Longitudinal stability and dynamic motions of a small passenger WIG craft", *Ocean Engineering,* (29), 1145–1162.

Cooper, G. and Harper, R. (1969) "The use of pilot rating in the evaluation of aircraft handling qualities", Technical Note D5153, NASA, USA.

Cronje, J. (1999) "Pitch flight simulator for the Exulans 2, final year thesis report", University of Pretoria, RSA.

Crosby, C. P. (1997) *Strategies for Glider Performance Improvement*, PhD thesis, Department of Mechanical and Aeronautical Engineering, University of Pretoria, RSA.

Crosby, C. P. (2000) "Aerodynamic coefficients for the Exulans 2 glider", Personal communication.

Dods, J. (1948) "Wind-tunnel investigation of horisontal tails. Part III - unswept and 35° swept-back plan forms of aspect ratio 6", Report RM A8H30, NACA, USA.

Drela, M. and Youngren, H. (2000) *XFoil 6.9 User Primer*, Department of Aeronautical and Astronautical Engineering, MIT, Boston, USA, Last updated edition.

Etkin, B. (1972) *Dynamics of Atmospheric Flight*, John Wiley & Sons, Inc., New York.

Fremaux, C. and Vairo, D. (1995) "Effect of geometry and mass distribution on tumbling characteristics of flying wings", *AIAA Journal of Aircraft, 32* (2).

Holly, P. (2005) "Under surveillance - the Boeing ScanEagle", *Aerospace Testing International, September issue.*

Horstmann, K. and Shürmeyer, C. (1985) "Development of airfoil sections for the swept-back tailless sailplane SB 13", Conference paper, Rieti, Italy.

Horstmann, K.-H. (1988) "Ein Mehrfach-Traglinienverfahren un seine Verwendung für Entwurf und Nachrechnen nichtplanarer Flügelanordnungen. (A multiple lifting line method and its application for the design and calculation of non-planar wing configurations.)", Forschungsbericht DFVLR-FB 87-51, DFVLR, Braunschweig.

Huyssen, R. J. (2000) "Mass properties of the Exulans 2 glider", Personal communication.

Huyssen, R. (1994) "Investigation into the feasibility of a new concept of ultra light hang glider", Master's thesis, Department of Mechanical and Aeronautical Engineering, University of Pretoria, RSA.

Kay, J.; Mason, W. H.; Durham, W.; Lutze, F. and Benoliel, A. (1996) *Control Authority Issues in Aircraft Conceptual Design: Critical Conditions, Estimation Methodology, Spreadsheet Assessment, Trim and Bibliography*, Department of Aerospace and Ocean Engineering, Virginia Polytechnic Institute and State University, Blacksburg, Virginia 24061, Unpublished edition.

Kroo, I. (2000) "Design and development of the SWIFT: A foot-launched sailplane", *AIAA Journal of Aircraft,* (AIAA-00-4336).

Kroo, I.; Beckman, E.; Robbins, B.; Morris, S. and Porter, B. (1991) "Development of the SWIFT - A tailless foot-launched sailplane", Website, `http://aero.stanford.edu/Reports/SWIFTArticle1991.html`, Accessed 4 May 2001.

Kuethe, A. M. and Chow, C. (1998) *Foundations of Aerodynamics - Bases of Aerodynamic Design*, John Wiley and Sons inc., USA.

McCormick, B. W. (1995) *Aerodynamics, Aeronautics and Flight Mechanics*, John Wiley and Sons inc., USA.

Melin, T. (2001) *Tornado 1.0 User's Guide Reference Manual*, Royal Institute of Technology (KTH), Department of Aeronautics, Sweden, Release 2.3 edition.

MIL-F-8785C (1980) "MIL Specification F8785C, Flying qualities of piloted airplanes", U.S. Department of Defense Military Specification.

Moes, T. and Iliff, K. (2002) "Stability and control estimation flight test results for the SR-71 aircraft with externally mounted experiments", Report TP-2002-210718, NASA, USA.

Mönnich, W. and Dalldorff, L. (1993) "A new flying qualities criterion for flying wings", *AIAA Journal of Aircraft,* (AIAA PAPER 93-3668).

Neal, T. and Smith, R. (1970) "An in-flight investigation to develop control system design criteria for fighter airplanes", *AFFDL-TR-70-74, Air Force Flight Dynamics Laboratory, Wright-Patterson AFB, Ohio, I and II.*

Nickel, K. and Wohlfahrt, M. (1994) *Tailless aircraft in theory and practice*, Edward Arnold, London first edition.

O'Hara, F. (1967) "Handling criteria", *Journal of the Royal Aeronautical Society, 71* (676), 271–291.

Park, M. (2000) "Steady-state computation of constant rotational rate dynamic stability derivatives", *AIAA Journal of Aircraft,* (AIAA 2000-4321).

Roskam, J. (1971) *Methods for Estimating Stability and Control Derivatives of Conventional Subsonic Airplanes*, The University of Kansas, Lawrence, Kansas, USA, First edition.

Shomber, H. and Gertsen, W. (1967) "Longitudinal handling qualities criteria: An evaluation", *Journal of Aircraft, 4* (4), 371–376.

Stevens, B. L. and Lewis, F. L. (1992) *Aircraft Control and Simulation*, John Wiley and Sons inc., USA.

Thomas, F. (1993) *Fundamentals of Sailplane Design*, College Park Press, College Park Maryland, USA.

Tobie, H.; Elliot, E. and Malcom, L. (1966) "A new longitudinal handling qualities criterion", Conference paper, National Aerospace Electronics Conference, Dayton, Ohio.

Toll, T. and Queijo, M. (1948) "Approximate relations and charts for low-speed stability derivatives of swept wings", Technical Note TN-1581, NACA, USA.

Wilson, J. (2003) "Battle of the X-Planes", *Popular Mechanics RSA, June edition.*

Zientek, A. (1992) "A polish flying experience with tailless gliders.", *Technical Soaring, 16* (2), 48–56.

Index

Appendix A

The Cooper-Harper Scale

The following table presents the Cooper-Harper scale that is used to express pilot rating (PR) of aircraft handling qualities.

Table A.1: Pilot opinion rating and flying qualities level. (The Cooper Harper scale)

Aircraft characteristics	Demands on pilot in selected task or required operation	Pilot rating	Flying qualities level
Excellent; highly desirable	Pilot compensation not a factor for desired performance	1	
Good; negligible deficiencies	Pilot compensation not a factor for desired performance	2	1
Fair; mildly unpleasant deficiencies	Minimal pilot compensation required for desired performance	3	
Minor but annoying deficiencies	Desired performance requires moderate pilot compensation	4	
Moderately objectionable deficiencies	Adequate performance requires considerable pilot compensation	5	2
Very objectionable but tolerable deficiencies	Adequate performance requires extensive pilot compensation	6	
Major deficiencies	Adequate performance not attainable with maximum tolerable pilot compensation. Controllability not in question	7	
Major deficiencies	Considerable pilot compensation required for control	8	3
Major deficiencies	Intense pilot compensation required to retain control	9	
Major deficiencies	Control will be lost during some portion of required operation	10	

Appendix B

Eigenvalue Analysis

Eigenvalue analysis of a mechanical system requires a mathematical description of the system dynamics. An aircraft can be modelled by means of the equations of motion just like any other mechanical system. It has inertial properties like mass and moment of inertia. It also has damping properties represented by the aerodynamic damping coefficients. It has properties that have similar characteristics to the stiffness of a spring that obeys Hooke's law. An example of a 'stiffness' is the lift force that has a linear dependence on the angle of attack (α).

The equations used to describe aircraft dynamics can be expressed in the following matrix form:

$$m\ddot{\overline{x}} + c\dot{\overline{x}} + k\overline{x} = \overline{F} \tag{B.1}$$

The variable $\overline{F}$ in this equation represents a column vector of external excitation forces and moments. In the case of the aircraft this represents forces and moments from the control surfaces. The control surfaces are controlled by the pilot of the aircraft. The velocity column vector is now defined as

$$\overline{y} = \dot{\overline{x}} \tag{B.2}$$

Equation B.2 can now be substituted into Equation B.1 in order to yield another form of the matrix equation:

$$m\dot{\overline{y}} + c\overline{y} + k\overline{x} = \overline{F} \tag{B.3}$$

Equations B.2 and B.3 are now combined:

$$\begin{bmatrix} m & 0 \\ 0 & I \end{bmatrix} \begin{bmatrix} \dot{\overline{y}} \\ \dot{\overline{x}} \end{bmatrix} + \begin{bmatrix} c & k \\ -I & 0 \end{bmatrix} \begin{bmatrix} \overline{y} \\ \overline{x} \end{bmatrix} = \begin{bmatrix} \overline{F} \\ 0 \end{bmatrix} \tag{B.4}$$

For the eigenvalue (modal) analysis that we want to perform, the inherent dynamics of the mechanical system have to be analysed. This means that the forced excitation $\overline{F}$ is set equal to zero before the eigenvalue analysis is performed. Having done this, Equation B.4 is rewritten and the following state space representation of the aircraft model follows:

$$\begin{bmatrix} \dot{y} \\ \dot{x} \end{bmatrix} = - \begin{bmatrix} m & 0 \\ 0 & I \end{bmatrix}^{-1} \begin{bmatrix} c & k \\ -I & 0 \end{bmatrix} \begin{bmatrix} y \\ x \end{bmatrix} \tag{B.5}$$

The state space representation is now of the form:

$$\dot{z} = Az \tag{B.6}$$

with

$$z = \begin{bmatrix} x^T & y^T \end{bmatrix}^T \tag{B.7}$$

where

$$A = - \begin{bmatrix} m & 0 \\ 0 & I \end{bmatrix}^{-1} \begin{bmatrix} c & k \\ -I & 0 \end{bmatrix} \tag{B.8}$$

The eigenvalues of matrix A are used to calculate the natural frequencies and damping ratios of the natural modes of the system.

The resulting eigenvalues are in real or conjugate pairs. Each complex conjugate pair can be associated with a natural oscillation mode and can be expressed in a form analogous to a single degree of freedom system, where ζ_r is the damping ratio and ω_r is the circular natural frequency corresponding to the r-th eigenvalue of the system:

$$s_r = -\zeta_r \omega_r + i\omega_r \sqrt{1-\zeta_r^2} \tag{B.9}$$

$$s_r^* = -\zeta_r \omega_r - i\omega_r \sqrt{1-\zeta_r^2} \tag{B.10}$$

The damped natural frequency is calculated with Equation B.11.

$$\omega_{d_r} = \omega_r \sqrt{1-\zeta_r^2} \tag{B.11}$$

The damped natural frequencies are important parameters in analysing the dynamics of a multi degree of freedom system.

The aircraft rigid body equations of motion are non-linear. Eigenvalue analysis require a set of linear differential equations. It is important to note that the matrix A of Equation B.6 may be considered as the coefficient matrix of a linearised version of the non-linear aircraft equations of motion at a particular aircraft flight regime or trim state.

Appendix C

Aircraft Planforms in this Study

The following aircraft planforms were part of the handling quality investigation.

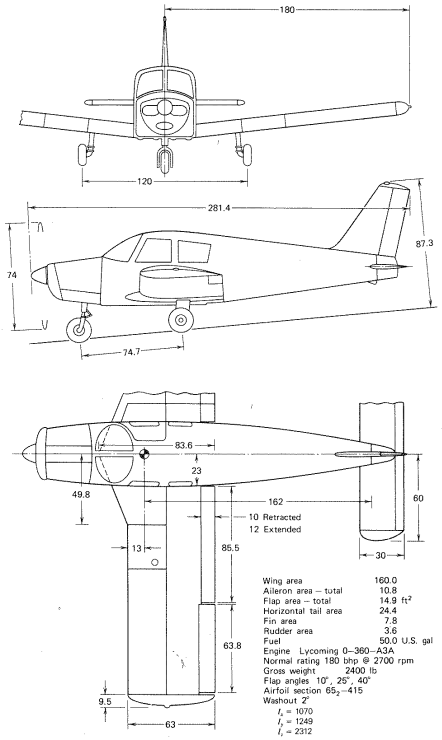

(a) Piper Cherokee PA-28-180 aircraft, all dimensions in inches (McCormick, 1995:123).

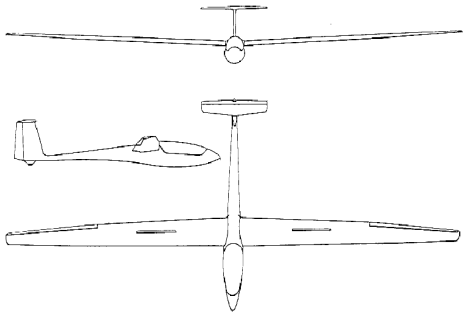

(b) The ASW-19 aircraft (Anonymous, n.d. j).

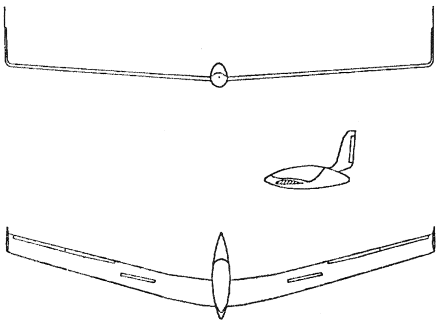

(c) The SB-13 aircraft (Mönnich & Dalldorff, 1993:448).

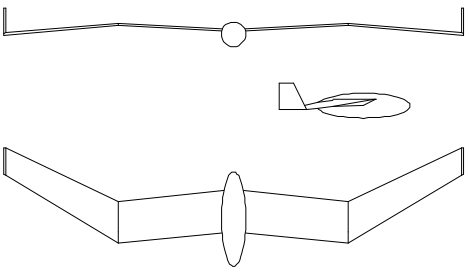

(d) The gull-wing configuration (30° sweep-back angle).

Figure C.1: Planforms that formed part of the handling quality investigation.

Appendix D

Time Step Size

Time domain simulations of aircraft dynamic responses were executed using a Runge Kutta fourth order method. This method was also used in Stevens & Lewis (1992). The effect of the time step size on the convergence of the simulation response was investigated by means of comparative simulations. This was done in order to optimise the time step size with respect to both convergence of the response and simulation execution time. The investigation revealed that simulations with a 0.01 second time step size yielded sufficiently converged time domain responses.

Figures D.1 to D.6 shows simulation results for four different time step sizes (0.1, 0.01, 0.001 and 0.0001 seconds). The simulation results show the gust response of an Exulans with 30° wing sweep and a static margin layout of 10.7% at 30°. A cosine gust model (with the same magnitude as described in Section 4.8.1) was used as the disturbance.

The results show that time step size has the largest influence on attitude and true airspeed response. Figure D.3 shows the effect of time step on the short period attitude response. This simulation result shows that a 0.01 second time step size calculates the attitude response with sufficient convergence.

A time step size of 0.01 seconds was consequently used for all simulations that are presented in this study.

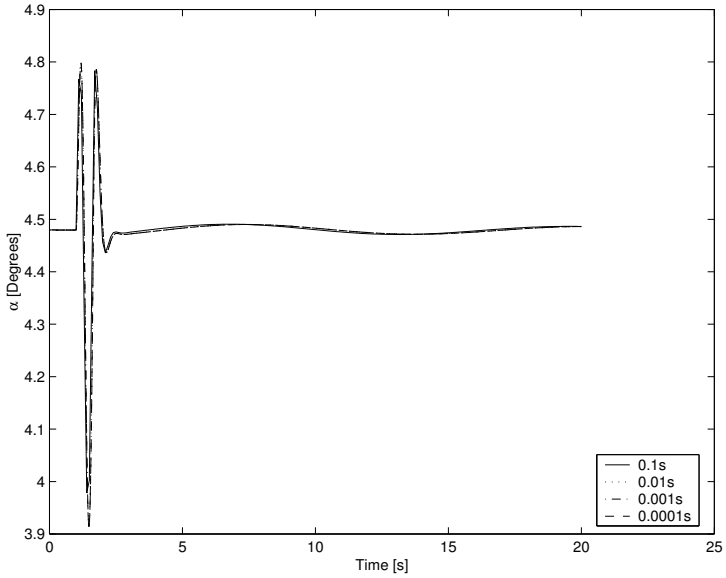

Figure D.1: The effect of step size on angle of attack (α) response for four step sizes.

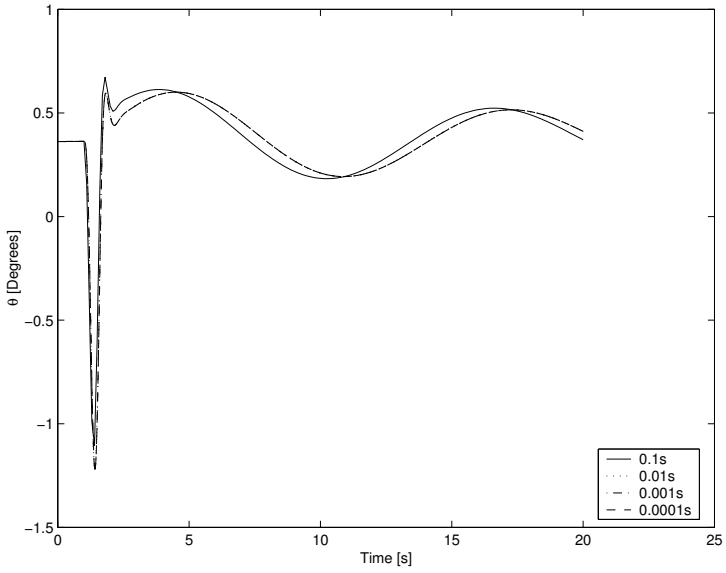

Figure D.2: The effect of step size on attitude (θ) response for four step sizes.

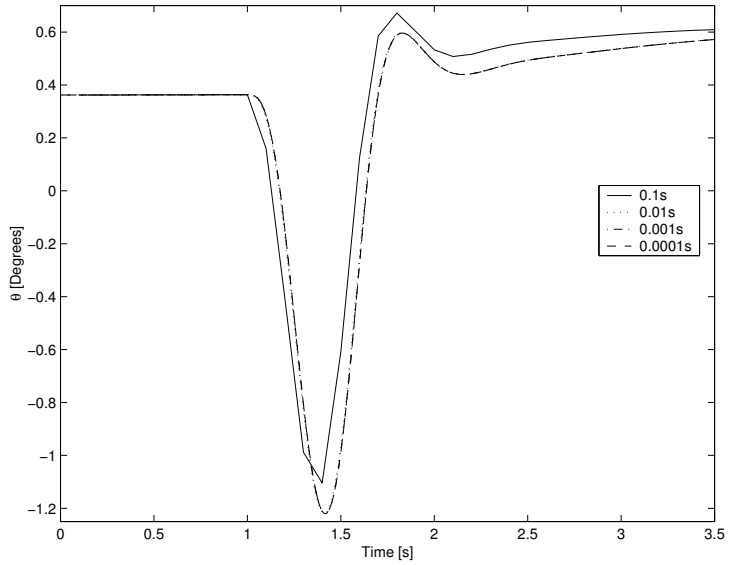

Figure D.3: The effect of step size on the short period attitude (θ) response for four step sizes (Zoomed-in portion of Figure D.2).

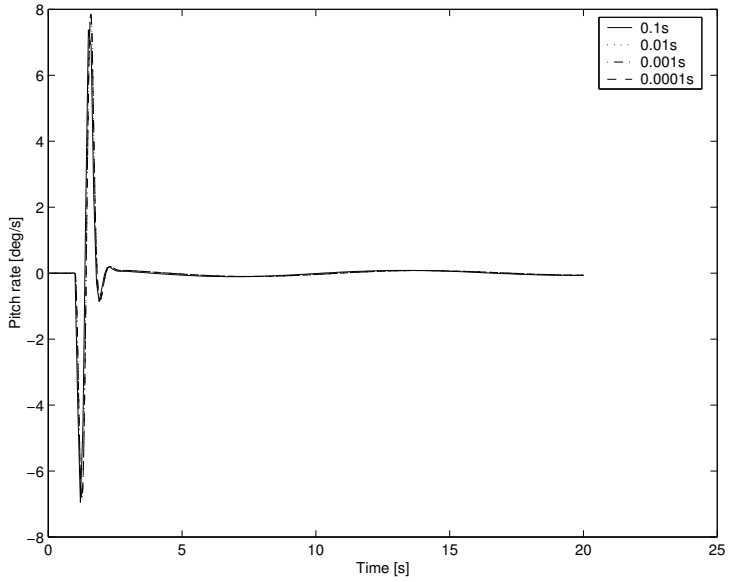

Figure D.4: The effect of step size on the pitch rate response for four step sizes.

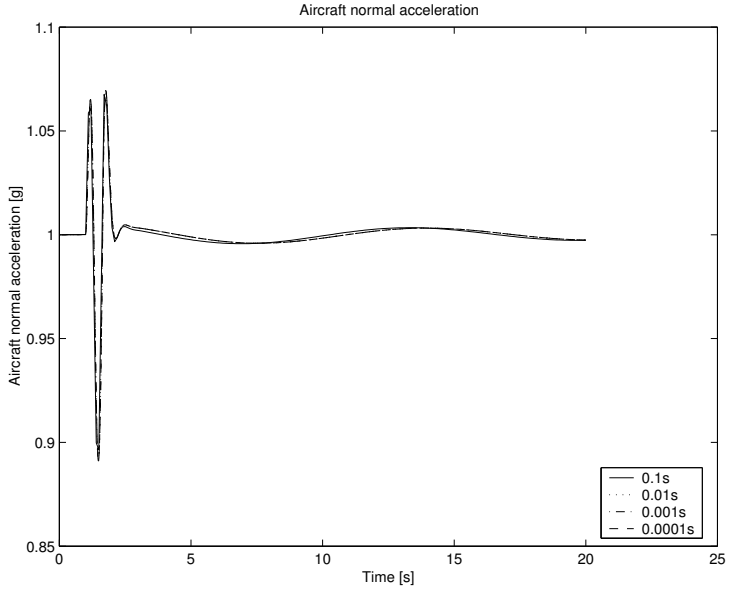

Figure D.5: The effect of step size on the normal acceleration response for four step sizes.

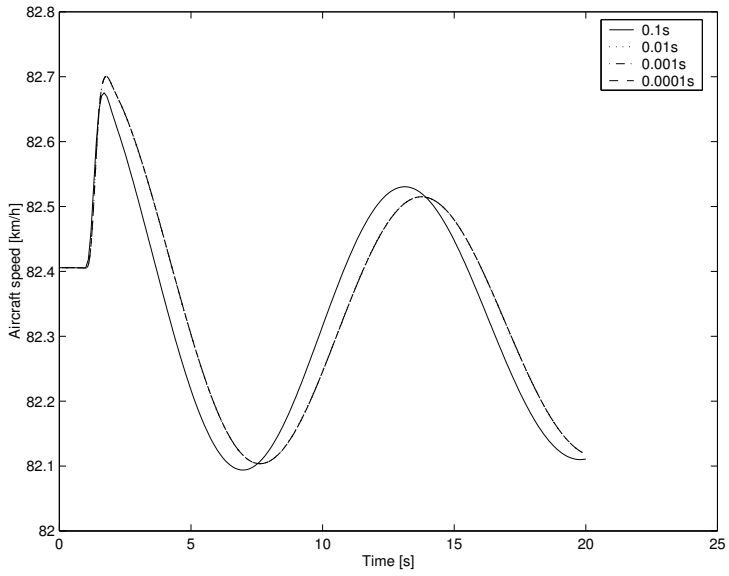

Figure D.6: The effect of step size on the true airspeed response for four step sizes.

Appendix E

C_{M_q} Benchmark Investigation

The damping coefficient (C_{M_q}) is an important parameter when calculating the natural frequencies and damping ratios of the phugoid and short period motions. It is therefore necessary to calculate or measure it accurately before using the damping coefficient values in calculations.

Damping coefficients can be obtained through wind tunnel measurements, numerical methods such as CFD or vortex lattice methods, or by means of system identification methods from measurements in real flight.

The vortex lattice method was chosen as the method with which to numerically estimate aircraft damping coefficients for the purpose of this study. It was chosen since this type of method is suitable for calculating the damping coefficients of complex planform geometries, while being less computationally intensive than Navier Stokes fluid dynamic numerical methods.

Since the calculation accuracy of the damping coefficient is important to this study, it was necessary to determine the level of accuracy of the vortex lattice method codes that were used in this study. Two different vortex lattice codes, namely JKVLM[1] and Tornado were used in this study.

The accuracy of the two vortex lattice methods was evaluated by means of comparison with the wind tunnel results of damping coefficients for four different wing planforms that are presented in Toll & Queijo (1948:52).

[1] J. Kay Vortex Lattice Method

E.1 Planforms under Investigation

The damping coefficients of the four different wing planforms of Toll & Queijo (1948:47) were calculated using the JKVLM and Tornado vortex lattice method implementations.

The wing planforms that were used in the investigation are presented in Figure E.1.

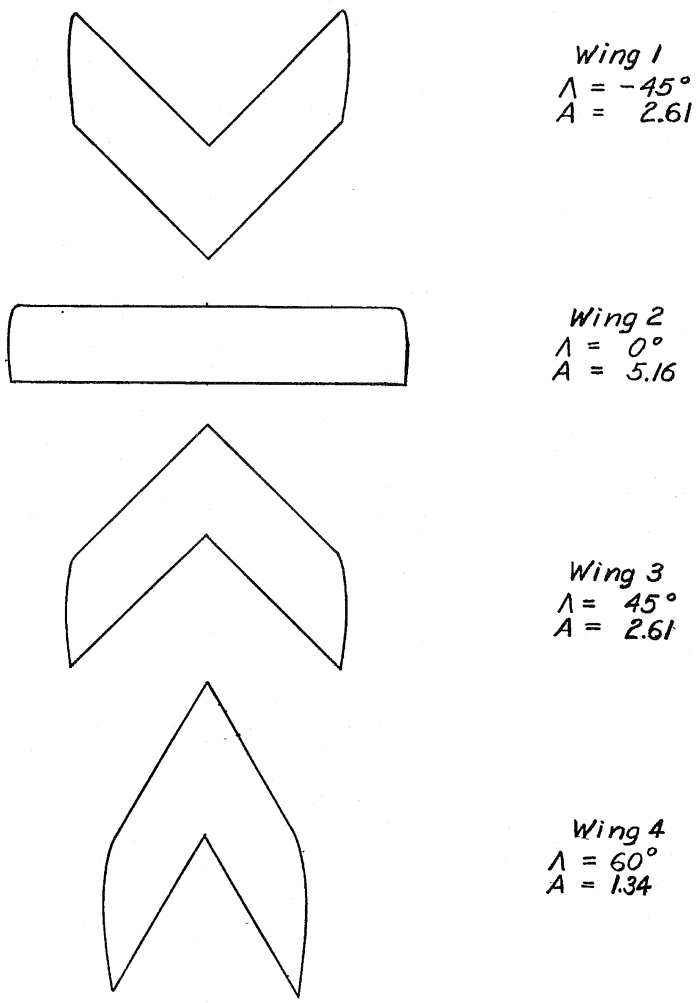

Figure E.1: The four wing planform types used in the vortex lattice method benchmark study. (Toll & Queijo, 1948:47)

E.2 Results and Conclusions

A sensitivity study of the value of C_{M_q} with respect to the number of elements on the wing was performed using the Tornado vortex lattice method. The results of this study are shown in Figure E.2. Inspection of this figure shows that convergence is reached with a relatively small number of elements.

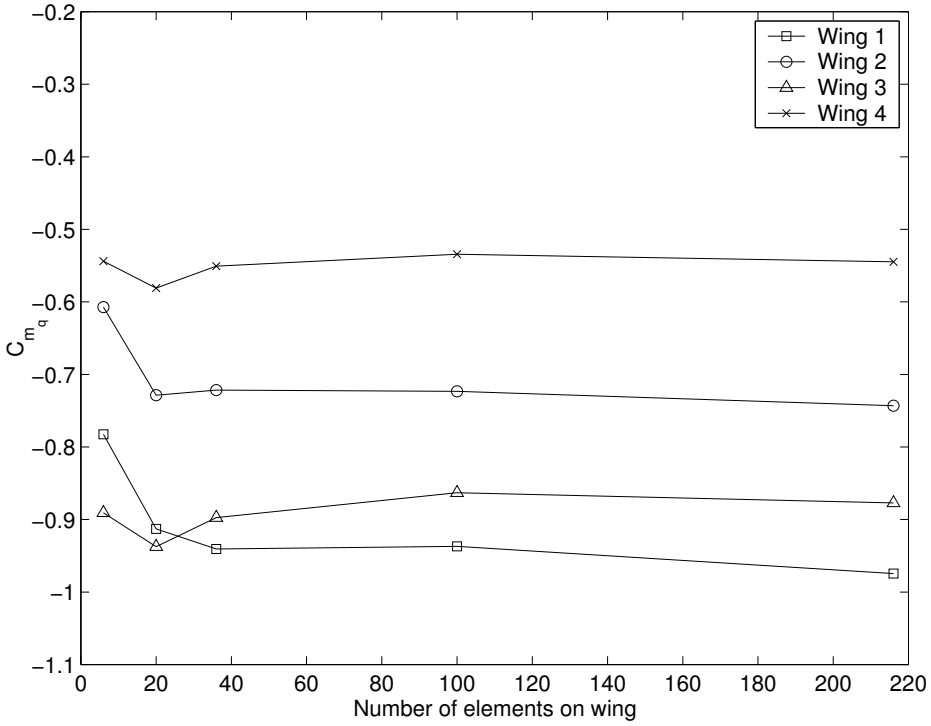

Figure E.2: Convergence of C_{M_q} values as calculated with the Tornado vortex lattice method.

The results of the benchmark study are shown in Figure E.3. The results are also presented in table format in Table E.1. The results of the two vortex lattice methods show good agreement with each other. The vortex lattice method results and wind tunnel results do not show very good agreement for C_{M_q} values (see results of Wing 2, Figure E.3), but are of the same order of magnitude. The results of the benchmark study indicate that poor results for C_{M_q} are obtained when a straight wing planform is analysed. Large discrepancies between experimental and calculated results for highly swept

wings at moderate and high lift coefficients are most likely caused by partial separation of flow which results in changes in the distributions of lift and drag along the wing span (Toll & Queijo, 1948:27). The gull-wing configuration is a combination of a forward swept and a backward swept wing. The vortex lattice method showed acceptable accuracy (within 20% for moderate lift coefficients) for these wing types. The damping coefficient resulting from the vortex lattice method is constant across the whole range of lift coefficients shown, as it is a linear method.

The value of C_{M_q} that is labelled as 'Calculated' in Figure E.3 and Table E.1 was obtained using Equation E.1 (Toll & Queijo, 1948:25)[2]. This equation can be used to calculate C_{M_q} for swept wings. The results show that the vortex lattice methods show very good agreement with this analytical approximation.

$$C_{M_q} = -a_0 \cos\Lambda \left\{ \frac{\chi\left[2\left(\frac{\overline{X}}{\overline{c}}\right)^2 + \frac{1}{2}\frac{\overline{X}}{\overline{c}}\right]}{\chi + 2\cos\Lambda} + \frac{1}{24}\frac{\chi^3 \tan^2\Lambda}{\chi + 6\cos\Lambda} + \frac{1}{8} \right\} \tag{E.1}$$

Table E.1: Comparison of values of C_{M_q} calculated by different methods

Wing number	Calculated	JKVLM	Tornado
1	-0.935	-0.939	-0.975
2	-0.709	-0.764	-0.743
3	-0.935	-0.951	-0.877
4	-0.551	-0.593	-0.545

The damping coefficient values calculated for the Exulans were used as inputs to a handling quality study. The baseline damping coefficient values (as calculated by vortex lattice methods) were varied by 20% above and below the baseline. This was done since the estimation error is roughly 20% above and below the baseline damping ratio. By varying the damping in this manner the effect of the estimation error on handling qualities can be

[2]Equation 50 in that document.

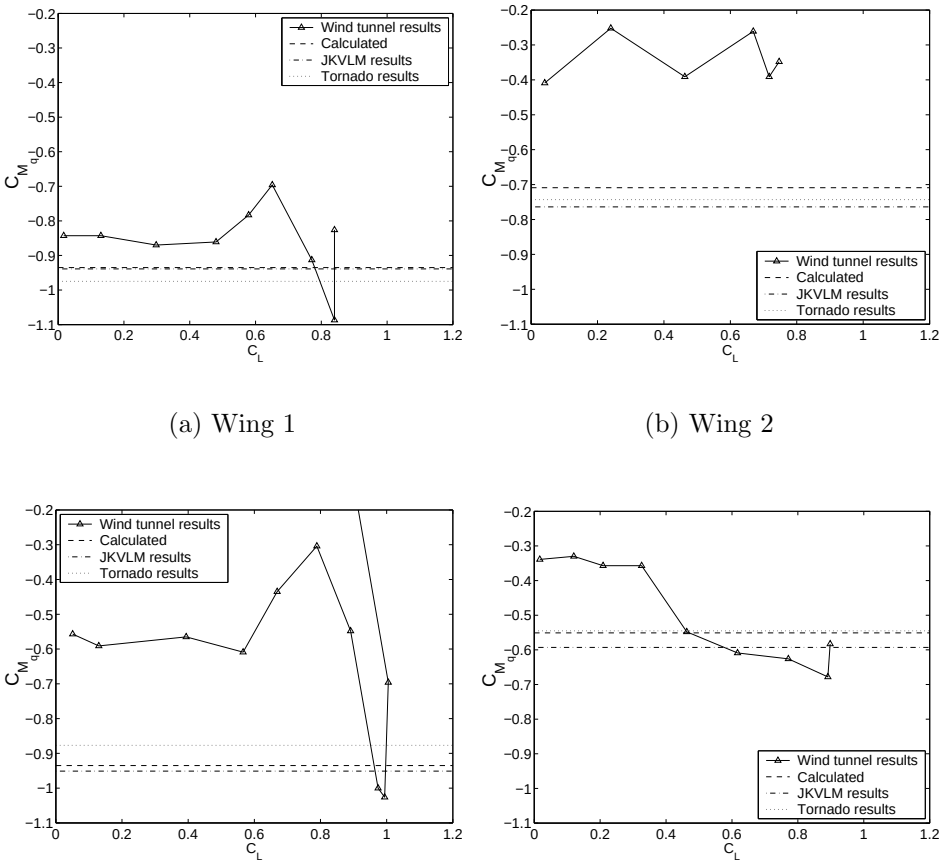

(a) Wing 1

(b) Wing 2

(c) Wing 3

(d) Wing 4

Figure E.3: C_{M_q} values for different angles of attack from experimental data (Toll & Queijo, 1948:58) compared with calculated values from vortex lattice methods.

determined. The aerodynamic damping was varied by 50% (as a worst case scenario) during the gull-wing sensitivity analysis to gauge the sensitivity of the handling qualities to such a large variation in damping.

Since the uncertainty in the damping coefficient was estimated, the uncertainty in the handling qualities analysis results resulting from this estimation error can be quantified. The handling qualities of the aircraft can therefore be determined to be within a certain band. The handling qualities can be judged to be acceptable or marginal by evaluating this band. This is sufficient for a preliminary handling quality analysis where a prototype aircraft is not yet available to measure handling qualities accurately by means of flight testing.

It is therefore concluded that the vortex lattice methods codes that are used in this study have the capability to calculate damping coefficients of swept wing aircraft with sufficient accuracy for handling qualities analysis.

Appendix F

$C_{M_{\delta e}}$ Benchmark Investigation

The accuracy with which the vortex lattice method, JKVLM, can predict the moment control surface derivative, $C_{M_{\delta_e}}$, was determined. $C_{M_{\delta_e}}$ is the aerodynamic moment resulting from elevon deflection. The ratio of $C_{M_{\delta_e}}$ to $C_{L_{\delta_e}}$ is important with respect to handling qualities for a tailless aircraft, since the elevon deflection on such an aircraft does not produce negligible aerodynamic lift. The aerodynamic lift may lead to an undesirable phenomenon called pancaking. $C_{L_{\delta_e}}$ is calculated with sufficient accuracy by VLM's, but not $C_{M_{\delta_e}}$.

This section presents JKVLM calculations that were used to determine the $C_{M_{\delta_e}}$ parameter for an elevator. An unswept elevator and a 35° swept-back elevator were analysed. The results were compared with wind tunnel results (see Dods (1948)) to determine the accuracy of the VLM predictions.

F.1 Planforms under Investigation

Two elevators having different planform characteristics (see Figure F.1) were used in the benchmark investigation. An unswept planform and one with a 35° sweep-back were used.

The models used to obtain the wind tunnel data for the different plan forms both had the NACA 64A010 airfoil. This is a symmetrical airfoil. The two planforms were modelled by flat plate panels in the vortex lattice models.

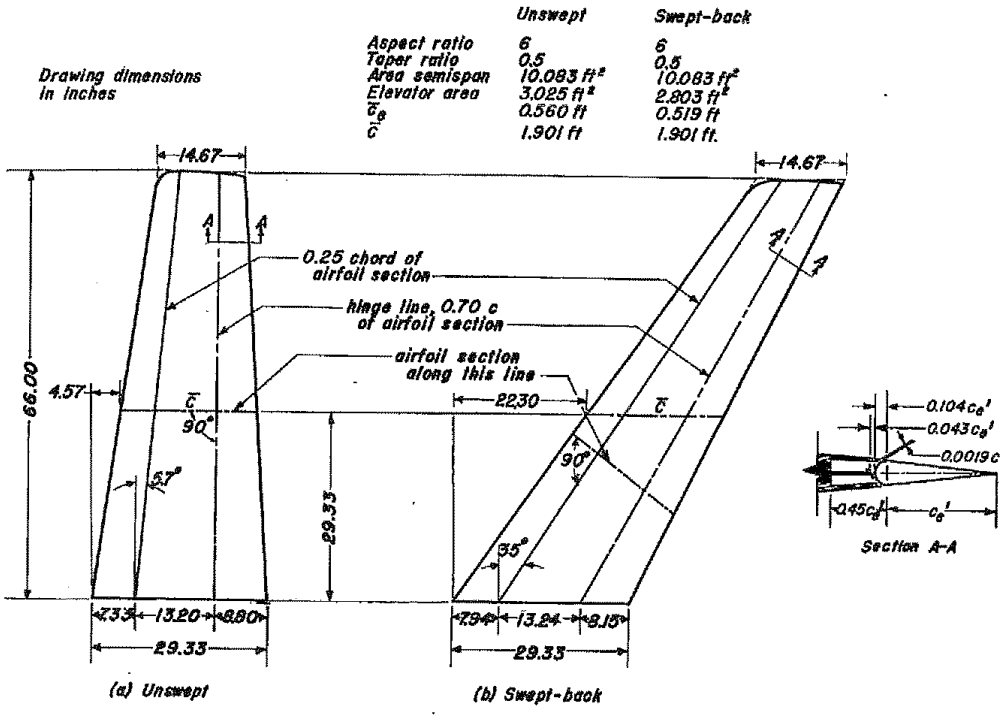

Figure F.1: Planforms of the horizontal tail models of aspect ratio 6 used in the benchmark investigation. (Dods, 1948:13)

F.2 Wind tunnel Data

The empirical lift and moment coefficient data presented in Dods (1948) was used to calculate $C_{M_{\delta_e}}$ for various angles of attack and elevator deflection angles. The wind tunnel data is presented in Figures F.3 to F.6.

The pitching moment coefficients shown in Figures F.4 and F.6 were measured around a lateral axis through a point at 25% the length of the mean aerodynamic chord. The position of the moment reference axis is presented in Figure F.2.

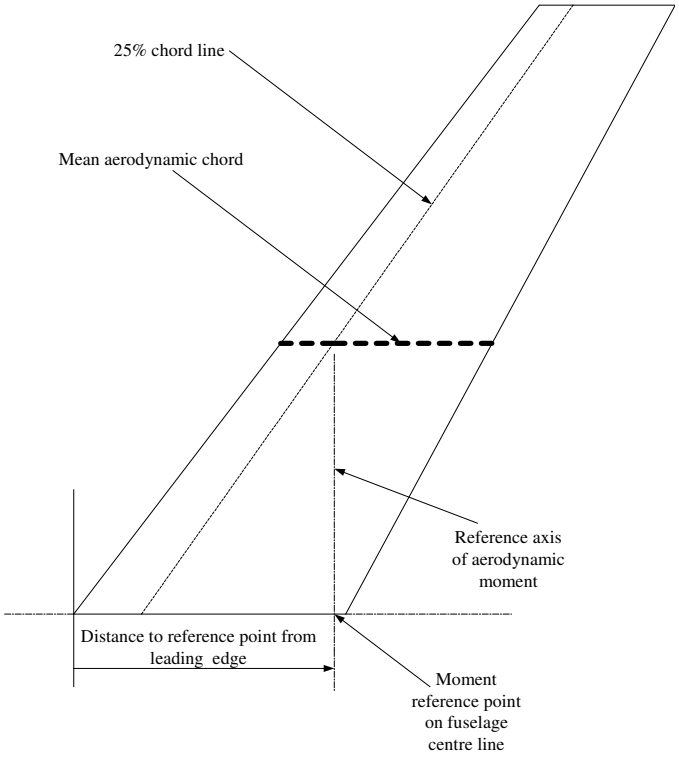

Figure F.2: Aerodynamic moment reference axis as used in Dods (1948:.)

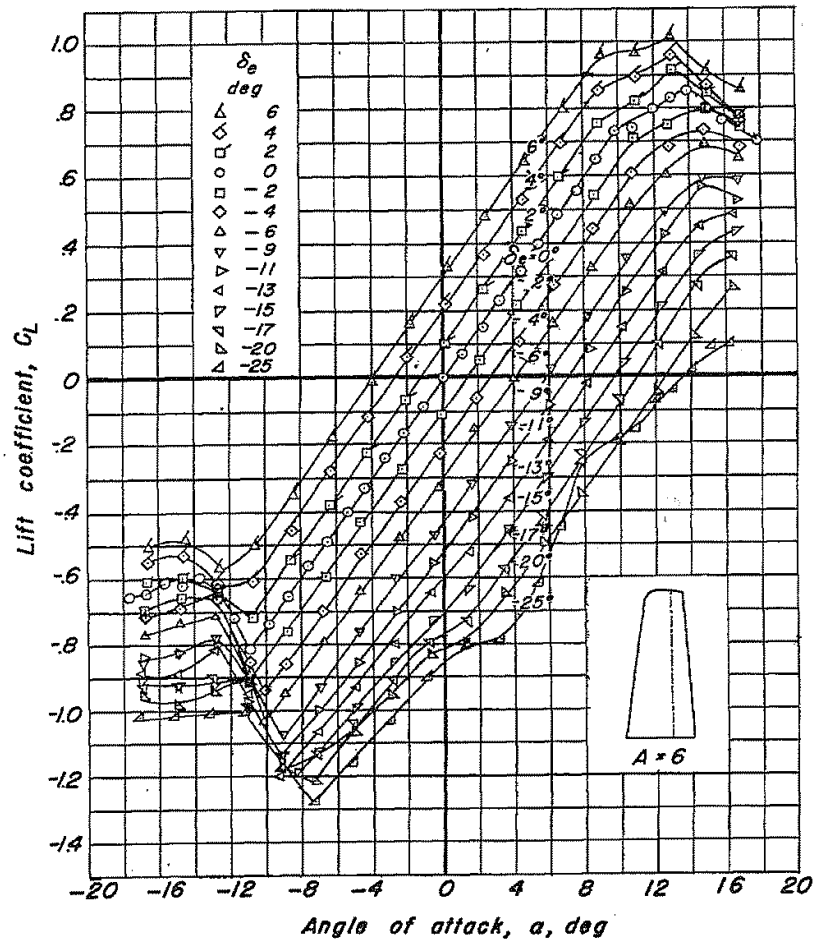

Figure F.3: Lift coefficients of an unswept tail. Aspect ratio, 6; R_e, 3.0×10^6. (Dods, 1948:19)

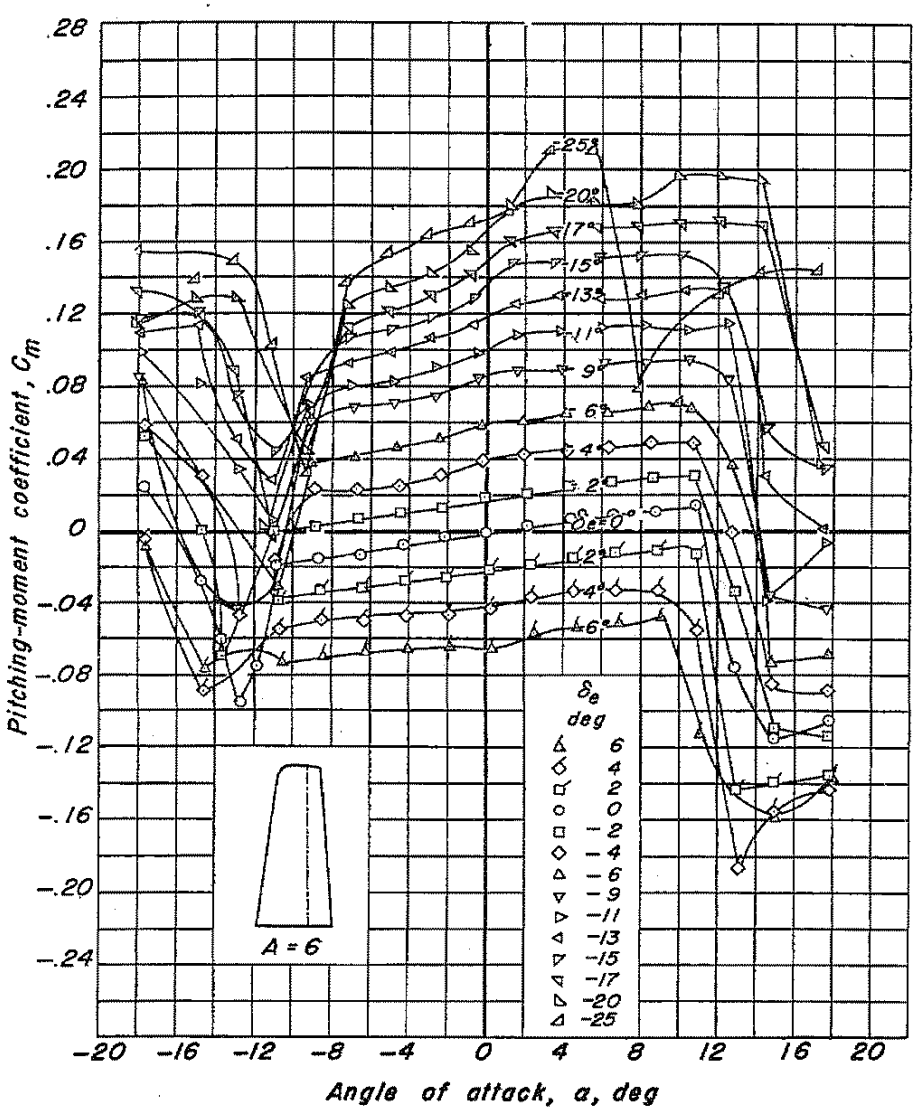

Figure F.4: Pitching moment coefficients of an unswept tail. Aspect ratio, 6; R_e, 3.0×10^6. The moments are measured around a lateral axis through a point that is 25% chordwise aft of the leading edge on the mean aerodynamic chord. (Dods, 1948:21)

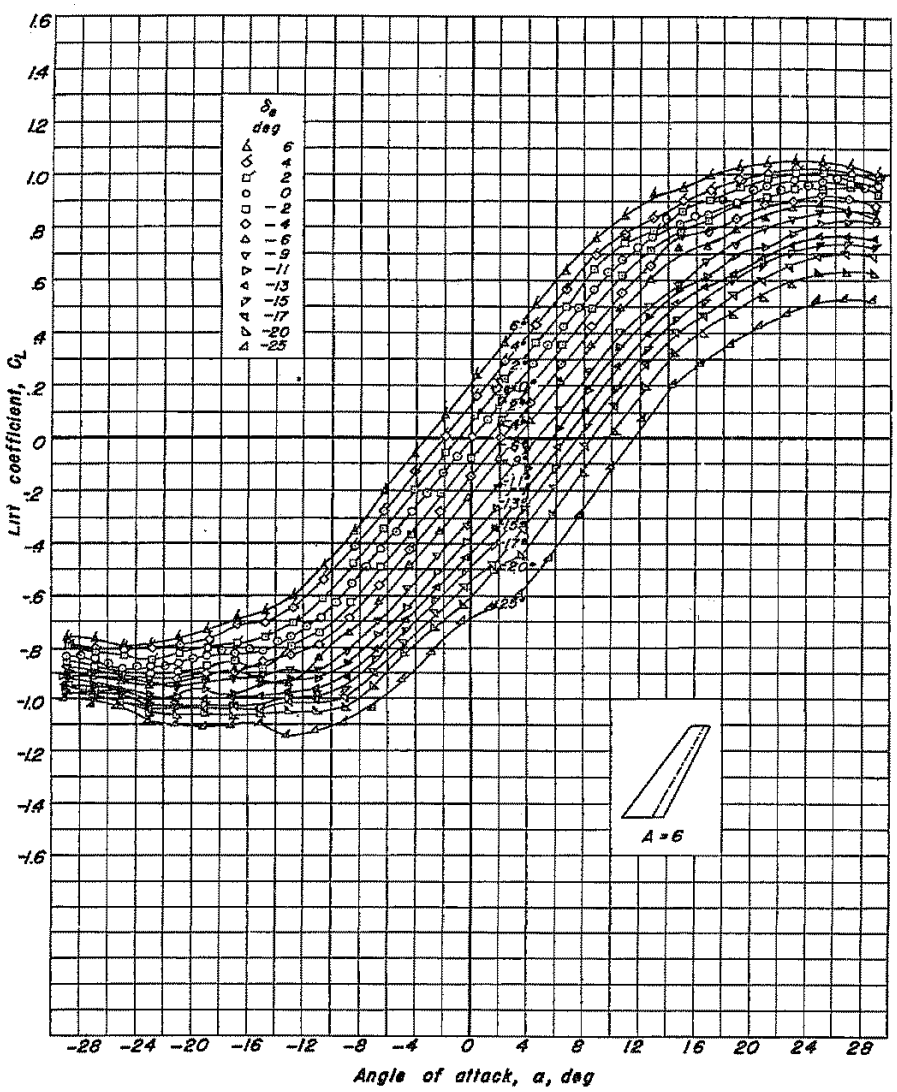

Figure F.5: Lift coefficients of a 35° swept-back tail. Aspect ratio, 6; R_e, 3.0×10^6. (Dods, 1948:29)

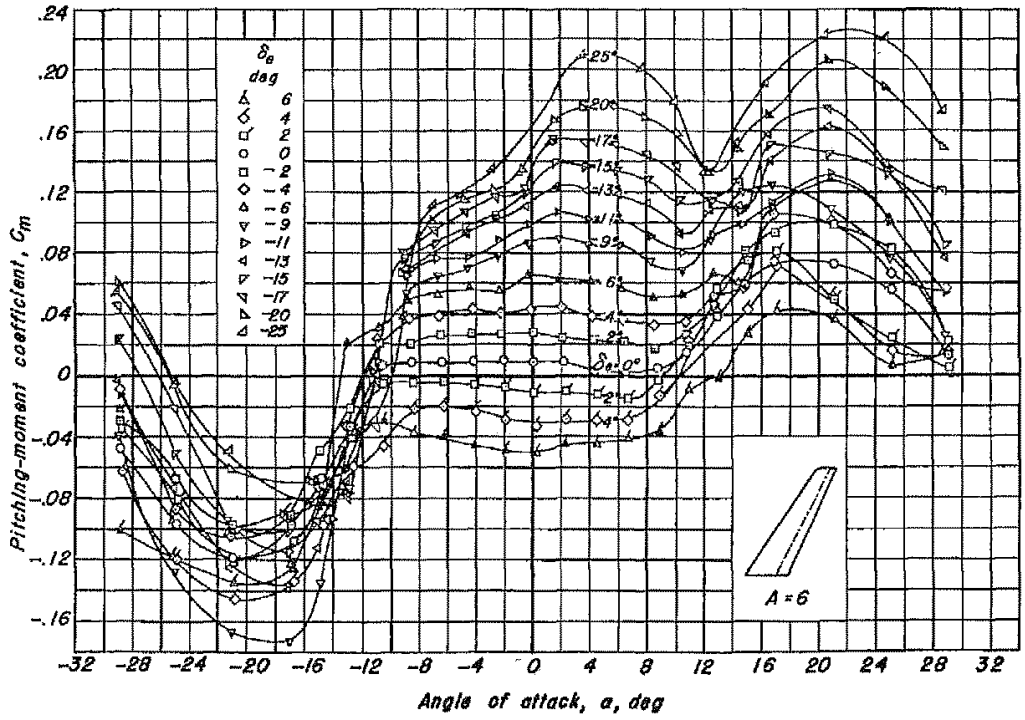

Figure F.6: Pitching moment coefficients of a 35° swept-back tail. Aspect ratio, 6; R_e, 3.0×10^6. The moments are measured around a lateral axis through a point that is 25% chordwise aft of the leading edge on the mean aerodynamic chord. (Dods, 1948:31)

F.3 The Sensitivity of $C_{M_{\delta_e}}$ with respect to Panel Size in VLM's.

A sensitivity study was performed to investigate the influence of the number of elements on the elevon panel on the magnitude of $C_{M_{\delta_e}}$. This parameter can not be adjusted in the JKVLM input file. The analysis was performed using the Tornado vortex lattice method that does have an input parameter for adjusting the number of elements on the elevon.

The sensitivity study was performed using the same elevator wing geometry described in Appendix F.2. Both the swept and unswept wing geometries were used in the sensitivity analysis.

The VLM panel layouts used in the sensitivity analysis are presented in Table F.1. The number of panels were increased on the control panel in order to investigate the effect of more panels on the convergence of the moment coefficient calculation.

Table F.1: VLM model sizes used for the $C_{M_{\delta_e}}$ sensitivity analysis.

Layout	Spanwise elements	Chordwise elements	Chordwise elements on control surface	Total elements
1	10	5	5	100
2	10	5	10	200
3	10	5	15	300
4	20	5	15	400
5	20	10	15	500

The results of the sensitivity study are presented in Figure F.7.

The sensitivity results indicate that the coefficients are already converged at 100 elements. Table F.2 presents JKVLM and Tornado results for the same geometric wing shapes that were used in the sensitivity analysis. The Tornado results are of the same order of magnitude as the JKVLM results. This indicates that the two codes give similar results and that the default number of elements of the JKVLM code produces a result that is sufficiently

converged.

Table F.2: Comparison of the JKVLM elevator deflection coefficients with Tornado results. All coefficients have the units [/rad]

	JKVLM		Tornado	
	Unswept wing	35° swept-back wing	Unswept wing	35° swept-back wing
$\partial C_L/\partial\alpha$	4.649	4.133	4.404	3.9482
$\partial C_M/\partial\alpha$	0.027	-0.167	0.065	-0.057
$\partial C_L/\partial\delta_e$	3.015	2.199	2.941	2.207
$\partial C_M/\partial\delta_e$	-0.634	-0.581	-0.598	-0.565

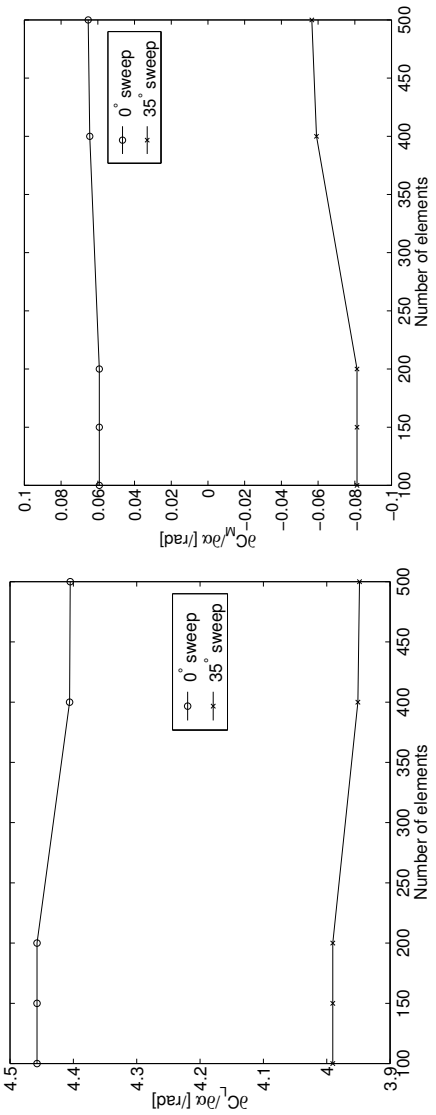

(a) C_{L_α} vs number of elements on wing for 0° and 35° sweep-back wing.

(b) C_{M_α} vs number of elements on wing for 0° and 35° sweep-back wing.

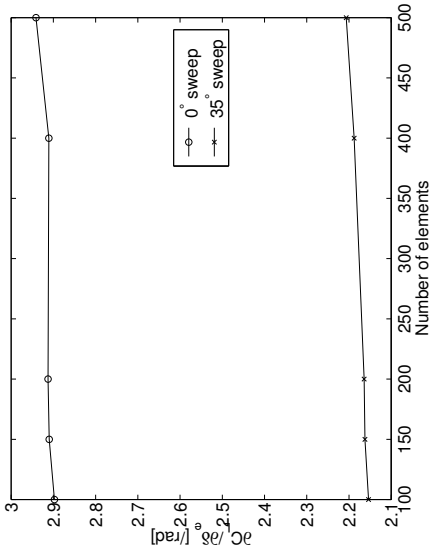

(c) $C_{L_{\delta_e}}$ vs number of elements on wing for 0° and 35° sweep-back wing.

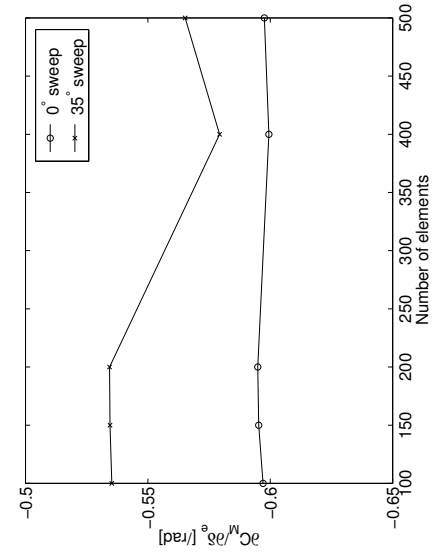

(d) $C_{M_{\delta_e}}$ vs number of elements on wing for 0° and 35° sweep-back wing.

Figure F.7: Sensitivity study with respect to the number of panel elements on the wing for the C_{L_α}, C_{M_α}, $C_{L_{\delta_e}}$ and $C_{M_{\delta_e}}$ parameters.

F.4 Results and Conclusions

The $C_{L_{\delta_e}}$ and $C_{M_{\delta_e}}$ estimates from JKVLM for the two types of elevator are presented in Table F.3. The JKVLM results are compared with wind tunnel results. The wind tunnel results presented in the table are for an angle of attack of 0°. The values of $C_{L_{\delta_e}}$ and $C_{M_{\delta_e}}$) presented in the table are average values for elevator deflections from -5° to 5°.

The reference position for the moment coefficients is around a lateral axis through the same reference point shown in F.2.

Table F.3: Comparison of the calculated elevator deflection coefficients with wind tunnel results for the same coefficients. All coefficients have the units [/rad]

	JKVLM		Wind tunnel	
	Unswept wing	35° swept-back wing	Unswept wing	35° swept-back wing
$\partial C_L/\partial\alpha$	4.649	4.133	4.257	3.581
$\partial C_M/\partial\alpha$	0.027	-0.167	0.082	0.000
$\partial C_L/\partial\delta_e$	3.015	2.199	3.063	1.910
$\partial C_M/\partial\delta_e$	-0.634	-0.581	-0.573	-0.537

The results from the JKVLM calculations for the two types of elevator for $C_{L_{\delta_e}}$ and $C_{M_{\delta_e}}$ are presented in Figure F.8. The JKVLM results are constant over the elevator deflection range. This is because the vortex lattice method is linear.

The following conclusions can be drawn from the results presented here:

- $C_{L_{\delta_e}}$ is predicted with satisfactory accuracy. For elevator deflection angles of -15° to 6° it is valid to treat the value of $C_{L_{\delta_e}}$ as constant. For more negative angles than -15° the value of the parameter cannot be considered constant any more. This can be attributed to viscous effects. This has little impact on the simulations presented in this study, since only small deflections (less than five degrees) are used.

- $C_{M_{\delta_e}}$ is not predicted very accurately by means of the vortex lattice

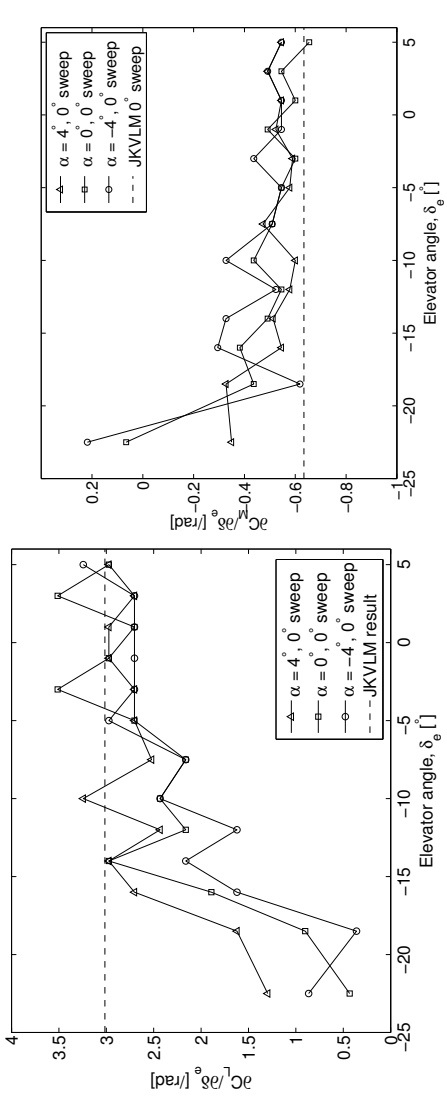

(a) $C_{L_{\delta_e}}$ vs elevator deflection for 0° sweep-back wing.

(b) $C_{M_{\delta_e}}$ vs elevator deflection for 0° sweep-back wing.

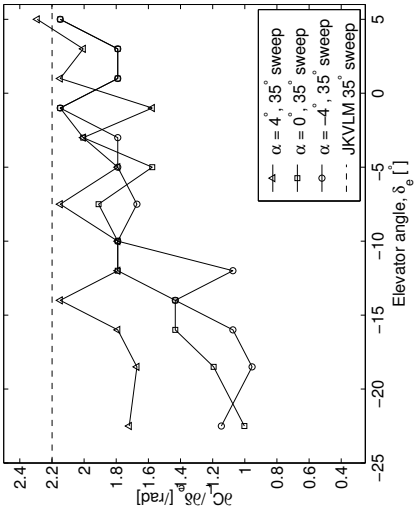

(c) $C_{L_{\delta_e}}$ vs elevator deflection for 35° sweep-back wing.

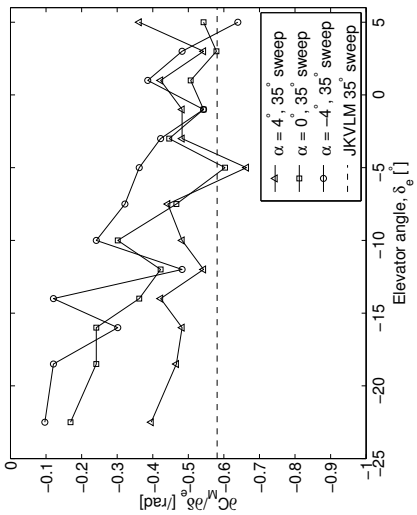

(d) $C_{M_{\delta_e}}$ vs elevator deflection for 35° sweep-back wing.

Figure F.8: Comparison of calculated values of $C_{L_{\delta_e}}$ and $C_{M_{\delta_e}}$ with wind tunnel data.

method. The estimation error is 20% from the vortex lattice baseline result for small angles of attack (less than four degrees) and small deflection angles (less than 5 degrees). This study is limited to small angles of attack and small deflection angles and therefore the estimation error figure of 20% shall be used in determining the sensitivity of the aircraft response to this error.

- C_{M_α} is not predicted accurately by means of the vortex lattice method. The discrepancy of the coefficient is larger for a swept-back wing than for an unswept wing. These errors are attributed to viscous effects and cross-flow that are not modelled in the vortex lattice method.

- As a general trend, prediction errors with respect to $C_{L_{\delta_e}}$, C_{L_α} and C_{M_α} are larger when the wing sweepback angle is larger.

- The accuracy of $C_{L_{\delta_e}}$ of the horizontal tail surface is important for the accurate simulation of the pitch plane dynamics of conventional aircraft with an empennage, while $C_{M_{\delta_e}}$ is more important for the accurate simulation of the pitch plane dynamics of tailless aircraft.

- The accuracy of the estimations of the aerodynamic coefficients is judged to be sufficient for a preliminary handling quality investigation such as the one presented in this work. The estimation error was quantified using the wind tunnel results. The handling qualities can be investigated for a range of the aerodynamic properties (particularly $C_{M_{\delta_e}}$). This range of handling quality results can then be used to determine the sensitivity with respect to the estimation error.

Appendix G

Neutral Point Benchmark Study

The accuracy of the prediction of the neutral point by means of the vortex lattice method was investigated. Wind tunnel results were used to estimate accuracy. The neutral point for two elevator models was calculated using the aerodynamic data presented in Dods (1948). The neutral points of the same two models were estimated using a VLM. The measured and estimated values for the two models are compared and presented here. The numerical convergence of the neutral point calculation with respect to the number of VLM elements used, is also investigated.

G.1 Wind tunnel results

The wind tunnel results used in the benchmark investigation of the moment control surface derivative, $C_{M_{\delta_e}}$, were also used for benchmarking of the neutral point. This data is presented in Appendix F.2. The wind tunnel results relevant to the neutral point are summarised in Table G.1. This table presents the neutral point and static margin for two elevator wind tunnel models. One model has no sweep and the other has 35° wing sweep. The position of the neutral point as presented in Table G.1 is expressed as a percentage of mean aerodynamic chord. The position is given as a distance

aft of the leading edge of the wing on the root chord. This convention is different from and should not be confused with the convention used in Dods (1948). In Dods (1948) the chordwise position on the wing is expressed as a fraction of the mean aerodynamic chord, aft of the leading edge of the wing at the spanwise position where the chord equals the mean aerodynamic chord.

Table G.1: Wind tunnel results for the neutral point. The neutral point position is given in percentage of mean aerodynamic chord.

Parameter	Unswept wing	35° swept-back wing
$\partial C_L/\partial\alpha$ [/rad]	4.257	3.581
$\partial C_M/\partial\alpha$ [/rad]	0.082	0.000
Static margin	-1.92%	0.00%
Neutral point	43.54%	122.90%

The neutral point of Table G.1 corresponds to an approximate position around the quarter chord, calculated at the mean aerodynamic chord. For the swept-back wing this position is significantly further aft of the leading edge at the root chord when compared to the unswept wing.

Table G.1 contains the item 'static margin'. For an aircraft the static margin is determined as the distance between the CG of the aircraft and the neutral point. In the case of the test specimen described here, the axis around which the aerodynamic moment was measured, was used as the chordwise 'CG' of the specimen and the static margin was calculated accordingly. The position of this axis was taken to be the chordwise quarter chord distance aft of the leading edge at that spanwise position where the chord of the test specimen equals the mean aerodynamic chord. This position is where one would expect the neutral point of a symmetrical profile to be. The actual neutral point is not at this position due to three dimensional flow effects.

The values of the neutral point and the static margin of the test specimen as presented in Table G.1 was obtained from the test results presented in Dods (1948).

G.2 Neutral Point Using VLM

The neutral point (and static margin) of the Exulans was estimated by means of a vortex lattice method (VLM). The vortex lattice method was chosen since it is often used to obtain a rapid estimation of aircraft properties while an aircraft is still in the concept phase. For a handling qualities investigation such as the one presented in this document, the fidelity of aircraft properties as calculated by the VLM is sufficient. This is justified by the fact that a general configuration is investigated (albeit with the Exulans as a specific example) and that a sensitivity analysis was performed to gauge the effect of inaccuracies in the aircraft model on predicted handling qualities. The VLM has some disadvantages (see Section G.3) leading to inaccurate predictions, but the accuracy can be quantified (see same Section) and has an acceptable magnitude.

In general a VLM models the wing or lifting surface of the aircraft as a series of closed trapezoidal vortex rings. The actual vortex ring is displaced downstream by a quarter chord of each panel. A control point is located at the center of each ring, where a non-penetration surface boundary condition is imposed. The strengths of each of the vortex rings must be found so that the vector sum of their induced velocity and the free-stream contribution at each control point satisfies the boundary conditions. The induced velocity at a point due to a straight line segment of a vortex filament is given by the Biot-Savart Law. The vortex strengths of the lifting surface panels are represented by a system of simultaneous linear equations. These equations are solved to obtain the vortex strengths. The vortex strengths are integrated over the surface to obtain the aerodynamic forces and moments. Once the moment distribution over the lifting surface is known, the sum of moments may be used to find the point on the lifting surface where the aerodynamic moment is a constant with respect to angle of attack. This point is known as the neutral point of the lifting surface. Kay et al. (1996) may be consulted for a more detailed description of the vortex lattice method theory.

The JKVLM programme was the vortex lattice method used for estimating the neutral point of the gull wing configuration. This programme has

static margin as one of its output parameters. The moment reference point of the aircraft is an input parameter for JKVLM. This point was varied until the calculated static margin was zero. At this point the neutral point coincides with the reference point. This method was also used to calculate the neutral point for the neutral point benchmark study.

The geometry of the wing models of Dods (1948) was entered into the JKVLM programme and the neutral point and static margin of these models were estimated. The results of this effort is presented in Table G.2. The sensitivity of the neutral point value with respect to the number of vortex lattice elements was also investigated. It showed that reasonable convergence was achieved from 120 elements on a wing model (Figure G.1). The position of the moment reference point that was used for the elevator test specimens of Dods (1948) was entered as a CG reference in the vortex lattice method with which the same geometry was analysed. The distance between the neutral point of the elevator geometry analysed with the VLM and this reference point is the static margin value that is presented in Figure G.1.

Table G.2: VLM results for the neutral point. The neutral point position is given in percentage of mean aerodynamic chord.

Parameter	Unswept wing	35° swept-back wing
$\partial C_L/\partial\alpha$ [/rad]	4.494	4.002
$\partial C_M/\partial\alpha$ [/rad]	0.047	-0.085
Static margin	-1.06%	2.13%
Neutral point	44.40%	125.03%

G.3 Wind tunnel and VLM Comparison

The neutral point and static margin from wind tunnel data for the models of Dods (1948) can be compared with the VLM estimates for the same models. The static margin of the wind tunnel elevator specimen was determined by measuring aerodynamic moments around a fixed reference point. The distance of this point to the neutral point of the elevator test specimen is defined

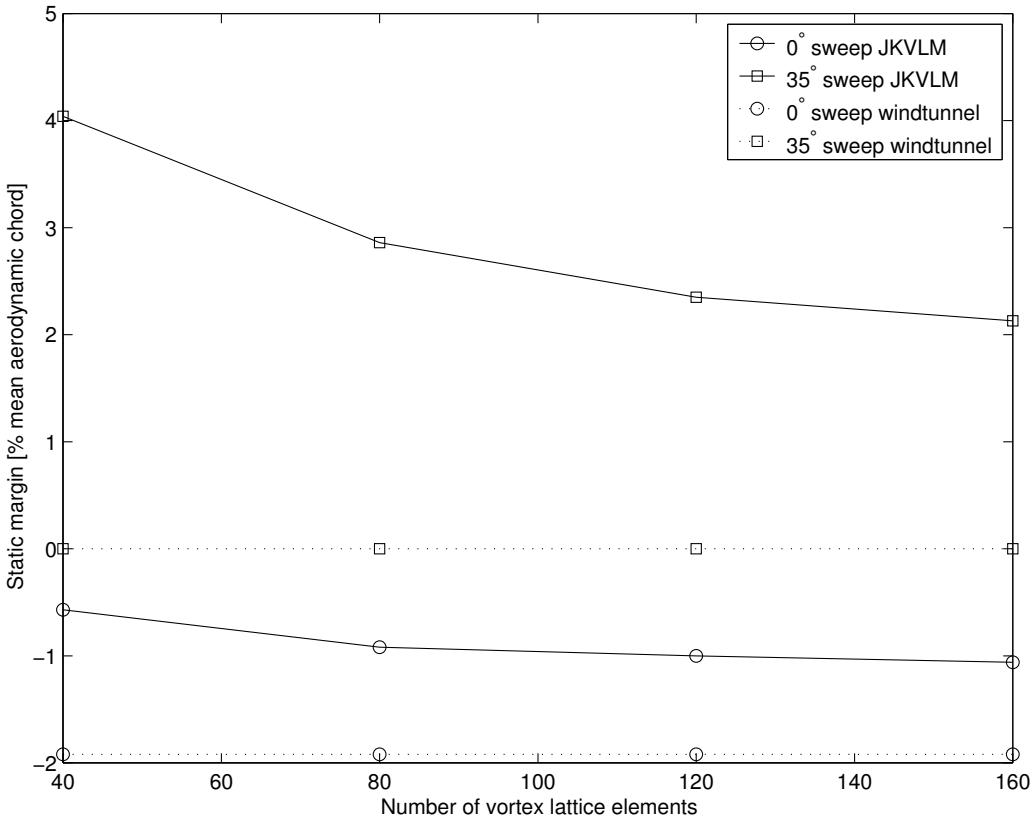

Figure G.1: Convergence of static margin with respect to number of VLM elements.

as the static margin for the test specimen. In the case of an aircraft, the CG of the aircraft would be used as this reference point. The comparison is presented in Table G.3. The following limitations of VLM's are important when making this comparison:

- Airfoil thickness is not modelled and this leads to the underestimation of aerodynamic lift in the case of very thick airfoil sections.
- JKVLM does not model wing camber. This leads to an incorrect estimate of the zero lift angle of attack.
- Viscous effects are neglected in VLM estimates.

- The VLM results are only valid in the linear region of aerodynamics and at small angles of attack (typically -5° to 5°). This is not a severe limitation for the current study since all simulations are with small disturbances and at small angles of attack.

Table G.3: Comparison of the wind tunnel and VLM results for the neutral point and static margin.

	JKVLM		Wind tunnel	
	Unswept wing	35° swept-back wing	Unswept wing	35° swept-back wing
Static margin	-1.06%	2.13%	-1.92%	0.00%
Neutral point	44.40%	125.03%	43.54%	122.90%

It may be concluded from the results presented in Table G.3 that JKVLM has a maximum error of around 3% for the estimation for the static margin at 30° sweep angles. The VLM tends to overestimate the magnitude of static margin. The prediction error becomes greater at higher wing sweep angles. The error in prediction at greater sweep angles may be ascribed to the fact that spanwise flow effects are not modelled. Viscous effects are also neglected and therefore lift and aerodynamic moment are predicted incorrectly. This in turns leads to incorrect neutral point and static margin estimates.

G.4 Conclusions

The prediction error of the neutral point (using VLM's) for unswept wings is less than 1% and less than 3% for swept wings. This should be viewed as sufficiently accurate for the purpose of a handling qualities investigation on a general configuration.

This level of accuracy is also sufficient for the case of the Exulans, since no complete design (or prototype aircraft) existed at the time of completion of this study. Possible future aerodynamic and fuselage shape design changes have the potential of changing the neutral point by a larger margin than

the error of the prediction method. Once the Exulans design is completed, the neutral point can be accurately estimated using methods such as CFD. The impact of any changes in neutral point may then be assessed by the sensitivity study presented in this document.

Furthermore it is possible to alter static margin within a limited range by changing aircraft CG. It should be possible to alter the CG of the Exulans by design changes within the 3% range.

Based on these points, the level of accuracy of the VLM is therefore judged to be acceptable for the purposes of this handling quality investigation.

Appendix H

Aircraft Configurations

The aircraft configurations listed in this section were used in the pitch control analysis simulations, as well as the gust response analysis simulations. The different configurations are described by means of codes. The legend of the codes is presented in the following table:

Legend for sweep symbols	
Symbol	Declaration
20°	20 degrees outboard wing sweep (γ)
24°	24 degrees outboard wing sweep (γ)
30°	30 degrees outboard wing sweep (γ)
36°	36 degrees outboard wing sweep (γ)

Legend for static margins	
Symbol	Declaration
2%	2% @ 30° sweep
5%	5% @ 30° sweep
10.7%	10.7% @ 30° sweep
15%	15% @ 30° sweep

Legend for control authority	
Symbol	Declaration
cm20	control baseline minus 20% ($C_{L_{\delta_e}}$ kept at the baseline and $C_{M_{\delta_e}}$ reduced by 20%)
cp20	control baseline plus 20% ($C_{L_{\delta_e}}$ kept at the baseline and $C_{M_{\delta_e}}$ increased by 20%)
c	control baseline

Legend for damping ratio	
Symbol	Declaration
dm20	damping baseline minus 20%
dp20	damping baseline plus 20%
d	damping baseline

The aircraft configurations presented in the following tables were used in the pitch control analysis simulations.

Table H.1: The aircraft configurations investigated in the pitch control effectiveness analysis.

Number	Description
1	20° 2% cm20 dm20
2	20° 2% cm20 dp20
3	20° 2% cm20 d
4	20° 2% cp20 dm20
5	20° 2% cp20 dp20
6	20° 2% cp20 d
7	20° 2% c dm20
8	20° 2% c dp20
9	20° 2% c d
10	20° 5% cm20 dm20
11	20° 5% cm20 dp20
12	20° 5% cm20 d
13	20° 5% cp20 dm20
14	20° 5% cp20 dp20
15	20° 5% cp20 d
16	20° 5% c dm20
17	20° 5% c dp20
18	20° 5% c d
19	20° 10.7% cm20 dm20
20	20° 10.7% cm20 dp20
21	20° 10.7% cm20 d
22	20° 10.7% cp20 dm20
23	20° 10.7% cp20 dp20
24	20° 10.7% cp20 d
25	20° 10.7% c dm20
26	20° 10.7% c dp20
27	20° 10.7% c d
28	20° 15% cm20 dm20
29	20° 15% cm20 dp20
30	20° 15% cm20 d
31	20° 15% cp20 dm20
32	20° 15% cp20 dp20
33	20° 15% cp20 d
34	20° 15% c dm20
35	20° 15% c dp20
36	20° 15% c d

Number	Description
37	24° 2% cm20 dm20
38	24° 2% cm20 dp20
39	24° 2% cm20 d
40	24° 2% cp20 dm20
41	24° 2% cp20 dp20
42	24° 2% cp20 d
43	24° 2% c dm20
44	24° 2% c dp20
45	24° 2% c d
46	24° 5% cm20 dm20
47	24° 5% cm20 dp20
48	24° 5% cm20 d
49	24° 5% cp20 dm20
50	24° 5% cp20 dp20
51	24° 5% cp20 d
52	24° 5% c dm20
53	24° 5% c dp20
54	24° 5% c d
55	24° 10.7% cm20 dm20
56	24° 10.7% cm20 dp20
57	24° 10.7% cm20 d
58	24° 10.7% cp20 dm20
59	24° 10.7% cp20 dp20
60	24° 10.7% cp20 d
61	24° 10.7% c dm20
62	24° 10.7% c dp20
63	24° 10.7% c d
64	24° 15% cm20 dm20
65	24° 15% cm20 dp20
66	24° 15% cm20 d
67	24° 15% cp20 dm20
68	24° 15% cp20 dp20
69	24° 15% cp20 d
70	24° 15% c dm20
71	24° 15% c dp20
72	24° 15% c d

Number	Description
73	30° 2% cm20 dm20
74	30° 2% cm20 dp20
75	30° 2% cm20 d
76	30° 2% cp20 dm20
77	30° 2% cp20 dp20
78	30° 2% cp20 d
79	30° 2% c dm20
80	30° 2% c dp20
81	30° 2% c d
82	30° 5% cm20 dm20
83	30° 5% cm20 dp20
84	30° 5% cm20 d
85	30° 5% cp20 dm20
86	30° 5% cp20 dp20
87	30° 5% cp20 d
88	30° 5% c dm20
89	30° 5% c dp20
90	30° 5% c d
91	30° 10.7% cm20 dm20
92	30° 10.7% cm20 dp20
93	30° 10.7% cm20 d
94	30° 10.7% cp20 dm20
95	30° 10.7% cp20 dp20
96	30° 10.7% cp20 d
97	30° 10.7% c dm20
98	30° 10.7% c dp20
99	30° 10.7% c d
100	30° 15% cm20 dm20
101	30° 15% cm20 dp20
102	30° 15% cm20 d
103	30° 15% cp20 dm20
104	30° 15% cp20 dp20
105	30° 15% cp20 d
106	30° 15% c dm20
107	30° 15% c dp20
108	30° 15% c d

Number	Description
109	36° 2% cm20 dm20
110	36° 2% cm20 dp20
111	36° 2% cm20 d
112	36° 2% cp20 dm20
113	36° 2% cp20 dp20
114	36° 2% cp20 d
115	36° 2% c dm20
116	36° 2% c dp20
117	36° 2% c d
118	36° 5% cm20 dm20
119	36° 5% cm20 dp20
120	36° 5% cm20 d
121	36° 5% cp20 dm20
122	36° 5% cp20 dp20
123	36° 5% cp20 d
124	36° 5% c dm20
125	36° 5% c dp20
126	36° 5% c d
127	36° 10.7% cm20 dm20
128	36° 10.7% cm20 dp20
129	36° 10.7% cm20 d
130	36° 10.7% cp20 dm20
131	36° 10.7% cp20 dp20
132	36° 10.7% cp20 d
133	36° 10.7% c dm20
134	36° 10.7% c dp20
135	36° 10.7% c d
136	36° 15% cm20 dm20
137	36° 15% cm20 dp20
138	36° 15% cm20 d
139	36° 15% cp20 dm20
140	36° 15% cp20 dp20
141	36° 15% cp20 d
142	36° 15% c dm20
143	36° 15% c dp20
144	36° 15% c d

The aircraft configurations presented in the following tables were used in the gust response analysis simulations.

Table H.2: The aircraft configurations investigated in the gust response and eigenvalue analysis.

Number	Description
1	20° 2% dm20
2	20° 2% dp20
3	20° 2% d
4	20° 5% dm20
5	20° 5% dp20
6	20° 5% d
7	20° 10.7% dm20
8	20° 10.7% dp20
9	20° 10.7% d
10	20° 15% dm20
11	20° 15% dp20
12	20° 15% d
13	24° 2% dm20
14	24° 2% dp20
15	24° 2% d
16	24° 5% dm20
17	24° 5% dp20
18	24° 5% d
19	24° 10.7% dm20
20	24° 10.7% dp20
21	24° 10.7% d
22	24° 15% dm20
23	24° 15% dp20
24	24° 15% d

Number	Description
25	30° 2% dm20
26	30° 2% dp20
27	30° 2% d
28	30° 5% dm20
29	30° 5% dp20
30	30° 5% d
31	30° 10.7% dm20
32	30° 10.7% dp20
33	30° 10.7% d
34	30° 15% dm20
35	30° 15% dp20
36	30° 15% d
37	36° 2% dm20
38	36° 2% dp20
39	36° 2% d
40	36° 5% dm20
41	36° 5% dp20
42	36° 5% d
43	36° 10.7% dm20
44	36° 10.7% dp20
45	36° 10.7% d
46	36° 15% dm20
47	36° 15% dp20
48	36° 15% d

Appendix I

Time Domain Simulations

I.1 Pitch Control Input Analysis

Simulations were performed with the gull-wing mathematical model in order to investigate pitch control input response. The damping, control authority and static margin of the model were varied to investigate the effect on the aircraft step response. The simulations of the pitch control input analysis differs from the gull wing sensitivity analysis (Section 5.4) in the sense that only one parameter value was changed in isolation in the case of the sensitivity study. In reality many of the parameters of the aircraft model have coupling effects with other parameters. A change in the CG, for example, has an influence on the aerodynamic pitch damping coefficient (C_{M_q})[1]. With the gull wing sensitivity analysis other parameters such as damping were held constant while CG was varied in order to investigate the effect and sensitivity of each parameter on the aircraft dynamics in isolation. With the pitch control input analysis the influence of parameter changes on other parameters was included in the simulation models.

The aircraft mathematical models were subjected to elevon step inputs (-1 degree, resulting in nose up rotation) during simulation runs.

A matrix of different aircraft configurations was defined for the use of

[1]The change in magnitude of pitch damping coefficient with a change in CG is not negligible in the case of tailless aircraft.

the pitch control input analysis. Each of the configurations was used in a simulation with an elevon step input. Inertia was kept constant at the baseline value for all configurations, because it was shown in Chapter 5 that a change in pitch inertia does not have a sufficiently large influence on the aircraft response.

The control authority was varied in the following ways: For one set of model configurations the control authority was 20% higher than the baseline and for the other the control authority was 20% lower than the baseline. The third model configuration had the baseline control authority.

The model parameter values for aerodynamic damping were varied as follows: A baseline damping configuration was used for one set of simulations. A configuration with 20% higher damping than the baseline configuration was used for another set of simulations and a configuration with 20% lower damping than the baseline configuration was used for yet another set of simulations.

The static margin was varied in the following ways for the different aircraft mathematical models used in the different simulations to provide the following configurations:

- 2% at 30° sweep
- 5% at 30° sweep
- 10.7% at 30° sweep
- 15% at 30° sweep

The static margin is specified at a certain sweep angle, because static margin is a function of the sweep angle of the outboard wing.

The variations of parameters were not implemented on the mathematical models in isolation of other parameters, as was the case with the sensitivity analysis of Chapter 5. In other words, if the static margin changed, the damping also changed along with the elevon control authority.

The control authority simulations were performed for the following values of wing sweep:

- 20° sweep
- 24° sweep
- 30° sweep
- 36° sweep

The parameter variations described here lead to a matrix of 144 aircraft configurations. The simulation schedule for the different models is noted in Appendix H. Each simulation configuration for the pitch response analysis is numbered there and the numbering system will be used to refer to the configurations and associated simulation results. The simulation results for all the configurations are not all displayed in this section or the rest of the document. The following simulation results were chosen for inclusion in the document:

- All static margin variations at 30° sweep having the baseline aerodynamic damping and control authority. (Configurations 81, 90, 99, 108) Only this set of configurations is plotted in the main document, while the other sets are documented in this Appendix. Baseline values refer to the calculated model parameter values as presented in Section 4.7.
- All static margin variations at 24° sweep having the baseline aerodynamic damping and control authority. (Configurations 45, 54, 63, 72. Configurations 45 and 54 are statically unstable and therefore no results are plotted)
- All static margin variations at 36° sweep having the baseline aerodynamic damping and control authority. (Configurations 117, 126, 135, 144)
- All control authority variations at 30° sweep with the baseline aerodynamic damping at a 10.7% (at 30°) static margin configuration. (Configurations 93, 96, 99)

- All control authority variations at 24° sweep with the baseline aerodynamic damping at a 10.7% (at 30°) static margin configuration. (Configurations 57, 60, 63)
- All damping variations at 30° sweep with the baseline control authority at a 10.7% (at 30°) static margin configuration. (Configurations 97, 98, 99)

The results of the first item are presented in this section. The rest are shown in Appendix I.2. All the results are discussed here.

The simulations shown here were performed with a step input as described in Section 4.8.2.

The time domain simulations predictably show that higher control authority leads to a more rapid initial aircraft response. Lower static margins show higher magnitude pitch responses than higher static margins. The higher pitch responses are accompanied by high pitch rates and normal accelerations.

Damping decreases the magnitude of the pitch response and makes the pitching moment less rapid. Damping has a smaller effect on the natural frequency of the aircraft modes than static margin.

The pitch step responses of the different gull-wing configurations are oscillatory in nature. The phugoid mode is not strongly damped. The step response is similar in shape to the step response of the SB-13 aircraft shown in Mönnich & Dalldorff (1993:349). The aircraft tends to pitch down after the initial upward pitching motion, even though the control input is held constant.

Configuration 45 was statically unstable. The simulation response of this configuration is not shown because it was divergent. This type of configuration needs to be investigated with controller (pilot) in the loop study. The pilot or controller may prevent a divergent response.

α, θ, pitch rate, normal acceleration and speed versus time were plotted as the output of this investigation. These parameters were chosen because they are most important for studying the aircraft modes. The normal acceleration is included because it is used in the calculation of the C-star response. Pitch

rate and normal acceleration have a large influence on the pilot opinion of an aircraft configuration.

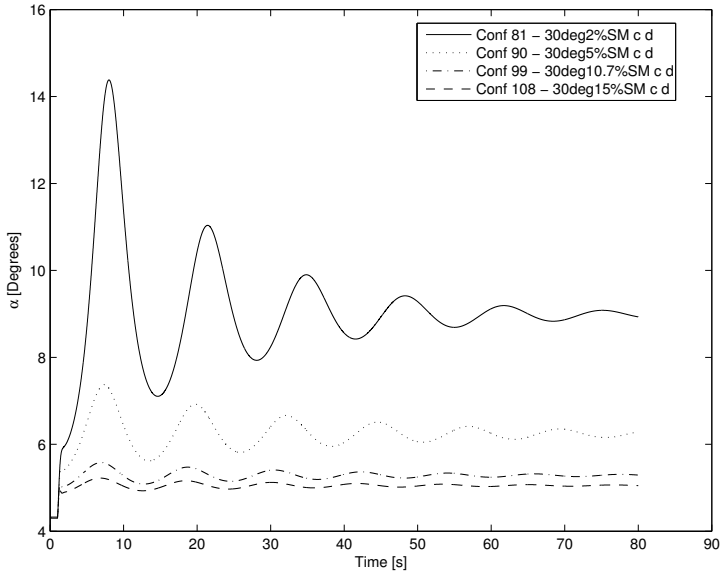

Figure I.1: Response in aircraft angle of attack (α) to a unit step elevon control input for 30° outboard wing sweep at different static margins with the baseline control authority and aerodynamic damping.

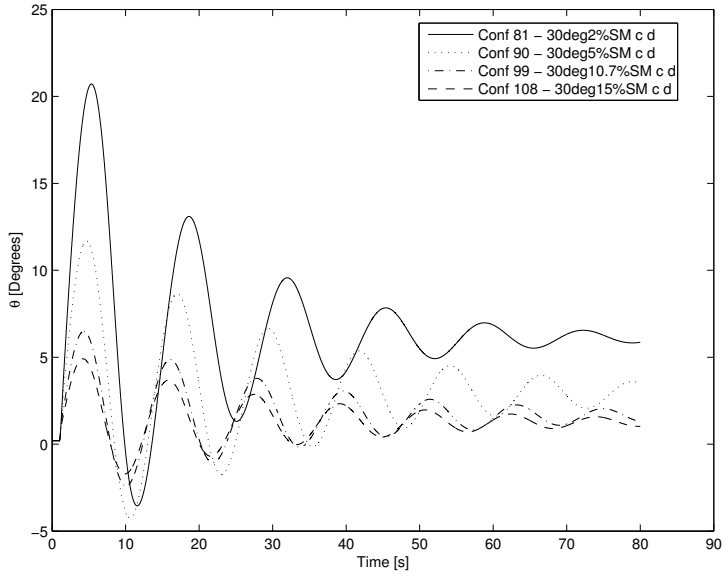

Figure I.2: Response in aircraft attitude (θ) to a unit step elevon control input to a unit step elevon control input for 30° outboard wing sweep at different static margins with the baseline control authority and aerodynamic damping.

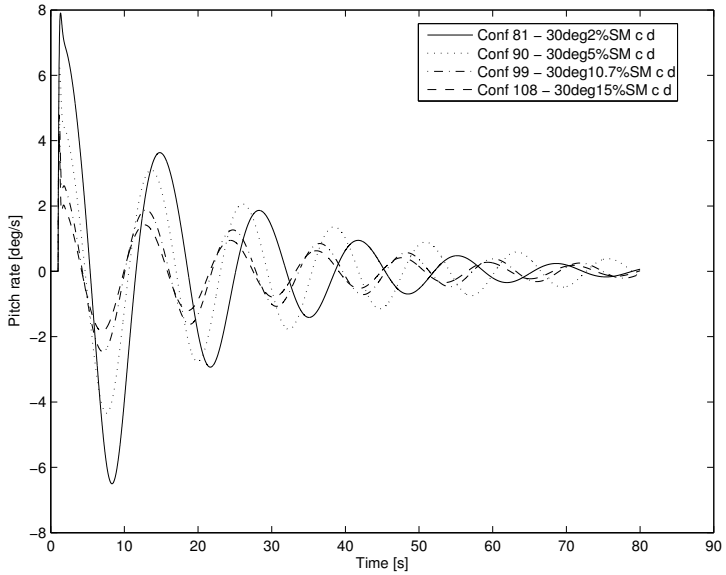

Figure I.3: Response in aircraft pitch rate to a unit step elevon control input for 30° outboard wing sweep at different static margins with the baseline control authority and aerodynamic damping.

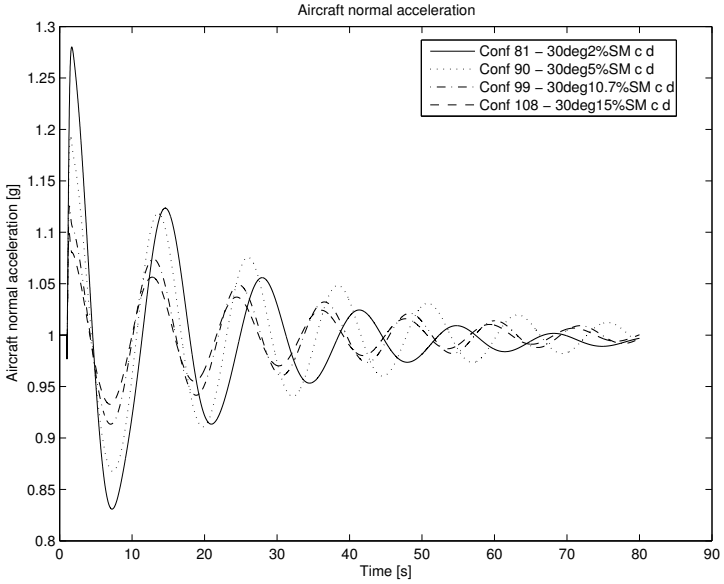

Figure I.4: Response in aircraft normal acceleration to a unit step elevon control input for 30° outboard wing sweep at different static margins with the baseline control authority and aerodynamic damping.

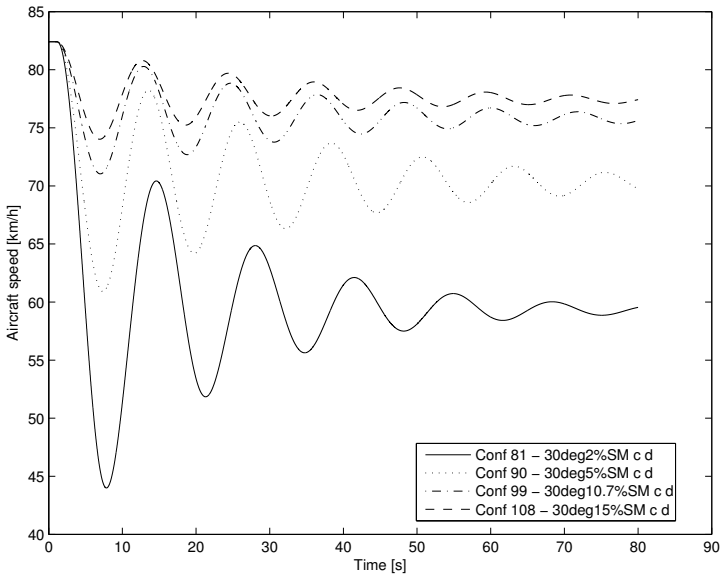

Figure I.5: Response in aircraft airspeed to a unit step elevon control input for 30° outboard wing sweep at different static margins with the baseline control authority and aerodynamic damping.

I.2 Pitch Control Input Simulations

I.2.1 Configurations 45, 54, 63, 72

Simulation results of all static margin variations at 24° sweep having the baseline aerodynamic damping and control authority. (Configurations 45 (unstable, not plotted), 54, 63, 72)

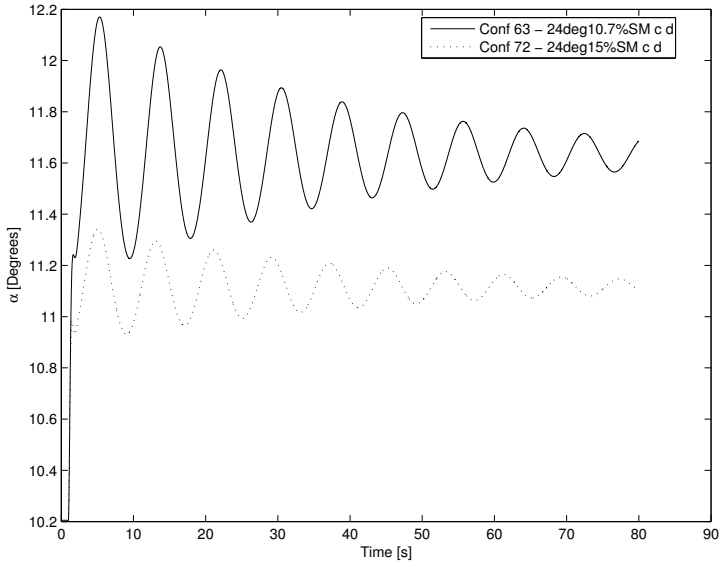

Figure I.6: Response in aircraft angle of attack (α) to a unit step elevon control input for 24° outboard wing sweep at different static margins with the baseline control authority and aerodynamic damping.

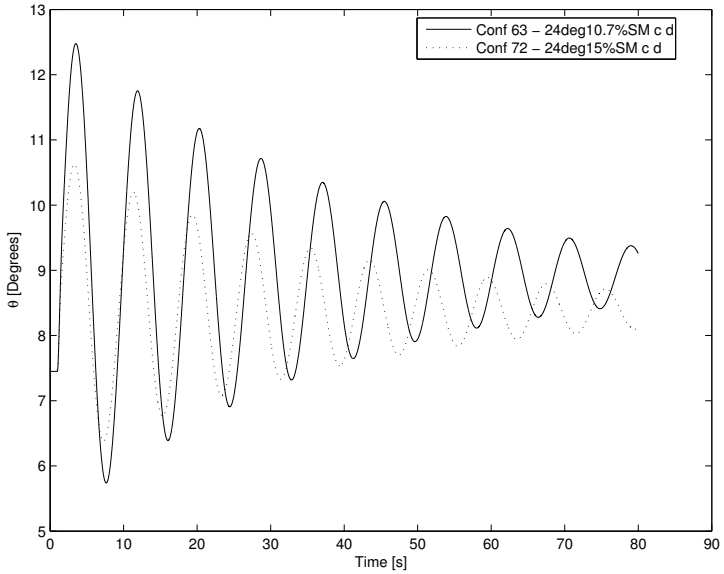

Figure I.7: Response in aircraft attitude (θ) to a unit step elevon control input for 24° outboard wing sweep at different static margins with the baseline control authority and aerodynamic damping.

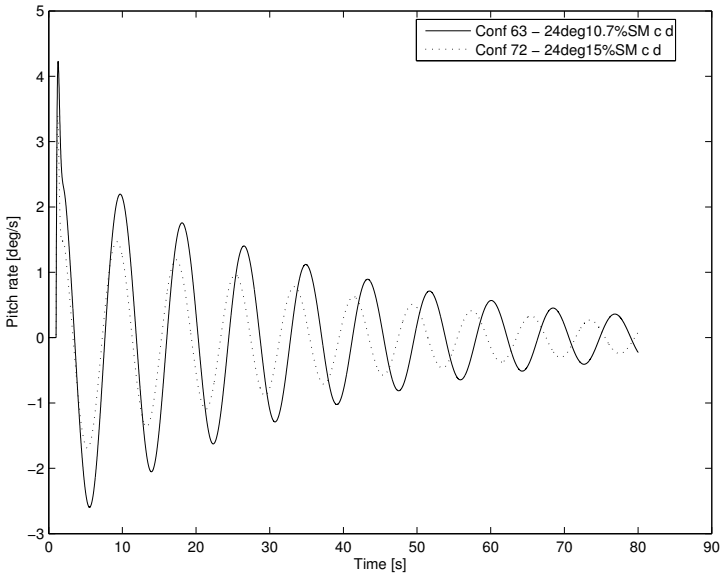

Figure I.8: Response in aircraft pitch rate to a unit step elevon control input for 24° outboard wing sweep at different static margins with the baseline control authority and aerodynamic damping.

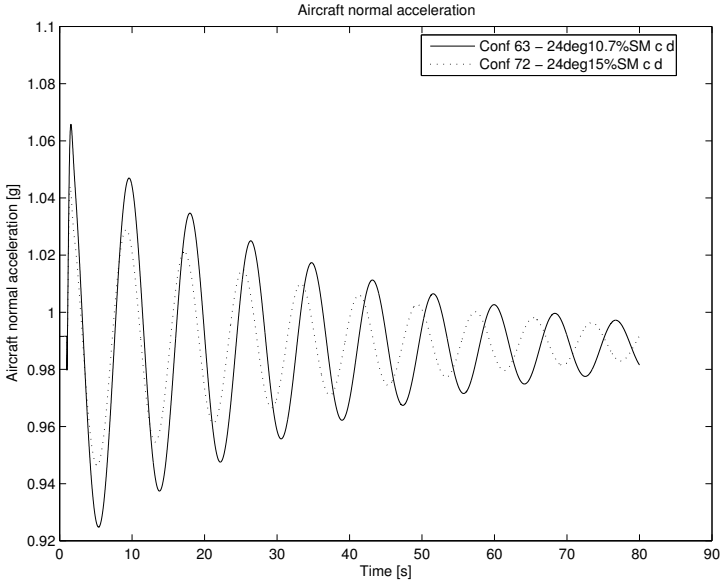

Figure I.9: Response in aircraft normal acceleration to a unit step elevon control input for 24° outboard wing sweep at different static margins with the baseline control authority and aerodynamic damping.

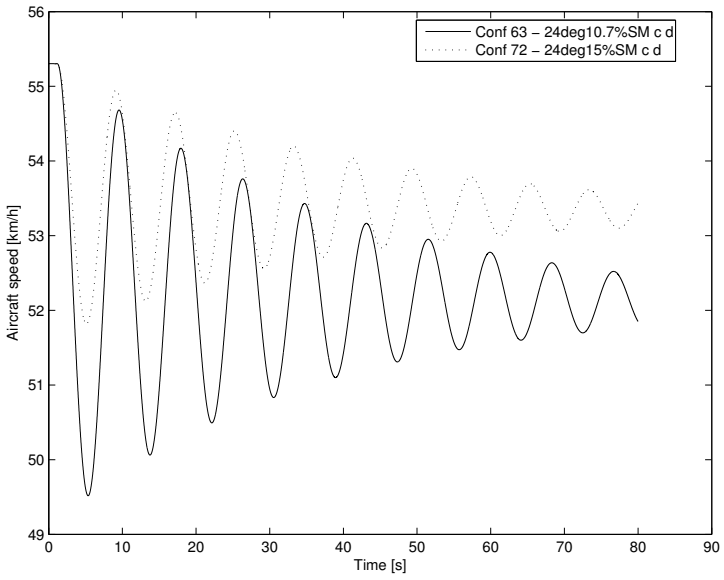

Figure I.10: Response in aircraft airspeed to a unit step elevon control input for 24° outboard wing sweep at different static margins with the baseline control authority and aerodynamic damping.

I.2.2 Configurations 117, 126, 135, 144

Simulation results of all static margin variations at 36° sweep having the baseline aerodynamic damping and control authority. (Configurations 117, 126, 135, 144)

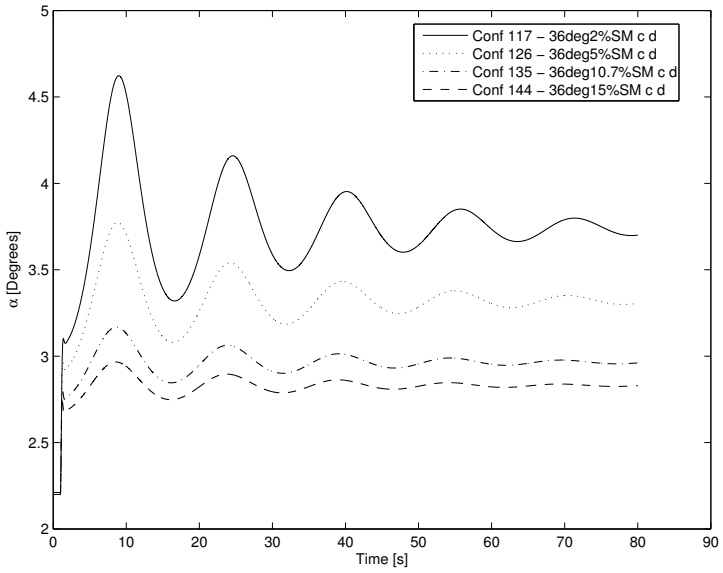

Figure I.11: Response in aircraft angle of attack (α) to a unit step elevon control input for 36° outboard wing sweep at different static margins with the baseline control authority and aerodynamic damping.

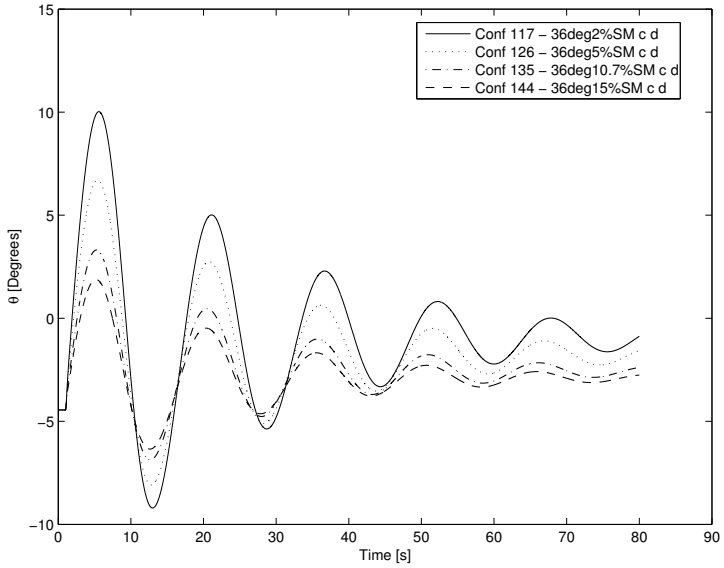

Figure I.12: Response in aircraft attitude (θ) to a unit step elevon control input for 36° outboard wing sweep at different static margins with the baseline control authority and aerodynamic damping.

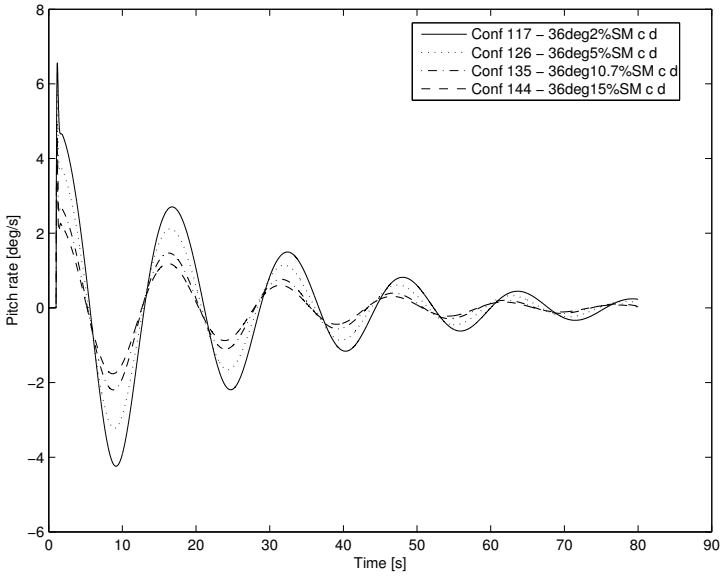

Figure I.13: Response in aircraft pitch rate to a unit step elevon control input for 36° outboard wing sweep at different static margins with the baseline control authority and aerodynamic damping.

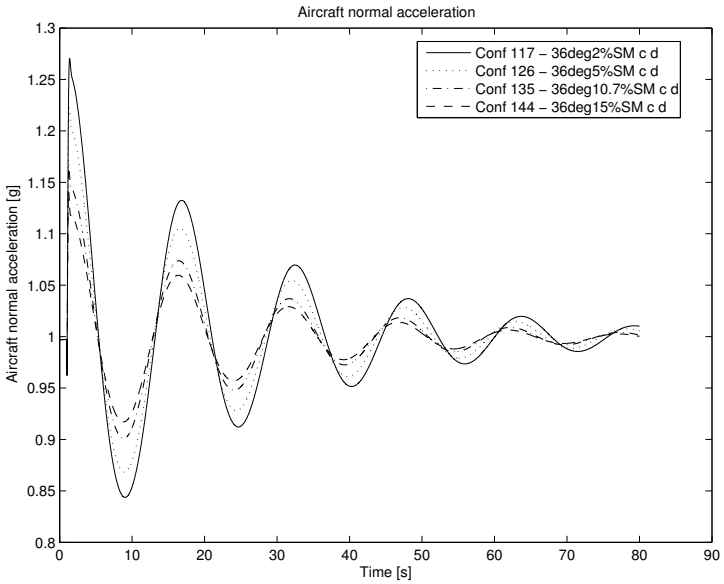

Figure I.14: Response in aircraft normal acceleration to a unit step elevon control input for 36° outboard wing sweep at different static margins with the baseline control authority and aerodynamic damping.

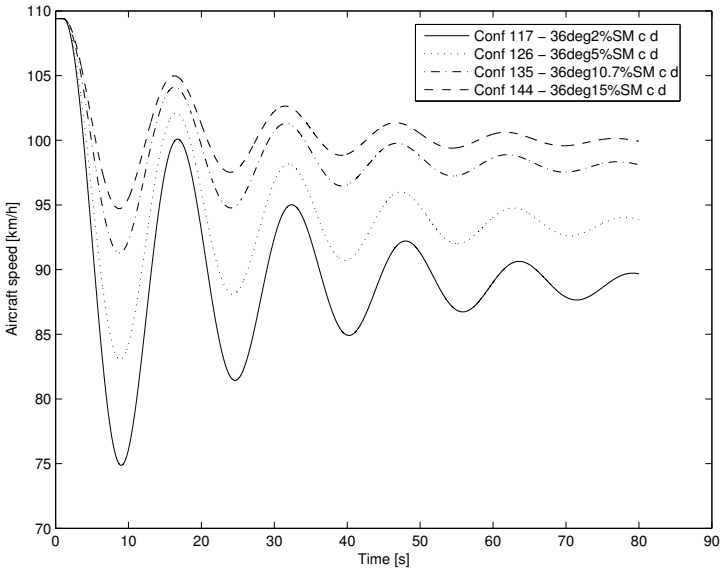

Figure I.15: Response in aircraft airspeed to a unit step elevon control input for 36° outboard wing sweep at different static margins with the baseline control authority and aerodynamic damping.

I.2.3 Configurations 93, 96, 99

Simulation results of all control authority variations at 30° sweep with the baseline aerodynamic damping at a 10.7% (at 30°) static margin configuration. (Configurations 93, 96, 99)

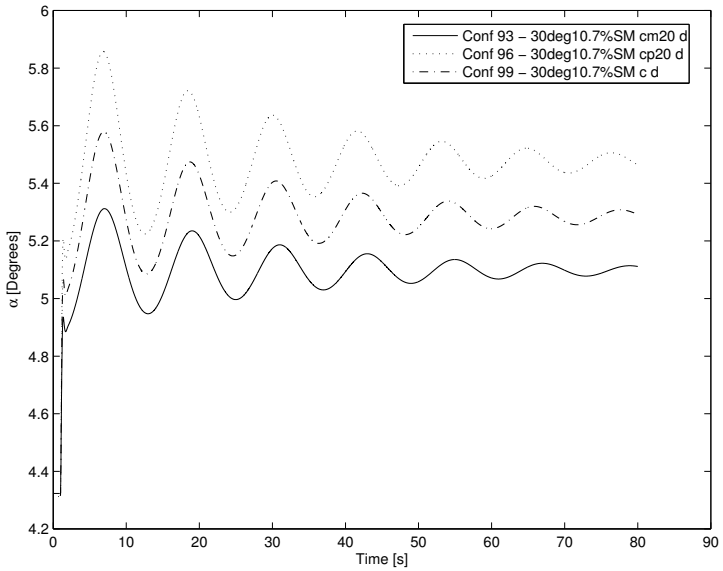

Figure I.16: Response in aircraft angle of attack (α) to a unit step elevon control input for 30° outboard wing sweep at a 10.7% static margin (at 30°) with the baseline aerodynamic damping with variations in control authority.

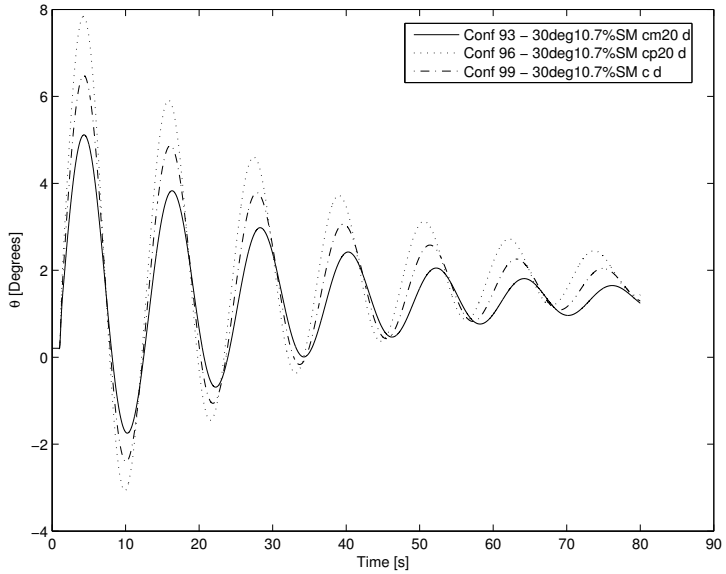

Figure I.17: Response in aircraft attitude (θ) to a unit step elevon control input for 30° outboard wing sweep at a 10.7% static margin (at 30°) with the baseline aerodynamic damping with variations in control authority.

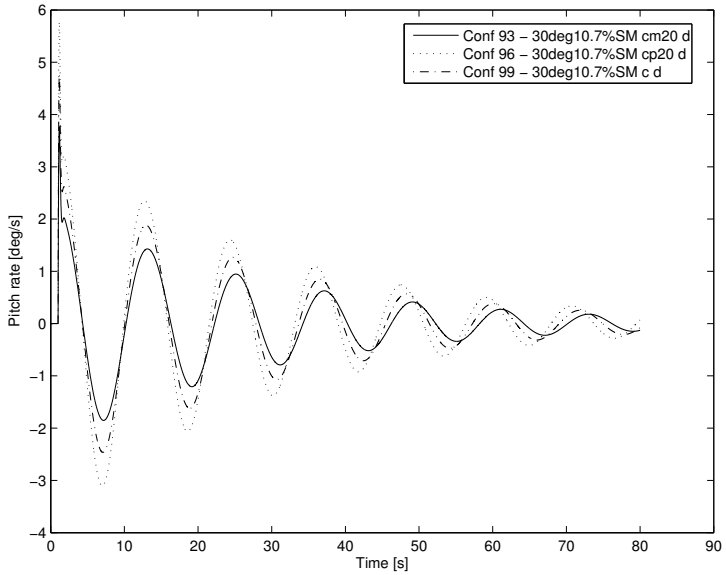

Figure I.18: Response in aircraft pitch rate to a unit step elevon control input for 30° outboard wing sweep at a 10.7% static margin (at 30°) with the baseline aerodynamic damping with variations in control authority.

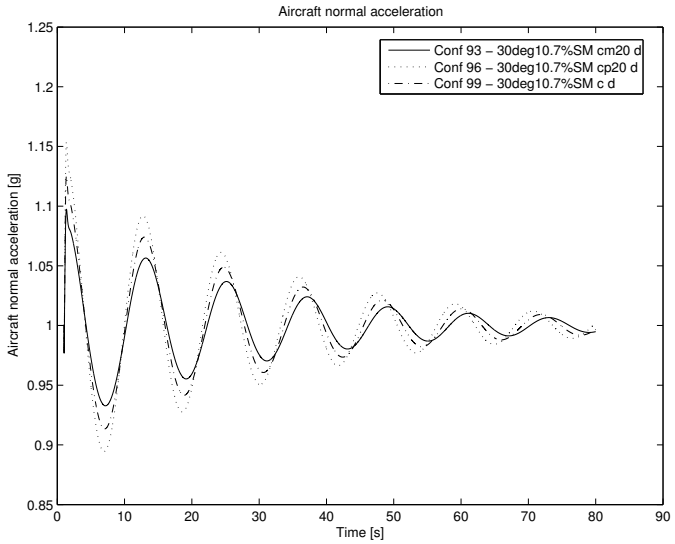

Figure I.19: Response in aircraft normal acceleration to a unit step elevon control input for 30° outboard wing sweep at a 10.7% static margin (at 30°) with the baseline aerodynamic damping with variations in control authority.

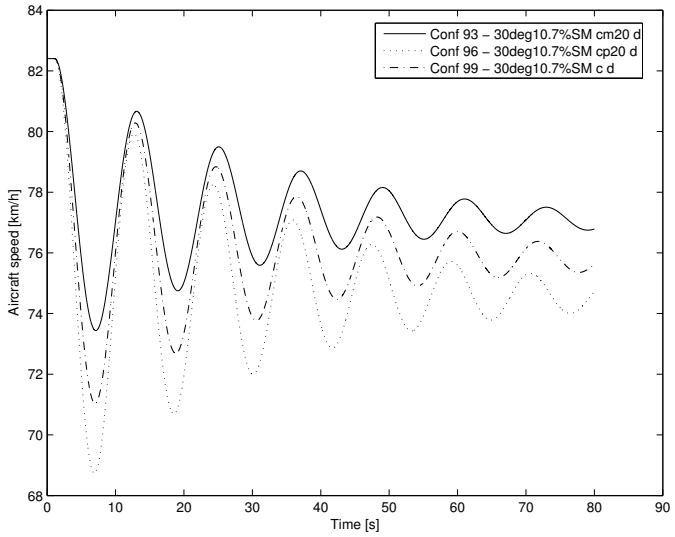

Figure I.20: Response in aircraft airspeed to a unit step elevon control input for 30° outboard wing sweep at a 10.7% static margin (at 30°) with the baseline aerodynamic damping with variations in control authority.

I.2.4 Configurations 57, 60, 63

Simulation results of all control authority variations at 24° sweep with the baseline aerodynamic damping at a 10.7% (at 30°) static margin configuration. (Configurations 57, 60, 63)

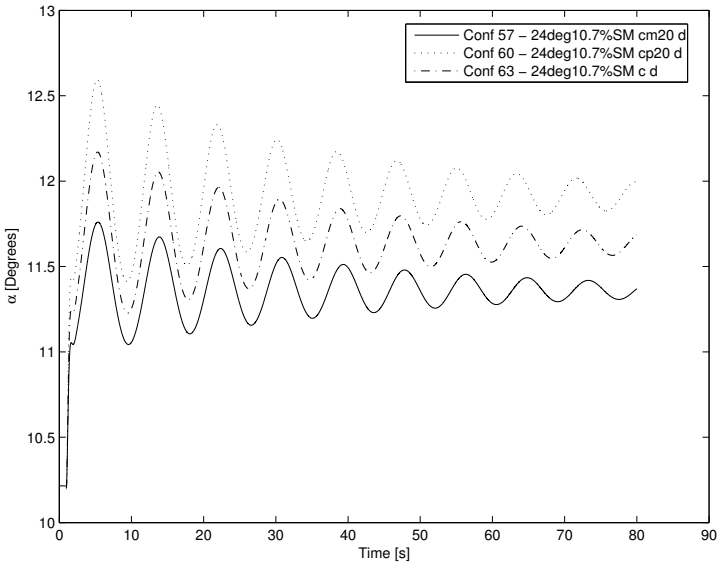

Figure I.21: Response in aircraft angle of attack (α) to a unit step elevon control input for 24° outboard wing sweep at a 10.7% static margin (at 30°) with the baseline aerodynamic damping with variations in control authority.

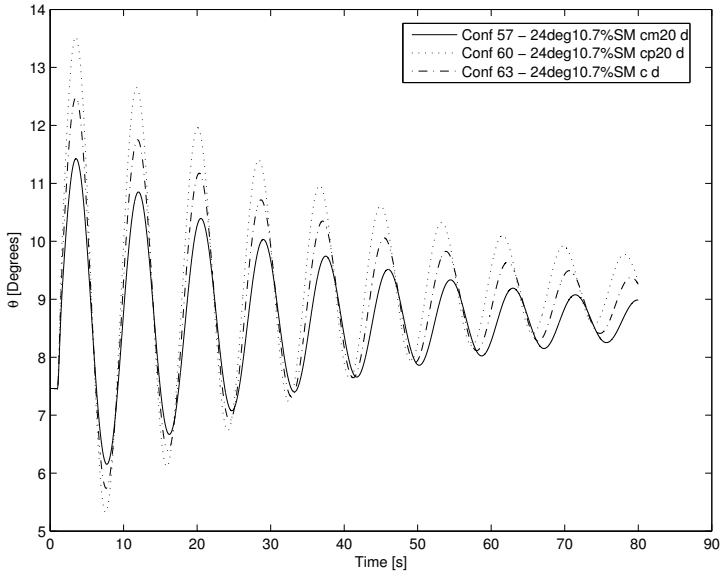

Figure I.22: Response in aircraft attitude (θ) to a unit step elevon control input for 24° outboard wing sweep at a 10.7% static margin (at 30°) with the baseline aerodynamic damping with variations in control authority.

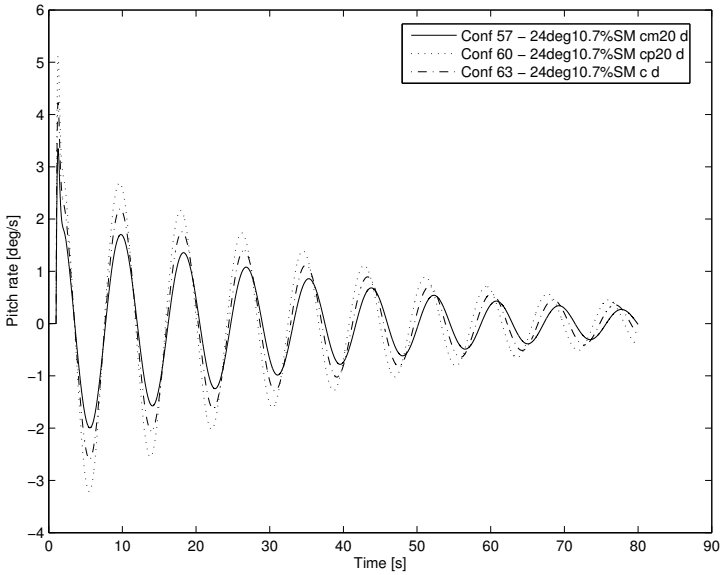

Figure I.23: Response in aircraft pitch rate to a unit step elevon control input for 24° outboard wing sweep at a 10.7% static margin (at 30°) with the baseline aerodynamic damping with variations in control authority.

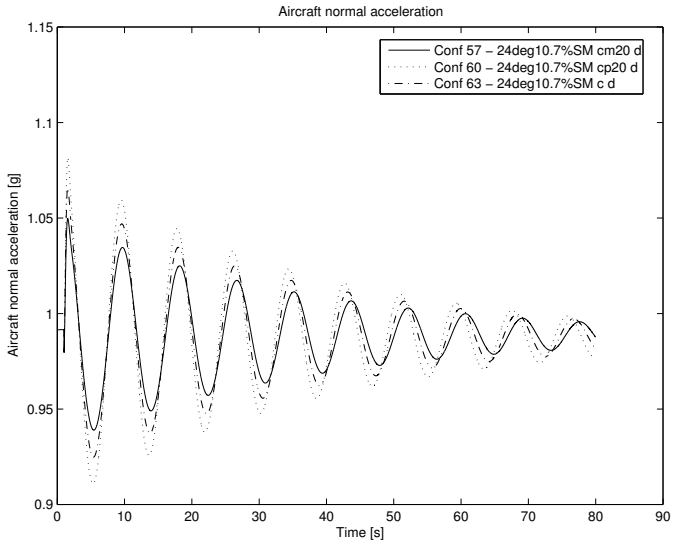

Figure I.24: Response in aircraft normal acceleration to a unit step elevon control input for 24° outboard wing sweep at a 10.7% static margin (at 30°) with the baseline aerodynamic damping with variations in control authority.

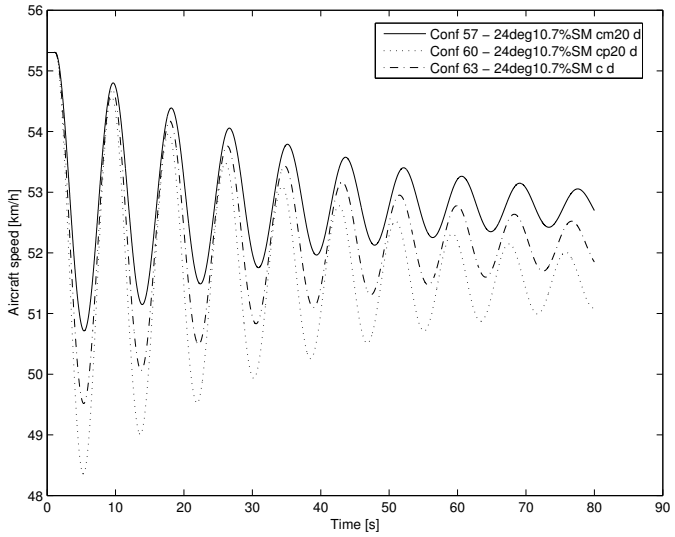

Figure I.25: Response in aircraft airspeed to a unit step elevon control input for 24° outboard wing sweep at a 10.7% static margin (at 30°) with the baseline aerodynamic damping with variations in control authority.

I.2.5 Configurations 97, 98, 99

Simulation results of all damping variations at 30° sweep with the baseline control authority at a 10.7% (at 30°) static margin configuration. (Configurations 97, 98, 99)

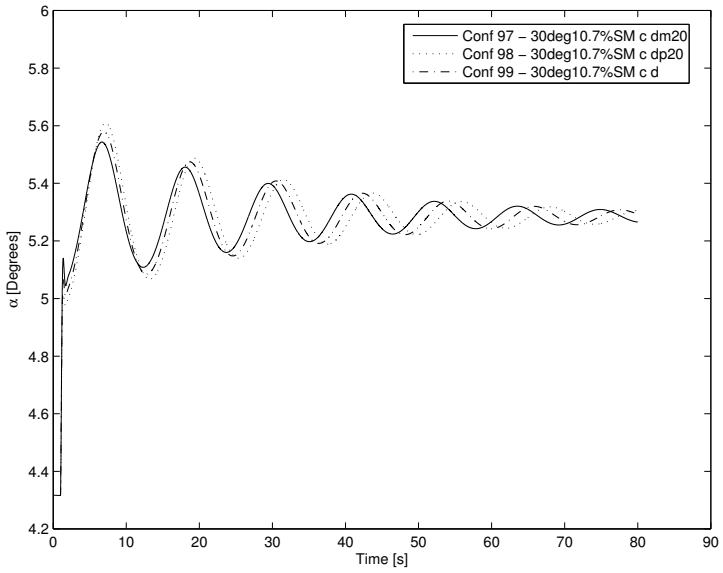

Figure I.26: Response in aircraft angle of attack (α) to a unit step elevon control input for 30° outboard wing sweep at a 10.7% static margin (at 30°) with the baseline control authority with variations in aerodynamic damping.

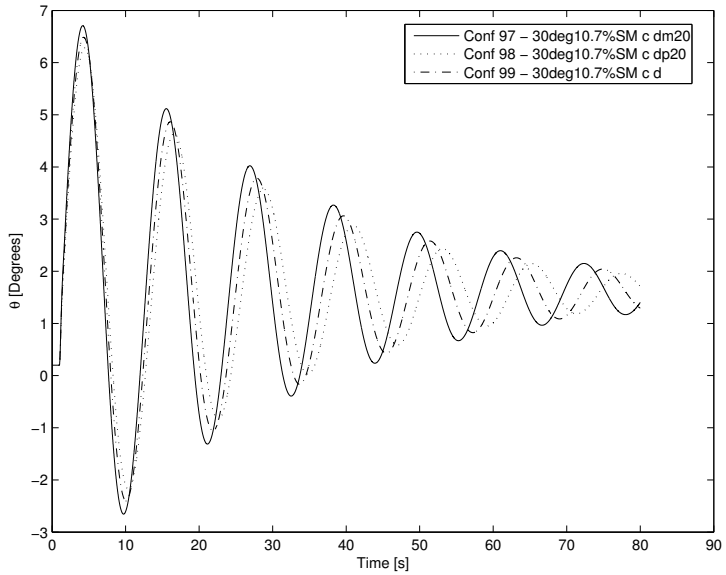

Figure I.27: Response in aircraft attitude (θ) to a unit step elevon control input for 30° outboard wing sweep at a 10.7% static margin (at 30°) with the baseline control authority with variations in aerodynamic damping.

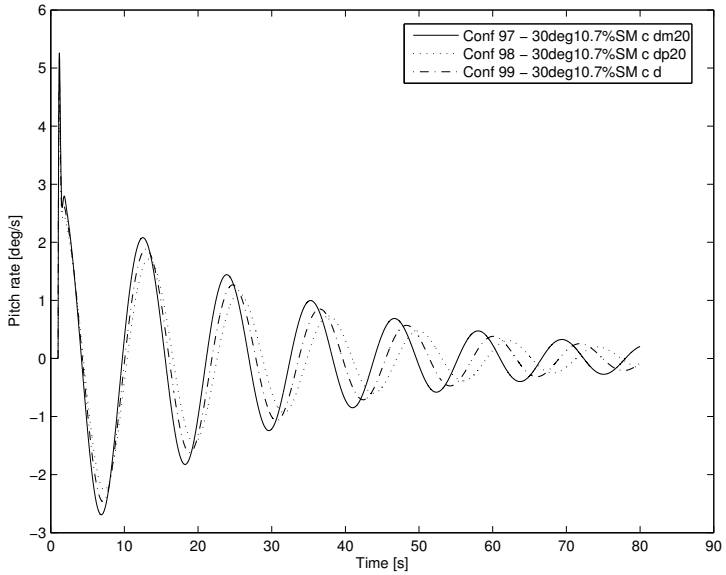

Figure I.28: Response in aircraft pitch rate to a unit step elevon control input for 30° outboard wing sweep at a 10.7% static margin (at 30°) with the baseline control authority with variations in aerodynamic damping.

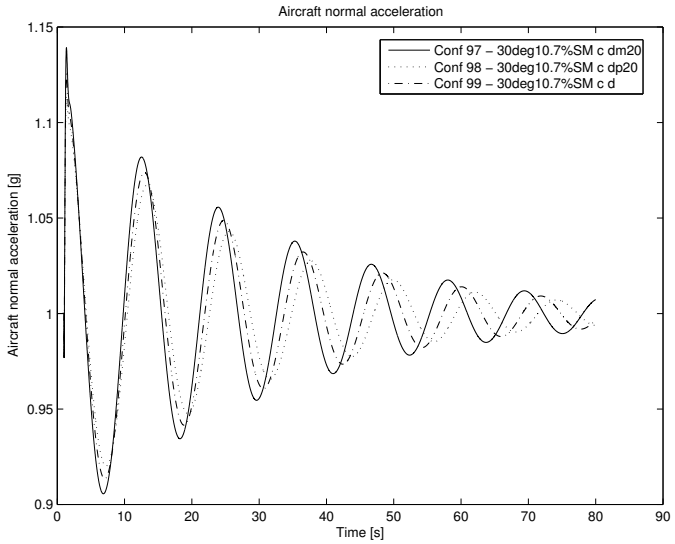

Figure I.29: Response in aircraft normal acceleration to a unit step elevon control input for 30° outboard wing sweep at a 10.7% static margin (at 30°) with the baseline control authority with variations in aerodynamic damping.

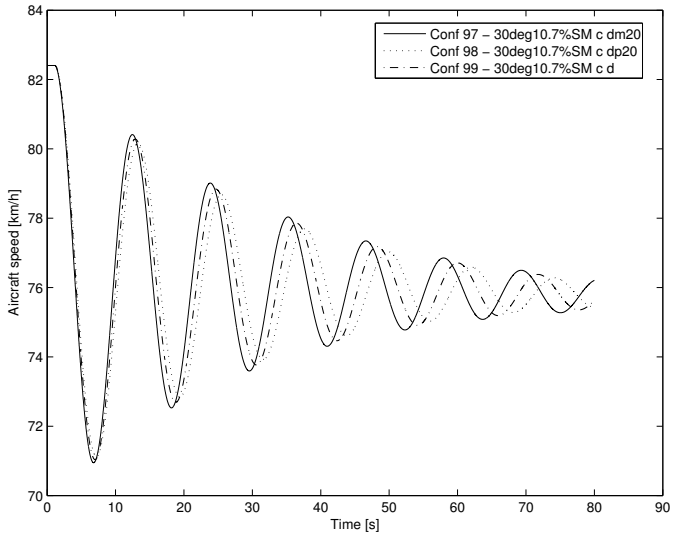

Figure I.30: Response in aircraft airspeed to a unit step elevon control input for 30° outboard wing sweep at a 10.7% static margin (at 30°) with the baseline control authority with variations in aerodynamic damping.

I.3 Gust Response Analysis

Simulations were performed in order to investigate gust response of the gull-wing configuration. The mathematical models of the aircraft which represented different aircraft configurations were subjected to a vertical gust of type $1 - \cos$ with a peak value of 2 m/s that was introduced 1 second following the start of the simulation. A graphical representation of the gust is shown in Figure 4.13.

It is necessary to perform a study with respect to gust response since an aircraft might have satisfactory handling qualities in calm atmosphere, whilst having unpleasant handling qualities in rough air as shown in Chalk (1963) and Mönnich & Dalldorff (1993).

The static margin, outboard wing sweep and damping parameter values of the gull-wing configuration mathematical model were varied for the purposes of investigating the effects of these changes on the gust response of the aircraft. The static margin and aerodynamic damping parameters were varied in the same way as described in the pitch response analysis of Section I.1. All the gust response simulations were performed with the control input assumed to be fixed.

The numbering system used for the aircraft configurations of the gust response study is different from that of the pitch control study. The aircraft configurations of the gust response analysis is defined in Table H.2 of Appendix H. All the simulation results for the gust response study are not shown in this document. The gust response simulation results of the following configurations were chosen to be shown here:

- All static margin variations at 30° sweep having the baseline aerodynamic damping. (Configurations 27, 30, 33, 36)
- All static margin variations at 24° sweep having the baseline aerodynamic damping. (Configurations 15, 18, 21, 24)
- All static margin variations at 36° sweep having the baseline aerodynamic damping. (Configurations 39, 42, 45, 48)

- All damping variations at 30° sweep at a 10.7% (at 30°) static margin configuration. (Configurations 31, 32, 33)

Only the responses of the first item are presented in this section (Figures I.31 to I.35). The responses of the other configurations described in the above list are shown in Appendix I.4 but are discussed here.

The following observations were made regarding the simulation results: Configuration 15 is statically unstable and therefore the simulation results with this configuration are not plotted.

Changes in static margin have a large influence on the magnitude of the aircraft pitch response and the natural frequencies of the aircraft modes. The simulated aircraft responses indicate that the low static margin configurations have smaller magnitudes and lower natural frequencies than the high static margin configurations.

The simulations with variations in damping showed that the damping influences the natural frequency as well as the damping of the aircraft response. The effect of damping is less significant than that of static margin.

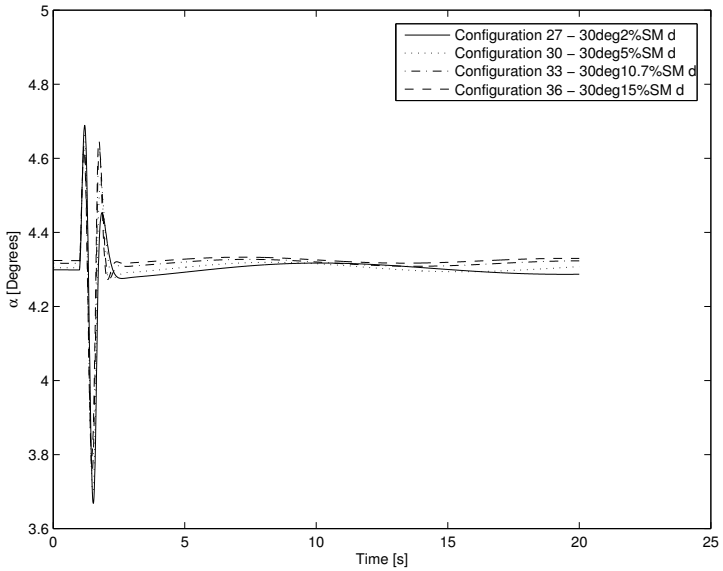

Figure I.31: Gust response for aircraft angle of attack (α) for 30° outboard wing sweep at different static margins with the baseline aerodynamic damping.

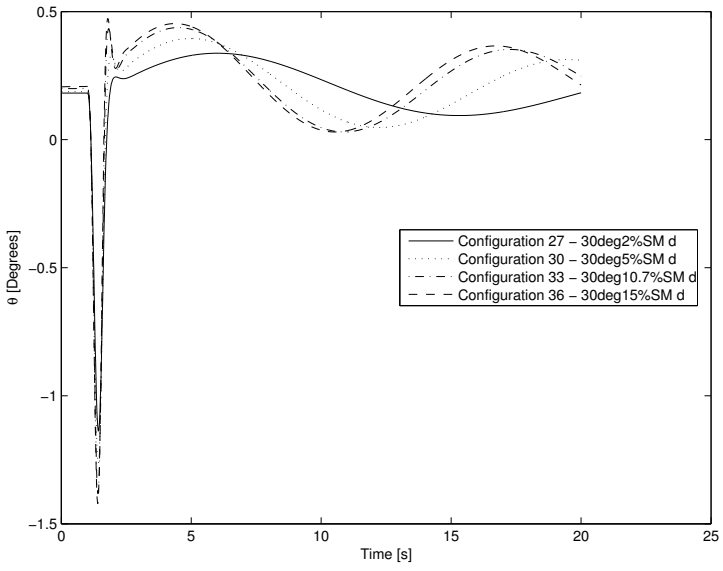

Figure I.32: Gust response for aircraft attitude (θ) for 30° outboard wing sweep at different static margins with the baseline aerodynamic damping.

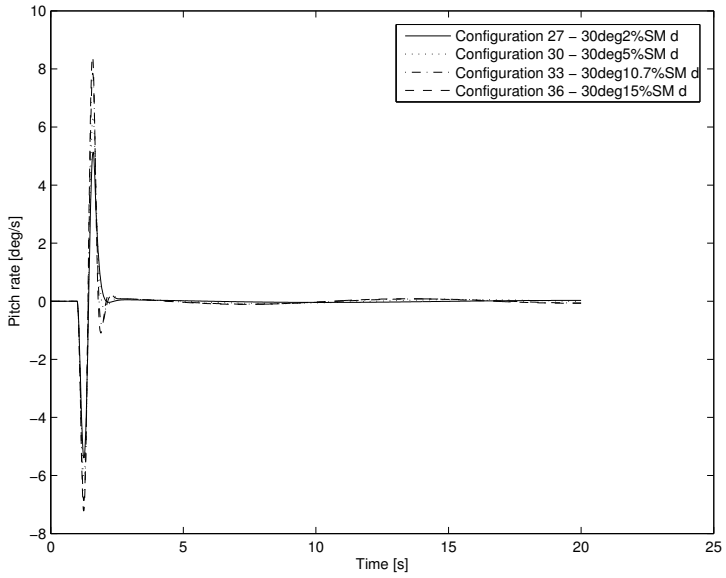

Figure I.33: Gust response for aircraft pitch rate for 30° outboard wing sweep at different static margins with the baseline aerodynamic damping.

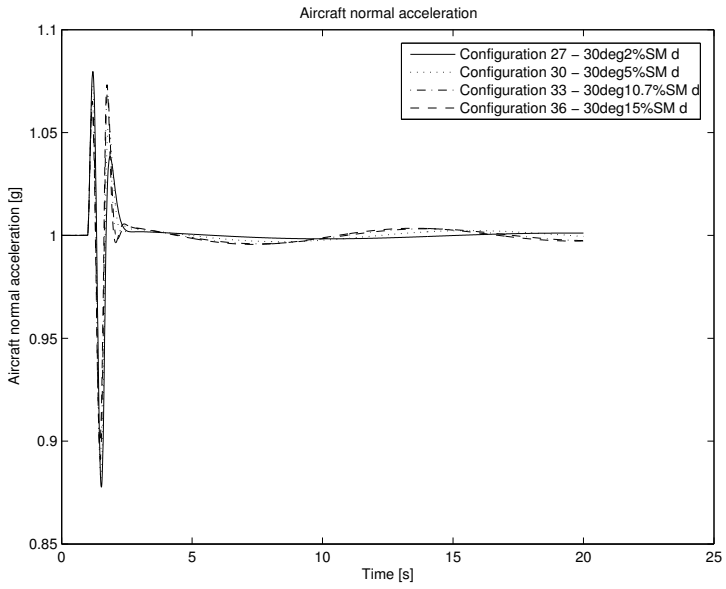

Figure I.34: Gust response for aircraft normal acceleration for 30° outboard wing sweep at different static margins with the baseline aerodynamic damping.

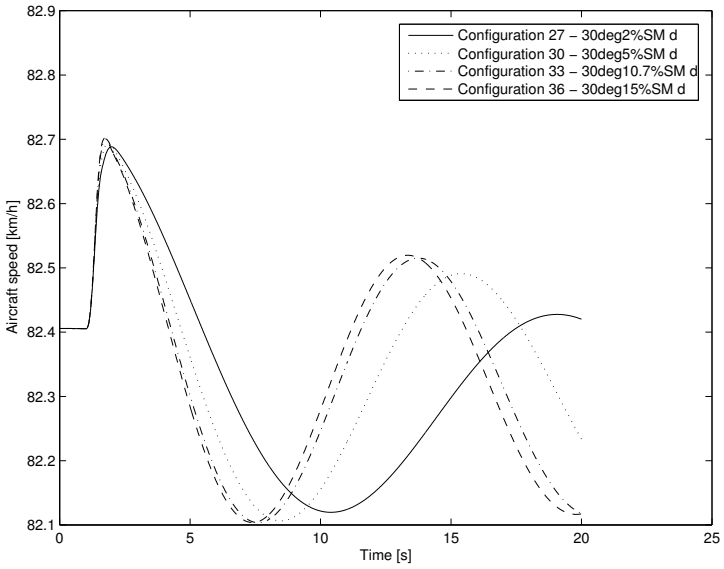

Figure I.35: Gust response for aircraft airspeed for 30° outboard wing sweep at different static margins with the baseline aerodynamic damping.

I.4 Gust Response Simulations

I.4.1 Configurations 15, 18, 21, 24

Simulation results of all static margin variations at 24° sweep having the baseline aerodynamic damping. (Configurations 15, 18, 21, 24)

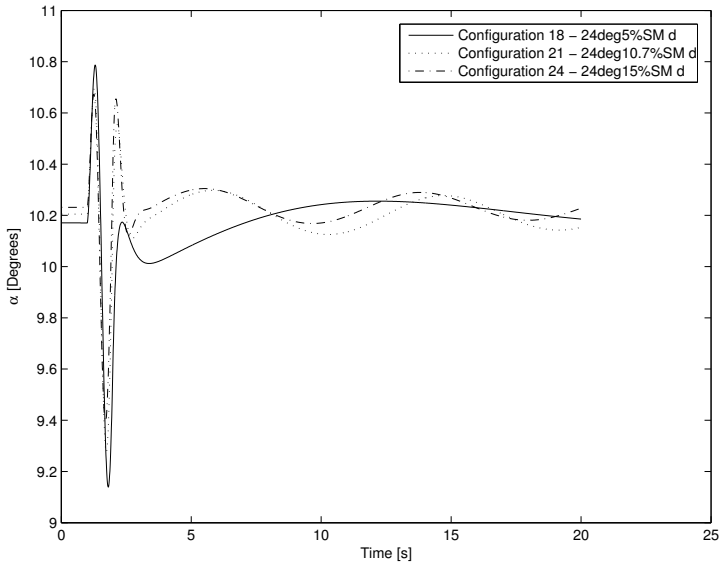

Figure I.36: Gust response for aircraft angle of attack (α) for 24° outboard wing sweep at different static margins with the baseline aerodynamic damping.

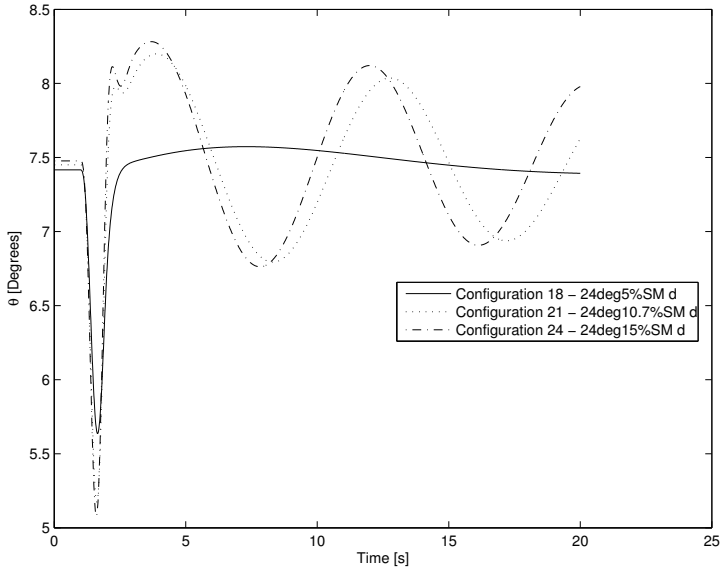

Figure I.37: Gust response for aircraft attitude (θ) for 24° outboard wing sweep at different static margins with the baseline aerodynamic damping.

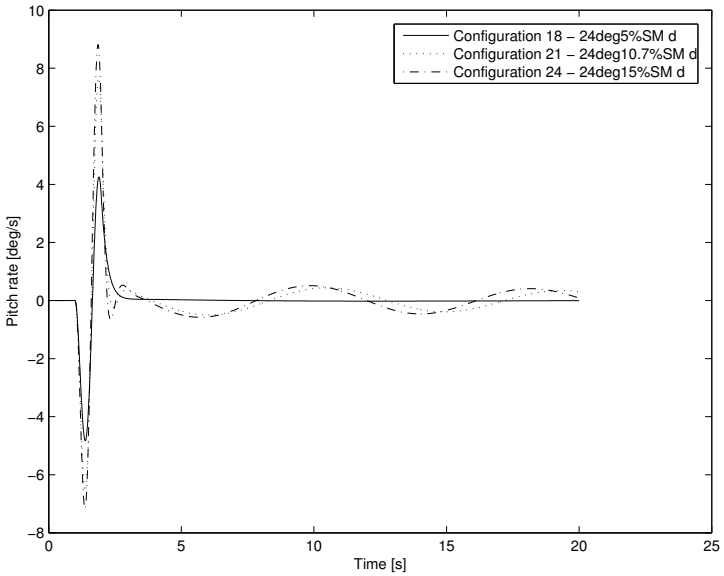

Figure I.38: Gust response for aircraft pitch rate for 24° outboard wing sweep at different static margins with the baseline aerodynamic damping.

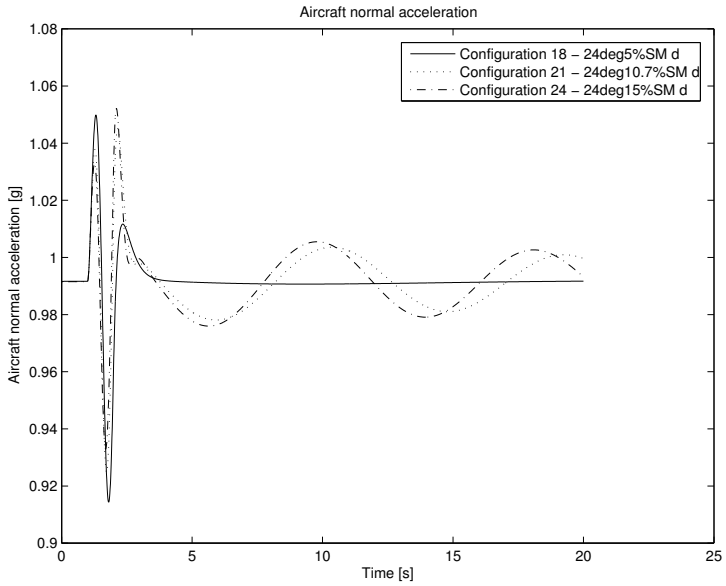

Figure I.39: Gust response for aircraft normal acceleration for 24° outboard wing sweep at different static margins with the baseline aerodynamic damping.

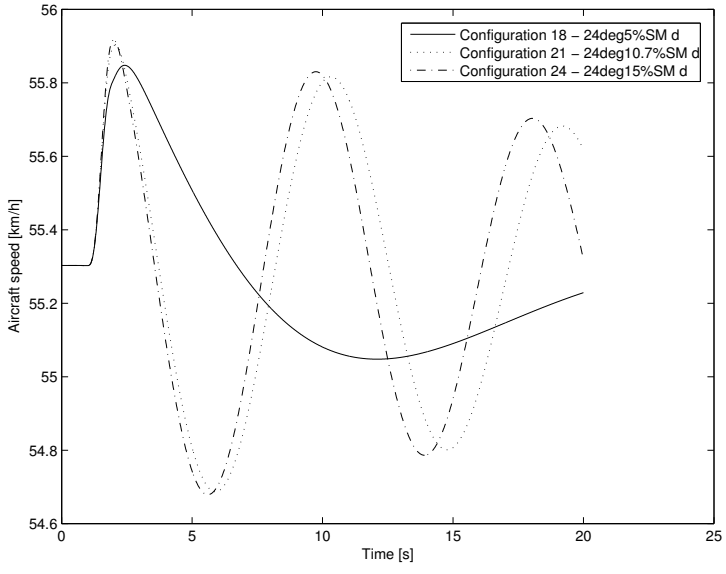

Figure I.40: Gust response for aircraft airspeed for 24° outboard wing sweep at different static margins with the baseline control authority and aerodynamic damping.

I.4.2 Configurations 39, 42, 45, 48

Simulation results of all static margin variations at 36° sweep having the baseline aerodynamic damping. (Configurations 39, 42, 45, 48)

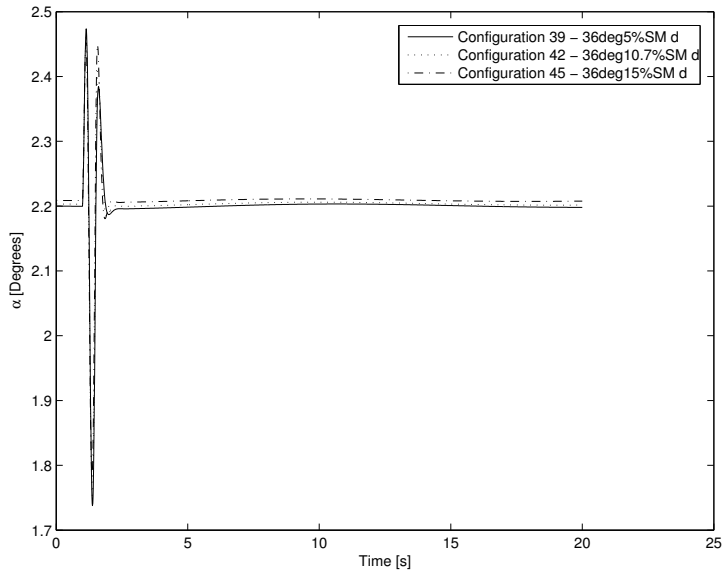

Figure I.41: Gust response for aircraft angle of attack (α) for 36° outboard wing sweep at different static margins with the baseline aerodynamic damping.

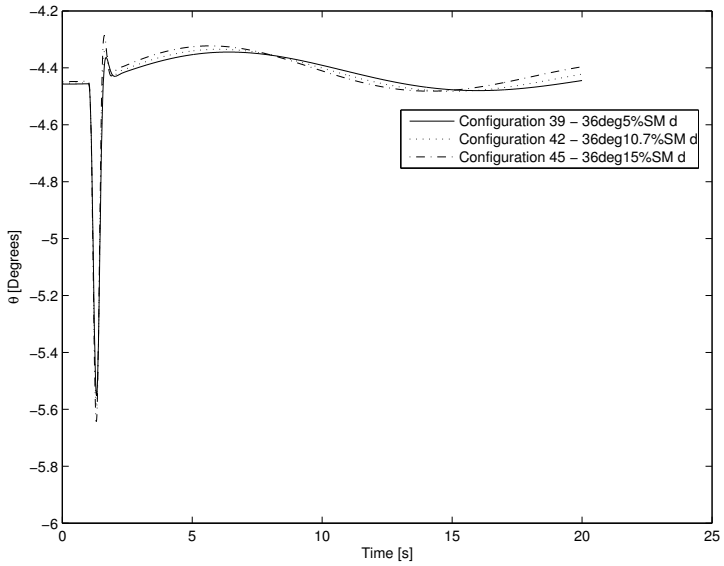

Figure I.42: Gust response for aircraft attitude (θ) for 36° outboard wing sweep at different static margins with the baseline aerodynamic damping.

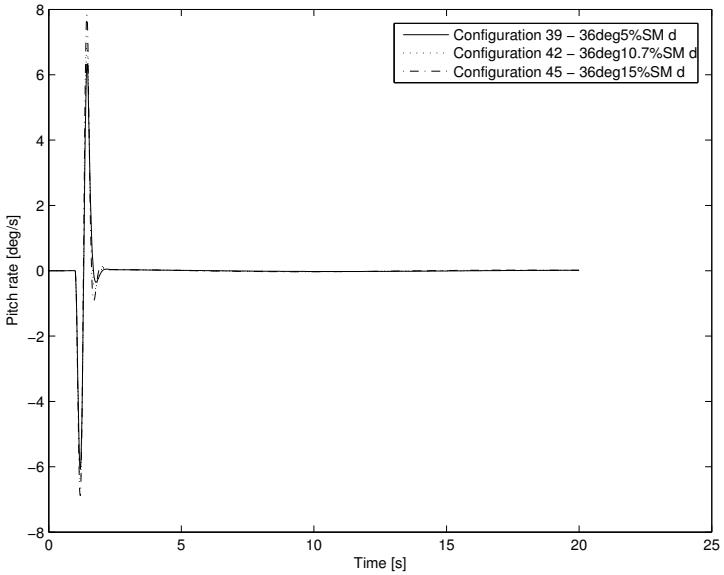

Figure I.43: Gust response for aircraft pitch rate for 36° outboard wing sweep at different static margins with the baseline aerodynamic damping.

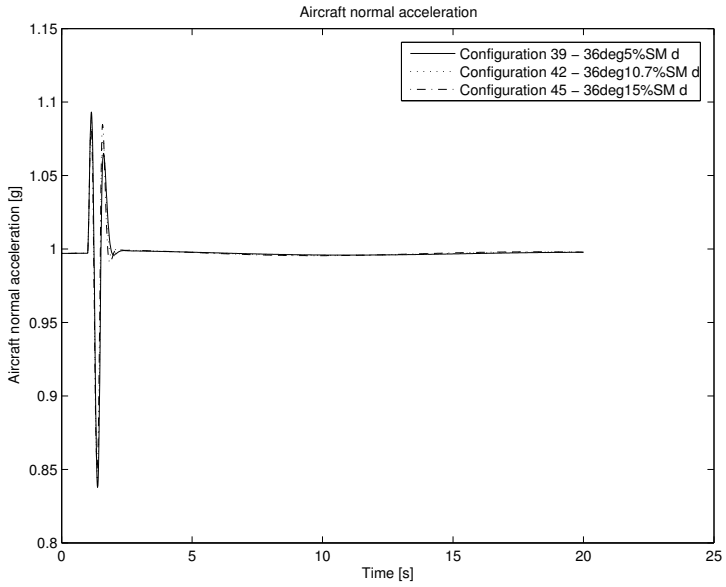

Figure I.44: Gust response for aircraft normal acceleration for 36° outboard wing sweep at different static margins with the baseline aerodynamic damping.

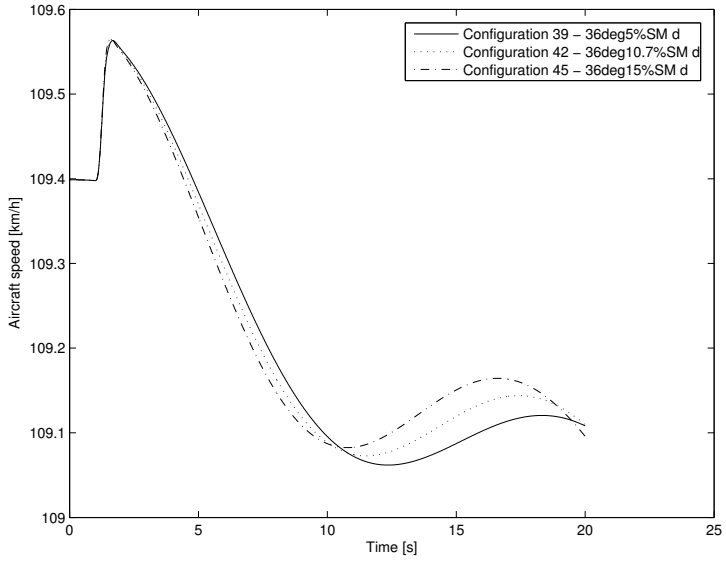

Figure I.45: Gust response for aircraft airspeed for 36° outboard wing sweep at different static margins with the baseline control authority and aerodynamic damping.

I.4.3 Configurations 31, 32, 33

Simulation results of all damping variations at 30° sweep at a 10.7% (at 30°) static margin configuration. (Configurations 31, 32, 33)

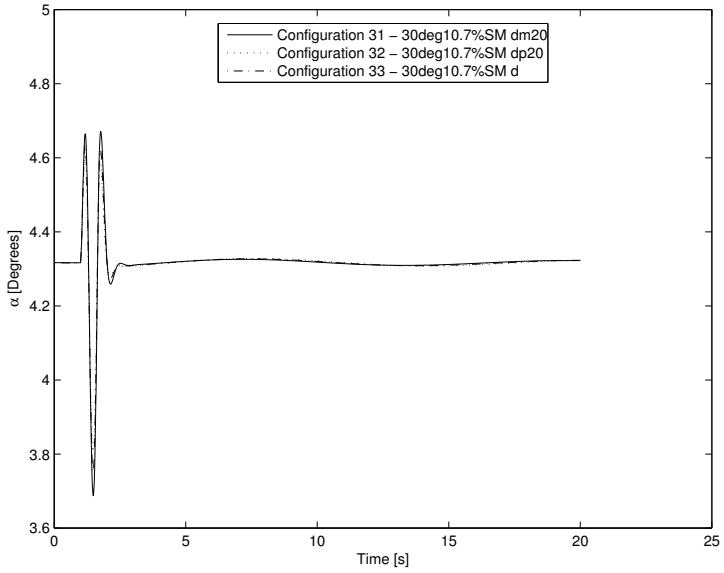

Figure I.46: Gust response for aircraft angle of attack (α) for 30° outboard wing sweep at a 10.7% static margin (at 30° sweep) with different configurations for aerodynamic damping.

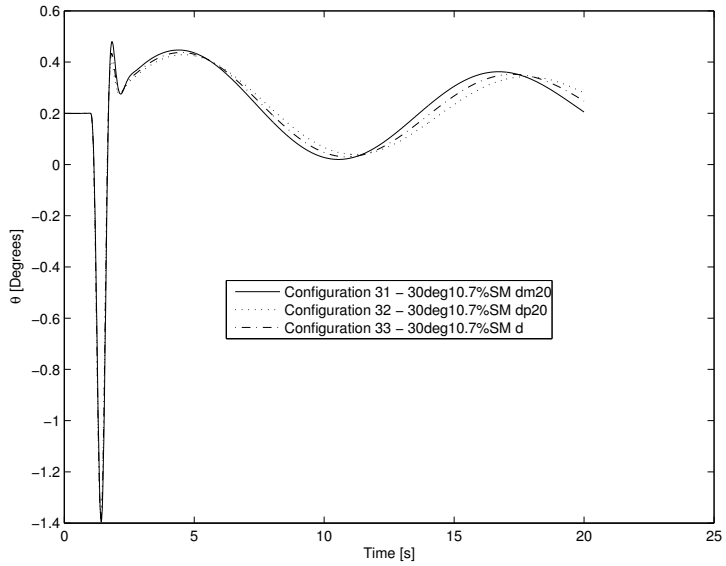

Figure I.47: Gust response for aircraft attitude (θ) for 30° outboard wing sweep at a 10.7% static margin (at 30° sweep) with different configurations for aerodynamic damping.

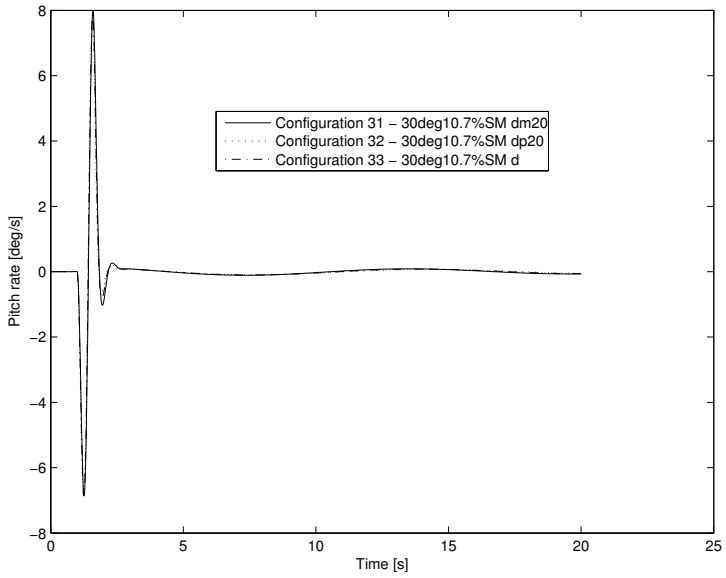

Figure I.48: Gust response for aircraft pitch rate for 30° outboard wing sweep at a 10.7% static margin (at 30° sweep) with different configurations for aerodynamic damping.

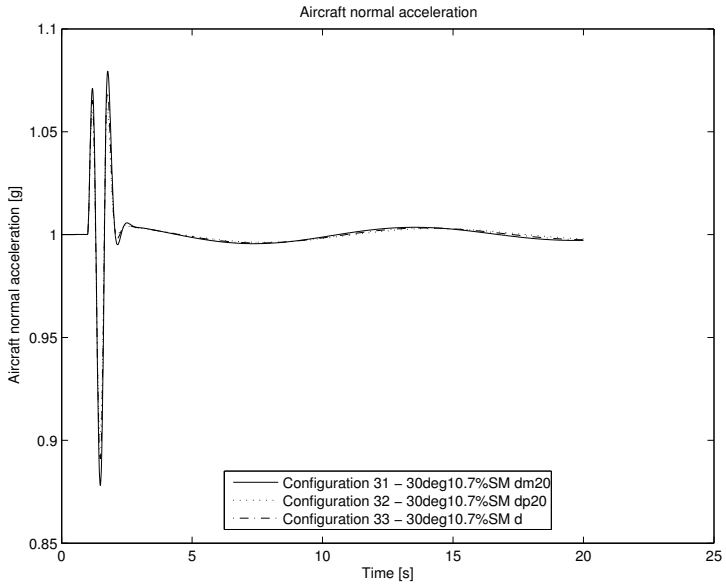

Figure I.49: Gust response for aircraft normal acceleration for 30° outboard wing sweep at a 10.7% static margin (at 30° sweep) with different configurations for aerodynamic damping.

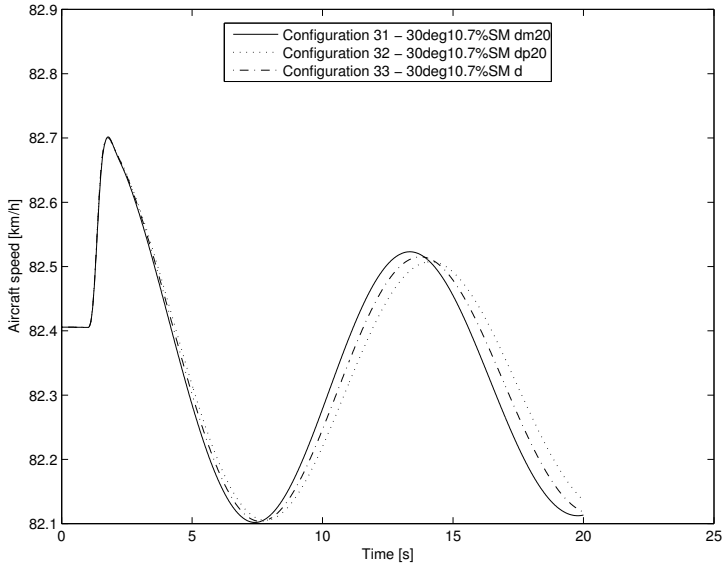

Figure I.50: Gust response for aircraft airspeed for 30° outboard wing sweep at a 10.7% static margin (at 30° sweep) with different configurations for aerodynamic damping.

I.5 C-star Analysis Results

The additional results of the C-star analysis are presented here.

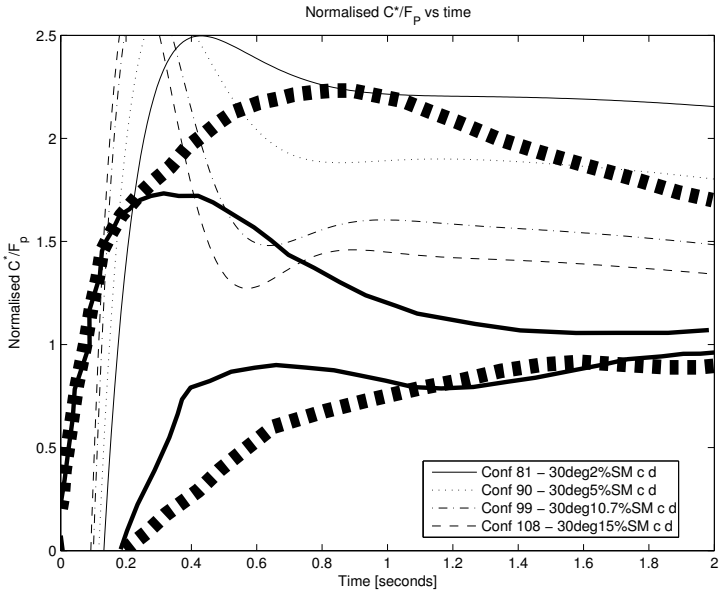

Figure I.51: The C-star analysis for all static margin variations at 30° sweep having the baseline aerodynamic damping and control authority. (Configurations 81, 90, 99, 108).

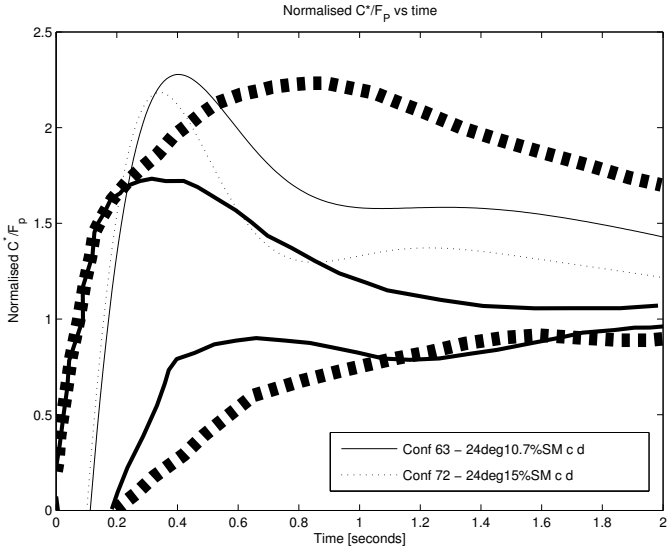

Figure I.52: The C-star analysis for all static margin variations at 24° sweep having the baseline aerodynamic damping and control authority. (Configurations 63, 72).

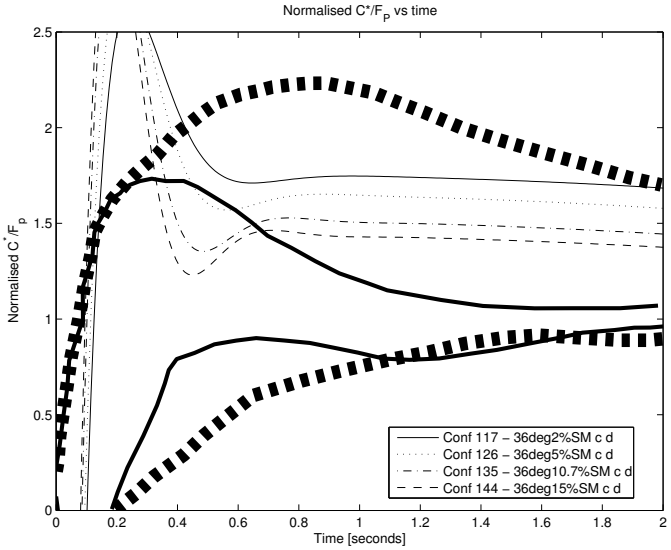

Figure I.53: The C-star analysis for all static margin variations at 36° sweep having the baseline aerodynamic damping and control authority. (Configurations 117, 126, 135, 144)

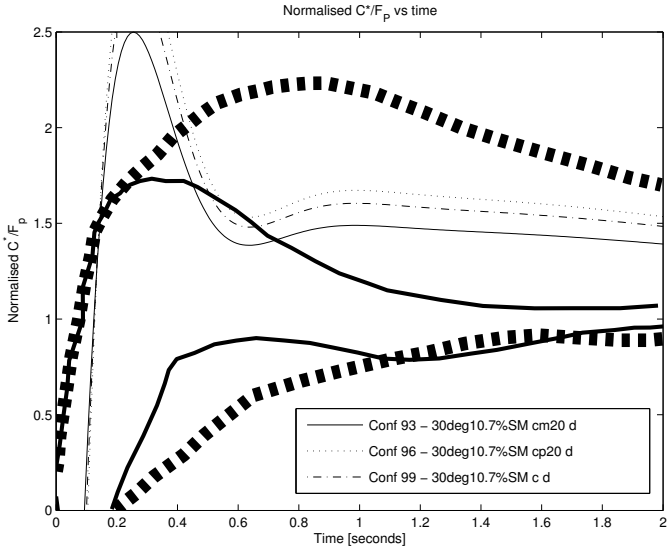

Figure I.54: The C-star analysis for all control authority variations at 30° sweep with the baseline aerodynamic damping at a 10.7% (at 30°) static margin configuration. (Configurations 93, 96, 99)

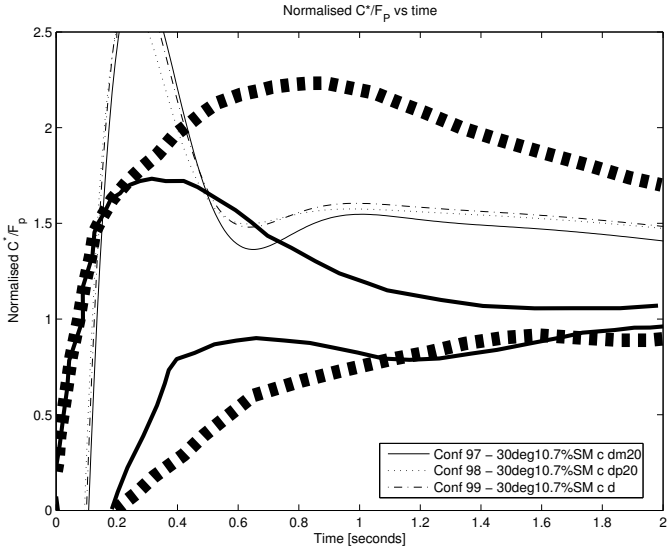

Figure I.55: The C-star analysis for all damping variations at 30° sweep with the baseline control authority at a 10.7% (at 30°) static margin configuration. (Configurations 97, 98, 99)

Appendix J

Frequency Domain Analysis Results

J.1 Thumbprint Criterion Analysis

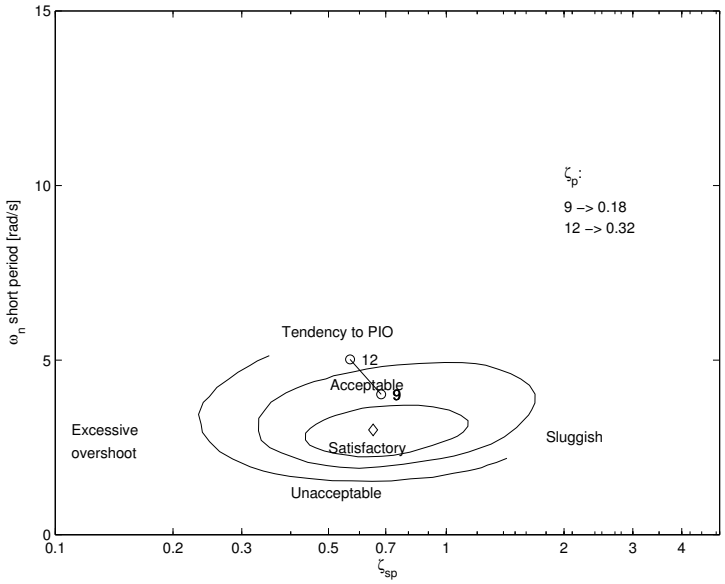

Figure J.1: Thumbprint analysis for 20° outboard wing sweep, at various static margin cases, with the baseline aerodynamic damping.

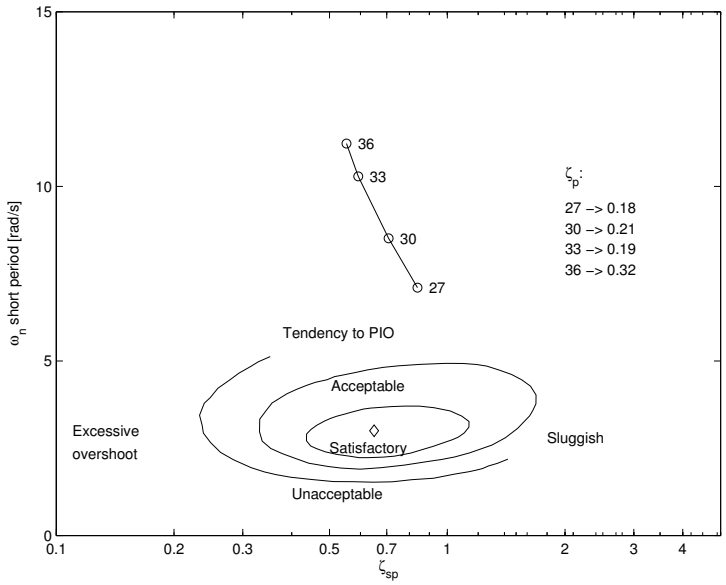

Figure J.2: Thumbprint analysis for 30° outboard wing sweep, at various static margin cases, with the baseline aerodynamic damping.

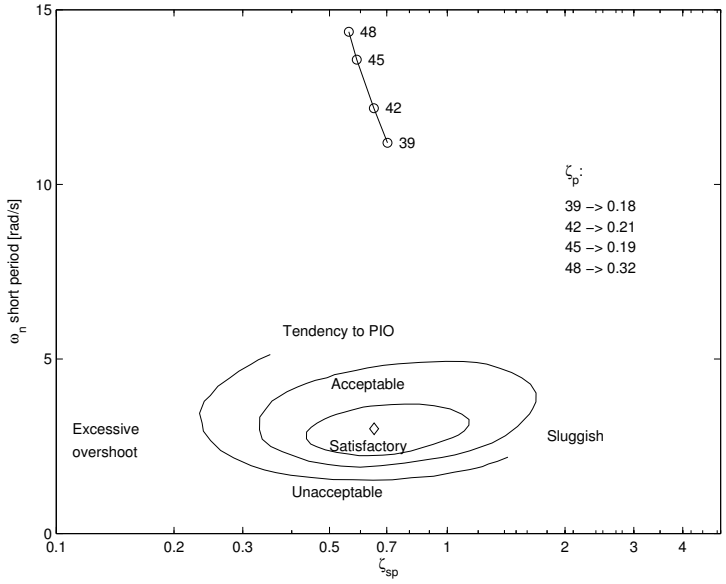

Figure J.3: Thumbprint analysis for 36° outboard wing sweep, at various static margin cases, with the baseline aerodynamic damping.

J.2 Military Flying Qualities Analysis

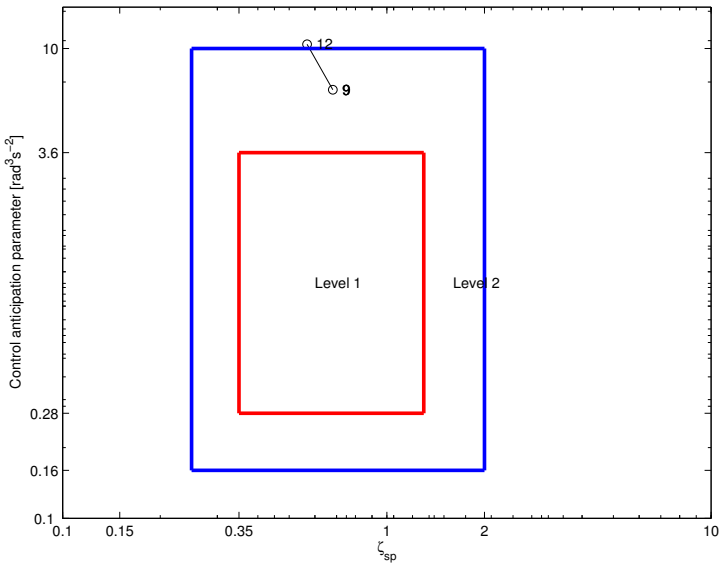

Figure J.4: *CAP* for 20° outboard wing sweep, at various static margin cases, with the baseline aerodynamic damping.

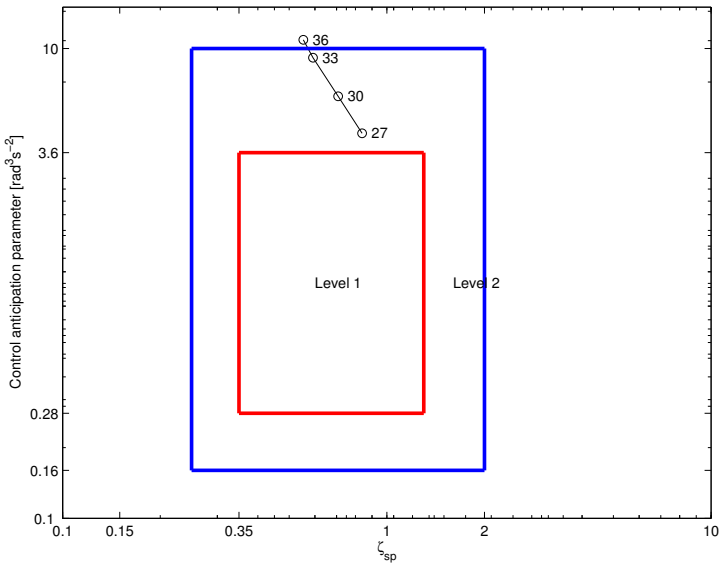

Figure J.5: *CAP* for 30° outboard wing sweep, at various static margin cases, with the baseline aerodynamic damping.

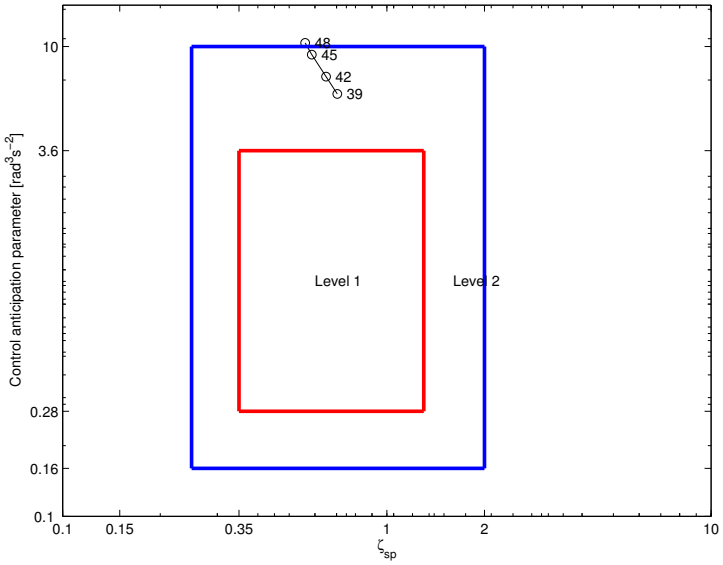

Figure J.6: *CAP* for 36° outboard wing sweep, at various static margin cases, with the baseline aerodynamic damping.

J.3 Shomber-Gertsen Analysis

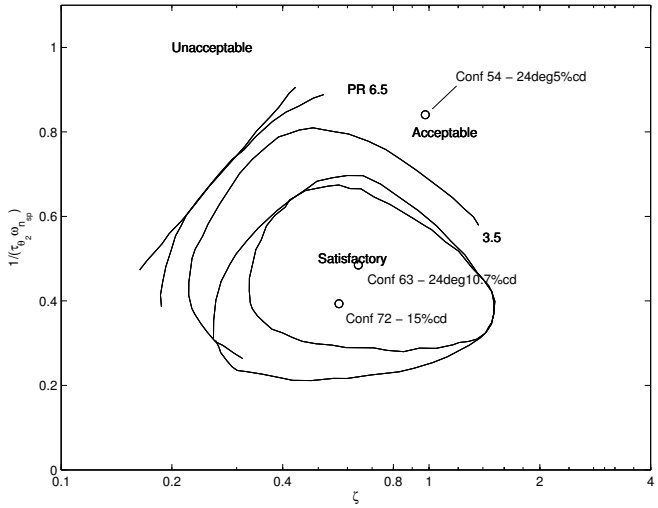

Figure J.7: Group two analysis results for $n_\alpha < 15$ g/rad.

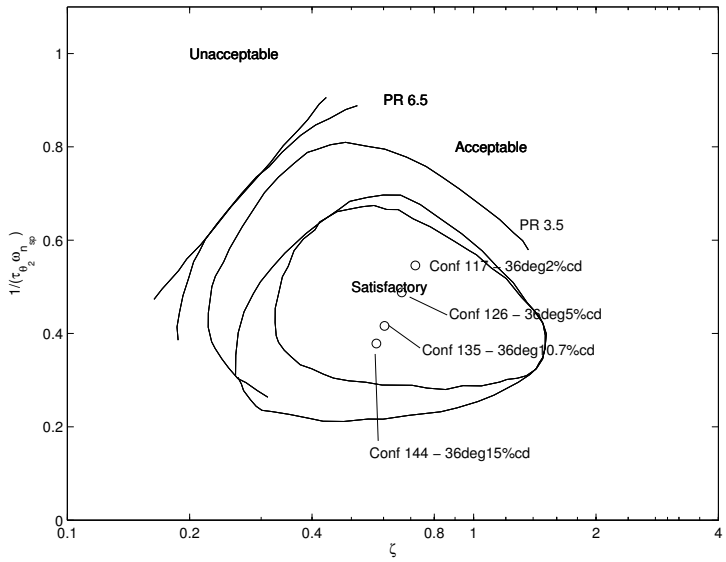

Figure J.8: Group three analysis results for $n_\alpha < 15$ g/rad.

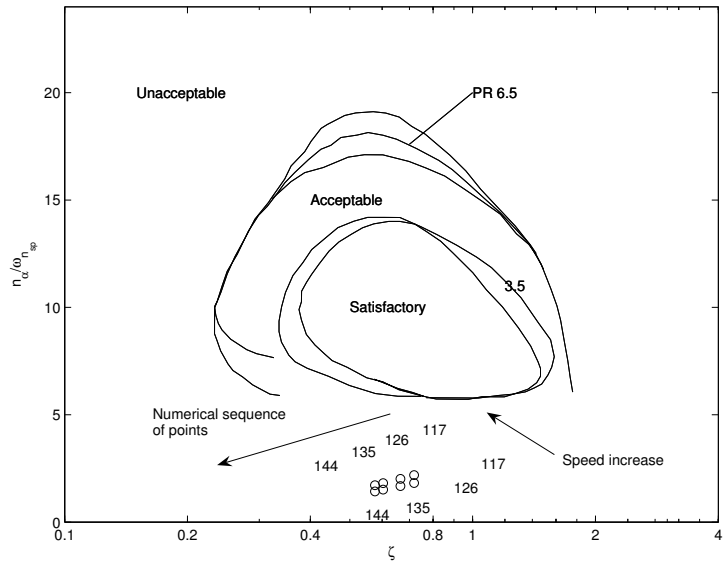

Figure J.9: Group three analysis results for $n_\alpha \geq 15$ g/rad.

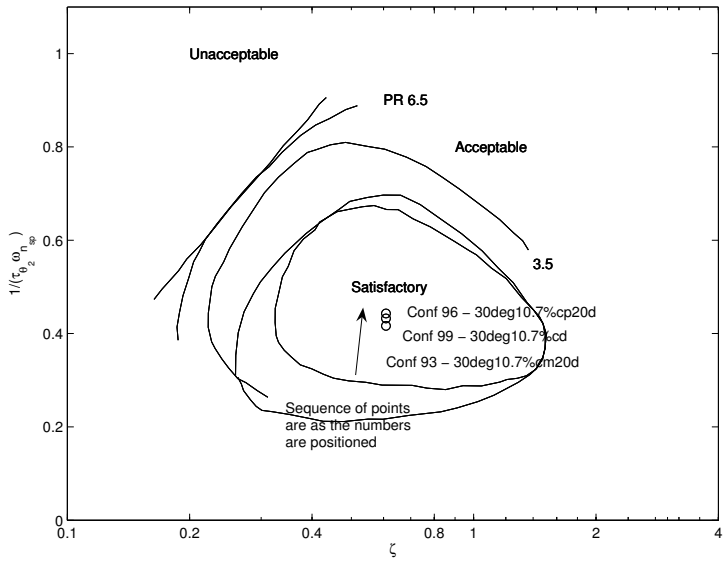

Figure J.10: Group four analysis results for $n_\alpha < 15$ g/rad.

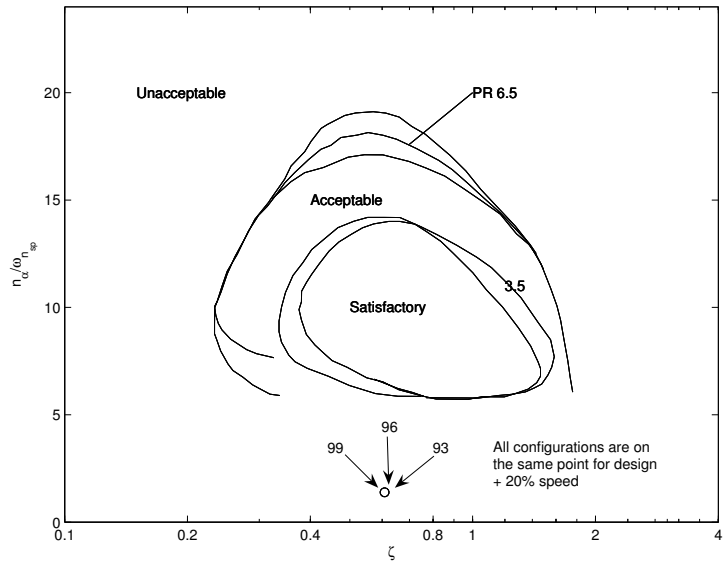

Figure J.11: Group four analysis results for $n_\alpha \geq 15$ g/rad.

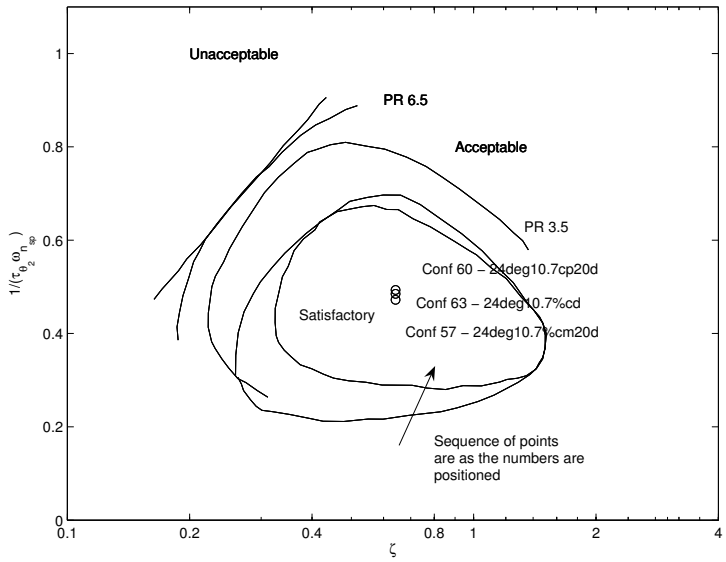

Figure J.12: Group five analysis results for $n_\alpha < 15$ g/rad.

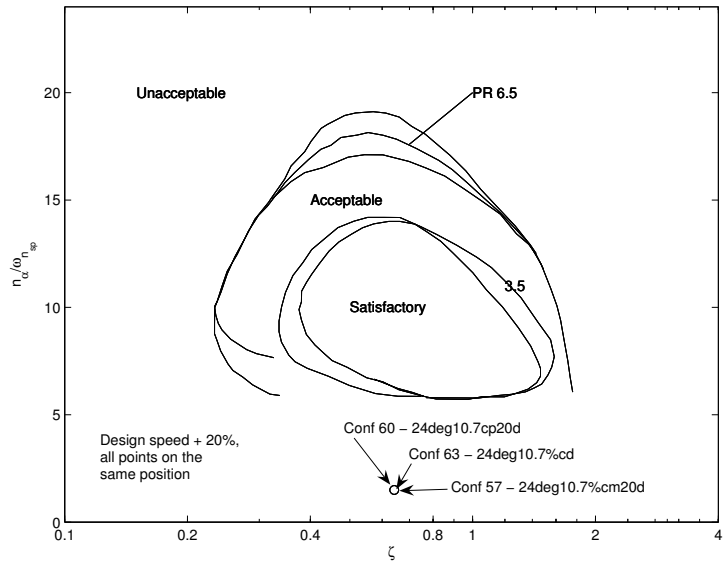

Figure J.13: Group five analysis results for $n_\alpha \geq 15$ g/rad.

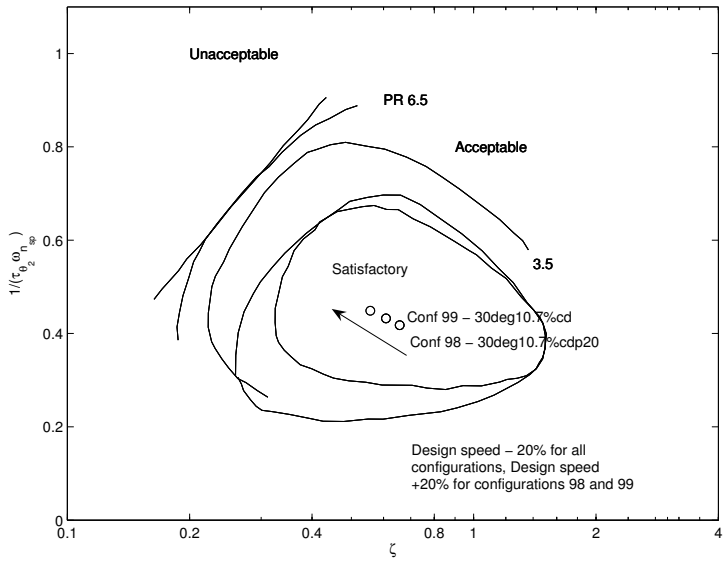

Figure J.14: Group six analysis results for $n_\alpha < 15$ g/rad.

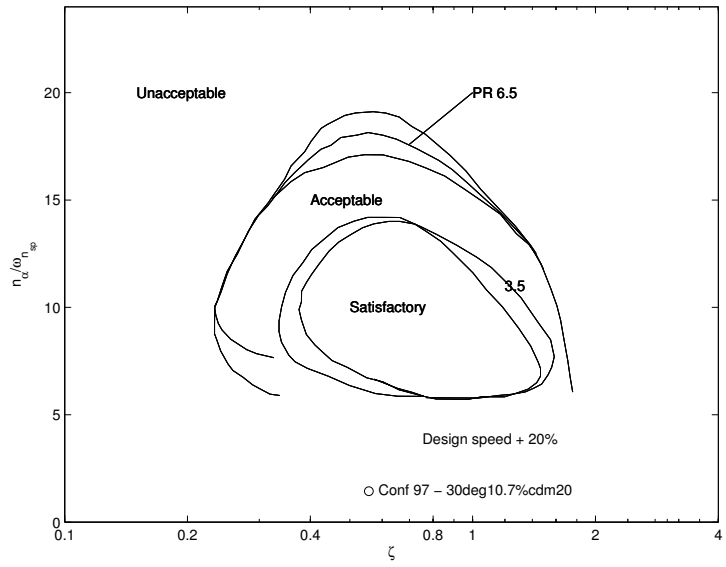

Figure J.15: Group six analysis results for $n_\alpha \geq 15$ g/rad.

Appendix K

Neal-Smith Example

The Neal-Smith method will now be presented by means of an example. A sample Neal-Smith analysis of configuration 99 (30° sweep, 10.7% static margin and the baseline control authority and aerodynamic damping) of the gull-wing configuration will be presented.

The first step of the Neal-Smith analysis of configuration 99 was to set up the transfer function of the aircraft configuration using Equation 3.9 and the aerodynamic coefficients for this configuration that was presented in Chapter 4:

$$\frac{\theta}{F_s} = \frac{K_\theta(\tau_{\theta_2}s + 1)}{s(\frac{s^2}{\omega_{sp}^2} + \frac{2\zeta_{sp}}{\omega_{n_{sp}}}s + 1)} \tag{K.1}$$

The open loop Bode amplitude and phase characteristics for the aircraft transfer function together with a pilot time delay and a gain of 1 was consequently calculated for a frequency range from 0 to 10 rad/s. The results were plotted onto a Nichols chart and translated vertically (which implies merely a open loop gain adjustment) until the 3.5 rad/s point fell on the 90° closed loop phase angle or alternatively until the hump of the graph fell onto the 3 dB droop boundary. The result of this plot is shown in Figure K.1.

After the gain adjusted uncompensated curve is plotted on the Nichols chart it is necessary to choose whether to use lead or lag in order to achieve the performance standards (3.5 rad/s bandwidth and the maximum of 3 dB droop). This process mimics the way a pilot would adapt to an aircraft in

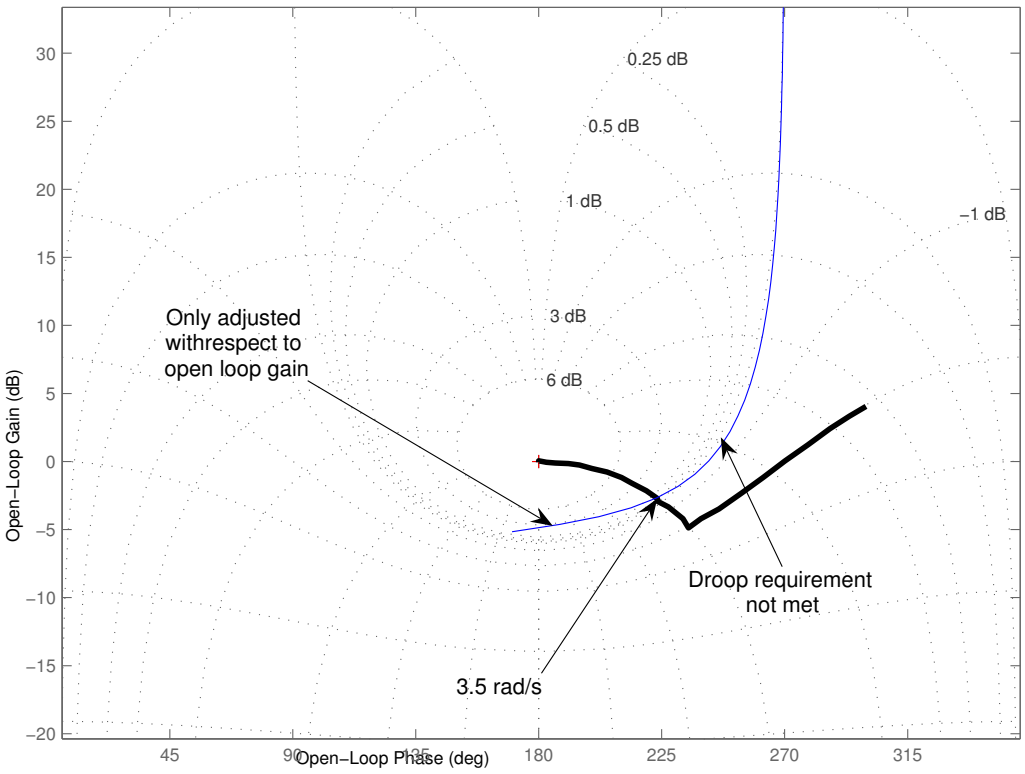

Figure K.1: Nichols chart for aircraft configuration 99 with only gain adjustment in order to achieve the performance standards.

order to perform flying tasks with the aircraft. Figure K.2 shows examples of configurations that require lead or lag compensation. Curve A is an example of an aircraft that requires lag compensation. The droop requirement is satisfied for this curve because the hump of the curve forms a tangent with the -3 dB line on the Nichols chart, but the 3.5 rad/s frequency does not lie on the -90° (or the 270°) phase line. Even though the bandwidth of this configuration might be higher than 3.5 rad/s, the closed loop resonance of the aircraft configuration that Curve A represents, will be high. This means that the aircraft will suffer from *PIO*. An aircraft will have reduced closed loop resonance (and accompanying good handling characteristics) only when both performance criteria (bandwidth and droop) are satisfied. Curve B is an example of an aircraft that requires lead compensation. The 3.5 rad/s frequency lies on the -90° phase line, but the hump of the curve does not

lie on the -3 dB boundary. Once again, even though the droop is less than 3 dB, the closed loop resonance is higher than what it could be with the lead compensation.

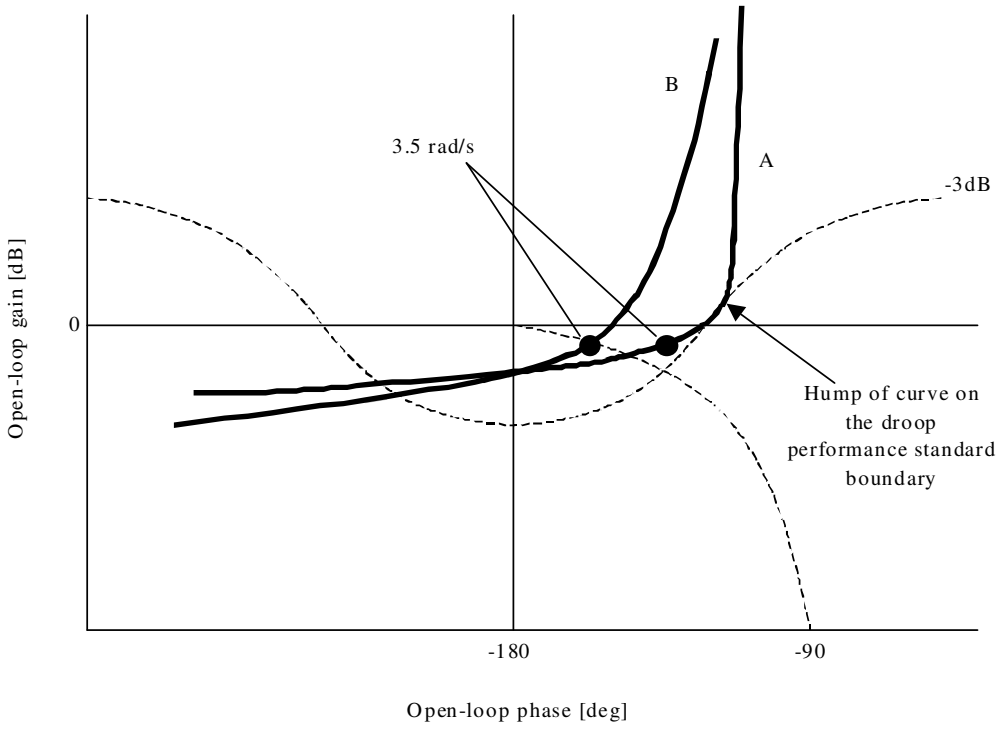

Figure K.2: Nichols chart illustrating the difference between a system that requires lead and lag compensation.

Neal & Smith (1970) defines 'rules' for determining the optimum lead or lag. The reference mentions that these rules might not represent the absolute optimum (such as would be achieved by a optimisation routine), but that the lead/lag guidelines provide very close to optimum compensation, as well as a repeatable process with which to determine compensation values. For purposes of comparison with the Neal-Smith document the same rules for determining lead and lag were employed in the gull-wing configuration analysis.

The lead/lag 'rules' state that if lead compensation is required, the lag time constant (τ_{p_2}) must be set to zero. The lead time constant is then varied

in an iterative process until the performance criteria are met.

If lag compensation is required, the optimum lead and lag time constants are chosen so that the lead and lag frequencies ($1/\tau_{p_1}$ and $1/\tau_{p_2}$) are logarithmically centred around the minimum bandwidth frequency (BW_{MIN}). This implies that the ratio between the lag and lead time constants or $\frac{\tau_{p_2}}{\tau_{p_1}}$ is chosen in an iterative process.

Once the ratio is chosen, the lead time constant is calculated using Equation K.2. The lag time constant may then be found using the ratio and the lead time constant value.

$$\tau_{p_1} = \frac{1}{x^{\frac{1}{2}} BW_{MIN}} \tag{K.2}$$

If Figure K.1 is studied, it is clear that lead compensation is required, because the droop requirement is not met. τ_{p_1} was consequently varied and the Nichols chart was plotted for the different values until all the requirements of the performance criteria were met. The result of the process is presented in Figure K.3. This graph represents a transfer function that satisfies the 3.5 rad/s bandwidth as well as the minimum droop requirement of 3 dB.

The Bode plot of the airframe that is compensated by the optimised compensation network can now be plotted and this is presented in Figure K.5. The resonant peak of the closed loop system (or peak of the $\frac{\theta}{\theta_c}$ magnitude Bode plot) may be read off from this graph. The phase angle of the pilot compensation at the bandwidth frequency of 3.5 rad/s may now be read off a Bode plot of the compensation network alone (see Figure K.4), or by using Figure 3.10. The resonant peak of the compensated airframe and the phase angle of pilot compensation are then used as y and x co-ordinates respectively and plotted on the pilot opinion map presented in Figure 3.6. A step response of the optimised closed loop transfer function is shown in Figure K.6.

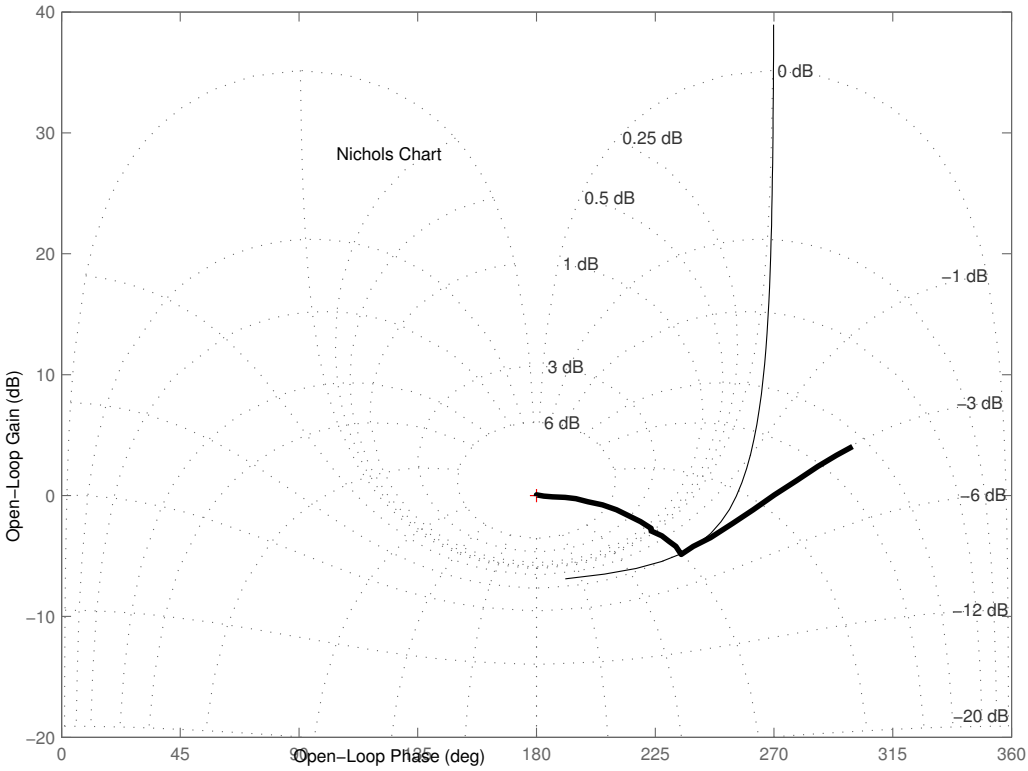

Figure K.3: Nichols chart for aircraft configuration 99 with lead, lag and gain adjustment in order to achieve the performance standards.

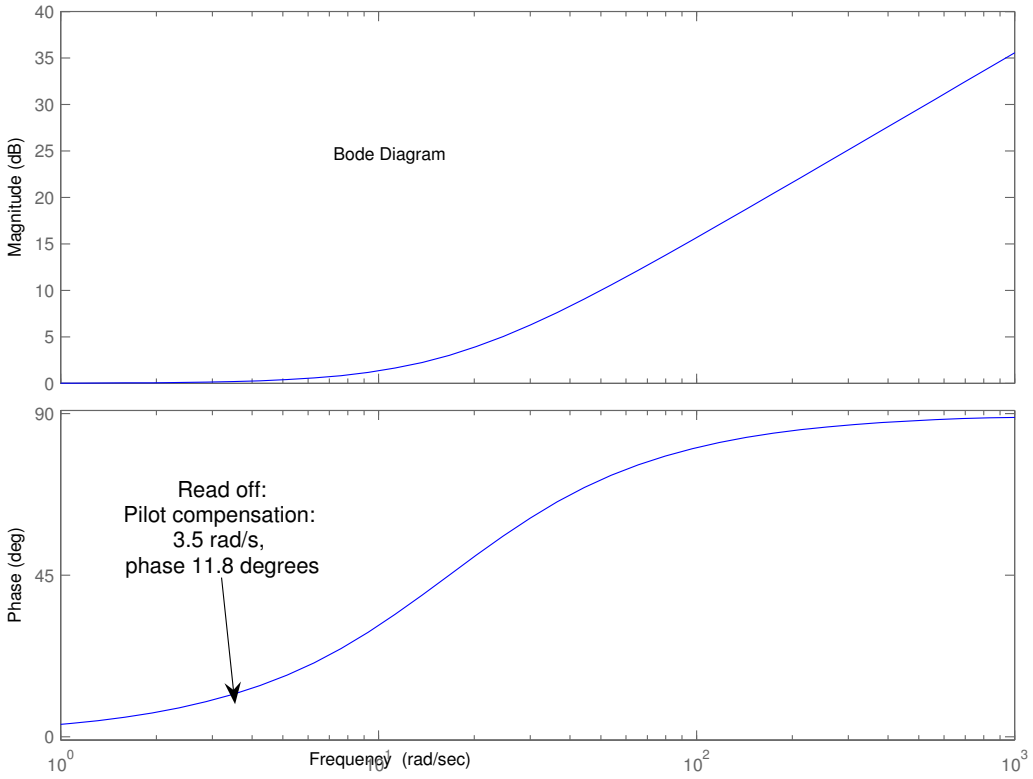

Figure K.4: Bode plot of the pilot compensation network. The phase angle at 3.5 rad/s is indicated by an arrow.

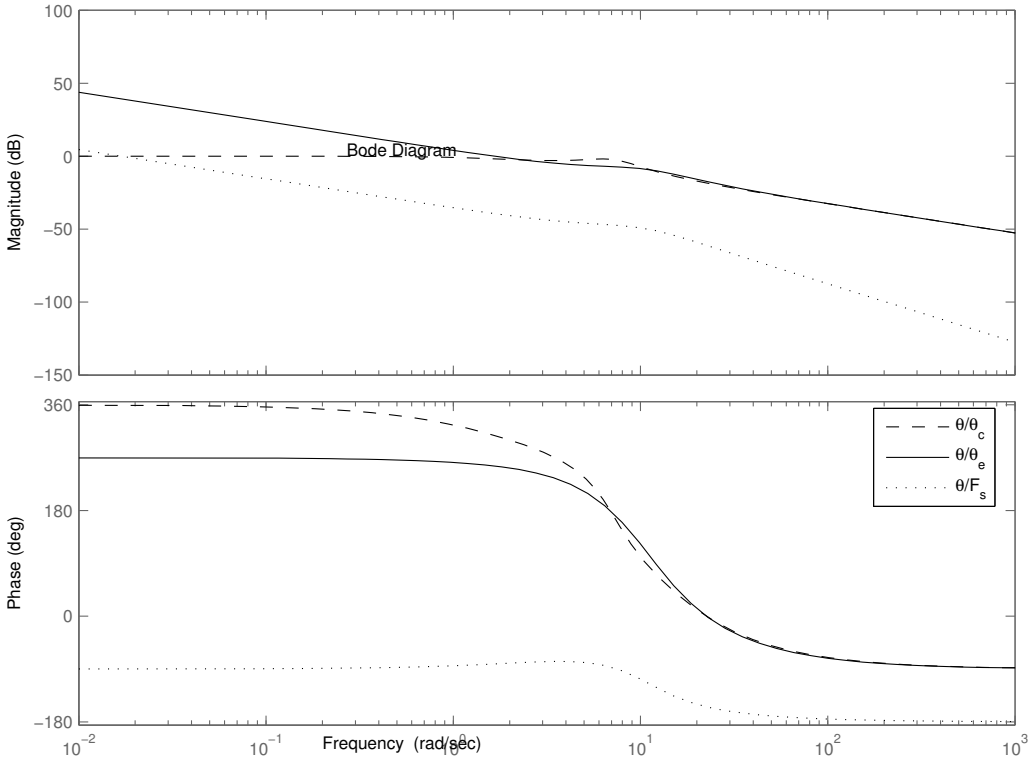

Figure K.5: Bode plots for aircraft configuration 99 showing the Bode characteristics of the airframe only, the open loop as well as the closed loop pilot compensated aircraft transfer function.

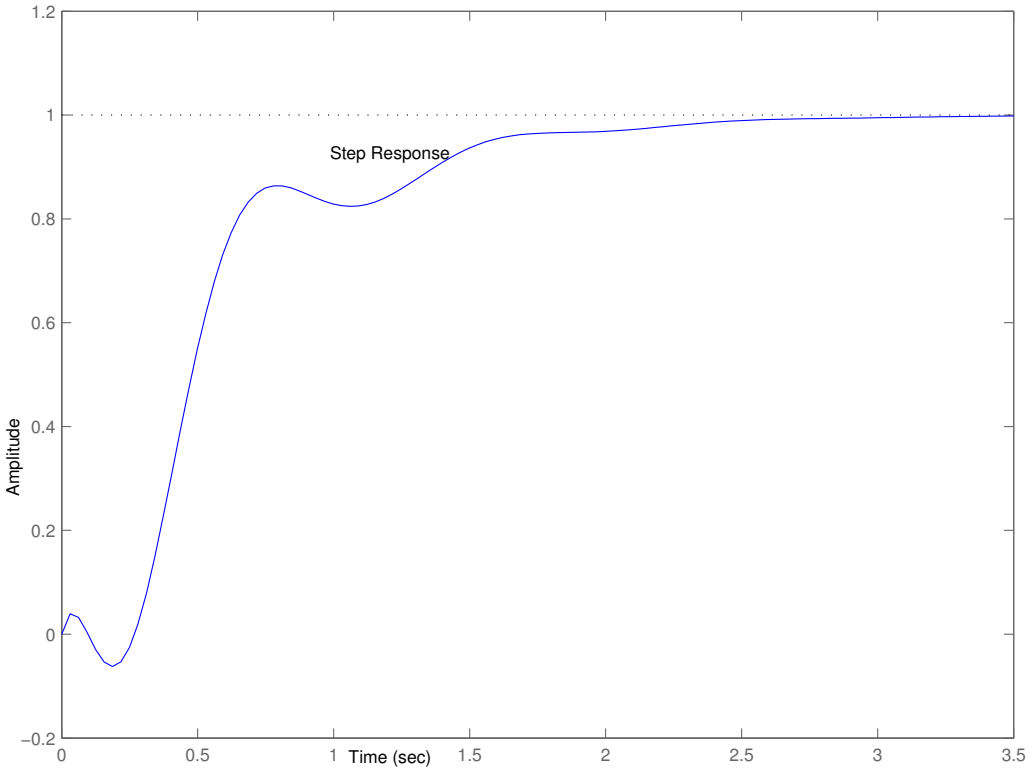

Figure K.6: Step response for the closed loop pilot compensated aircraft configuration 99.

Appendix L

Longitudinal Transfer Functions

The equations presented here were obtained from Appendix IV of Neal & Smith (1970). These equations represent the linearised version of Equation 4.1. The linearisation is performed at an arbitrary trim point. The equations are included for purposes of completeness and serve to support the Neal-Smith analysis presented in Section 7.4. The Neal-Smith analysis uses the transfer functions presented in this section.

Several simplified longitudinal transfer functions are presented in the following paragraphs. The following equations of motion are used to represent the airplane pitch dynamics. They assume constant speed and neglect incremental effects of gravity.

$$\begin{aligned} \ddot{\theta} &= M_q\dot{\theta} + M_{\dot{\alpha}}\dot{\alpha} + M_\alpha\alpha + M_{\delta_e}\delta_e \\ \dot{\alpha} &= \dot{\theta} - L_\alpha\alpha - L_{\delta_e}\delta_e \\ n &= \frac{V_T}{g}(\dot{\theta} - \dot{\alpha}) \end{aligned} \tag{L.1}$$

The equations imply that the reference axes are stability axes and that the wings are always level so that $\dot{\theta} = q$ and $\theta(s) = \frac{1}{s}\dot{\theta}(s)$. Small disturbances

are assumed, so that the variables θ, α, n and δ_e differ only by small amounts from their respective trim conditions.

The following transfer functions in Laplace notation arise from the above equations:

$$\begin{aligned}
\frac{q}{\delta_e} &= \frac{(M_{\delta_e} - L_{\delta_e}M_{\dot{\alpha}})s + (M_{\delta_e}L_\alpha - M_\alpha L_{\delta_e})}{s^2 + (L_\alpha - M_q - M_{\dot{\alpha}})s - (M_\alpha + M_q L_\alpha)} \\
\frac{\alpha}{\delta_e} &= \frac{-L_{\delta_e}s + (M_{\delta_e} + M_q L_{\delta_e})}{s^2 + (L_\alpha - M_q - M_{\dot{\alpha}})s - (M_\alpha + M_q L_\alpha)} \\
\frac{n}{\delta_e} &= \left(\frac{V_T}{g}\right)\frac{L_{\delta_e}s^2 + (-L_{\delta_e}M_q - L_{\delta_e}M_{\dot{\alpha}})s + (M_{\delta_e}L_\alpha - M_\alpha L_{\delta_e})}{s^2 + (L_\alpha - M_q - M_{\dot{\alpha}})s - (M_\alpha + M_q L_\alpha)}
\end{aligned} \tag{L.2}$$

Assuming that the product of small terms is negligible $L_{\delta_e}M_q \approx L_{\delta_e}M_{\dot{\alpha}} \approx 0$:

$$\begin{aligned}
\frac{q}{\delta_e} &= \frac{M_{\delta_e}s + (M_{\delta_e}L_\alpha - M_\alpha L_{\delta_e})}{s^2 + (L_\alpha - M_q - M_{\dot{\alpha}})s - (M_\alpha + M_q L_\alpha)} \\
\frac{\alpha}{\delta_e} &= \frac{-L_{\delta_e}s + M_{\delta_e}}{s^2 + (L_\alpha - M_q - M_{\dot{\alpha}})s - (M_\alpha + M_q L_\alpha)} \\
\frac{n}{\delta_e} &= \left(\frac{V_T}{g}\right)\frac{L_{\delta_e}s^2 + (M_{\delta_e}L_\alpha - M_\alpha L_{\delta_e})}{s^2 + (L_\alpha - M_q - M_{\dot{\alpha}})s - (M_\alpha + M_q + L_\alpha)}
\end{aligned} \tag{L.3}$$

The short-period natural frequency and damping ratio can be expressed as:

$$\begin{aligned}
\omega_{n_{sp}}^2 &= -M_\alpha - M_q L_\alpha \\
2\zeta_{sp}\omega_{n_{sp}} &= L_\alpha - M_q - M_{\dot{\alpha}} \\
\zeta_{sp} &= \frac{L_\alpha - M_q - M_{\dot{\alpha}}}{2\sqrt{-M_\alpha - M_q L_\alpha}}
\end{aligned} \tag{L.4}$$

and:

$$\frac{1}{\tau_{\theta_2}} = \frac{M_{\delta_e} L_\alpha - M_\alpha L_{\delta_e}}{M_{\delta_e}} \tag{L.5}$$

Making these substitutions and rearranging,

$$\begin{aligned}
\frac{q}{\delta_e} &= \frac{M_{\delta_e}}{\omega_{n_{sp}}^2} \frac{1}{\tau_{\theta_2}} \frac{(\tau_{\theta_2} s + 1)}{\frac{s^2}{\omega_{n_{sp}}^2} + \frac{2\zeta_{sp}}{\omega_{n_{sp}}} s + 1} \\
\frac{\alpha}{\delta_e} &= \frac{M_{\delta_e}}{\omega_{n_{sp}}^2} \frac{(-\frac{L_{\delta_e}}{M_{\delta_e}} s + 1)}{\frac{s^2}{\omega_{n_{sp}}^2} + \frac{2\zeta_{sp}}{\omega_{n_{sp}}} s + 1} \\
\frac{n}{\delta_e} &= \frac{M_{\delta_e}}{\omega_{n_{sp}}^2} \left(\frac{V_T}{g} \frac{1}{\tau_{\theta_2}}\right) \frac{\tau_{\theta_2} \frac{L_{\delta_e}}{M_{\delta_e}} s^2 + 1}{\frac{s^2}{\omega_{n_{sp}}^2} + \frac{2\zeta_{sp}}{\omega_{n_{sp}}} s + 1}
\end{aligned} \tag{L.6}$$

For most conventional airplanes, the numerator time constants in the $\frac{\alpha}{\delta_e}$ and $\frac{n}{\delta_e}$ transfer functions are negligible. However, for airplanes having a tail length which is quite short, these numerator terms can be important.

The following relationships are now derived for use in the Neal-Smith handling characteristics analysis:

1. n/α:
   For a step input in elevon/elevator deflection,

$$\begin{aligned}
\left(\frac{n}{\delta_e}\right)_{SS} &= \left(\frac{n}{\delta_e}\right)|_{s\to 0} = \frac{M_{\delta_e}}{\omega_{n_{sp}}^2} \left(\frac{V_T}{g} \frac{1}{\tau_{\theta_2}}\right) \\
\left(\frac{\alpha}{\delta_e}\right)_{SS} &= \left(\frac{\alpha}{\delta_e}\right)|_{s\to 0} = \frac{M_{\delta_e}}{\omega_{n_{sp}}^2}
\end{aligned}$$

   therefore,

$$\left(\frac{n}{\alpha}\right)_{SS} = \frac{(n/\delta_e)_{SS}}{(\alpha/\delta_e)_{SS}} = \frac{V_T}{g} \frac{1}{\tau_{\theta_2}}$$

2. F_s/n:

$$\left(\frac{n}{F_s}\right)_{SS} = \left(\frac{n}{\delta_e}\right)_{SS}\left(\frac{\delta_e}{F_s}\right)_{SS}$$

and

$$M_{F_s} = M_{\delta_e}\left(\frac{\delta_e}{F_s}\right)_{SS}$$

therefore,

$$\left(\frac{F_s}{n}\right)_{SS} = \left(\frac{n}{F_s}\right)_{SS}^{-1} = \frac{\omega_{n_{sp}}^2}{M_{F_s}(n/\alpha)_{SS}}$$

3. θ/F_s transfer function (no control system dynamics):

$$\frac{\theta}{F_s} = \frac{\theta}{\delta_e}\left(\frac{\delta_e}{F_s}\right)_{SS} = \frac{M_{F_s}}{\omega_{n_{sp}}^2}\left(\frac{1}{\tau_{\theta_2}}\right)\frac{\tau_{\theta_2}s+1}{s\left(\frac{s^2}{\omega_{n_{sp}}^2}+\frac{2\zeta_{sp}}{\omega_{n_{sp}}}s+1\right)}$$

or

$$\frac{\theta}{F_s} = \frac{K_\theta(\tau_{\theta_2}s+1)}{s\left(\frac{s^2}{\omega_{n_{sp}}^2}+\frac{2\zeta_{sp}}{\omega_{n_{sp}}}s+1\right)}$$

where

$$K_\theta = \frac{M_{F_s}}{\omega_{n_{sp}}^2\tau_{\theta_2}} = \frac{g}{V_T(F_s/n)_{SS}}$$

Note: K_θ as defined above is the same as the steady-state value of q/F_s